

Development of a Virtual Testing Methodology for Structural Fatigue Testing Setups



Author: Ing. Noë C. Eenkhoorn

Supervisors TU Delft: Prof. dr. ir. Fred van Keulen and Ir. Chris Valentin

Supervisors NLR: Ir. Paul Arendsen and Ir. Cees de Mareé

*Delft University of Technology
Faculty of Mechanical Engineering and Marine Technology
Section Precision and Microsystems Engineering
Delft, The Netherlands*

July 3, 2010

SUMMARY

Full-scale structural testing of aircraft structures has been and still is the task of the aircraft industry when new aircrafts are developed. The NLR performs structural testing of aircraft structures for certification, this is done using structural test setups. Structural testing consists out of static testing (ultimate load) and fatigue testing (lifetime). The NLR is developing a new structural testing methodology whereby the testing behaviour is predicted using computational models before the certification test is actually performed, called *virtual testing*. This has the advantage of performance prediction as well as a reduction in costs and risks. This thesis covers the development of a virtual testing methodology for structural test setups, to simulate its static and dynamic behaviour.

Structural test setups consist out of three main systems, the hydraulic system, mechanical system and control system. Currently design of the mechanical system and hydraulic system takes place in separate processes. Controller parameters are tuned when the test setup is built and in operation. As a result the total system performance is currently only known if the test setup is actually built. To improve design and performance of structural test setups a virtual testing methodology has been developed. The virtual testing methodology combines mechanical, hydraulic and control system in a simulation model to simulate the system performance of the test setup before it is built, called *virtual testing*.

To develop and to verify the proposed virtual testing methodology a demonstration test setup is developed. This demonstration test setup is derived from the general architecture of structural test setups. Assumptions regarding the modelling were made to obtain a demonstration test setup which represents the essence of a general structural test setup.

Reference signals used in fatigue tests are interpolated sinusoidal signals, therefore dynamic modelling of the demonstration test setup is applied. To obtain a measure of the bandwidth of fatigue reference signals, the frequency content of fatigue profiles were analyzed. This analysis obtained a maximum bandwidth of 5 [Hz].

Dynamic models of the three main systems, the hydraulic system, mechanical system and control system were developed and coupled, describing the system behaviour of a demonstration test setup. The control architecture as presently used is implemented in the model. Using the simulation models it is possible to obtain controller parameter and provide also the possibility to investigate non-linear effects, such as play and friction. The simulation models obtain physical knowledge of the system behaviour, which can be analyzed in the time domain or frequency domain.

Measurements on the demonstration test setup were performed to verify the simulation models. Each component of the demonstration test setup was measured and verified individually. Coupled system measurements were performed for verification of the coupled mechanical, hydraulic and control system. The coupled system response is verified up to 40 [Hz], compared with the linear frequency response of the model. The simulation model proved to predict the frequency response of the demonstration test setup.

This thesis proved the ability of virtual testing of structural test setups before they are actually build. Using these simulation models it is possible to investigate system performance and non-linear effects. Further research is needed on extending these models to full scale structural test setups.

ACKNOWLEDGEMENTS

From February 2009 and onwards, the National Aerospace Laboratory (NLR) provide me with the opportunity to fulfill my M.Sc. thesis at the *Structures Testing and Evaluation* department. During this period of time I developed my engineering skills but also my project management skills, in setting up the M.Sc. project as provided by NLR.

First of all I would like to thank Ir. Paul Arendsen for providing me the opportunity to fulfill my M.Sc. thesis project at NLR, his support and the discussions we had from time to time. For the support during my M.Sc. project, I would especially like to thank Ir. Cees de Mareé. Cees provided me with the physical and technical know length of hydraulic systems, and helped me solving signal errors in the demonstration test setup. In general I would like to thank all NLR colleagues who contributed to my work by providing me support in various ways.

Many thanks go to Prof. Dr. Ir. Fred van Keulen and Ir. Chris Valentin of the T.U. Delft for their evaluations and comments to my work. On the technical side but also on the project management side. Thank you both, it improved my work a lot.

Last but not least, I would like to thank the people who where not directly involved to my work, but provided me a lot of support to complete my M.Sc. thesis.

First of all I would like to thank my parents and my sister for their continuous support and encouragements during my studies. Thank you Mom and Dad. Appreciation goes also to my friends who encouraged me during my studies, thank you all. Finally, I would like to thank the Lord for His blessing and support in my study and my life.

Sassenheim,
July 2010

Noë Eenkhoorn

CONTENTS

Summary	iii
Acknowledgements	v
1 Introduction	1
1.1 History of Structural testing	2
1.2 State-of-the-art Structural testing	3
1.3 Virtual Testing project	7
1.4 Assignment Definition	10
1.5 Thesis Outline	10
2 Testing Methodology	11
2.1 Current and proposed structural testing methodology	12
2.2 Fatigue loading methodology	18
2.3 Summary	23
3 Fatigue Testing Setups	25
3.1 Architecture and Operation of Fatigue Testing Setups	25
3.2 Modelling Assumptions of the Demonstration Test Setup	28
3.3 Demonstration Test Setup	32
3.4 Summary	38
4 Modelling Theory	39
4.1 Mechanical Modelling	39

4.2	Servo-Hydraulic Modelling	45
4.3	Controller Modelling	52
4.4	Summary	56
5	Demonstration Test Setups Models	59
5.1	Mechanical System Model	60
5.2	Servo-Hydraulic System Model	66
5.3	Coupling Mechanical Model and Servo-Hydraulic model	80
5.4	Controller Models	83
5.5	Summary	93
6	Measurements and Verification on Demonstration Test Setup	95
6.1	Mechanical System Measurements and Verification	96
6.2	Servo-Hydraulic measurements and verification	101
6.3	Coupled Mechanical System and Hydraulic System Measurement and Verification	112
6.4	Verification of Controller Parameters	117
6.5	Summary Measurement and Verification	122
7	Conclusion and Recommendations	125
7.1	Conclusions	125
7.2	Recommendations	130
A	Thesis Assignment defined by NLR	135
B	Demonstration Test Setup Component Details	137
B.1	Mechanical system	137
B.2	Hydraulic system	142
B.3	Measurement System	155
C	Derivations Modelling Theory	159
C.1	Mechanical Modelling	159
C.2	Servo-Hydraulic Modelling	166
D	Demonstration Test Setup Model Parameters	175
D.1	Mechanical System Model	175
D.2	Hydraulic System Model	180
E	Simulink Modelling	185
E.1	Energy Based Modelling	185
E.2	Force Input Calculation	186

E.3	Linearization of Simulation Models	188
F	Measurement Settings	191
F.1	Mechanical System	191
F.2	Hydraulic System	192
F.3	Control System Settings	194
G	Model Updating	199
G.1	Test Article Model Updating	199
G.2	Hydraulic System Model Updating	204
H	Measurement Results	205
H.1	Mechanical System	205
H.2	Hydraulic System	209
H.3	Coupled Mechanical and Hydraulic System	212
H.4	Control System	214
H.5	Signal Conditioning	214

NOTATIONS

Nomenclature

δ	play interface structure	m
\mathbf{C}_{MS}	Damping matrix of mechanical system	Ns/m
$\mathbf{F}_{\text{extern}}$	External applied force	N
\mathbf{K}_{MS}	Stiffness matrix of mechanical system	N/m
\mathbf{M}_{MS}	Mass matrix of mechanical system	kg
ω_n	Eigenfrequency mechanical system	rad/s
ω_v	Natural frequency of the servo valve	rad/s
ρ_{oil}	Density of hydraulic fluid	kg/m
ρ_{TA}	Density test article	kg/m ³
ζ	Damping factor of mechanical system	-
A_p	Piston area hydraulic actuator	m ²
C_d	Discharge coefficient	-
c_s	Stribeck velocity	m/s
D_v	Damping coefficient of the servo valve	Ns/m

E	Bulk modulus hydraulic fluid	Pa
F_c	Coulomb friction	N
F_s	Static friction	N
F_v	Viscous friction	Ns/m
I_{TA}	Inertia test article	m ⁴
K_v	Servo valve gain	-
K_d	Controller damping gain	-
K_i	Controller integral gain	-
K_p	Controller proportional gain	-
m_{HA}	Hydraulic actuator mass	kg
P_A	Pressure chamber A of HA	Pa
P_B	Pressure chamber B of HA	Pa
P_s	Supply pressure	Pa
P_t	Return pressure to tank	Pa
Q_A	Servo valve flow to HA chamber A	m ³ /s
Q_B	Servo valve flow to HA chamber B	m ³ /s
S	Hydraulic actuator maximum stroke	m
S_{port}	Valve spool position gain	m
V_0	Dead oil volume of oil pipelines between servo valve and hydraulic actuator	m ³
x_p	Piston displacement hydraulic actuator	m
D_{IS}	Interface structure damping	Ns/m
F_{IS}	Interface structure Interaction force	N
K_{IS}	Interface structure stiffness	N/m
x_v	Servo valve position	m
x_v^*	Normalized servo valve displacement	-

List of abbreviations

AC	Accumulator
BS	Backup Structure
CS	Control System
CT	Controller
EMA	Experimental Modal Analysis
FE	Finite Element
FR	Frequency Response
FRF	Frequency Response Function
HA	Hydraulic Actuator
HF	Hydraulic Fluid
HP	Hydraulic Pump
HS	Hydraulic System
IS	Interface Structure
LC	Load Cell
MB	Manifold Blocks
MS	Mechanical System
OC	Oil Cooler
OR	Oil Reservoir
SD	Servo valve Driver
SISO	Single Input Single Output
SV	Servo Valve
TA	Test Article
TL	Transmission Lines

CHAPTER

1

INTRODUCTION

The National Aerospace Laboratory (NLR) is a research centre for aerospace technology in the Netherlands. Two important activities performed by the NLR are research in computational structural analysis methods and certification tests of aerospace materials or components. The NLR is developing a novel structural testing methodology whereby the testing behaviour is predicted using computational models before the certification test is actually performed. This has the following potential advantages:

- Performance prediction of a pre-designed test setup by using simulation models.
- Reduction in costs and risks.

Performance prediction on structural testing setups is only possible if simulation models are verified. The verification on these simulation models needs to be done component wise, since it is then possible to be able to model and predict system performance of novel structural testing setups.

This thesis assignment covers the development and verification of an elasto-mechanical and servo-hydraulic computational method, a so-called virtual testing environment, to enable simulation of the dynamic and static behaviour of large structural test setups.

In this introduction, a brief history of certification testing of aerospace structures is presented. A brief summary on the state of the art on structural testing is presented.

Then, the virtual testing project is outlined and explained, resulting in the thesis assignment. Finally the outline of this thesis is presented.

1.1 History of Structural testing

Full-scale structural testing of aircraft structures has been and still is the task of the aircraft industry when new aircrafts are developed. The first structural tests were performed around 1920 to prove structural integrity by “People Standing on Wings”, see Figure 1.1-(a) [8]. This developed to putting sand bags on wings, to simulate a static load, as shown in Figure 1.1-(b). Wing structures evolved from wooden wings into metal structures. In the 1930’s after the Second World War both static and fatigue loading of wings became important. Emphasis on fatigue testing became intensive after the accidents with the De Havilland Comets in 1954¹. Fatigue of aircraft structures has

¹The problem of metal fatigue can be defined as the failure of metal components subjected to many cyclic loads which are much smaller than the loads that would be required for failure under a static



Figure a

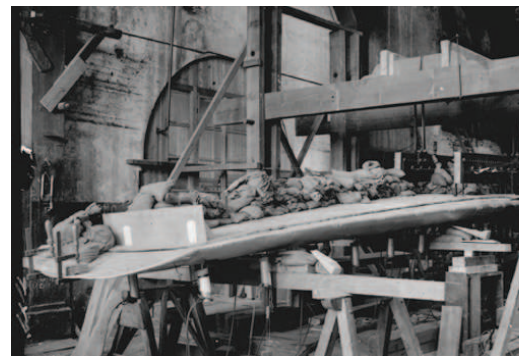


Figure b



Figure c



Figure d

Figure 1.1 – History of Structural testing with (a) “People Standing on Wings” 1919 photograph of a Fokker D.VII fighter, (b) Simulation of static loads on aircraft wing using sand bags, (c) Fatigue testing of Fokker F27 wing using cable systems, (d) Fatigue testing of Fokker F100 tail section, using hydraulic actuators.

become of great importance to flight safety, and the subject transcends personal, company and national interests. Since the second World War, NLR has obtained contracts from the Netherlands Institute for Aerospace Programs (NIVR) to carry out part of the structural testing of Fokker aircraft. Figure 1.1-(c) shows the testing of a Fokker F27 wing, during the period of 1966-1971, when a total of 180,000 simulated flights were applied. During the 1980's improved servo-hydraulic systems were applied for full-scale testing. These have the advantage applying loading conditions for a large number of cycles. An example is the application of servo-hydraulic systems for the T-tail tests of the Fokker 100 during the period of 1987-1992, shown in Figure 1.1-(d).

1.2 State-of-the-art Structural testing

Structural testing is not only performed in the aerospace industry. Indeed, other application areas for example the automotive industry and wind power industry utilize structural testing methodologies. This section presents the different methodologies used for structural fatigue testing.

Structural testing consists out of two fields:

- *Static testing*, ultimate strength of a structure or component.
- *Fatigue testing*, and durability tests of a structure or component by cyclic loading of the structure with a certain loading profile².

The emphasis of this section will be on fatigue testing. Fatigue testing can be divided into two types of testing methods, namely:

- *Dynamic testing*, which uses load time profile repetition to simulate fatigue loading.
- *Quasi-static testing*, which uses load profile repetition, see Section 2.2.

Different testing methodologies and their application can be summarized into a flowchart figure which is presented in Figure 1.2.

loading.

²Loading profiles are called in the industry loading spectra, but since spectra imply frequency domain loading, the name loading profile is used instead. Loading profiles are time domain loading conditions.

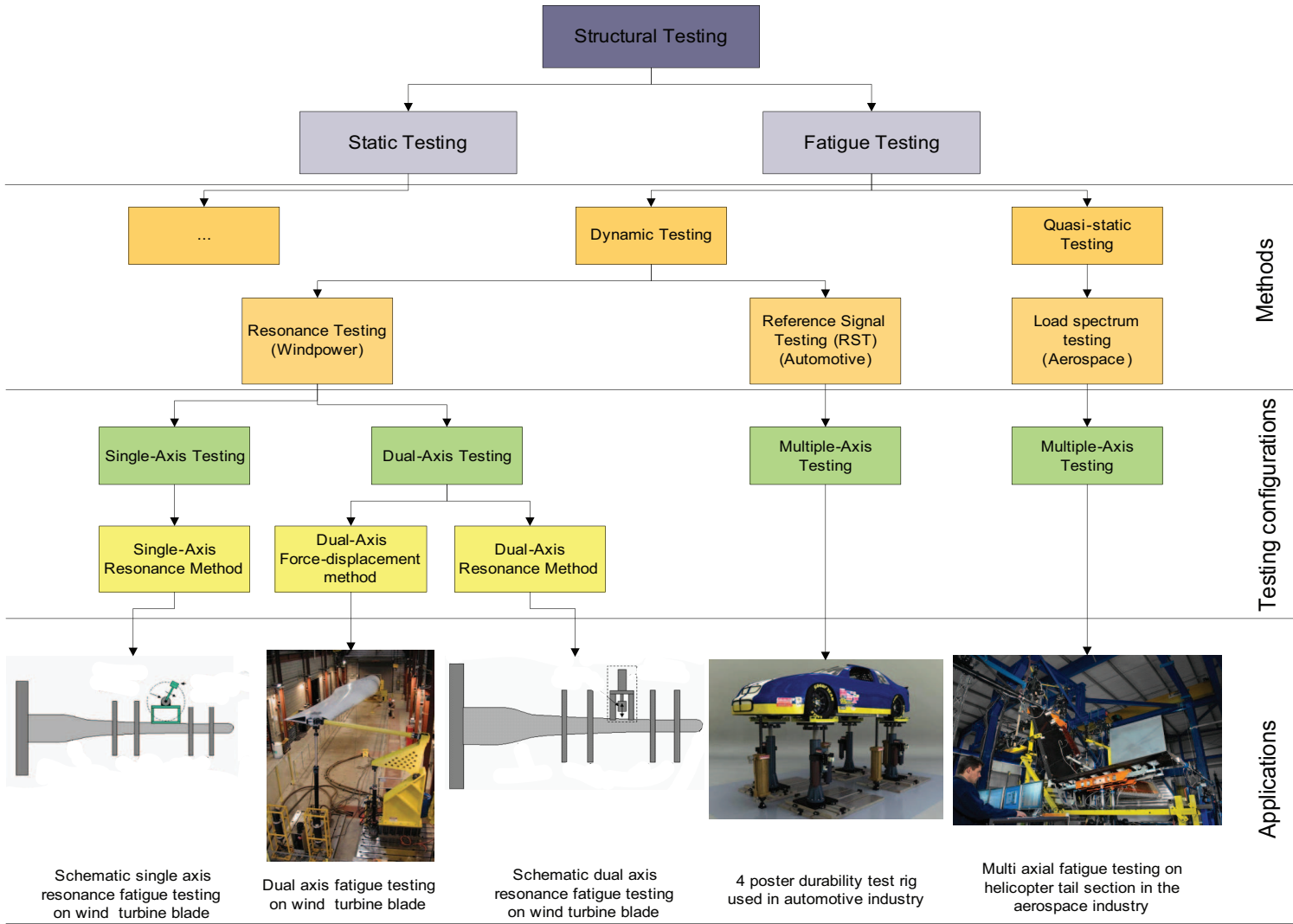


Figure 1.2 – Present state-of-the-art fatigue testing methodologies used in industry, application figures are found in [16, 17].

Windpower industry is a largely developing industry, since a necessary amount of wind turbines are used for electricity generation in the society. To obtain the lifetime of a wind turbine blade accelerated lifetime tests (fatigue tests) are performed. The International Electrotechnical Commission (IEC) which is an international institute for standardization, prescribes static and modal testing of wind turbine blades. Requirements for fatigue testing are expected in 2009 [3].

Fatigue loads for wind turbine blades are composed of periodic loads that are dependent on rotational frequencies and natural frequencies of the blade [10]. Since loads depend on rotational and bending frequencies, fatigue loading is performed using dynamic testing, see Figure 1.2. To the authors' knowledge there are three methods for fatigue testing of wind turbine blades, namely:

- Single-axis resonance testing,
- Dual-axis force displacement testing,
- Dual-axis resonance testing [24].

Single-axis resonance testing uses an electric motor to excite the system around the resonance frequency. Masses are added on the blade to lower the eigenfrequency. Furthermore the masses define the bending moment distribution of the blade. Single-axis resonance testing takes advantage of the magnification of the vibration of the blade near the resonance frequency, resulting in faster testing, lowering costs and more efficient use of test space. Single-axis testing requires multiple tests if multiple directions need to be tested. Therefore single-axis testing is time consuming in comparison to dual-axis testing [24].

Dual-axis force displacement testing uses a servo-hydraulic system with hydraulic actuators to excite the the system in multiple directions. As a result, only one test is needed. Loads can be applied accurately each cycle. Disadvantages of this method are the need of large stroke hydraulic actuators, and the large energy costs. Furthermore, there are also limitations on test speed due to limitation in maximum hydraulic flow. It is not possible to test the entire blade length. Costs of large stroke hydraulic equipment are expensive [24].

Dual-axis resonance testing takes the advantage of resonance testing using a hydraulic actuator with a mass as exciter for the vertical direction, and an other hydraulic actuator for the horizontal direction. The advantages of this method are faster testing, compared to single-axis resonance testing and relatively low energy costs compared to dual-axis force displacement testing [24].

Automotive industry uses structural test setups not only for fatigue testing but also for comfort testing. Durability of components and comfort of the driver is essential for the automotive industry. Different types of test setups are used in automotive industry to study durability and comfort. Examples of test setups are, suspension test rigs, 4-poster test rigs³ and multi-axial shaker test rigs. Fatigue testing and comfort testing is usually done using Reference signal testing (RST) [4].

Reference signal testing is a testing methodology where reference signals are measured on a test track and reproduced on the test rig. The reference signal is reproduced as measured on the test track. Reasons for using this method are:

- Test track reference signals provide information on the fatigue life of a vehicle. To obtain the same fatigue life in testing laboratory, exact replication of measured signals is needed.
- If a component is re-designed, a new fatigue test has to be performed. To ensure that the results are comparable, the same fatigue loading is applied to identify performance improvement.
- Fatigue life has a logarithmic nature between number of cycles and applied force. Therefore exact replication is needed. A test rig obtains a controlled environment to generate exact replication of fatigue loading.

Aerospace industry full scale fatigue testing is performed to ensure structural integrity during lifetime operation of an aerospace vehicle. Fatigue loading profiles are composed on the basis of aeroelastic calculations. These loading profiles are updated and verified using measured load profiles during test flights of the aerospace vehicle [21]. A full set of load profile data representing the entire fatigue life of an aerospace vehicle is called a fatigue load spectrum⁴, the layout of loading spectra is presented in Section 2.2.1 [20, 18]. Description of the methods to generate load profile databases can be found in [21, 18].

Load spectrum testing uses multiple servo-hydraulic systems to apply fatigue loading profiles on the tested specimen. Loading is applied quasi-static, since it is unwanted to excite the dynamics of the test specimen. Excitation of dynamics results in unwanted displacements and forces of the test specimen.

³4-poster test rigs are test rigs where a full vehicle is tested usually for comfort optimization. The vehicle wheels are supported by hydraulic actuators which apply the reference loading.

⁴In the remaining of this thesis fatigue load spectra will be called fatigue load profiles, since the word spectra implies that dynamics is present, but the loading is quasi-static.

1.3. Virtual Testing project

The complete system, where servo-hydraulic systems and test specimen are mounted in a test rig, is called a structural test setup. Advantages of structural test setups are, applying accurately fatigue loading profiles, obtaining a lot of information on fatigue life, structural integrity certification for airworthiness the component tested. Disadvantages are that, tests are expensive to perform due to costs of hydraulic equipment and test specimen, hydraulic energy costs are large, structural testing is very complex which imply a lot of risks.

1.3 Virtual Testing project

Thousands of tests need to be performed to ensure structural integrity of any newly developed aircraft and allow it to take off for the first time [12]. The costs and risks associated with these tests can be very large, depending on the amount of testing and the test complexity. Costs of re-design of a structural test increase during the development phase of the test. If changes have to be made in a late stadium, for example if the test setup is already completed, costs will be high see Figure 1.3. It is therefore more cost effective to apply changes in an early stage of the design. Influences of design choices can be investigated at an early stage using virtual testing.

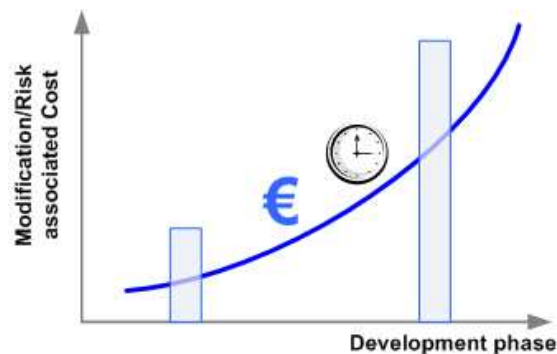


Figure 1.3 – Cost of modifying the design or test associated with the development phase in the developing structural test setups.

Virtual testing is “simulation of the behaviour of test articles in their test environment, reducing the overall costs and risks of actual tests” [12]. This is done using mathematical models of the physical components. These models can be updated by comparing them with the actual structural test results, thereby resulting in model refinements and improved predictions.

Structural tests enable the aircraft to be certified for flight during a certain lifespan, with the inclusion of inspection intervals, maintenance and repair plans. Because of

the complexity of an aircraft tests are performed on different levels, as is shown in the testing pyramid of figure 1.4. Complexity of the certification tests increases with the complexity of the test article. Full-scale tests require multi-axial loading, whereas coupon tests are small uniaxial tests. The levels of the testing pyramid can be explained as:

- **Full-scale** is a complete aerospace vehicle for example, aircraft or Helicopter.
- **Component** is a structure of an aerospace vehicle for example, a wing or stabilizer.
- **Subcomponent** is a piece of a component for example, a flap.
- **Details** is piece of a subcomponent for example, a stiffened panel.
- **Coupons** are standardized material samples⁵.

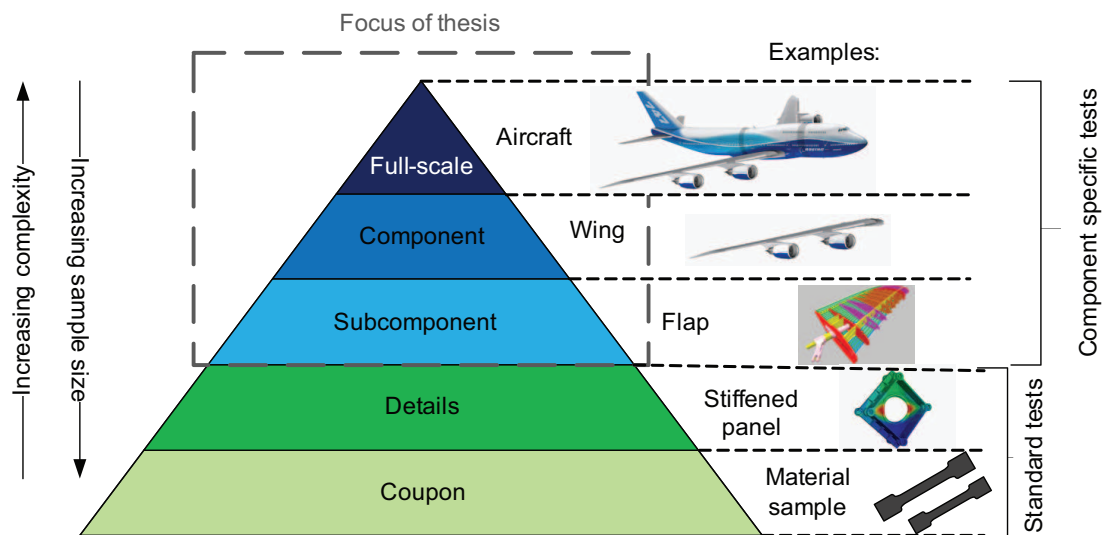


Figure 1.4 – Testing pyramid, describing the different levels of structural testing, similar picture in [10, 12]. Example figures are from [1, 2, 12].

Currently virtual testing is applied on coupon level and detailed level, using finite element simulations [12]. Uniaxial or biaxial structural tests are performed to obtain the actual material and structural properties of the test object. Simulation models can be updated using actual structural test results, resulting in more accurate predictions of subcomponent and full-scale system models.

⁵Coupons are test specimens, each sample is extracted from batch-material or a component. Coupons are generally produced with constant dimensions according to the prescribed test protocol.

1.3. Virtual Testing project

Fatigue testing employs quasi-static loading conditions. Customers want to perform endurance tests at low test speed because this is proven technology. Institutes that perform the fatigue tests want to increase test speed, however to reduce costs, increase total number of tests a year and subsequently increase their revenue. Increasing test speed results in the risk of exciting the dynamics in the system. To convince customers to decrease step-time between loads and subsequently increase the test speed, and show the effect on testing performance, virtual testing is desired.

To be able to perform virtual testing verified numerical models representing servo-hydraulic and elasto-mechanical behaviour of fatigue test setups are needed. The simulation models of component specific fatigue test setups, need to be able to:

- Reduce risks and costs,
- Reduce time of the fatigue test,

Challenges of developing the virtual testing environment are:

- Developing robust models that predict dynamic behaviour of (multi)-axial test setups.
- Including non-linear phenomena that disturb ideal dynamic behaviour, for example:
 - Friction in hydraulic cylinders,
 - Play in mechanical interfaces,

enables the prediction of allowable levels for these phenomena.

- Including controller model for test setups.

Benefits of developing the virtual testing environment are:

- Possibility to improve design choices by performing more design iterations, to gain optimal system performance.
- Physical insight in the behaviour of the test setup.
- Obtaining a set of controller parameters, which can be used for fine tuning of these parameters.

These benefits need to contribute to a reduction in costs and risks for performing actual structural fatigue testing.

The focus of thesis is investigation into virtual testing methodology for component specific fatigue testing. The assignment definition is given in the next section.

1.4 Assignment Definition

As mentioned above and to the authors knowledge, a virtual testing environment has not yet been developed for component specific fatigue testing setups. This is especially the case at NLR. Owing to the complexity, costs and risks of designing, constructing and performing of such tests, there is a need to predict the actual behaviour of the complete test setup. A solution would be to create a physically-based model of the structural test setup that quantifies the static and dynamic hydraulic and mechanical system behaviour before actually building the setup.

These considerations led to the following thesis assignment:

Development of a virtual testing methodology for structural fatigue testing setups, using elasto-mechanical and servo-hydraulic models as a foundation for virtual testing.

1.5 Thesis Outline

This thesis consists out of 7 chapters, where *Chapter 1* is already discussed. Further on the thesis is built up as followed:

- *Chapter 2* presents the current and proposed structural testing methodology. The proposed methodology will be developed and verified in this thesis. Fatigue loading profiles are discussed and analyzed since they play a key role in the performance of the fatigue test setup.
- *Chapter 3* discusses the general architecture of fatigue test setups and the principle of operation on the specific components. Thereafter modelling assumptions are made, to obtain a demonstration test setup. Finally this chapter discussed the layout of the demonstration test setup.
- *Chapter 4* presents the modelling theory used to model the demonstration test setup. Mechanical, hydraulic and control models are presented.
- *Chapter 5* applies the modelling theory on the demonstration test setup and discusses its physical characteristics. In this chapter the coupling is made between the mechanical, hydraulic and control system.
- *Chapter 6* presents the measurement results and verification on the demonstration test setup model. The verification is performed on each system component and on the coupled systems.
- *Chapter 7* ends this thesis with conclusions and recommendations.

CHAPTER

2

TESTING METHODOLOGY

Chapter 1 discussed the need of a virtual testing methodology, for structural fatigue testing setups. Improvement on design and system performance of structural fatigue testing can be performed by:

- (a). Numerical models that predict system performance in the design process.
- (b). Reducing step time between load conditions in the testing process.

Where point (b) affects point (a). Change of step times affects system performance in mechanical and dynamic behaviour of structural test setups.

To improve and accelerate structural fatigue testing, this chapter gives a detailed description of the structural testing methodology of aerospace components. An overview on the present methodology is provided, including a discussion involving its advantages and disadvantages. Conclusions on the present methodology result into development of a novel virtual testing methodology, which takes into account point (a). The chapter ends with a description of fatigue loading profiles and their frequency content used in fatigue testing, which takes into account point (b).

2.1 Current and proposed structural testing methodology

This section presents the current methodology of structural testing and proposes a novel methodology. Advantages for implementing a novel methodology are discussed as well.

2.1.1 Current structural testing methodology

The current method of structural testing is presented in Figure 2.1. The process can be divided into three different stages:

- Specification stage (blue box in Figure 2.1).
- Design stage (red box in Figure 2.1).
- Production & Testing stage (green box in Figure 2.1).

The different stages are described below.

Specification stage

Before designing a structural test setup, the customer defines loading conditions, maximum displacements and stiffness specifications in the specification stage. The designer of the test setup specifies a list of properties for the components in the test setup, for example the maximum displacement of the backup structure. The block “*load specification*” represents the static and fatigue loading conditions for the structural test, defined by the customer. Maximum loads and displacements for each actuator provide an input for the design of the backup structure and hydraulic actuator. The expected displacements of the test article are provided, to the block “*displacements test article*”. Each component connected to the aircraft has a certain connection stiffness, therefore the block “*Stiffness Specification*” defines the stiffness conditions for the backup structure or interface structures. All these different constraints provide input for the design stage.

Design stage

In the design stage, design of the hydraulic system and the backup structure takes place in two separate processes. Currently, design of the backup structure is done using static stiffnesses and deflections calculations. No modal analysis is performed of the backup structure and test article, resulting in unknown dynamic behaviour. Design of the hydraulic system is done by choosing hydraulic actuators on the basis of load capacity and maximum actuator stroke. Servo valves are chosen on the basis of estimation of the required flow through the servo valve. If both hydraulic system and backup

2.1. Current and proposed structural testing methodology

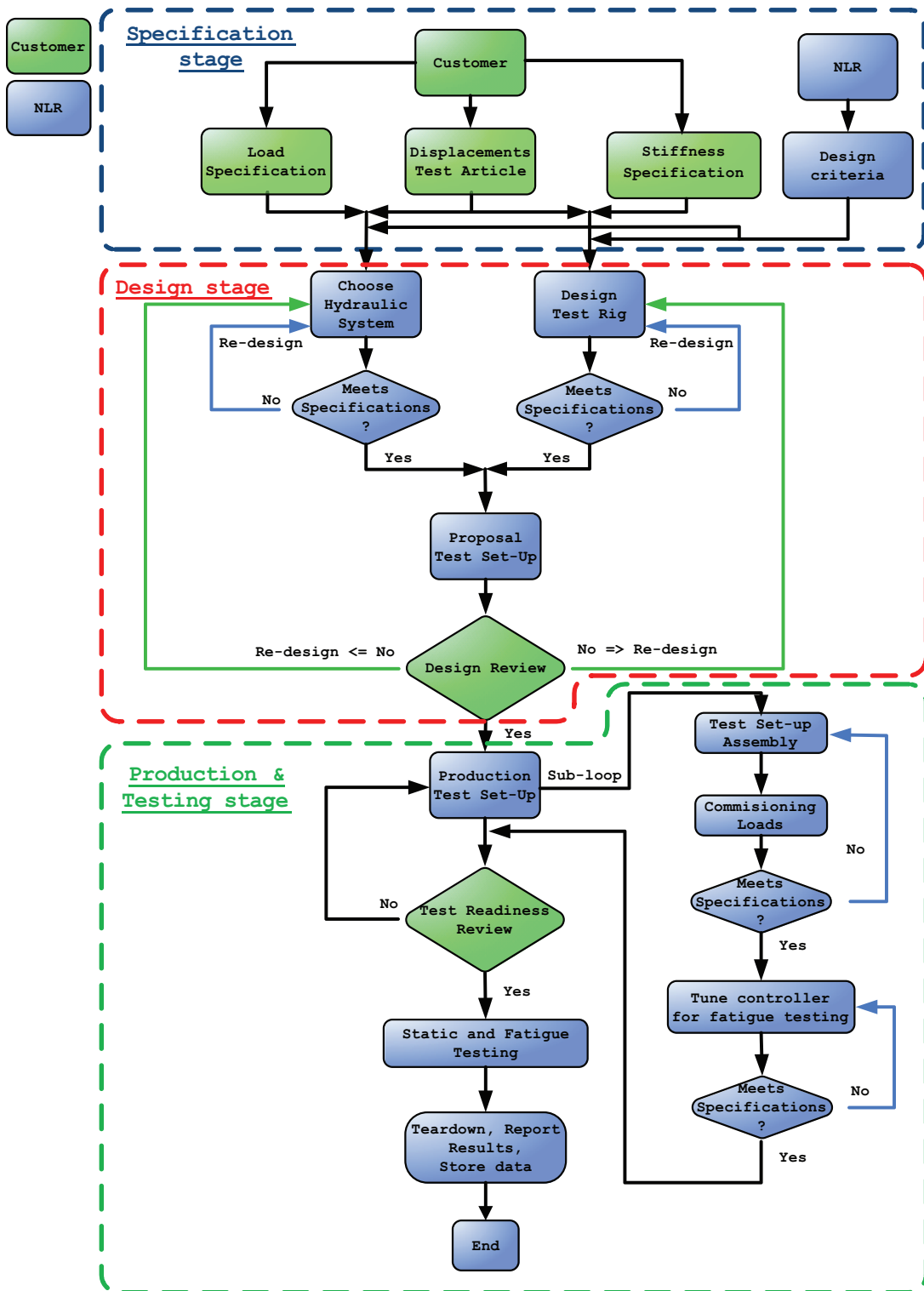


Figure 2.1 – Flow chart of the current structural testing methodology, describing specifications (blue), design process (red) and testing process (green).

structure are designed, the test setup is proposed to the customer. The customer performs a design review. During the review, the proposal is checked whether it meets the specifications from the design stage. If the customer agrees with the proposed design, the process moves to the production and testing stage, see Figure 2.1.

Production and Testing stage

After design of the structural test setup, the production and testing takes place. Production consists of building the complete backup structure and test article in addition to getting the test setup working. Important aspects for a working test setup are commissioning loads for static testing and controller tuning for fatigue testing. Commissioning loading is a process where the static load is gradually increased. The displacements and strains are measured and used to verify the actual test article measurement with the FE model. If the commissioning stage is completed and the results of the static tests have been adopted, controller tuning is performed for fatigue testing. Controller parameters are estimated on the basis of experience. If each hydraulic actuator applies the condition in the specified error range¹, the controller tuning is satisfied.

The behaviour of the complete test setup is currently only known if the complete test setup is actually built. This could be a disadvantage if phenomena exist which can drastically influence system performance, such as:

- Dynamic coupling between test article and backup structure, if eigenfrequencies are the same.
- Hydraulic actuators have coupling terms with each other through the test article and/or backup structure.
- Mechanical play in the interface structures, which can change over time because it transfers the fatigue loading to the test article.
- Friction effects of the hydraulic actuators at low actuator speeds.

After completion of the structural test setup, a “*test readiness review*” is conducted. During a test readiness review the test setup is checked by the customer to see if it meets the specifications for static and fatigue testing. If the test setup passes the test readiness review, then the static and fatigue testing process is started. The test article is inspected, during fatigue testing. Inspections are non-destructive inspections, to find possible cracks in the structure. When the process of static and fatigue testing is completed, the test setup is dismantled (teardown) and results are reported. Finally, the data is stored and the aircraft will be certified for service if the results were satisfying.

¹Generally the error range between reference signal and feedback signal is 1% for load conditions, between load conditions the error may vary up to maximum of 5 %, more information in section 2.2.1.

2.1.2 Conclusions about the current structural testing process

The previous section described the current structural testing process. The main conclusions about this process are:

- Design of the hydraulic system and the mechanical backup structure are two separate processes, resulting in unknown system performance.
- Controller tuning is based on experience. As a result, controller settings could not be optimal. Operators only know how to obtain these controller settings.
- Backup structures are designed only using static calculations, therefore dynamic effects are unknown at the design stage.
- Hydraulic components are chosen on the basis of maximum force and stroke for static responses. Dynamic behaviour of hydraulic components is not taken into account, resulting in unknown dynamic behaviour of the design stage.
- Performance of the test setup is known only if the test setup is actually built, no performance prediction is obtained a priori.

Concluding, design and operation of test setups can be improved using interaction between design of the hydraulic system, the mechanical system and by including controller models. Combining system design in a mechatronic manner, system performance will increase and a reduction in costs and risks will be obtained. Consequently, potential exists for a systematic design approach of structural test setups. The next section proposes a novel structural testing methodology.

2.1.3 Proposed structural testing method

Figure 2.2 presents the proposed method for structural testing. The new method consist of 4 stages, which are:

- Specification stage (blue box in Figure 2.2),
- Design stage (red box in Figure 2.2),
- Production and Testing stage (green box in Figure 2.2),
- Verification stage (orange box in Figure 2.2).

To indicate the difference with respect to the conventional method (presented in Figure 2.1), new blocks or modified blocks are coloured red. Other blocks remain the same colours, i.e. blue for NLR and green for the customer. A discussion on the differences between current and proposed methodology is given below.

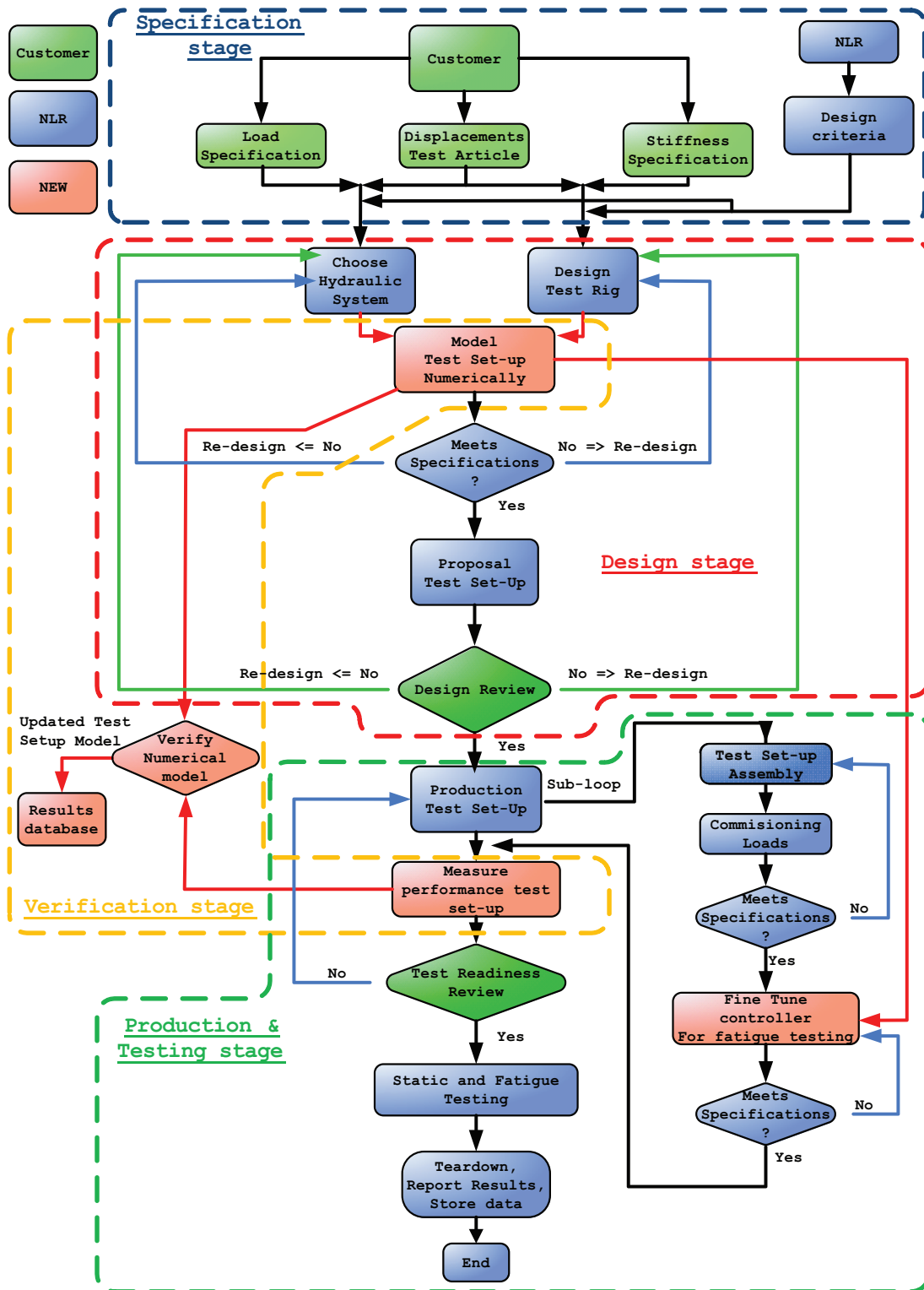


Figure 2.2 – Future structural testing methodology, describing new design (red), testing (green) and verification (orange) stages

Design stage

After the specification of the test setup, the design stage follows. The hydraulic system and the mechanical system are combined into a numerical model that predicts system performance. The numerical model uses a dynamic modelling approach to describe the dynamic behaviour of the systems. A controller model as currently used in structural testing, is included to obtain controller settings. Using the dynamic modelling approach, it is possible to predict system performance over a predefined frequency range. The inclusion of this novel virtual testing model does not affect the current modelling already performed on the design of structural fatigue test setups, it is an addition.

Production and Testing stage

Difference in the production and testing stage between the current and proposed methodology, is that the controller will be provided with a set of controller parameters from the numerical model. If the performance of the system needs to increase, then fine tuning of these parameters will be needed. Implementing a controller in this manner will save time.

Verification stage

An added stage in the proposed methodology is the verification stage. During this stage the numerical model is verified with the actual test setup. There are two ways to verify the setup:

- Verification of each component².
- Verification of the complete test setup.

In the first method each individual component is analyzed with respect to its dynamic behaviour. Coupling of the components results into a model of the complete test setup. In the second method the dynamic behaviour of the test setup is determined including all components. The response of the system can be determined by measuring input and output of the system, where the input is the force and the output is the position. Using these two different methods, it is possible to identify differences between the model and the real test setup. Obtaining information on multiple hydraulic system components and multiple test setups, will lead to improvement of the numerical model and modelling process. Subsequently, it will be possible to predict the performance of future test setups accurately.

²This is performed once for hydraulic actuators and servo valves, test dependent components backup structure and test article have to be verified each test.

Advantages of Virtual Testing

- Combining the hydraulic, mechanical and control system makes it possible to obtain system performance. Which obtains know length about possibilities for increase of test speeds.
- Ability to perform design iterations, for design modifications and prediction of the behaviour of the test setup by using simulation models.
- Providing first set of control parameters for the real test setup.
- Reducing risks in design and testing, due to verified numerical simulation models.

Disadvantages of Virtual Testing

- Time consuming to verify simulation models of each component in the test setup.
- If a new test setup is build, specific components will change. For example the backup structure or test article. Therefore new models have to be made for each new test.

2.2 Fatigue loading methodology

In order to understand more about structural fatigue loading, the methodology of fatigue loading profiles is discussed in this section. As stated in the Introduction of this chapter, increase of test speed can be obtained by reduction of step time between load conditions. This will lead to increase of frequency content in the applied loading. The fatigue loading profile will be transformed from time domain to frequency domain to determine the frequency content of fatigue loading profiles. The frequency content will be used throughout this thesis as an input specification parameter for virtual testing of structural fatigue test setups.

A general description of fatigue loading is: *“the ensemble of individually occurring structural load variations having a certain magnitude and, above all, appearing in a certain sequence”* [20]. A fatigue load profile consists out of different levels, see Figure 2.3. These levels are:

- *Sequence of flight during operation*, representing the number of flights to be performed for certification³.

³An average aircraft, for example a Fokker 100, around 90.000 simulated test flights have to be performed, in the test environment. The total number of flights certified is approximately, $\frac{1}{2}$ to $\frac{1}{3}$ of the number of test-flights simulated in the test environment.

2.2. Fatigue loading methodology

- *Sequence of instructions*, representing different events during flights, for example taxiing manoeuvres, flight phases and single operational procedures.
- *Sequence of conditions*, represent loading conditions during the flight events. These fatigue loads, define the type hydraulic actuators chosen in the test setup.

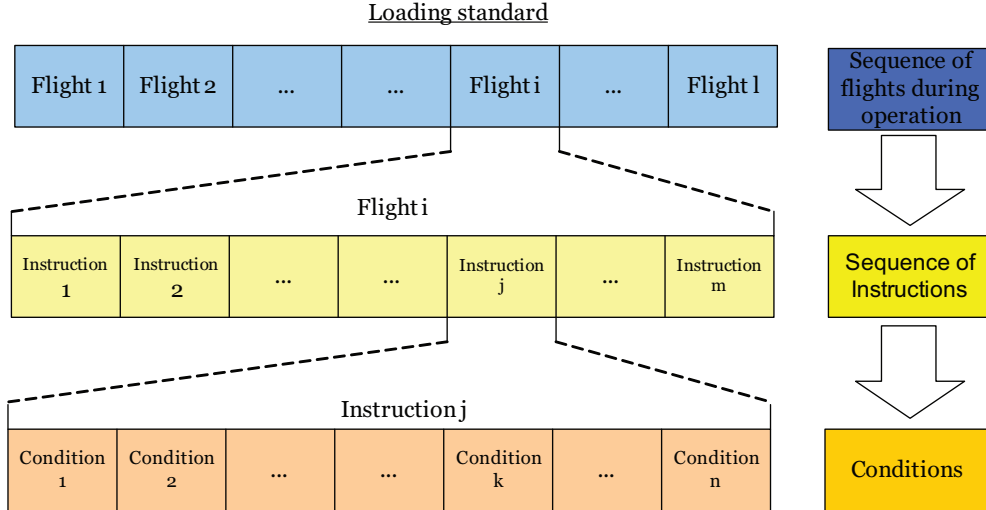


Figure 2.3 – Schematic on defining loading profiles, consisting out of flights, instructions and conditions [20].

2.2.1 Flight load profile

Figure 2.4 displays the applied load of different hydraulic actuators, representing a part of a flight load profile. Each hydraulic actuator in the test setup has its own colour in the graph. For one of the hydraulic actuators, Figure 2.4 indicates the condition loads and the step time between these loads.

The load profile in Figure 2.4 is composed of a sequence of condition loads. To obtain the loads between conditions an interpolation function is used, which is defined as:

$$F_{intp}(t_{intp}) = B - A \cos\left(\pi \frac{t_{intp}}{t_{step}}\right) \quad (2.1)$$

From Figure 2.5 is seen that B defines the average between two conditions, A defines the amplitude between two conditions and cos function defines the magnitude at interpolation time t_{intp} . Using Figure 2.5 Equation 2.1 the interpolation function results in:

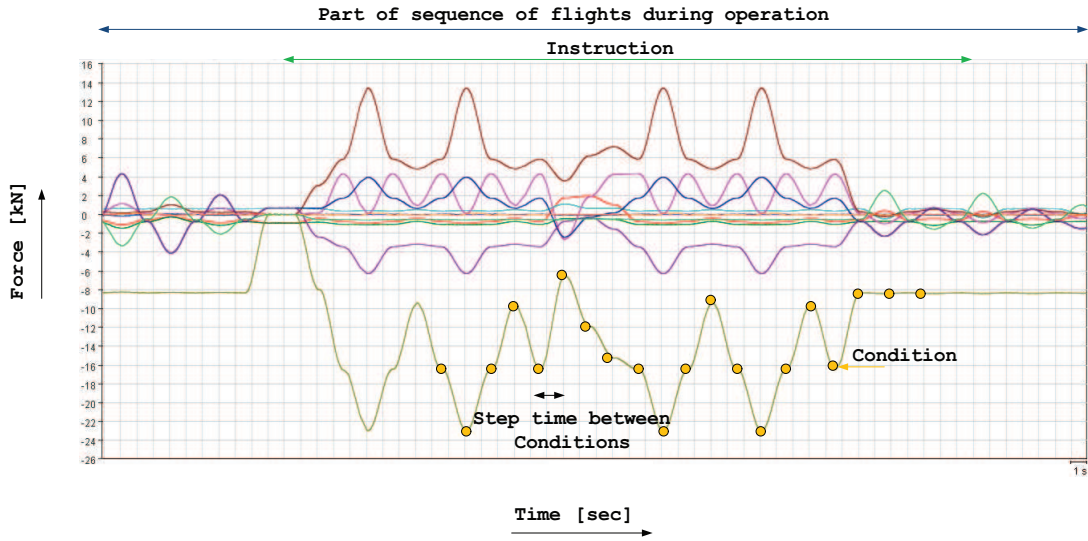


Figure 2.4 – Loading profile for fatigue loading of an aerospace structure, displaying load conditions and the steptime between conditions.

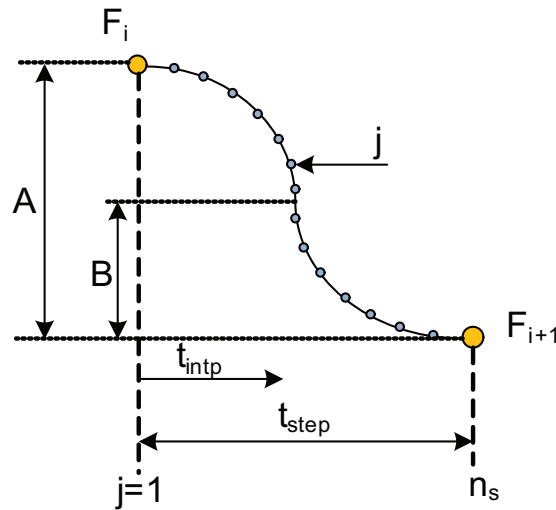


Figure 2.5 – Interpolation variables between loading conditions.

$$F_{intp}(j) = \frac{F_{i+1} + F_i}{2} - \frac{F_{i+1} - F_i}{2} \cos\left(\pi \frac{j}{n_s}\right) \quad (2.2)$$

where:

$$t_{intp} = \frac{j}{n_s} t_{step}$$

with:

$$t_{intp} = 0 \dots t_{step}$$

2.2. Fatigue loading methodology

$$j = 1, 2, \dots, n_s$$

$$i = 1, 2, \dots, n_c - 1$$

Interpolated load	F_{intp}	[N]
Condition load i	F_i	[N]
Total number of samples between two conditions	n_s	[-]
Number of Conditions	n_c	[-]
Sample	j	[-]
Condition	i	[-]
Interpolation time	t_{intp}	[sec]
Step time	t_{step}	[sec]

Equation 2.2 obtains the fatigue loading profile as used in fatigue testing. Structural testing is performed in a quasi static manner, conditions are applied with a step time large enough so that system dynamics are not to excited. Minimum step time between conditions depends also on the amplitude of the condition and the hydraulic servo-system to generate the condition. The servo valve provides a limited flow, therefore hydraulic actuators do have a limited speed. Large load difference between conditions, result in longer time periods between these conditions.

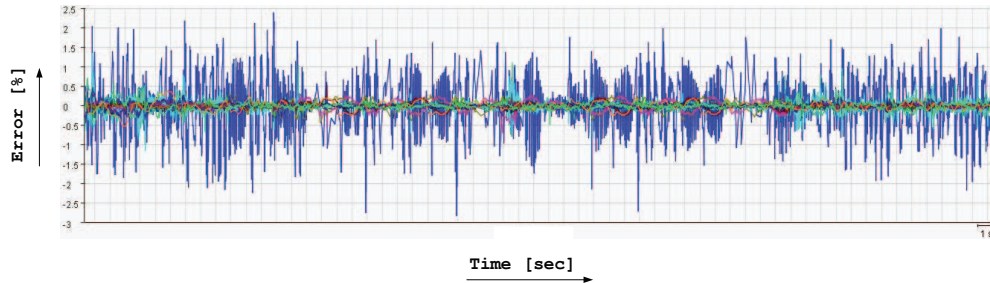


Figure 2.6 – Error in [%] between applied load and measured load.

Fatigue loading as displayed in Figure 2.4 has a certain error between reference and applied force or displacement. Figure 2.6 displays the error between the measured load at the load cell and the applied load from the predefined load profile. Between the applied conditions the force error is in the range of 3-5%. On the condition itself the error is 1% or less ⁴. The fail safe system shuts the system down when the force error is above 5%.

⁴This excludes error effects from calibration of load cells.

2.2.2 Frequency content of structural fatigue loading profiles

Previous section showed that fatigue loading profiles are sinusoidal signals which depend on the step-time between loading conditions. Since fatigue loading profiles are sinusoidal signals they obtain a certain frequency content. This section investigates the frequency content and the effect of reducing the step-time between load conditions on the frequency content of the fatigue load profile.

Because fatigue loading profiles are sinusoidal, dynamic modelling will be used to model structural test setups. It is important to know the the frequency content for modelling of structural test setups. The frequency content is used as a reference for verification of virtual model robustness, verification on measured system performance and for design of controller models.

In current testing setups the step-time generally varies between 1 or 2 seconds to travel from one condition to the next. Figure 2.7 displays part of the load profile of Figure 2.4 and is calculated using Equation 2.2. The conditions under which the fatigue load profile of Figure 2.7 was generated are:

Step-time	t_{step}	1	[sec]
Total number of samples between 2 conditions	n_s	1024	[-]
Number of Conditions	n_c	37	[-]

To obtain a measure for the loading profile frequency content, the loading profile is transferred to the frequency domain. Which is performed for a step-time of 1 second and a step-time of 0.2 seconds. The reduction of step-time is taken into account to obtain a measure of the frequency content when test speed is increased. The frequency spectrum obtained is only applicable on this set of load profile.

Figure 2.8 presents the frequency content of the fatigue loading profile for a step-time of 1 second and a step-time of 0.2 seconds. Analysis was performed using Fast Fourier Transformation (FFT) and a hanning window to eliminate the effects of leakage. Figure 2.8 shows that if the step-time is 1 second, the frequencies will remain below 1 Hz. The load spectrum of Figure 2.7 can be assumed to be quasi-static, since step times between 1 and 2 seconds are used. If the step-time is reduced by an factor 5 till 0.2 seconds, the frequency increases with a factor five. Which obtains a frequency range till 3 [Hz]. Since it is not possible to analyze the complete load profile it is assumed that the maximum frequency content will remain under 5 [Hz]. A bandwidth of 5 [Hz] will be used as a reference input for development of virtual testing models of structural

2.3. Summary

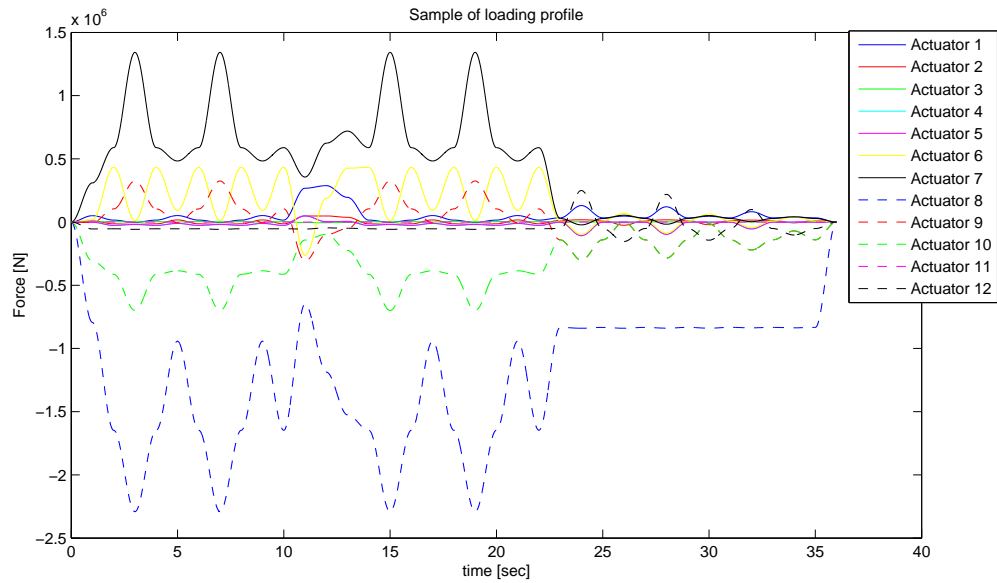


Figure 2.7 – Sample load profile calculated in MATLAB, using 1 second step time.

test setups.

2.3 Summary

Structural fatigue testing can be improved in two manners by:

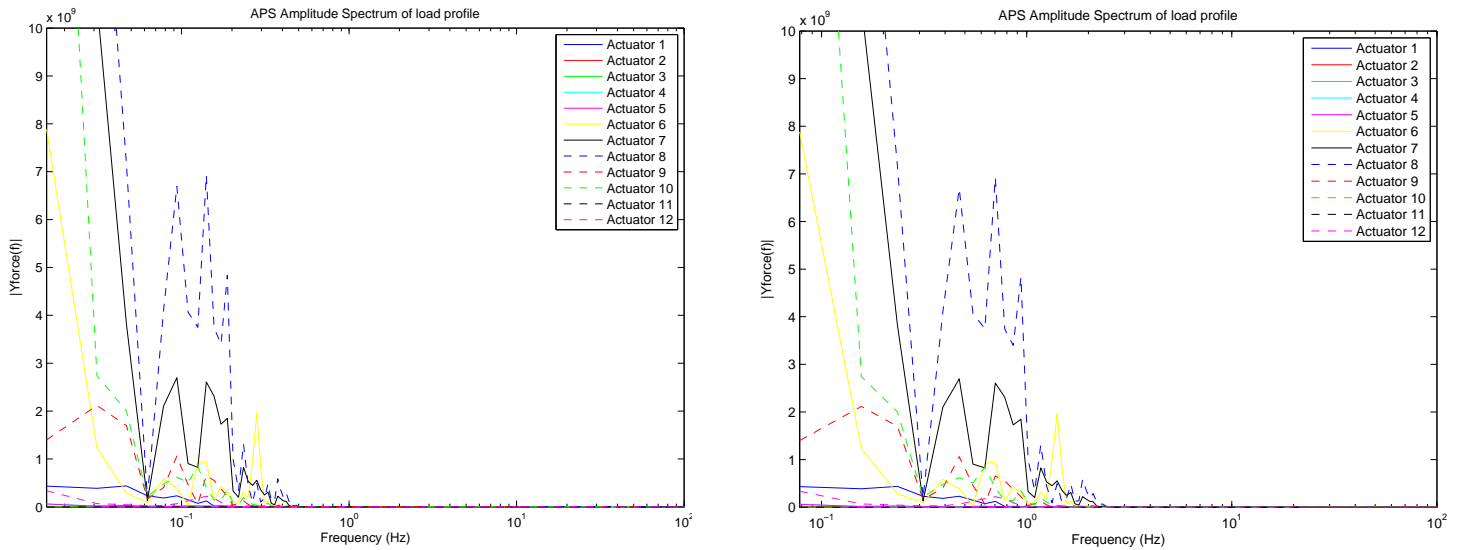
- a). Numerical models that predict system performance, in the design process.
- b). Reducing step time between load conditions, in the testing process.

To improve structural fatigue testing by (a), a novel testing methodology was proposed. The difference between the current method and the proposed method is use of mechatronic simulation models to:

- Reduce costs and risks by performing more design iterations.
- Predict the behaviour of the test setup by verification of numerical modelling.
- Tune controller parameters to reduce tuning when test setup is working.

To improve structural fatigue testing, also (b) fatigue loading profiles were investigated. From this investigation it resulted into the conclusions that:

- Current fatigue loading profiles are quasi-static, therefore the dynamics of the system will not be excited.



(a) 1 seconds step time

(b) 0.2 seconds step time

Figure 2.8 – FFT transformation of sample load profile (see Figure 2.7).

- For virtual testing models, fatigue loading profiles are assumed to have a maximum bandwidth of 5 [Hz]⁵.

Increase of speed of fatigue loading influences the novel testing methodology by new design specifications. The discussed advantages of improving structural fatigue testing will lead to better engineering of structural fatigue test setups, by using virtual testing for simulation of the physical behaviour before the test setup is built.

⁵This bandwidth was determined on a specific part of fatigue loading profile, see Section 2.2.2. Each fatigue loading profile is different and therefore the bandwidth should be calculated for each specific test.

CHAPTER

3

FATIGUE TESTING SETUPS

Chapter 2 discussed a novel structural testing methodology. To be able to verify this novel methodology this chapter will present the derivation of a demonstration test setup used for numerical modelling and experimental verification. This chapter introduces the general architecture of fatigue testing setups and the principle of operation on specific components. Physical modelling assumptions are made on each of the components described in the general architecture. Furthermore a demonstration test setup is derived from the modelling assumptions. This demonstration test setup will be used for experimental verification and for numerical modelling. Finally, the chapter concludes with a flowchart on the measurement signals of the demonstration test setup.

3.1 Architecture and Operation of Fatigue Testing Setups

This section presents the general architecture of fatigue testing setups. Furthermore the working principle of the different components is discussed.

3.1.1 General Architecture of Fatigue Test Setups

Fatigue testing setups can be categorized into three main systems:

- **Mechanical system (MS)**, consists of the test article, interface structures and backup structure.

- **Hydraulic system (HS)**, which main components are, hydraulic pump, servo valve and the hydraulic actuator¹. These components apply the fatigue loading onto the test article.
- **Control system (CS)**, controls the applied forces or displacements by the hydraulic system.

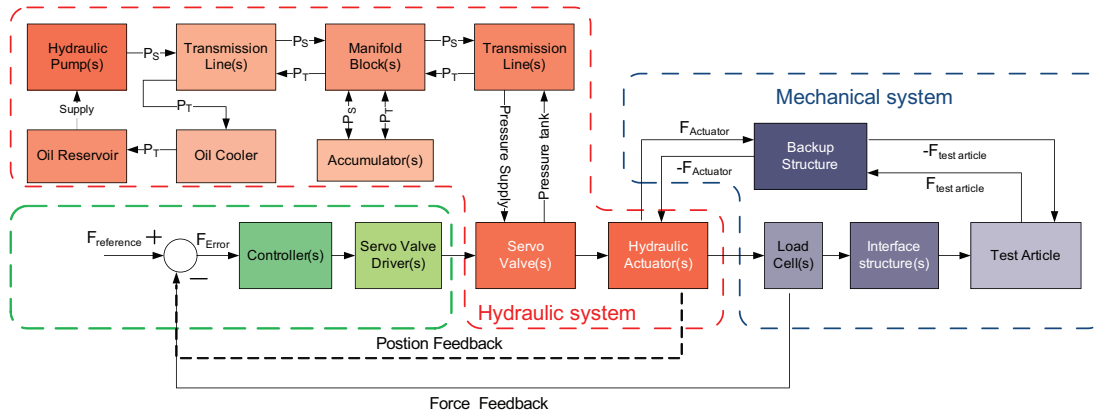


Figure 3.1 – General architecture of fatigue test setups, describing the different systems and their components.

The general architecture of fatigue testing setups is presented in Figure 3.1. The three main subsystems MS, HS and CS consist out of different components. The principle of operation of the different components will be discussed in the next Section 3.1.2.

The block representation in Figure 3.1 displays force feedback. It can be also possible that the system uses position feedback. In that case the position of the hydraulic actuator rod will provide the position feedback to the control system.

3.1.2 Principle of Operation of Fatigue Test setups

Each component has its own task in the fatigue testing setup. This section describes the working principle and tasks of the most important components, that are included in Figure 3.1.

Mechanical System

The *mechanical system* consists out of the following components:

- **Test Articles (TA)**, are the structures that must undergo fatigue testing or static testing. Two test articles are supplied by the customer, one for fatigue

¹Hydraulic actuators are generally used in aerospace testing, for other types of fatigue testing there is the possibility that other types of actuators are used.

testing and one for static load testing. The one for static load testing is also used for ultimate load testing. The TA is connected with the backup structure and the interface structure.

- **Backup Structure (BS)**, is a mechanical structure which provides mechanical stiffness for connection of TA and hydraulic actuators. Backup structures are non-standard components in fatigue testing. If a new fatigue test is developed also a new BS is designed.
- **Interface Structures (IS)**, are used to transmit the loads from the hydraulic actuator to the test article. IS are needed to introduce the loading to the TA in a correct manner. IS are different for single loading or distributed loading. For distributed loading are whiffletrees used. An advantage of whiffletrees is that they reduce the amount of hydraulic actuators needed to apply the fatigue or static loading. A disadvantage of IS is that often mechanical play is present, which increases during testing because the IS also undergoes the fatigue loading.
- **Load Cells (LC)**, measure the applied loading on the test article. This information is fed back to the control loop when force feedback is desired. LCs measure the force on the basis of strain gages.

Hydraulic System

To apply fatigue loading profiles a *hydraulic system* is used, which consists out of the following components:

- **Hydraulic Pump (HP)**, pressurizes the hydraulic fluid and creates flow.
- **Transmission Lines (TL)**, transmit the hydraulic fluid.
- **Manifold Blocks (MB)**, are connection blocks to distribute hydraulic fluid to the different hydraulic actuators.
- **Accumulators (AC)**, are used to reduce pressure fluctuations of the hydraulic fluid in the transmission lines created by the hydraulic pump.
- **Oil Cooler (OC)**, cools down the return oil, which is heated by the hydraulic actuator and hydraulic pump. Oil return temperature is on average 60 degrees and oil supply temperature is on average 40 degrees.
- **Oil Reservoir (OR)**, stores hydraulic fluid and is used as a supply buffer.

- **Servo Valve (SV)**, regulates the hydraulic fluid flows to the hydraulic actuator by varying its valve position. The position of the valve generates an opening area where hydraulic fluid passes through to an actuator chamber. Flow passing through the SV to the hydraulic actuator generates a motion of the piston. Valve positions are controlled using either a mechanical or electrical internal feedback. In the demonstration test setup an electrically feedback used, because electrical feedback SV are more accurate than mechanical feedback SV.
- **Hydraulic Actuator (HA)**, is used apply fatigue loading on the TA. The loading is generated by the flow passing through the SV to the HA. Flow passing through a SV generates a volume difference in the HA chambers, resulting into a motion of the HA piston and rod. In essence hydraulic actuators are flow regulated and subsequently realize piston velocity. Consequently, HA are integrators. In HAs friction is present, it consist of static friction, viscous friction and coulomb friction and are combined a non-linear effect.

Control System

To control the fatigue loading applied to the TA, a control system is needed. The *control system* consists of the following components:

- **Controller (CT)**, minimizes the error between the reference and feedback signal. To obtain this, parameters in the control system are tuned to achieve desired system performance. Fatigue testing can be either position controlled or force controlled. Generally all structural testing is force controlled, only a small amount of specific tests is displacement controlled. Each HA has its own controller and is therefore Single Input Single Output (SISO) controlled. Interaction between actuators is not taken into account.
- **Servo valve Driver (SD)**, converts the digital output of the digital controller to an analog output signal appropriate to control the servo valve position.

3.2 Modelling Assumptions of the Demonstration Test Setup

The previous section discussed the general architecture of fatigue test setups. The aim of this thesis is to be able to model fatigue testing setups. To model these fatigue testing setups, modelling assumptions are made.

This section is divided into three sections, the *mechanical system*, *hydraulic system* and *control system assumptions*.

3.2.1 Mechanical System Assumptions

The mechanical system consists out of different components as already discussed in Section 3.1.2. Physical modelling assumptions made for these components are:

- **Test Article**

- Elastic behaviour is assumed. To achieve this, the TA maximum loading for elastic deformation is calculated.
- Clamping with the backup structure (BS) is rigid, because stiffness of the BS is estimated to be a factor $7.5 \cdot 10^2$ larger than the stiffness of the TA.

- **Backup Structure**

- The backup structure is assumed to be rigid and connected rigidly to the ground, because of estimated stiffness ratio between BS and TA. The modelling of the backup structure is neglected.

- **Interface Structure**

- Elastic behaviour of the interface structure is assumed. The stiffness is a factor $2.8 \cdot 10^3$ larger than the TA.
- It is assumed that mechanical play is constant over time. Where in reality the mechanical play is different since interface structures are also fatigue loaded.

- **Load Cell**

- Ideal transformation of the applied force through the load cell is assumed. In reality the load cell has a small elastic deformation (0.05 [mm] at 22.24 [kN]). Its natural frequency is 6.6 [kHz]. These values are out of the modelling range, therefore the servo valve is assumed to be rigid.

These mechanical modelling assumptions were made to reduce complexity of the mechanical system, which enables verification of the hydraulic system models. If the coupling of the TA with the BS has not infinite stiffness, it will result in a difference in eigenfrequencies of the TA between model and real system. If the clamping is not stiff enough with respect to the TA, it will not be possible to apply the correct displacement and loading onto the TA.

3.2.2 Hydraulic System Assumptions

As presented in Figure 3.1 the hydraulic system consists out of 8 subsystems. To model the hydraulic system of fatigue testing setups modelling assumptions are made, which are:

- **Hydraulic Pump**

- Constant supply pressure is assumed.
- Ideal hydraulic fluid flow.
- Pressure dynamics due to the rotation speed of the pump is neglected.

These assumption are made because measurements on the demonstration test setup, verified a maximum of 2 [%] pressure fluctuation on the supply pressure to the SV. Details are provided in Appendix H.2.3. The demonstration test setup used one HA and one HP. If multiple HAs are used it could be possible that more pressure fluctuotons are present. Which depends on the amount of flow needed by the HAs.

- **Transmission Lines**

- Fluid inertia is not taken into account, which plays a role if pressure fluctuations occur. These are neglected.
- Friction losses over the TL are not taken into account, because a constant supply pressure to the SV is assumed.

Because of these assumptions TL are not included in the modelling.

- **Manifold Blocks**

- Friction losses by MB are not taken into account, it is assumed that the fluid is transmitted in an ideal way.

Friction in TL and MB results into a pressure drop. Therefore the supply pressure on to the SV will be lower then the pressure provided by the HP.

- **Accumulators**

- Since pressure dynamics is neglected, accumulators will not be modelled. As stated it is assumed that supply pressure is constant.

- **Hydraulic Fluid**

- Constant system temperature of 60 degrees, therefore constant viscosity and constant density and constant bulk modulus of the hydraulic fluid is assumed.

- Entrained air into the hydraulic fluid is neglected, resulting in constant bulk modulus over the complete pressure range.

Entrained air reduces the bulk modulus of the hydraulic fluid and is dependent on the pressure. Especially pressures below 100 [bar] result into a substantial influence in bulk modulus [9]. The bulk modulus influences the eigenfrequency of the HA. Entrained air could lower the eigenfrequency. A lower system temperature results into a higher bulk modulus and increase of density. For details see Appendix D.2.1.

- **Oil Cooler**

- Since a constant system temperature is assumed, the oil cooler is neglected in the system modelling.

- **Oil Reservoir**

- It is assumed that the oil reservoir has atmospheric pressure.

- **Servo Valve**

- SV hysteresis will be neglected, since it is very small ($< 0.5\%$, see Appendix F.2.1) for electronic feedback servo valves.
- Orifices are assumed to be sharp edged, therefore turbulent flow is always present through the servo valve [23].
- Leakage of flows through the servo valve are neglected, therefore the valve is assumed to be critical centered.

Generally under lapped valves are used in structural testing. Under lapped valve provide accurate control but are less energy efficient. Hydraulic systems are effected by some energy losses, an under lapped valves do not decrease therefore largely energy efficiency. The manufacturer of the servo valve provided a critical centered flow current diagram, see Appendix B.2.4. Therefore the servo valve is modelled as critical centered.

- **Hydraulic Actuator**

- Leakage of flows across the piston and seals are neglected.
- Dead oil volume of both chambers is constant and the same for both supply lines to the HA.
- Operating position of the HA piston is always centered.

Leakage flows are neglected because hydrostatic bearings are not present in the HA. It is assumed that they can be neglected. The operating position will be centered, because then lowest eigenfrequency of the HA, see Section 5.2.1.

3.2.3 Control System Assumptions

The control system controls the applied force or displacement to the TA. To include a control system in the modelling, the following choices and assumptions are made:

- **Controller**

- It was chosen to implement a controller architecture as already used in fatigue testing. Subsequently no new controller architectures will be developed in this thesis.
- Safety systems will not be modelled, but will be included in the demonstration test setup.

- **Servo valve Driver**

- The SD will be modelled as a scaling gain. It is assumed that the SD behaves in an ideal way and that no dynamics is present.

In practice it could be that the servo valve driver has hysteresis, which could result in non-ideal behaviour.

3.3 Demonstration Test Setup

To demonstrate the novel structural testing methodology as proposed in Section 2.1.3, a demonstration test setup is needed. This section discusses the architecture and development of the demonstration test setup and explains why components were chosen. This demonstration test setup will be modelled and used for verification of the servo-hydraulic and elasto-mechanical modelling.

3.3.1 Final Architecture of Modelled Fatigue Test Setup

Section 3.2 presented the modelling assumption made. The most important assumptions are:

- The backup structure will be modelled as rigid.
- Supply pressure is assumed to be constant.
- A control architecture as presently used will be implemented.

3.3. Demonstration Test Setup

These assumptions of previous sections lead to a reduction in the number of components that need to be modelled. As a result the general architecture of Figure 3.1 reduces to a final architecture of the to be modelled and build demonstration test setup, is presented in Figure 3.2.

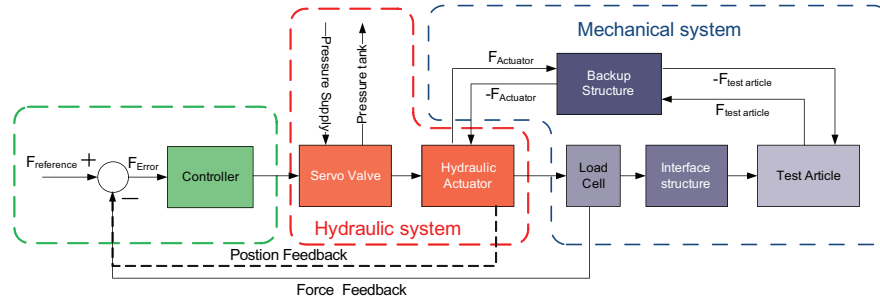


Figure 3.2 – Final architecture of the to be modelled and build demonstration test setup.

3.3.2 Overview demonstration test set-up

A block description of the demonstration test setup is presented in Figure 3.2. Figures 3.3, 3.4, 3.5 and 3.6 shows the hardware layout of the demonstration test setup. The objective is to have an as simple as possible but relevant demonstration test setup.

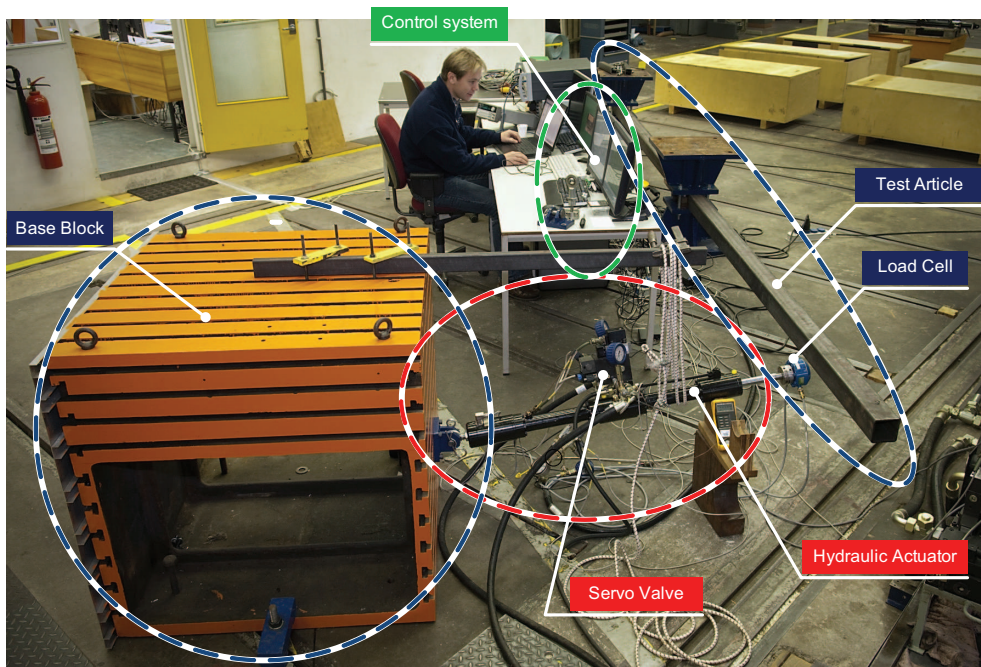


Figure 3.3 – Overview of the experimental test set-up, the colors of the component scheme of Figure 3.2 are linked to the photo.

The demonstration test setup will therefore only use one hydraulic actuator and one control system, where both force feedback and position feedback is possible. The following sections discuss the mechanical system, the hydraulic system and control system. Furthermore, the measurement system is presented.

3.3.3 Mechanical system

For the TA of the mechanical system it was chosen to use a 6 meter steel beam. It was chosen to use a steel beam since its physical properties are known. This simple structure is relatively easy to model in comparison with a full wing structure. The beam structure will be used for verification of the coupled system response. Therefore it is important to know the physical response correctly. To be able to simulate different mechanical system configurations, flexibility in the tested structure was created. The steel beam can be clamped at different clamping lengths simulating different physical responses.

For the backup structure of the test article is provided by *clamping blocks*. These large steel blocks were mounted onto a concrete floor. The backup structure of the hydraulic actuator is provided by a *base block*, see Figure 3.3. The backup structure is chosen to be flexible in the setup of the TA and to obtain ideal physical response of the TA.

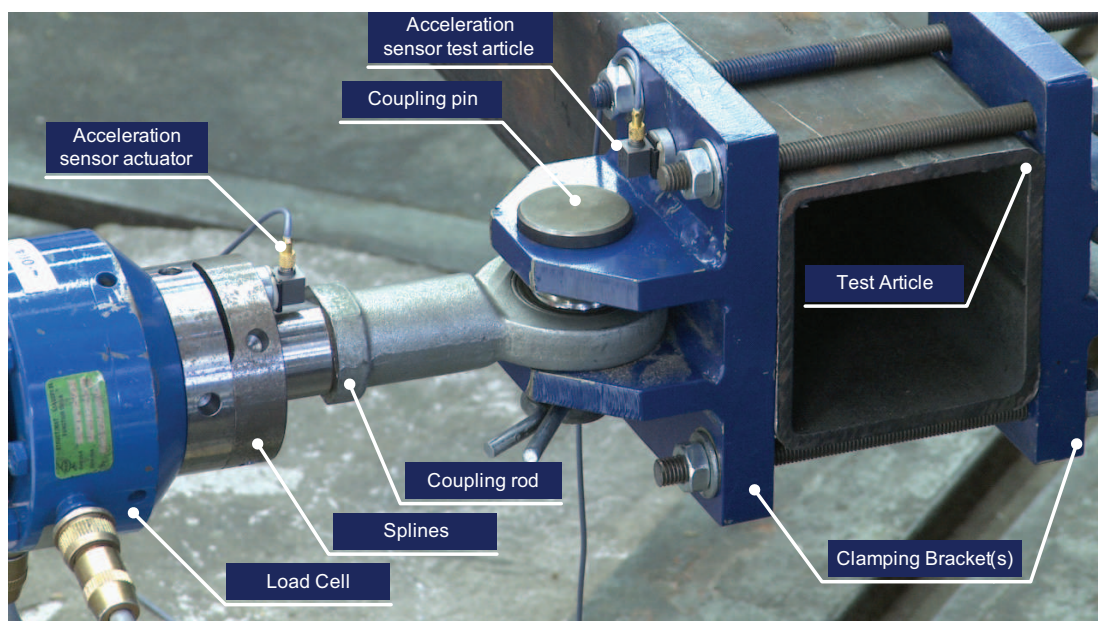


Figure 3.4 – Interface structure used for coupled system measurements.

3.3. Demonstration Test Setup

The coupling between mechanical system and hydraulic system is provided by the interface structure, which components are presented in Figure 3.4. Brackets are used to provide coupling with the TA. Generally the coupling in fatigue test setups is done using glued pads on the TA. Brackets were mounted since it is an easy coupling for the demonstration test setup and cost efficient.

3.3.4 Hydraulic System

The hydraulic system of the demonstration test setup including instrumentation sensors for measurements, is presented in Figure 3.5.

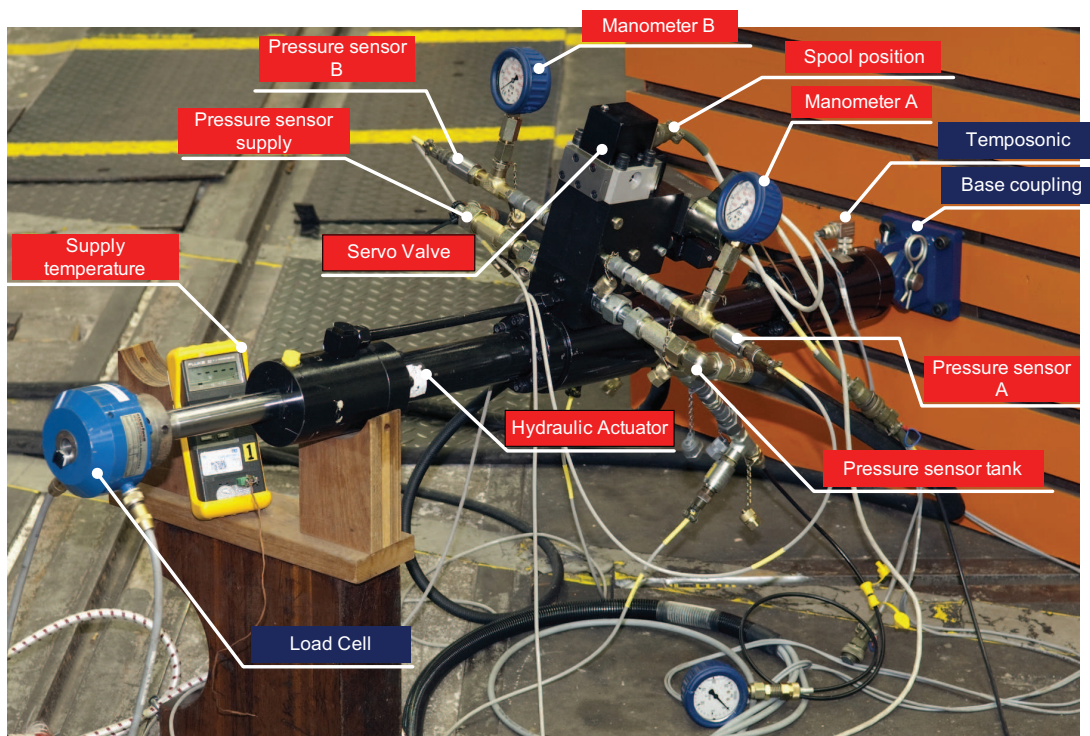


Figure 3.5 – Hydraulic system, including instrumentation sensors used during measurements.

The test setup uses a 10 [kN] hydraulic actuator with a maximum stroke of 0.250 [m], details are provided in Appendix B.2.1. For verification of the modelling the hydraulic actuator is equipped with the following sensors:

- Position tempo-sonic, measures the position of the actuator piston.
- Pressure supply strain gage sensor, measures the supply pressure.
- Pressure tank strain gage sensor, measures the return pressure.

- Pressure chamber A strain gage sensor, measures the pressure in chamber A.
- Pressure chamber B strain gage sensor, measures the pressure in chamber B.

Specifications of these sensors are provided in Appendix B.2.

To supply the HA with hydraulic fluid a servo valve is chosen, which has a nominal oil capacity of 10 liters / minute and internal electronic feedback loop to regulate the valve position set point². The valve position is measured using a break out wire on the servo valve itself. Furthermore the servo valve command signal is measured. These two signals characterize the servo valve dynamic behaviour. Details of the servo valve are provided in Appendix B.2.

3.3.5 Control system

The hydraulic system is used in a closed loop control configuration to control force or displacement prescribed by the reference signal. The demonstration test setup uses a real time Xpc-Target system, consisting out of two desktop computers. One for running real time controller, and one to access the controller parameters on the real time target. The advantage of this system is that it is possible to adapt the controller architecture using MATLAB-Simulink and to adapt controller parameters while the test setup is in operation. Figure 3.6 shows the desktop computers used for the real-time controller setup.

3.3.6 Measurement System

To be able to verify the physical response of the test setup with simulation models, the test setup is equipped with a dynamic measurement system. A dynamic measurement system is used because the modelling of the test setup will be performed dynamically.

The dynamic measurement system is indicated by the yellow labels in Figure 3.6. This measurement system has the capability to measure multiple signals at once using multiple channels. To indicate the signals measured and their path through signal conditioning units to the measurement system, a signal flowchart figure is created, which is presented in Figure 3.7.

Figure 3.7 displays a closed loop configuration with force feedback. It is also possible to have a closed loop configuration with position feedback. If position feedback is used, then the position signal of the hydraulic actuator is subtracted from the reference signal.

²The nominal flow capacity was chosen as the maximum flow through the servo valve, above the nominal flow the servo valve its electronic feedback loop does not provide feedback anymore.

3.3. Demonstration Test Setup

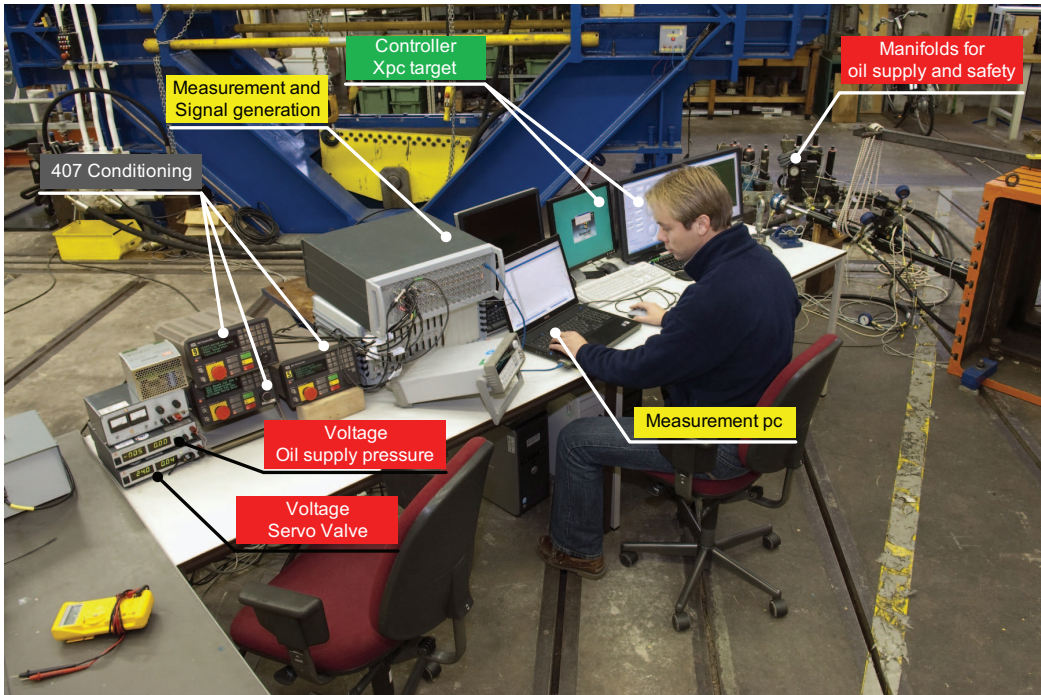


Figure 3.6 – Demonstration test setup, measurement and controller hardware.

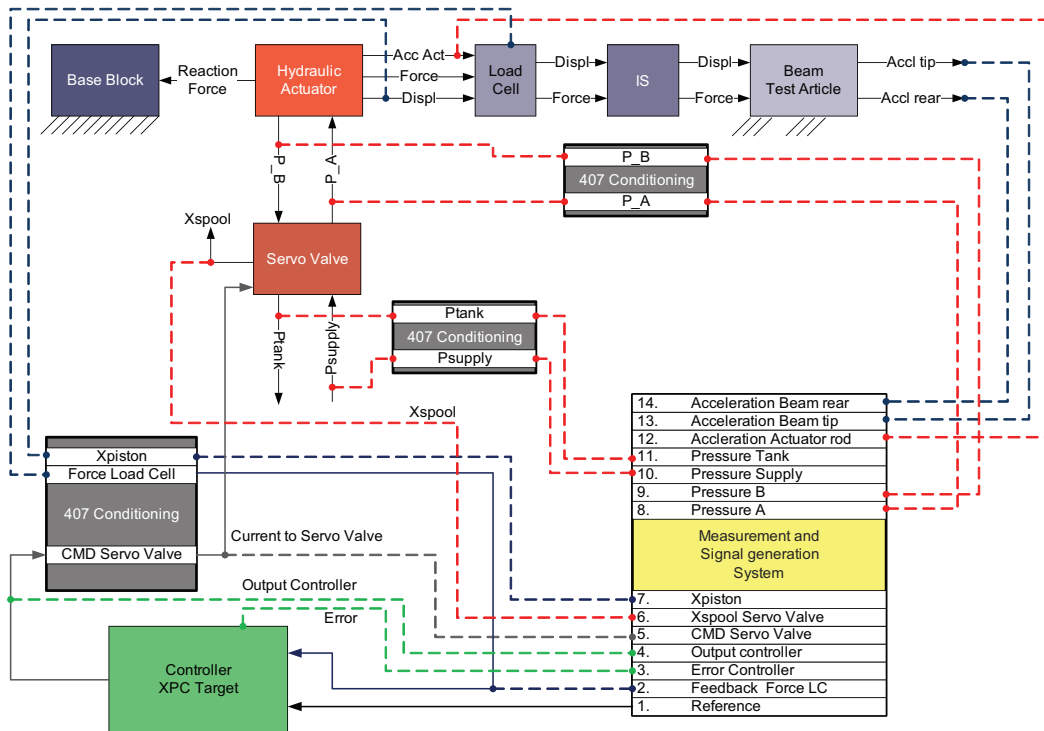


Figure 3.7 – Measurement signal flowchart of the demonstration test setup. Presenting the measured signals and their path through signal conditioning units.

The 407 conditioning in Figure 3.7 are signal conditioning units, which are used for:

- Apply calibration gains, for correct scaling of the measured signals.
- A/D conversion of the measured signals.
- Conditioning of the servo valve command signal from voltage to current.

The measured signals in Figure 3.7 were chosen in such a way that the dynamic response of each component can be determined and related back to the simulation model.

3.4 Summary

To prove the novel structural testing methodology of Chapter 2 several steps should be made. This chapter presented a general architecture of fatigue testing setups. Structural test setups, consist out three important systems:

- Mechanical System (MS),
- Hydraulic System (HS),
- Control System (CS).

These systems consist out of a multiple components. The principle of operation of the different subcomponents was presented in this chapter.

Physical modelling assumptions on the different subcomponents were made. This resulted into a demonstration test setup architecture which represents the essence of fatigue testing setups. The demonstration test setup architecture was translated to a physical demonstration test setup. This test setup will be used for modelling and verification of the novel structural testing methodology. Verification will be performed using measurements, therefore this chapter presented a measurement signal flowchart, to obtain an overview on the measured signals.

The next chapter will present the modelling theory to model the different subcomponents of the demonstration test setup.

CHAPTER

4

MODELLING THEORY

This chapter summarizes important theorems and formula's found in literature [7, 9, 22, 23] which are used model the components of structural test setups. Derivations of the formulas will be provided in Appendix C. As presented in the previous chapter, structural test setups consist of three main systems: the mechanical system, the hydraulic system, and control system. This chapter first discusses modelling theory for mechanical systems, followed by the theory for hydraulic systems and finally the control architecture and control methods used for control of the hydraulic system.

4.1 Mechanical Modelling

The mechanical system consists of different mechanical parts. As described, in an earlier chapter important parts are the Test Article (TA), Backup Structure (BS) and Interface Structure (IS). Generally the TA is the most complex structure of the mechanical system, since it is a component¹ of an aerospace vehicle. BS are usually build using beam constructions. IS can occur as a mechanical connection or as a whiffletree. IS can have non-linear characteristics such as play and hysteresis. These structures are therefore modelled as lumped-mass models, which will be discussed in Section 4.1.3.

¹Parts of aerospace vehicles tend to be more and more made from composite materials. Modelling of composite parts is difficult since they to not obtain the same material properties in each direction.

4.1.1 Finite Element Modelling

The current approach of modelling a TA is done using Finite Element (FE) models, with which stresses and strains under applied forces are calculated. Considering fatigue test setups specific interest is on the dynamic part of TA modelling, because of the applied frequency dependent loading. To obtain the frequency dependent behaviour of the TA it is chosen to use dynamic modelling. Dynamic models contain FE stiffness and mass matrices to describe the frequency dependent behaviour of the TA, see Section 4.1.2.

Chapter 3 presented the mechanical structure of the demonstration test setup which is a mechanical clamped beam, see Section 3.3.3 and Figure 4.1.



Figure 4.1 – Finite Element clamped beam, consisting of n elements.

The TA is modelled as a 2D structure and divided into a number of elements n . Each element has four degrees of freedom, two rotations and two translations see Figure 4.2.

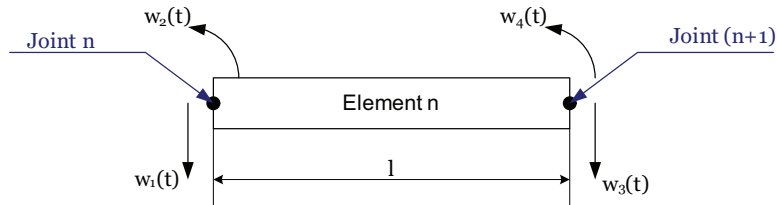


Figure 4.2 – Element n , representing the degrees of freedom.

Using kinetic, strain and virtual work energy theorems it is possible to derive the mass and stiffness element matrices [19], which are:

$$\mathbf{M}_e = \frac{\rho_{TA} A_{TA} l_e}{420} \begin{bmatrix} 156 & 22l & 54 & -13l \\ 22l & 4l^2 & 13l & -3l^2 \\ 54 & 13l & 156 & -22l \\ -13l & -3l^2 & -22l & 4l^2 \end{bmatrix}, \quad \mathbf{K}_e = \frac{E_{TA} I_{TA}}{l^3} \begin{bmatrix} 12 & 6l & -12 & 6l \\ 6l & 4l^2 & -6l & 2l^2 \\ -12 & -6l & 12 & -6l \\ 6l & -2l^2 & -6l & 4l^2 \end{bmatrix} \quad (4.1)$$

Element stiffness matrix	\mathbf{K}_e	[N/m]
Element mass matrix	\mathbf{M}_e	[kg]
Element length	l_e	[m]
Density test article	ρ_{TA}	[kg/m ³]
Elasticity modulus test article	E_{TA}	[N/m ²]
Inertia test article	I_{TA}	[m ⁴]

The derivation of the element matrices is provided in Appendix C.1.1. To obtain the full system representation as presented in Figure 4.1, the element mass and stiffness matrices are assembled to a global mass and a global stiffness matrices. The assembling process and applying boundary conditions is presented in Appendix C.1.2.

The obtained global mass and stiffness matrices are used to build a state space representation of the mechanical system, describes its dynamic behaviour. Derivation is presented in the next section.

4.1.2 State Space Representations

The advantage of a mechanical state space model is that it can be coupled with the dynamic models of the hydraulic system. Therefore a state space model needs to be obtained. A state space representation describes the dynamic system behaviour using only first order differential equations and are often used in control theory for developing controllers for a system. This section describes the state space representation obtained from the physical system and by modal analysis.

Physical State Space Equations

To derive a state space representation general dynamic equations of the physical system are needed. The general dynamic equations are described by Equation (4.2).

$$\mathbf{M}_{MS}\ddot{\mathbf{w}} + \mathbf{C}_{MS}\dot{\mathbf{w}} + \mathbf{K}_{MS}\mathbf{w} = \mathbf{F}_{extern} \quad (4.2)$$

Mechanical system mass matrix	\mathbf{M}_{MS}	[kg]
Mechanical system stiffness matrix	\mathbf{K}_{MS}	[N/m]
Mechanical system damping matrix	\mathbf{C}_{MS}	[Ns/m]
Mechanical system external applied force matrix	\mathbf{F}_{extern}	[N]
Mechanical system displacement matrix	\mathbf{w}	[m]

To obtain a first order system a state vector \mathbf{z} is introduced, see Equation (4.3).

$$\mathbf{z} = \begin{bmatrix} \mathbf{w} \\ \dot{\mathbf{w}} \end{bmatrix} \quad (4.3)$$

The general representation of a state space form is defined as in Equation (4.4).

$$\begin{aligned} \dot{\mathbf{z}} &= \mathbf{A}\mathbf{z} + \mathbf{B}\mathbf{u} \\ \mathbf{y} &= \mathbf{C}\mathbf{z} + \mathbf{D}\mathbf{u} \end{aligned} \quad (4.4)$$

In Equation (4.4) the \mathbf{A} matrix defines the dynamics of the system, \mathbf{B} the input in the system, \mathbf{C} the output of the system and the \mathbf{D} the direct feed through to the output of the system. The vector \mathbf{z} contains the states, where vectors \mathbf{u} and \mathbf{y} define the input and output vector. Equation (4.2) can be written in to physical state space form with the following matrices [6, 11]:

$$\begin{aligned} \mathbf{A}_p &= \begin{bmatrix} \mathbf{0} & \mathbf{I} \\ -\mathbf{M}_{MS}^{-1}\mathbf{K}_{MS} & -\mathbf{M}_{MS}^{-1}\mathbf{C}_{MS} \end{bmatrix} & \mathbf{B}_p &= \begin{bmatrix} \mathbf{0} \\ -\mathbf{M}_{MS}^{-1}\mathbf{F}_{ext} \end{bmatrix} \\ \mathbf{C}_p &= \begin{bmatrix} \mathbf{I} & \mathbf{0} \\ \mathbf{0} & \mathbf{I} \end{bmatrix} & \mathbf{D}_p &= \begin{bmatrix} \mathbf{0} \\ \mathbf{0} \end{bmatrix} \end{aligned} \quad (4.5)$$

The complete derivation is provided in Appendix C.1.3.

Normalized State Space Equations

By introducing state space modelling, the number of states is increased by a factor 2, which increases the computational time. To decrease the number of states it is possible to perform a modal analysis and obtain a state space representation using eigenfrequencies and eigenvectors, which is called a normalized state space [7]. The normalized state space equations can be obtained from the physical Equation (4.2). The system response is expressed through modal expansion, using Equation (4.6).

$$\mathbf{w}(\mathbf{t}) = \sum_{s=1}^n \eta_s(t)\mathbf{v}_s \quad (4.6)$$

In Equation (4.6), \mathbf{v}_s represent the s^{th} eigenmode and $\eta_s(t)$ the time-dependent amplitude of the modal component. If Equation (4.6) is substituted into Equation (4.2) and pre multiplied by each eigenmode $\mathbf{v}_{(r)}$, the result is the normal equations:

$$\mathbf{v}_{(r)}^T \left(\mathbf{M}_{MS} \sum_{s=1}^n \mathbf{v}_{(s)} \ddot{\eta}_s(t) + \mathbf{C}_{MS} \sum_{s=1}^n \mathbf{v}_{(s)} \dot{\eta}_s(t) + \mathbf{K}_{MS} \sum_{s=1}^n \mathbf{v}_{(s)} \eta_s(t) \right) = \mathbf{v}_{(r)}^T \mathbf{F}_{extern} \quad (4.7)$$

Using mode orthogonality it is possible to rewrite Equation (4.7) into the decoupled differential equations:

$$\ddot{\eta}_r + 2\zeta\omega_n\dot{\eta}_r + \omega_n^2\eta_r = \phi_r(t) \quad (4.8)$$

$$\omega_n^2 = \frac{\mathbf{v}_{(r)}^T \mathbf{K}_{MS} \mathbf{v}_{(r)}}{\mathbf{v}_{(r)}^T \mathbf{M}_{MS} \mathbf{v}_{(r)}} = \frac{\gamma_r}{\mu_r}$$

$$\zeta = \frac{\mathbf{v}_{(r)}^T \mathbf{C}_{MS} \mathbf{v}_{(s)}}{2\sqrt{\mathbf{v}_{(r)}^T \mathbf{K}_{MS} \mathbf{v}_{(r)} \mathbf{v}_{(r)}^T \mathbf{M}_{MS} \mathbf{v}_{(r)}}} = \frac{\beta_{rs}}{2\sqrt{\gamma_r \mu_r}}$$

$$\phi_r(t) = \frac{\mathbf{v}_{(r)}^T \mathbf{F}_{extern}}{\mathbf{v}_{(r)}^T \mathbf{M}_{MS} \mathbf{v}_{(r)}}$$

With μ_r the normalized mass matrix, β_{rs} the normalized damping matrix and γ_r the normalized stiffness matrix. The eigenfrequencies of the system are represented by ω_n and the damping is represented by ζ . Equation (4.8) can be written into the following normal state space form:

$$\mathbf{A}_n = \begin{bmatrix} \mathbf{0} & \mathbf{I} \\ -\mathbf{\Lambda} & -2\zeta\mathbf{\Lambda}^{1/2} \end{bmatrix} \quad \mathbf{B}_n = \begin{bmatrix} \mathbf{0} \\ -\mathbf{\Phi}_r \end{bmatrix} \quad \mathbf{C}_n = \mathbf{C} \begin{bmatrix} \mathbf{V} & \mathbf{0} \\ \mathbf{0} & \mathbf{V} \end{bmatrix} \quad \mathbf{D}_n = \begin{bmatrix} \mathbf{0} \\ \mathbf{0} \end{bmatrix} \quad (4.9)$$

These derived set of equations provide the system response, obtained from modal analysis. To generate the same output as the physical state space, the \mathbf{C}_n matrix is multiplied with the output matrix \mathbf{C}_p . The eigenfrequencies are represented by the $\mathbf{\Lambda}$ matrix, which is a diagonal matrix and the matrix \mathbf{V} represents the eigenvectors of the system. Each column of the \mathbf{V} matrix represents an eigenvector. Damping is defined by the ζ , which is chosen to be a scalar. Input of the system is generated by the normalized $\mathbf{\Phi}_r$ vector.

Reduction of State Space model

To simplify the complexity of the modelling and reduce computational time, reduction of the normalized state space model can be applied. In the case of fatigue testing setups, the interest is only on the low frequency dependent behaviour of the system, because fatigue testing is only performed quasi-statically, see Section 2.2. It is therefore

possible to truncate the number of modes used to describe the system dynamics.

Truncation is performed by taking into account only the first n eigenfrequencies of the \mathbf{A} matrix, and the first n number of columns of the eigenvector matrix \mathbf{V} . As a result sizes of the identity matrix \mathbf{I} and zero matrix $\mathbf{0}$ in the \mathbf{A} matrix change also to the size of $n \times n$. Truncation simplifies the complexity of the model and reduces computational time. An example on this reduction method will be provided in Chapter 5.

4.1.3 Modeling Interface Structures

Interface Structures (IS) are needed to connect the HS with the MS. An example of such an IS is presented in Figure 3.4 of Section 3.3.3. This section focuses on the modelling of a single degree of freedom IS. The modelling of whiffletrees will be excluded in this thesis. IS have the problem that there is always a certain amount of play present in the connection. Modelling this play and interface dynamics can be done using a *translational hard stop block* in MATLAB-Simulink, which is presented in Figure 4.3. In Figure 4.3 R is connected with the HA and C is connected with the TA.

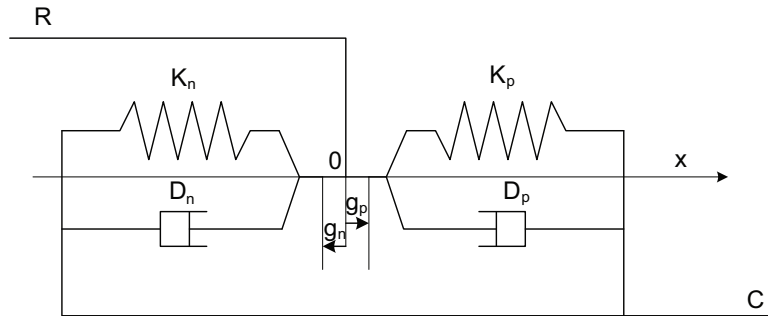


Figure 4.3 – Translational hard stop, used for modelling of IS dynamics.

The translational hard stop uses the following equations, which are presented in [13].

$$F_{IS} = \begin{cases} K_{IS} \cdot \delta + D_{IS}(\dot{x}_R - \dot{x}_C) & \text{for } \delta \geq g_p \\ 0 & \text{for } g_n < \delta < g_p \\ K_{IS} \cdot \delta + D_{IS}(\dot{x}_R - \dot{x}_C) & \text{for } \delta \leq g_n \end{cases} \quad (4.10)$$

$$\delta = x_R - x_C$$

F_{IS}	Interaction force between R and C	[N]
δ	Relative displacement between R and C	[m]
g_p	Gap between R and C in positive direction	[m]

g_n	Gap between R and C in negative direction	[m]
x_R, x_C	Absolute displacements of R and C	[m]
K_{IS}	Contact stiffness	[N/m]
D_{IS}	Damping coefficient	[Ns/m]

The dynamics due to the inertia in interface structure will be taken into account by adding mass to the test article. An example on modelling IFS and simulation results will be discussed in Section 5.1.2.

4.2 Servo-Hydraulic Modelling

This section introduces the models that are used to include the servo-hydraulic system in the virtual testing environment. Section 4.2.1 presents the modelling of a hydraulic actuator and Section 4.2.2 treats the modelling of a servo valve.

4.2.1 Fundamental Modelling Hydraulic Actuator

This section presents the modelling of a hydraulic actuators. The model consists of two parts, namely the pressure dynamics and piston motion dynamics. Figure 4.4 represents the dynamics present in HAs and their physical influences on the dynamics.

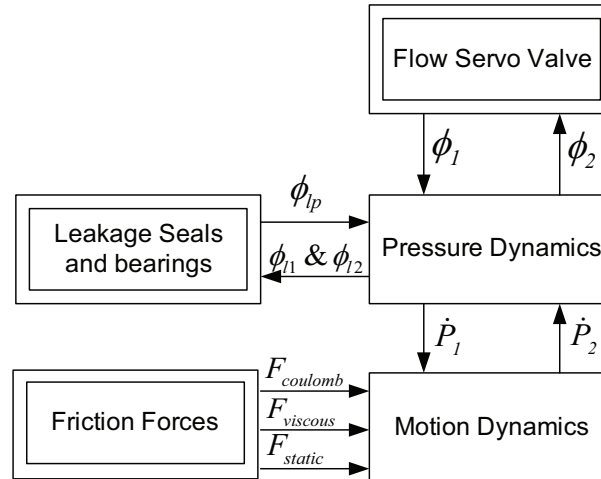


Figure 4.4 – Block scheme representing the dynamics of the HA and their inputs [22].

The equations of piston motion are dependent on the pressure dynamics of the HA. Non-linear inputs are the flow from the servo valve, leakage of seals ϕ_{l1} ϕ_{l2} , piston ϕ_{lp} and friction forces in the HA. Three important friction components are present in the hydraulic actuator namely, Coulomb friction ($F_{coulomb}$), Viscous friction ($F_{viscous}$) and

Static friction (F_{static}) [9]. First the pressure dynamics will be discussed where after the piston motion dynamics will be treated.

Pressure Dynamics

The pressure dynamics of the hydraulic actuator is obtained by continuity of volume flow to and from the actuator. Figure 4.5 presents a schematic of the hydraulic actuator flows and parameters. Using Figure 4.5 and the continuity of oil flow in the chambers the pressure dynamic equations are obtained. Derivation of these equations is presented in Appendix C.2 and in [9, 22, 23].

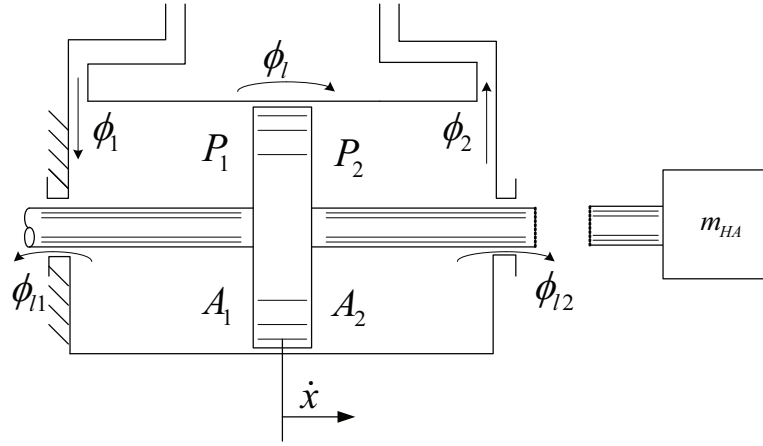


Figure 4.5 – Schematic of hydraulic actuator with the different parameters used for modelling [22].

$$\dot{P}_1 = \frac{E(P_1)}{(V_0 + x_p A_p)} (\Phi_1 - \dot{x}_p A_p - \Phi_{lp} - \Phi_{l1}) \quad (4.11)$$

$$\dot{P}_2 = \frac{E(P_2)}{(V_0 + x_p A_p)} (-\Phi_2 + \alpha \dot{x}_p A_p + \Phi_{lp} - \Phi_{l2}) \quad (4.12)$$

Φ_i	Servo valve flows 1 and 2	$[\text{m}^3/\text{s}]$
Φ_{lp}	Leakage flow piston	$[\text{m}^3/\text{s}]$
Φ_{li}	Leakage flow seals 1 and 2	$[\text{m}^3/\text{s}]$
V_0	Dead oil volume of oil pipelines between SV and HA	$[\text{m}^3]$
x_p	Piston displacement	$[\text{m}]$
A_p	Piston area	$[\text{m}^2]$
α	Correction factor for difference in piston area	$[-]$
E	Bulk modulus oil which is dependent on the type of oil used	$[\text{Pa}]$
\dot{P}_i	Pressure sensitivity with respect to time	$[\text{Pa}/\text{s}]$

In the remainder of this thesis, leakage across the piston and seals are neglected. Furthermore, $\alpha = 1$ since double acting hydraulic actuators are used which have the same piston area. Using these assumptions results in the following hydraulic actuator dynamics:

$$\begin{aligned}\dot{P}_1 &= \frac{E(P_1)}{(V_0 + x_p A_p)} (\Phi_1 - \dot{x}_p A_p) \\ \dot{P}_2 &= \frac{E(P_2)}{(V_0 + x_p A_p)} (-\Phi_2 + \dot{x}_p A_p)\end{aligned}$$

Equations of Motion

The equation of motion of a HA are derived from Figure 4.4 and Figure 4.5 and are also provided in literature [9, 22, 23]. The basic set of equations of motion can be written as:

$$\sum m_{HA} \ddot{x}_p = (P_1 - P_2) A_p + \sum F_{HA} \quad (4.13)$$

Where:

$$\begin{aligned}\sum F_{HA} &= F_{external} - F_{coulomb} - F_{viscous} - F_{static} \\ \sum m_{HA} &= m_{piston} + m_{rod} + m_{fluid,1} + m_{fluid,2}\end{aligned}$$

The hydraulic actuator inertia m_{HA} is the inertia of the rod, the piston and the hydraulic fluid. Inertias of the hydraulic fluid are not taken into account, since the amount of mass is relatively small compared to the mass of the actuator rod. Formulas for calculating the fluid inertias are provided in Appendix C.2.1. The inertia and acceleration of the test article and test rig is taken into account by the external forces ($F_{external}$). The friction forces, coulomb, viscous and static friction are calculated using [9]:

$$F_{coulomb} = F_c \text{sign}(\dot{x}_p) \quad (4.14)$$

$$F_{viscous} = F_v \dot{x}_p \quad (4.15)$$

$$F_{static} = F_s \text{sign}(\dot{x}_p) \exp\left(-\frac{|\dot{x}_p|}{c_s}\right) \quad (4.16)$$

F_c	Parameter for Coulomb friction	[N]
F_v	Parameter for Viscous friction	[Ns/m]
F_s	Parameter for Static friction	[N]
c_s	Stribeck velocity	[m/s]

Coulomb friction is present due to the seal friction. Viscous friction is dependent on the viscosity of the oil and static friction is a threshold force that needs to be applied before motion is achieved of the HA rod.

4.2.2 Fundamental Modeling Servo Valve

In this section, the fundamental modelling of a servo valve is introduced. The servo valve has an influence on the pressure dynamics and subsequently also on the piston motion. Modelling equations from literature will be presented [9, 22, 23].

Figure 4.6a displays a schematic block diagram on the most important dynamic components of a servo valve, a full schematic is provided in Appendix C.2.

Figure 4.6b displays the physical layout of the servo valve. The valve position defines the hydraulic fluid flow to the hydraulic actuator. The valve displacement has a internal feedback loop as shown in Figure 4.6b. The set point results in a net i_{ca} , changing the flapper position. This gives unequal flows through the nozzles ϕ_{n1} en ϕ_{n2} , a pressure difference builds up over both ends of the spool. Force unbalance pushes the spool to another position until the position feedback compensates for the set point altering. In the meantime results the new spool position in changed flows Q_A and Q_B . Dynamics of the servo valve is characterized between the current input and valve position output.

This section presents first the dynamic modelling equation used to model the dynamic characteristics of the servo valve. Thereafter the non-linear flow modelling through the servo valve is presented.

Dynamic Characteristics of Servo Valve

Dynamic behaviour of servo valves is characterized by the non-linear mechatronic system, pressure dynamics and spool dynamics. The different dynamic subsystems contain a large number of parameters. Due to high number of parameters it will be extremely difficult to determine all these different parameters and to validate the dynamic behaviour [9, 22]. Because of this reason detailed modelling of servo valve dynamics will not be performed, detailed modelling equations are presented in Appendix C.2.2.

Manufacturers often provide detailed frequency response functions (FRF) of the servo valve. These FRFs describe the input current to the output spool position behaviour of the servo valve, are dependent on the input current and the nominal flow through the servo valve. For a certain frequency bandwidth it is possible to approximate the servo valve dynamic response by a second-order model [9]:

4.2. Servo-Hydraulic Modelling

$$\frac{1}{\omega_v^2} \ddot{x}_v^* + \frac{2D_v}{\omega_v} \dot{x}_v^* + x_v^* + f_{hs} \text{sign}(\dot{x}_v^*) = K_v u_v^* \quad (4.17)$$

x_v^*	Normalized valve displacement	[-]
ω_v	Natural frequency of the valve	[rad/s]
D_v	Damping coefficient	[Ns/m]
f_{hs}	Valve hysteresis	[-]
K_v	Valve gain	[-]
u_v	Valve control input	[V]

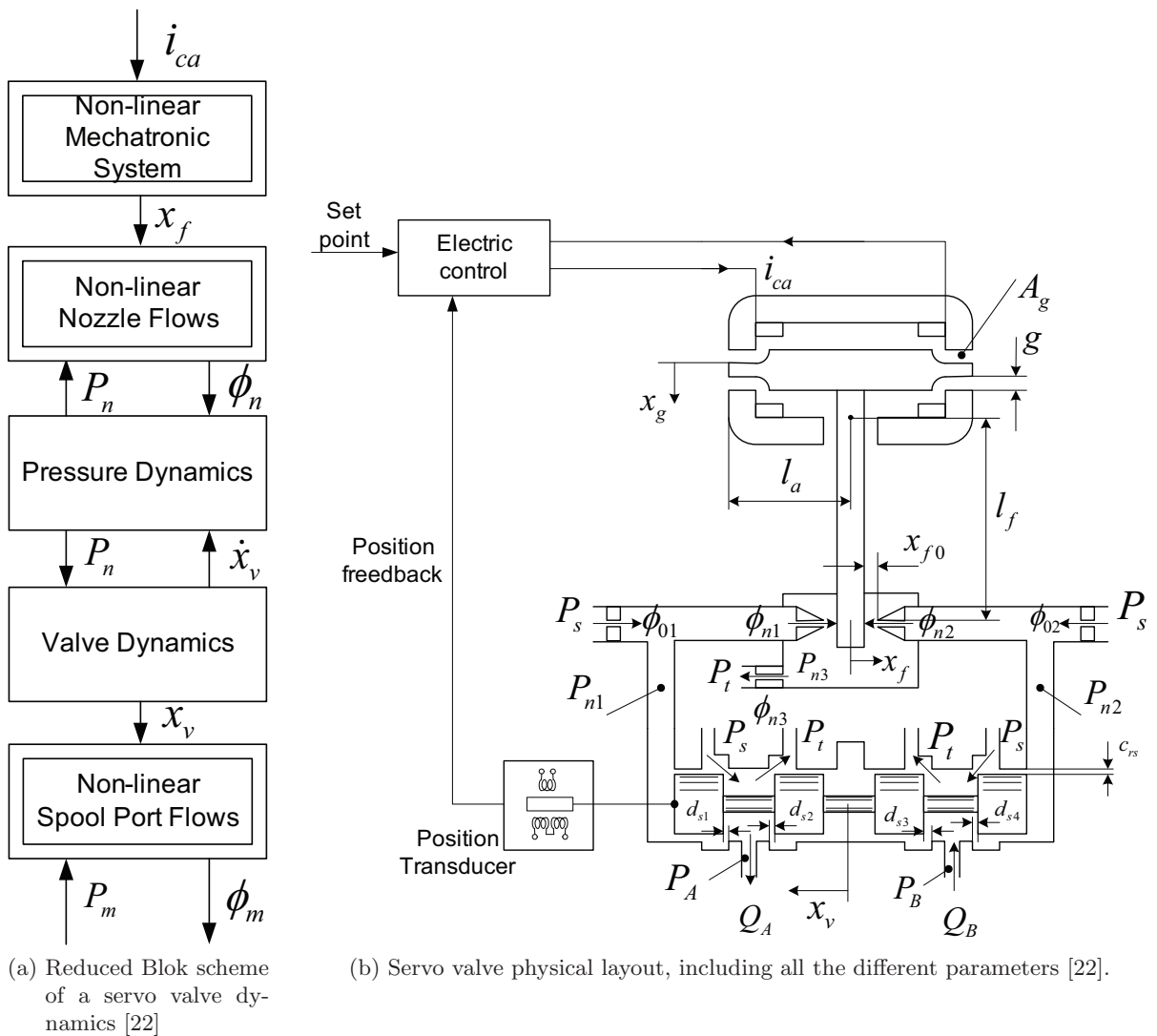


Figure 4.6 – Servo valve schematic and physical layout

Valve hysteresis is the result from frictional forces between spool and valve which are not distributed equally over the entire spool stroke. Normalized valve position, velocity and acceleration are presented in Equations, (4.18), (4.19) and (4.20).

$$x_v^* = \frac{x_v}{x_{v,max}} \quad \text{for } -1 \leq x_v^* \leq 1 \quad (4.18)$$

$$\dot{x}_v^* = \frac{\dot{x}_v}{x_{v,max}} \quad \text{for } -\dot{x}_{v,lim} \leq \dot{x}_v^* \leq \dot{x}_{v,lim} \quad (4.19)$$

$$\ddot{x}_v^* = \frac{\ddot{x}_v}{x_{v,max}} \quad (4.20)$$

$x_{v,max}$	Maximum valve displacement	[m]
$\dot{x}_{v,lim}$	Limited valve speed	[m/s]

Valve hysteresis will be neglected in this thesis, since the manufacturer specifies a valve hysteresis $< 0.5\%$, see Appendix B.2.4. Taken these assumptions into account, Equation (4.17) results in:

$$\frac{1}{\omega_v^2} \ddot{x}_v^* + \frac{2D_v}{\omega_v} \dot{x}_v^* + x_v^* = K_v u_v^*$$

This formula will be used for modelling of dynamic response of the servo valve. The next section will discuss the modelling of the flow through the servo valve, which is related to the valve position x_v .

Spool port flows

The spool port flows are related to the valve dynamics, and are an important non-linear effect in the servo valve dynamics. The valve dynamics places the valve at a certain position x_v , providing an opening of the orifices. Flow through an orifice can be calculated using equation by [9]:

$$Q_o = A_o \cdot v_{oil} = AC_d \sqrt{\frac{2\Delta P}{\rho}} \text{sign}(\Delta P) \quad (4.21)$$

Q_o	Orifice flow	[m ³ /s]
A_o	Orifice opening area	[m ²]
v_{oil}	Velocity of the oil	[m/s]
C_d	Discharge coefficient	[-]
ΔP	Pressure drop between inlet and outlet	[Pa]
ρ_{oil}	Density of oil	[kg/m ³]

Where the orifice opening area is calculated by:

$$A_o(h) = \begin{cases} h \cdot A_{max}/h_{max} + A_{leak} & \text{for } h > 0 \\ A_{leak} & \text{for } h < 0 \end{cases} \quad (4.22)$$

$$h = x_{v0} + x_v \cdot or \quad (4.23)$$

A_o	Orifice opening area	[m ²]
A_{leak}	Orifice leakage area	[m ²]
x_{v0}	Initial valve position	[m]
x_v	Valve position	[m]
or	Orifice orientation indicator, -1 or +1	[-]
h	Orifice opening	[m]

Knowing the equations for the flow through an orifice, it is possible to obtain the servo valve flows through and from the hydraulic actuator, which are:

$$Q_A = Q_{P_S-P_A} - Q_{P_A-P_T} \quad (4.24)$$

$$Q_B = Q_{P_B-P_T} - Q_{P_S-P_B} \quad (4.25)$$

Q_A	Valve flow to HA chamber A	[m ³ /s]
Q_B	Valve flow from HA chamber B	[m ³ /s]
$Q_{P_S-P_A}$	Orifice flow from supply to HA chamber A	[m ³ /s]
$Q_{P_A-P_T}$	Orifice flow from HA chamber A to tank	[m ³ /s]
$Q_{P_S-P_B}$	Orifice flow from supply to HA chamber B	[m ³ /s]
$Q_{P_B-P_T}$	Orifice flow from HA chamber B to tank	[m ³ /s]

If Equation 4.21 is substituted into Equations 4.24 and 4.25 the result is:

$$Q_A = A_{v1} C_d \sqrt{\frac{2(P_S - P_A)}{\rho}} \text{sign}(P_S - P_A) - A_{v2} C_d \sqrt{\frac{2(P_A - P_T)}{\rho}} \text{sign}(P_A - P_T)$$

$$Q_B = A_{v3} C_d \sqrt{\frac{2(P_B - P_T)}{\rho}} \text{sign}(P_B - P_T) - A_{v4} C_d \sqrt{\frac{2(P_S - P_B)}{\rho}} \text{sign}(P_S - P_B)$$

P_s	Supply pressure	[Pa]
P_t	Return pressure to tank	[Pa]
P_A	Pressure chamber A of HA	[Pa]
P_B	Pressure chamber B of HA	[Pa]
A_{vi}	Valve opening area of port i	[m ²]

The servo valve was assumed to have sharp edges. According to Viersma [23] it can be assumed that flow through the servo valve is turbulent having a discharge coefficient of $C_d = 0.611$.

In the modelling of a servo valve leakage flows will be neglected, because the servo valve is modelled as critical centered. The valve will be modelled as a critical centered valve, therefore underlap will be neglected. Underlapped servo valves are more efficient than overlapped ones. This is because overlapped valves have a relatively large response time due to the dead band. Underlapped valves have a small response time because they have a continuous flow of oil. The flow passing through at neutral position will be compensated by friction effects present in the hydraulic actuator.

4.3 Controller Modelling

The previous section presented the modelling equations of the hydraulic actuator and the servo valve. This section first presents the general control architecture for controlling the hydraulic system. Thereafter the present control method as used in fatigue testing is presented. Finally this section concludes with tuning approaches to obtain controller settings of the present controller.

The focus is on investigating the current control method as used in fatigue testing to obtain maximal system performance. No new controller models will be developed, which is a topic for future research.

4.3.1 General Controller Architecture

Control of the hydraulic system (HS) is needed since piston position drift is present in open loop configuration. Piston position drift is present due to the fact that the HA is supplied by oil flow. To prevent the HS from drifting a feedback controller is implemented.

Figure 4.7 presents the general control architecture of the fatigue testing setups. Fatigue testing setups are generally Single Input Single Output (SISO) controlled. Each

4.3. Controller Modelling

hydraulic actuator present in the test setup has its own individual controller.

Mainly two types of feedback loop configurations can be applied in fatigue testing, which are:

- Position feedback, where the hydraulic actuator piston position provides feedback.
- Force feedback, where the load cell provides feedback.

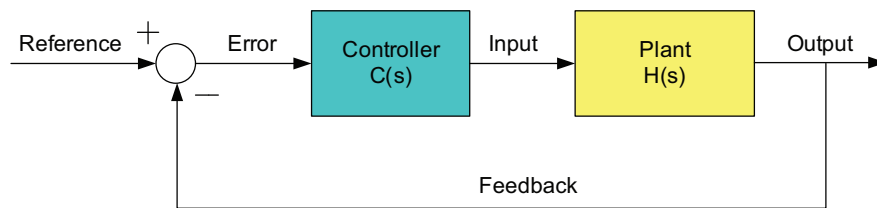


Figure 4.7 – General control architecture of fatigue test setup.

Generally force feedback is applied, since force signals are the reference signals for fatigue loading. The plant in Figure 4.7 represents the mechanical system and hydraulic system of the fatigue test setup.

4.3.2 Present Controller Method and Architecture

Control of fatigue testing is done using the basic control model as presented in Figure 4.8. This control model is used for position or force control. Change of feedback signal makes it possible to use either force or position control.

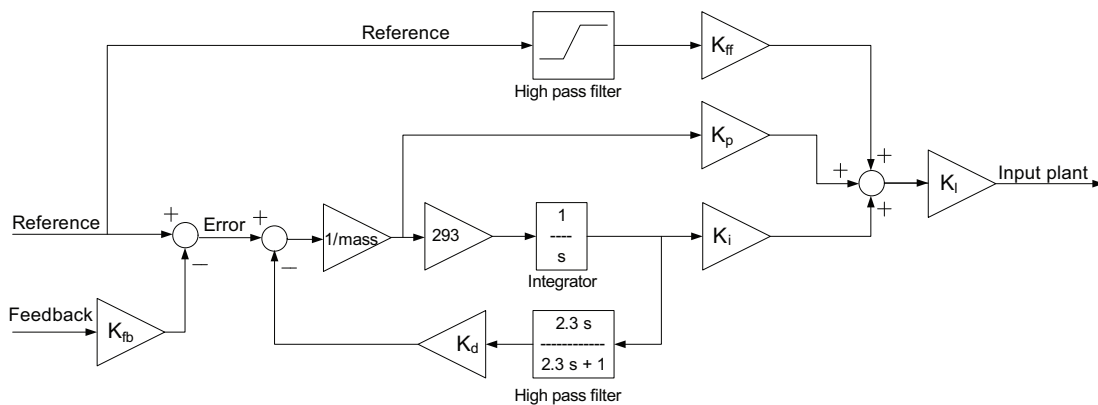


Figure 4.8 – Control architecture used for position and force control, in discrete time domain patented by Fokker Control Systems.

The controller displayed in Figure 4.8 has a number of parameters which can be tuned. These parameters and their effects are:

- *Feedback gain* K_{fb} , used to manipulate the amplitude of the feedback signal. The feedback gain is used to simulate open loop configuration of the system. Normally this gain is set to 1.
- *Feedforward gain* K_{ff} , provides high pass filtered feed through which can be used to improve the response on the (sinusoidal) command signal².
- *Proportional gain* K_p , is the acceleration gain used to amplify the error signal and to make system response faster. Disadvantage can be that the system becomes unstable.
- *Integral gain* K_i , if it is not possible to obtain the amplitude of the reference signal by using K_p , the integral gain is used. The integral gain minimizes the steady state error between reference and feedback signal.
- *Damping gain* K_d , the damping gain is used to damp resonance frequencies of the test article. Effectively it is a velocity dependent reaction force.
- *Loop gain* K_l , is an amplifying gain to increase the output signal of the controller. Normally this gain is set to 1 or -1, which depends on the chosen positive direction of applied force or displacement. The loop gain is an overall gain to boost the current output to the servo valve.
- *Mass gain* $1/mass$, is a reducing gain which reduces the magnitudes of K_p , K_i and K_d gains. Normally this gain is set to 1.

Currently controller settings are obtained when the test setup is build and in operation. Controller settings are obtained by systematic tuning of the parameters while the test setup is in operation. This approach does not provide information on the system preformance, regarding the frequency bandwidth achieved. Therefore it is currently unknown if system performance can be increased even further. The next section will presents novel methods to obtain controller settings for the controller presented in Figure 4.8.

4.3.3 Controller Tuning Methods

This section presents the methods to obtain controller settings for the controller presented in Figure 4.8. To obtain controller settings there are three options, which are:

- Simulation model time domain tuning (novel method),
- Simulation model frequency response tuning (novel method),

²The high pass filter before the feed forward gain can be set to different crossover frequencies. Therefore its transfer function is not presented in Figure 4.8.

- Test setup tuning (present method).

Time Domain Tuning, uses simulation models to obtain controller settings. The controller settings are obtained by systematic tuning of the controller parameters during continuous time domain simulation. Which is done using engineering sense. Advantage of this method is that non-linearities are included in the system. Disadvantage of this method is that it can be time consuming to obtain optimal controller parameters.

Frequency Domain Tuning, uses a linearization to obtain the open loop frequency response function of plant and controller. Using the open loop frequency response it is possible to determine stability and the bandwidth of the system. The bandwidth is a measure for the system performance. Indicators for system stability are the *gain margin* and *phase margin*, which will be explained in Section 5.4.2. These parameters indicate if the controller parameters should be increased or decreased to obtain stable system performance. The advantages of this method are that it is possible to determine if a stable system is obtained, and the frequency bandwidth of the system. Disadvantage of this method is that a linearized model is used for the plant model. Non-linearities such as coulomb-friction are excluded. Therefore obtained controller parameters need fine tuning using time domain tuning. An example on this method will be provided in Section 5.4.3.

Test Setup Tuning, tunes the controller parameters while the demonstration test setup is in operation. This method uses engineering sense to tune the controller parameters. Advantage of this method is that tuning controller parameters, obtains good know length on the influences of parameters on system response. Disadvantage of this method is that there is a possibility that optimal system performance is not reached.

Chosen Methods for Obtaining Controller Parameters

For the verification of the simulation model by measuring system response on the demonstration test setup, it was chosen to use *Test Setup Tuning*. The reason to do this is that each tested frequency needed its own controller parameters, to obtain the applied displacement or applied force. The applied displacement and force were correlated to a percentage of hydraulic flow through the servo valve. More information on testing and verification is provided in Section 6.3.

For the simulation models both *Time Domain Tuning* and *Frequency Domain Tuning* will be used. Time domain tuning is used because non-linear effects are present in the system. Frequency domain tuning is used to obtain a measure of the system performance. Frequency domain tuning provides a fundamental method based on con-

trol theory to obtain the controller parameters and is therefore preferred. It is advised to apply both methods, because non-linearities affect system performance. To show the potential of Time and Frequency Domain Tuning an example is provided in Section 5.4.2.

4.4 Summary

This Chapter presented the mechanical, servo-hydraulic and control system modelling. The chosen modelling methods have advantages and disadvantages, which are discussed and will be presented in this section.

4.4.1 Summary Mechanical modelling

In the current design process FE models of the test setup created. It is chosen to model the demonstration test setup MATLAB-Simulink. To couple the mechanical system with the hydraulic system dynamic state space models are needed. The advantage of these state space models is that it is possible to extract them from FE models. The disadvantage is that a physical state space models increase the number of states. To reduce computational time normalized state space models are obtained and model truncation is applied. The state space models obtain velocity and position output and have a force input.

Interface structures (IS) where modeled as lumped mass models with a translational play gab. Using these models it is possible to investigate the effects of force transfer through IS. The advantage of these models is that it are relatively simple models.

4.4.2 Summary Servo-Hydraulic Modelling

Hydraulic actuators and servo valves have two types of dynamics, motion dynamics and pressure dynamics. Specific parameters such as friction have to be measured to be included in the modelling, which is time consuming and therefore is a disadvantage. Literature [9, 22, 23] did not provide estimation rules for all parameters. The reduction of the model parameters lead to a less complex model, which is an advantage.

Servo valves are complex mechatronic systems where a lot of different components are used, each of them having their its own dynamics. As a result modelling of the coupled system dynamics is very complex, therefore the valve dynamics was approached by a second order model. This reduces model complexity, but can reduce modelling accuracy.

4.4.3 Summary Control Modelling

For controller modelling the present architecture of the control loop is presented. Including this control architecture obtains the possibility to analyze the system behaviour as presently is obtained. Tuning of controller parameters can be performed either in time domain or in the frequency domain. The time domain tuning has as advantage that includes non-linearities are included. Frequency domain tuning has as advantage that system system performance using control theory and is therefore preferred. It is recommended to verify the non-linear behaviour using time domain simulation.

CHAPTER

5

DEMONSTRATION TEST SETUPS MODELS

Chapter 4 discussed the modelling theory of structural test setups. This chapter will utilize the knowledge of Chapter 4 to model the demonstration test setup of Chapter 3. Chapter 5 is divided into four sections, the mechanical system, hydraulic system, coupled mechanical hydraulic system and control system. A description of the complete system is provided in Figure 5.1.

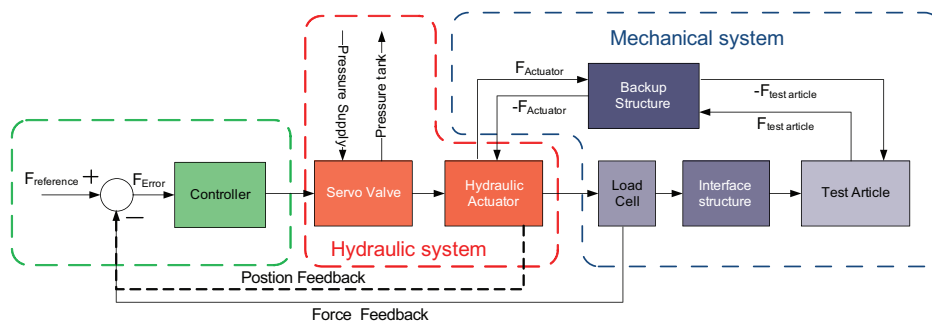


Figure 5.1 – Block description of the demonstration test setup.

A model of the total system is synthesized from sub-models of each component. The different sub-models are linked together, to create a total model that represents the static and dynamic response of the total system.

5.1 Mechanical System Model

Currently fatigue testing setups are only modelled using static Finite Element (FE) model calculations. Using these FE models, deformation and stresses of the Backup Structure (BS) are determined. Maximum loads of the load profile provide input forces on the Test Article (TA) and reaction forces on the BS. The static FE model do not provide information on the dynamic behaviour of the TA and BS. Therefore, a dynamic model is used. It is assumed that the FE models of the TA are generated and supplied by the customer.

A schematic representation of the modelled mechanical system is provided in Figure 5.2. The model described in Figure 5.2 does not include the SS. A BS is omitted in our model because it is assumed to be rigid.

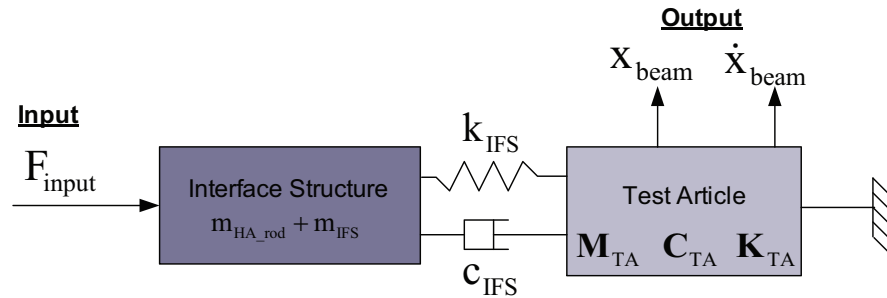


Figure 5.2 – Mechanical system description.

This section will first describe the state space modelling of the TA. Followed by the derived reduced order state space model. Finally, the coupling of the TA with an IF structure and effects of play are set out using time responses of the system.

5.1.1 Test Article model

This section discusses the state space model of the TA. In the demonstration test setup, a TA was used having the following properties:

Clamping length	L_{clamp}	3	[m]
Density	ρ_{steel}	7456,14	[kg/m ³]
Elasticity Modulus	E_{steel}	$210 \cdot 10^9$	[Pa]
Inertia	I_{beam}	$2.8658 \cdot 10^{-6}$	[m ⁴]

5.1. Mechanical System Model

The input force is applied on the tip, whilst the output displacement and velocity are measured at the same location. Figure 5.3a displays the physical schematic of the build test setup. It consists of a mechanical beam which is constrained at 3 and 6 meters from the tip. This system will be modelled as a clamped beam with a clamping length of 3 meters, see Figure 5.3b. Which is done to simulate coupled mechanical and hydraulic behaviour at a low eigenfrequency. In the modelling it is assumed that the dynamics of the second section can be neglected.

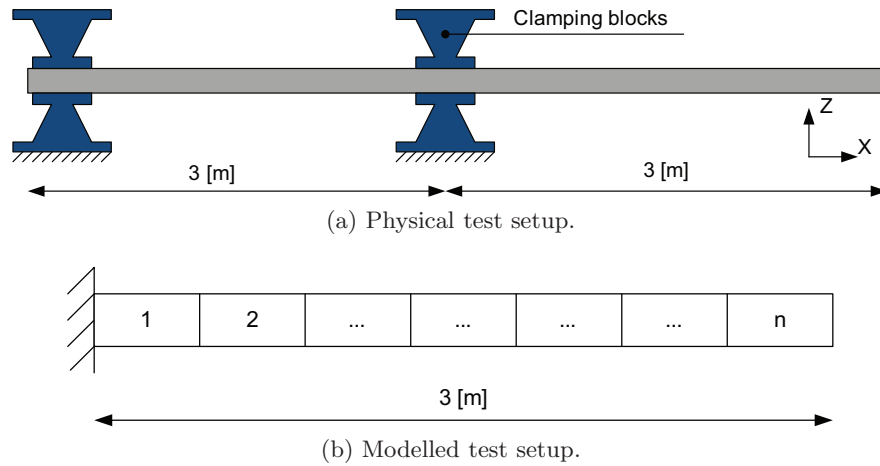


Figure 5.3 – Demonstration test setup mechanical structure.

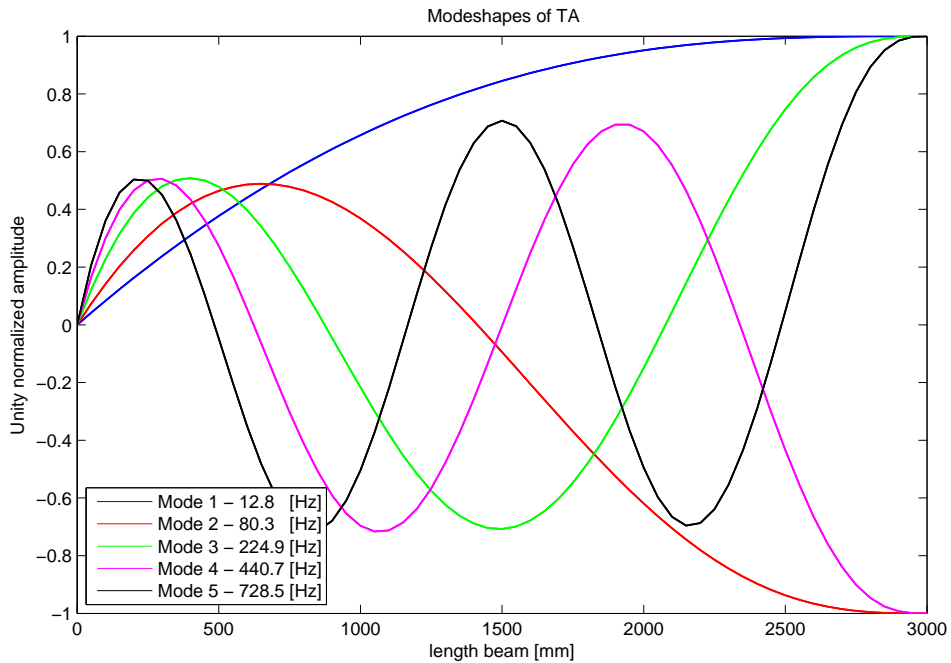


Figure 5.4 – Modeshapes and their eigenfrequencies of a 3 [m] clamped beam

Chapter 4 discussed the different state space derivation, namely the physical state space, normalized state space and the reduced order state space. A comparison of the models for the TA is given. Modal analysis provided the eigenfrequencies and eigenmodes of the system. Eigenfrequencies and eigenmodes are presented in Figure 5.4. From the TA mass and stiffness matrices, it is possible to construct a physical state space model of the TA, using Equation 4.5. The eigenvalue and eigenfrequency analysis results in a modal state space model. The physical and model model is presented in Figure 5.5. For the input a unity force is applied on the tip of the beam.

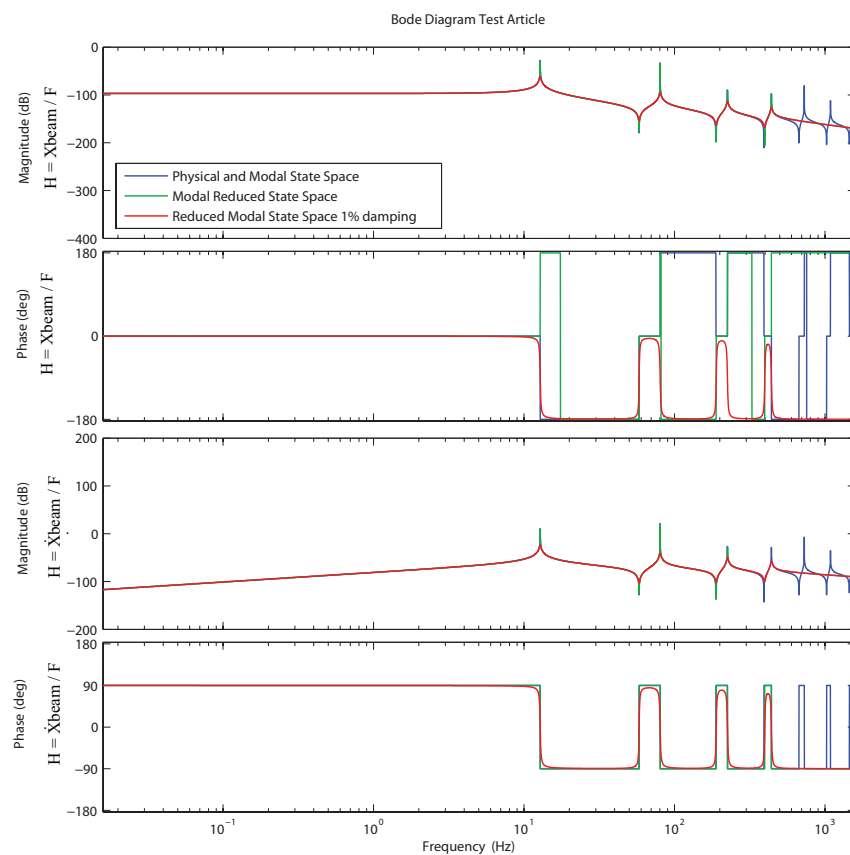


Figure 5.5 – Bode Diagram TA, presenting physical, modal, modal reduced and modal reduced damping state space models.

The next step is obtaining a reduced state space, which is described in Section 4.1.2. The current state space model is calculated from a finite element model using 60 elements in total, because the interest is on the low frequency depended behaviour up to 1000 [Hz]. As a result 120 eigenfrequencies are obtained from the eigenvalue analysis, since $\mathbf{M}^{-1}\mathbf{K}$ results in a 120×120 matrix. 120 Eigenfrequencies and a 120×120

5.1. Mechanical System Model

eigenvector matrix is large (for our application), since fatigue testing is performed in a frequency range till 5 [Hz]. Reduction of the state space system is needed to reduce computational time. For the reduction step, model truncation is used (see Section 4.1.2), taking into account the first 4 eigenmodes and eigenfrequencies of the system. This resulted in an accurate description of the system behaviour up to 100 [Hz], which is sufficient because the fatigue loading reference signal has a low frequency content.

In reality the system also has damping. Since it is a steel structure, damping will be estimated to be 1 [%], which is obtained from experimental analysis. Inclusion of this [1%] damping is done by the damping factor ζ as is included in Equation (4.8).

$$\zeta = \frac{\mathbf{v}_{(r)}^T \mathbf{C}_{MS} \mathbf{v}_{(s)}}{2\sqrt{\mathbf{v}_{(r)}^T \mathbf{K}_{MS} \mathbf{v}_{(r)} \mathbf{v}_{(r)}^T \mathbf{M}_{MS} \mathbf{v}_{(r)}}$$

The result of this inclusion and the difference between the state space models is presented in Figure 5.5.

5.1.2 Interface Structures Model

Chapter 4 already discussed the modelling of Interface Structures (IS). The model is include in order to obtain insight in the effects of play. The combined model of the TA and IS is shown in Figure 5.6.

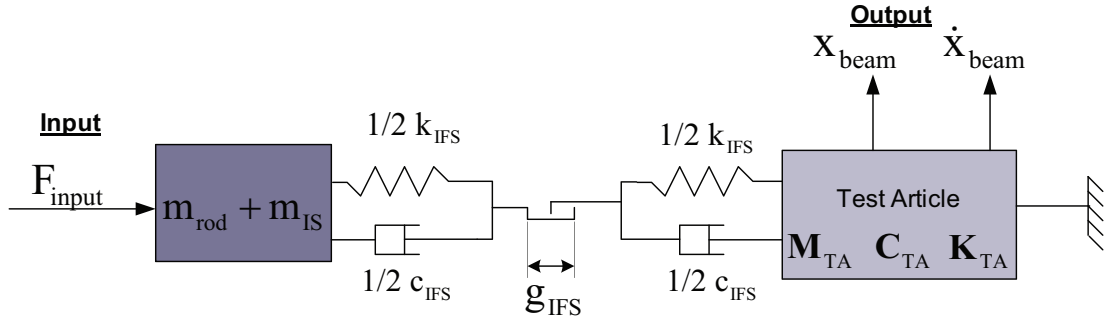


Figure 5.6 – The IS coupled with the TA.

IS structure mass is added to the system, to represent the moving mass of the coupling structure and the mass of the hydraulic actuator rod. The moving mass of the HA and IF structure is estimated to be 10 kg. The IS stiffness is obtained by calculating the coupling pin stiffness of the interface structure, see Appendix D.1.2. Damping is estimated to be 10% of the critical damping, because of the presence of some oil lubrication. Mechanical play, of the demonstration test setup was measured to be 0.17 [mm]. Applied modelling parameters of Equation 4.1.3 are:

Positive play gab	g_p	$0.085 \cdot 10^{-3}$	[m]
Negative play gab	g_n	$-0.085 \cdot 10^{-3}$	[m]
1/2 Stiffness IS positive	K_p	$100 \cdot 10^6$	[N/m]
1/2 Stiffness IS negative	K_n	$100 \cdot 10^6$	[N/m]
1/2 Damping IS positive	D_p	$10 \cdot 10^4$	[Ns/m]
1/2 Damping IS negative	D_n	$10 \cdot 10^4$	[Ns/m]
Mass IS	M_{IS}	2	[kg]
Mass HA _{rod}	M_{rod}	8	[kg]

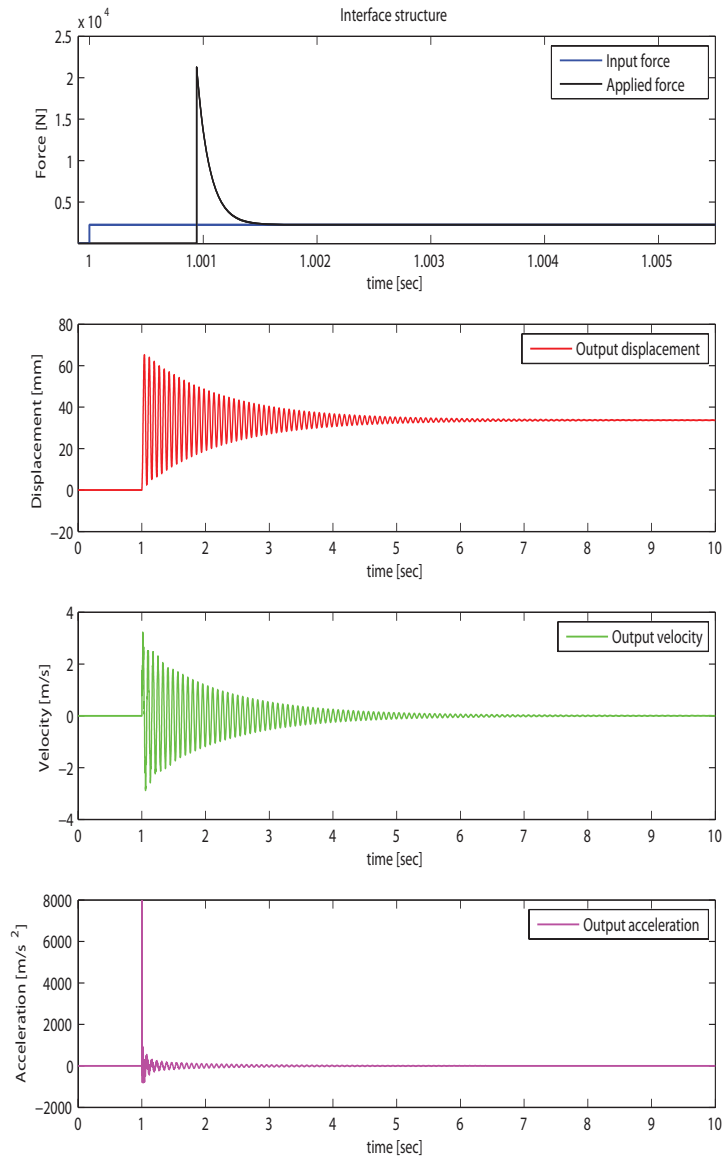
Play Effects

Figures 5.7a and 5.7b show simulation results in time domain of the applied force to the TA by the IS. In Figure 5.7a a step response is applied to the system whilst Figure 5.7b shows the response to an applied sinusoidal reference.

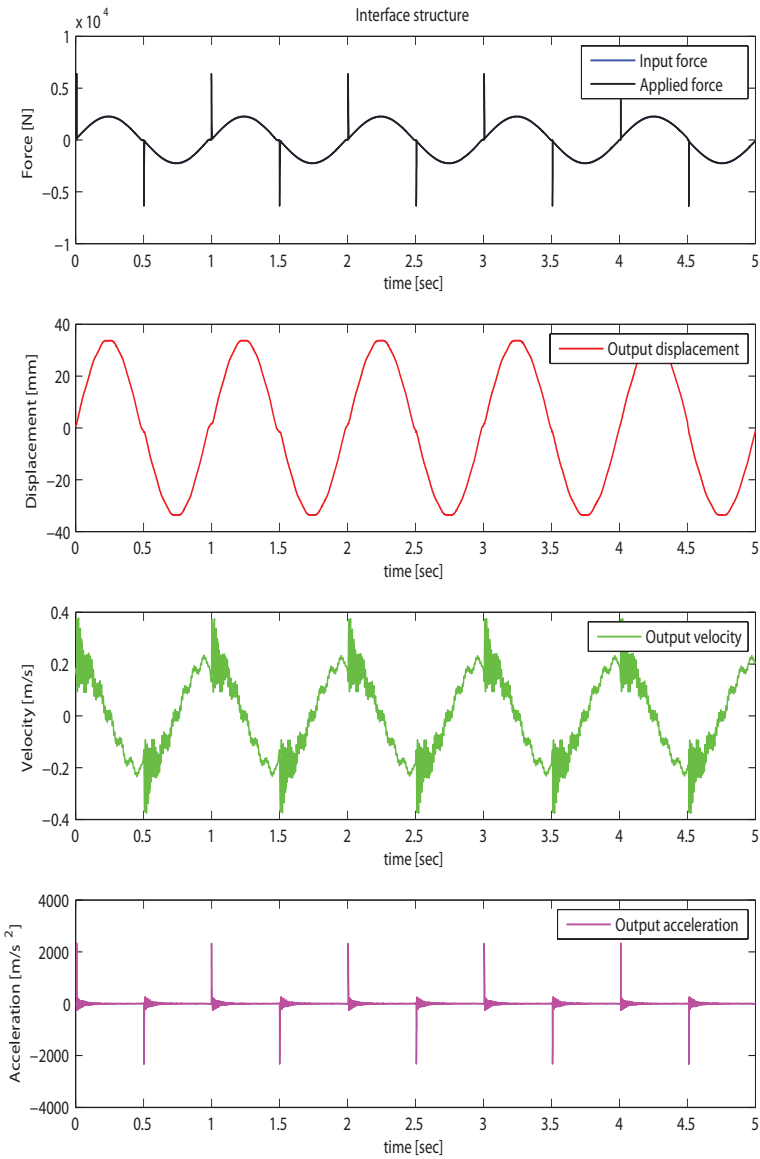
Step response The step response applies a 2255 [N] step force on the system, which is the maximum force applied on the demonstration test setup. From Figure 5.7a it can be concluded that effects of mechanical play are present at a short time after applying the step response. Play creates an impulse force onto the TA, which is applied in a very short time period. Overshoot of the applied force is not wanted in fatigue structural testing, because it applies unwanted loads and load cycles to the TA.

Sinus response Applying a step input to the structure is an extreme load case. The effect of play is investigated on a sinusoidal load profile of 1 [Hz], with an amplitude of 2255 [N]. This is combined the maximum force and frequency applied on the demonstration test setup, during verification. Figure 5.7b shows the sinusoidal reference and applied force and the responses of the TA. From Figure 5.7b can be concluded that play results into an impulse force applied when the displacement moves through the zero. The impulse force results into peak forces applied to the structure, which is unwanted because it applies unwanted loads and load cycles to the TA.

Concluding, play is an unwanted effect in fatigue testing setups, but should be taken into account. Mechanical play and damping are important parameters for future research. Because damping is not obtained from measurements and mechanical play is different for each IS. Therefore IS models will not be included in the total model of the demonstration test setup. Further research on mechanical play needs to be performed.



(a) Step response, presenting the input force on IS and the applied force on TA by IS.



(b) Sinus response, presenting the input force on IS and the applied force on TA, the peak forces are due to mechanical play.

Figure 5.7 – IS responses, showing the effects of mechanical play.

5.2 Servo-Hydraulic System Model

Currently the servo-hydraulic system of structural test setups is designed on their load, stroke and flow capacity, see Section 2.1.1. Dynamics is not taken into account during the design stage. Subsequently, there is no information about the physical response of servo-hydraulic system in combination with other subsystems. To obtain information about the physical response of servo-hydraulic system dynamic models needs to be constructed. The dynamic models are used to predict fatigue load profile tracking performance.

This section discusses the dynamic modelling results of a Hydraulic Actuator (HA) based on Section 4.2.1. Friction is included in the model and its physical influence will be discussed. Furthermore, the Servo Valve (SV) model is discussed. Finally, the hydraulic actuator and servo valve are coupled to model the hydraulic system as used in the total system model.

5.2.1 Hydraulic Actuator Model

This section presents the hydraulic actuator modelling. First a basic hydraulic actuator is modelled, without friction. This model will be extended by applying friction models to represent physical system response. Finally, the physical behaviour of the HA in the frequency domain is covered.

Basic Hydraulic Actuator Model

Section 4.2.1 presented the modelling equations of a simple hydraulic actuator, which consisted out of motion dynamics and pressure dynamics. To simulate the physical behaviour of a simple hydraulic actuator, which is connected to ideal flow sources. These provide hydraulic flow to the hydraulic actuator with a constant supply pressure. Ideal flow sources provide flow regardless of the opposite pressure in the hydraulic actuator. Pressure in the can only be build up by including external forces, friction or flow resistances. Important parameters in the modelling of the basic HA model are, the properties of the hydraulic fluid and the HA parameters itself.

Oil parameters are viscosity, bulk modulus, density, supply temperature and the amount of trapped air. The operating temperature of the hydraulic actuator is in general 60 degrees. It will be assumed in the modelling that the amount of trapped air is zero. Trapped air has a significant influence on system pressures below 100 [bar] [9]. If trapped air is included in the flow sources model its effect will be overestimated, because the system pressure is determined from its external applied force. Viscosity,

5.2. Servo-Hydraulic System Model

bulkmodulus and density are depended on the type of oil. Mobile UNIVIS N 46 hydraulic fluid was chosen, having the following properties ¹:

Viscosity	C_{oil}	21.36	[cSt]
Density	ρ_{oil}	855.6	[kg/m ³]
Bulk Modulus	E_{oil}	$1.295 \cdot 10^9$	[Pa]

HA parameters are included in the modelling equations which are described in Section 4.2.1. The hydraulic actuator is modelled with a *double-acting hydraulic actuator* block in Simulink-Simscape, which excludes mass, friction and external forces in Equation 4.13. Parameters are determined from design drawings of the manufacturer displayed in Appendix B.2.1. From manufacturer drawings it was not possible to obtain a accurate parameter for the dead oil volume. Which is estimated to be the same as the hydraulic actuator chamber volume. Leakage flows of the hydraulic actuator seals and leakage across the piston is neglected. The applied parameters are:

Dead oil volume of each chamber	V_0	$1.37 \cdot 10^{-4}$	[m ³]
Piston area	A_p	$5.497 \cdot 10^{-4}$	[m ²]
Correction factor	α	1	[—]
Maximum distance full extraction	x_E	0.125	[m]
Maximum distance full retraction	x_R	-0.125	[m]

Hydraulic actuators only build up internal pressure differences over the piston if they are loaded by mechanical forces. These forces can be generated by mass, external stiffnesses, friction and so on. To obtain internal pressure the ideal hydraulic system is coupled with an external mass spring damper system, which represents the first eigenfrequency of the mechanical beam. From the first eigenfrequency, the effective mass and the stiffness where calculated. A damping of 1% is applied. This resulted in the following parameters:

Effective mass	m_{eff}	10	[kg]
Stiffness	k_{eff}	$6.7 \cdot 10^4$	[N/m]
Damping	c_{eff}	32	[Ns/m]

Flow sources To supply the hydraulic actuator with hydraulic fluid, ideal flow rate sources are used. Which are controlled by an external input signal. In this example an external sinus function is applied of 0.5 Hz.

In the simulation a maximum nominal flow of 10 [l/min] is applied to the hydraulic

¹The bulkmodulus is generally unknown by the manufacturer or supplier of the hydraulic fluid, but is an important parameter because it influences the oil column stiffness.

actuator, which is also the nominal flow of the servo valve. The flow rate is proportional to the speed of the actuator movement:

$$Q_{HA} = \dot{x}_p A_p$$

where Q_{HA} represents the flow to the hydraulic actuator chamber, \dot{x}_p represents the piston velocity and A_p represents the piston area. A ideal hydraulic actuator simulation is presented in Figure 5.8. The reason for a asymmetric pressures of chamber A and B is because chamber A needs to overcome the externally force. Chamber B is used for retraction of the actuator rod. Figure 5.8 presents the obtained results from the simulation.

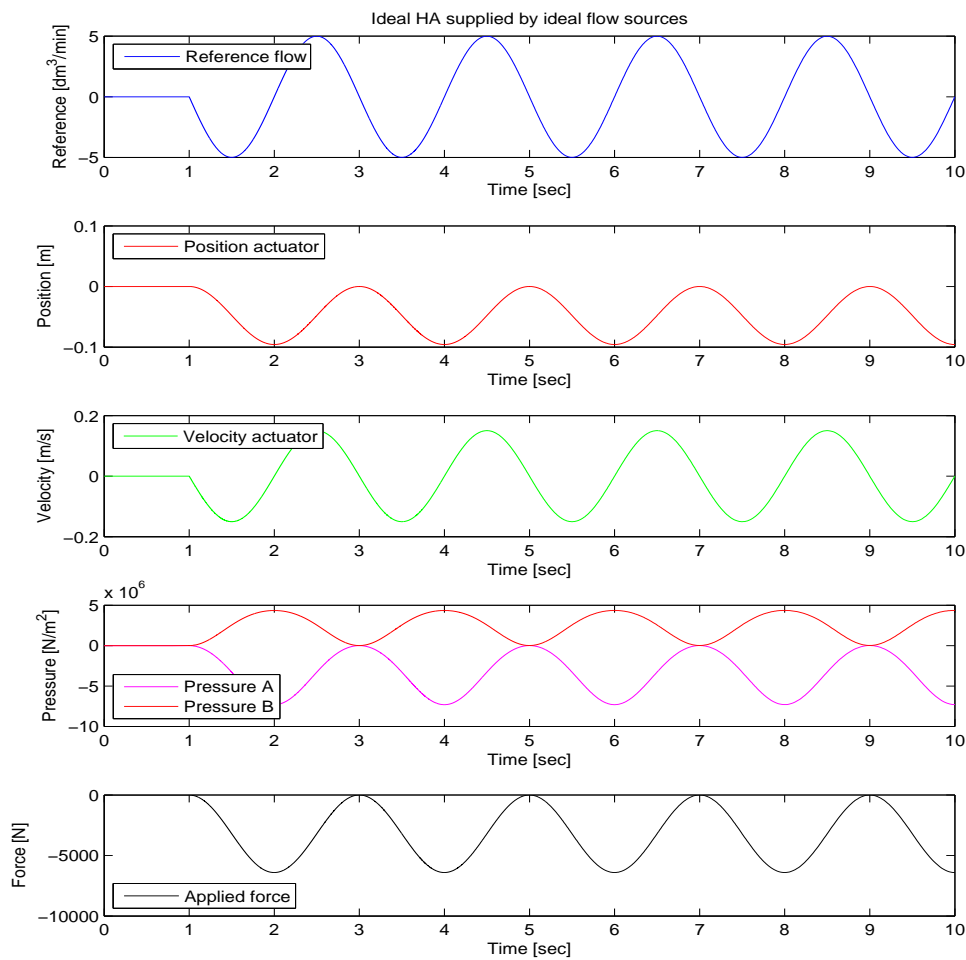


Figure 5.8 – Ideal hydraulic actuator simulation, presenting the applied flow and the outputs of position, velocity, pressures and force.

Friction model

In reality friction is present in hydraulic actuators. Section 4.2.1 presented a friction model for hydraulic actuators, representing a “*Stribeck curve*” [9], see figure 5.9. Friction in hydraulic actuators consists out of Coulomb, viscous and static friction.

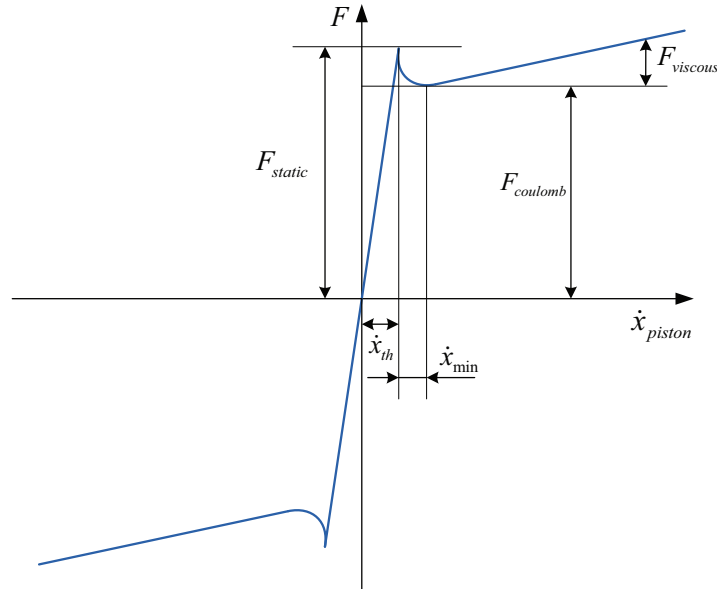


Figure 5.9 – Stribeck curve, representing the friction forces of a HA.

Literature [9, 22, 23] did not provide accurate rules or methods for friction parameters in a hydraulic actuator, therefore friction parameters were measured. This is done by measuring the pressures in the hydraulic actuator chambers and the velocity of the hydraulic actuator rod. From the pressure difference and the piston area is the force obtained. As a result the friction force versus the velocity is known. The parameters used in the hydraulic actuator model are:

Coulomb friction	F_c	260	[N]
Viscous friction	F_v	218.75	[N/(m/s)]
Static friction	F_s	600	[N]
Linear transition	$1/\dot{x}_{min}$	25	[s/m]
Linear velocity threshold	\dot{x}_{th}	$1 \cdot 10^{-4}$	[m/s]

These modelling parameters obtained a first estimated friction curve related to the single averaged friction curve, which will be discussed in Section 6.2.3.

Coulomb friction:

Figure 5.10 presents the applied Coulomb friction to the hydraulic actuator. Results of the simulation are presented in Figure 5.11. From Figure 5.11 is concluded that coulomb friction is visible when the velocity of the actuator rod moves through zero. As a result of coulomb friction, the dynamics of the hydraulic actuator is excited which is seen in the vibrations occurring in the velocity profile. Dynamics is excited due to the step of friction at zero velocity, which is presented in Figure 5.11. The coulomb friction of 260 [N] is 2.6 [%] from the maximum HA capacity of 10 [kN].

Coulomb and static friction:

Figure 5.10 presents the Coulomb and static friction curve. Static friction is the friction that needs to be overcome before motion is realized. The static friction is extrapolated from the measurement to be 600 [N], 6 [%] of the maximum hydraulic actuator capacity. Figure 5.12a displays the time response of the combined Coulomb and static friction. Static friction excites the actuator dynamics, which is seen in the velocity profile. This is due to the larger step force made at zero velocity. Static friction is therefore an unwanted behaviour. Use of hydrostatic actuators decrease the effect of static and coulomb friction, and are therefore preferably used in structural test setups.

Coulomb, static and viscous friction:

In reality there this always damping present. Damping in hydraulic actuators is provided by the viscosity of the hydraulic fluid. Viscous damping is dependent on the velocity of the hydraulic actuator and is represented by the increasing linear line in the stribek friction curve, see Figure 5.9. Figure 5.10 presents the total friction curve applied in modelling. Results of this friction model on the ideal hydraulic actuator model are presented in Figure 5.12b. From Figure 5.12b can be seen that the viscous damping damps the vibrations of the hydraulic actuator after the velocity moves through the zero ².

Conclusion:

Friction is an important non-linear effect in the dynamics of the hydraulic actuator which is difficult to characterize from literature. Literature did not provide valuable rules to characterize the amount of friction in a hydraulic actuator. Therefore the amount of friction needs to be measured. measuring the amount of friction. Friction is an unwanted behaviour since it excites the hydraulic actuator dynamics if the velocity changes sign. As a result the TA is loaded with unwanted loads and load cycles if this excitation occurs.

²To present the effect of viscous friction, the static friction was reduced to 340 [N] Otherwise the system would still resonate due to static friction.

5.2. Servo-Hydraulic System Model

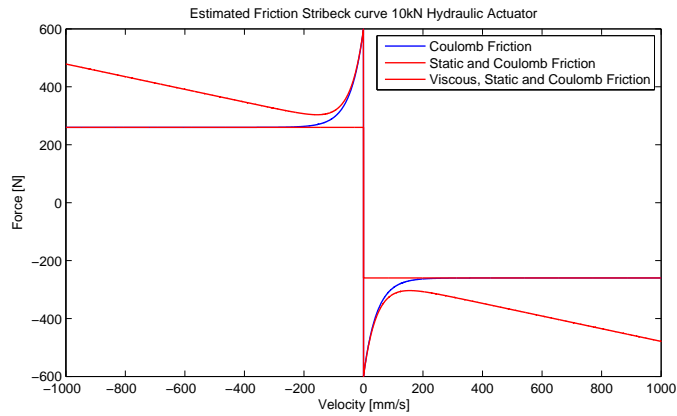


Figure 5.10 – Estimated friction curves of the HA, presenting Coulomb, static and viscous friction.

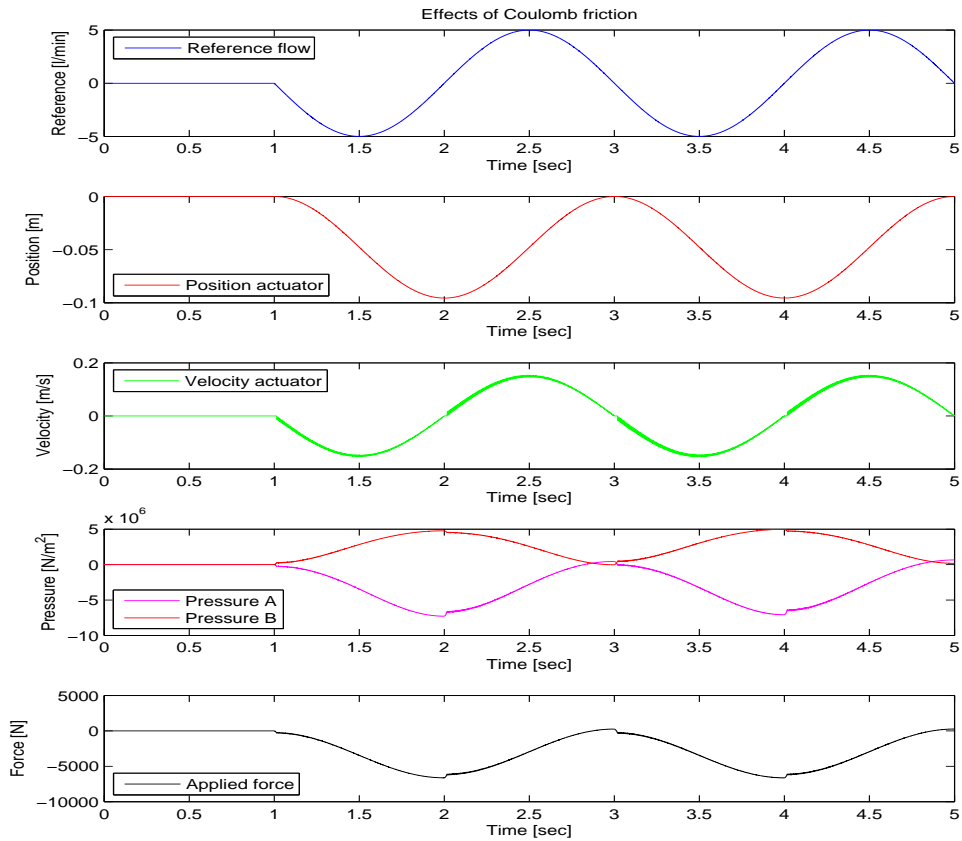
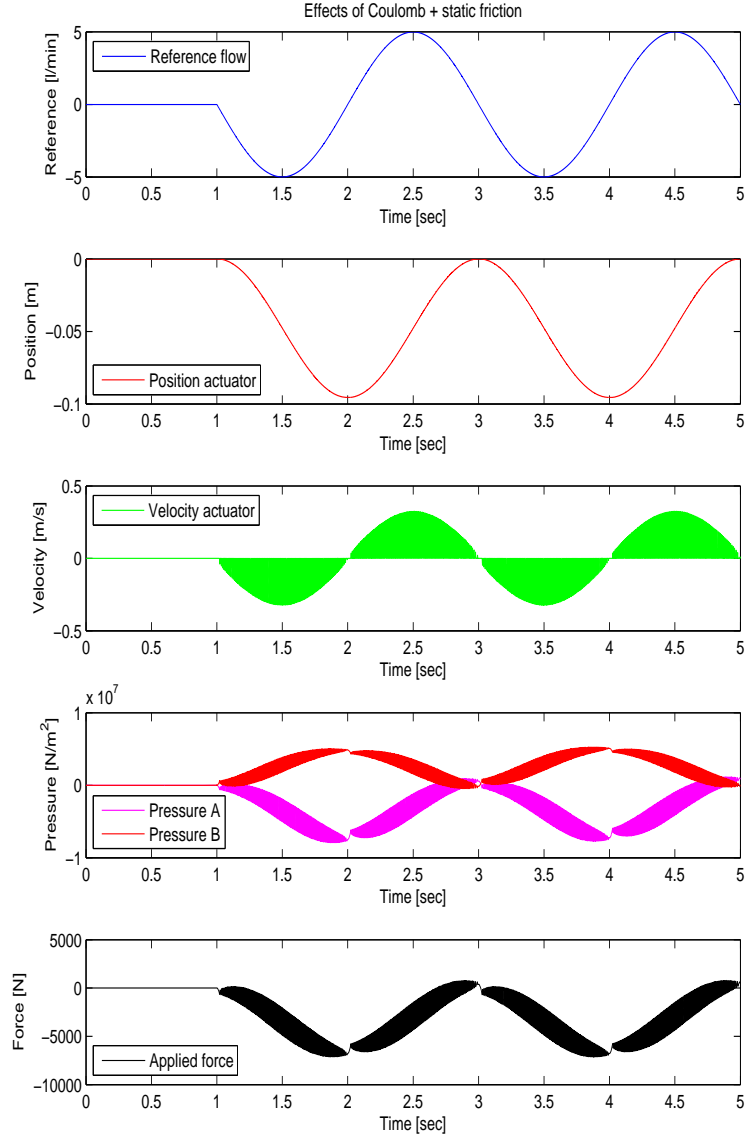
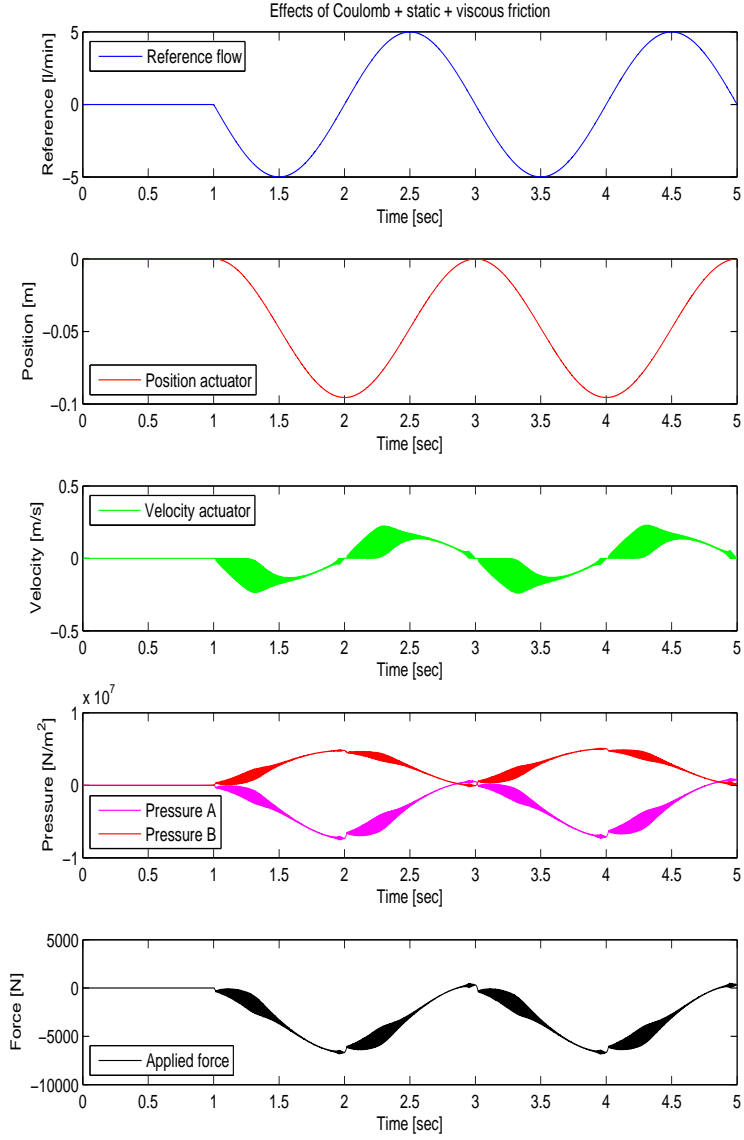


Figure 5.11 – Coulomb friction simulation results, showing position, velocity, pressure and force responses

(a) Coulomb and static friction simulation results, showing position, velocity, pressure and force responses. (b) Coulomb, static and viscous friction simulation results, showing position, velocity, pressure and force responses.



Physical Behaviour of Hydraulic Actuators

As stated, structural fatigue testing is performed with an excitation signal having low frequency content. It is therefore important to know the frequency dependent behaviour of hydraulic actuators. Hydraulic actuators have an eigenfrequency, which is dependent on the stroke position, mass of the piston, piston area and bulk modulus of the oil. According to Viersma [23] the eigenfrequency can be estimated using:

$$\omega_{HA} = \sqrt{\frac{K_{HA}}{M_{HA}}}$$

$$K_{HA} = \frac{A_{piston}^2 E_{oil}}{A_{piston} L_1 + \frac{1}{2} V_L} + \frac{A_{piston}^2 E_{oil}}{A_{piston} L_2 + \frac{1}{2} V_L}$$

ω_{HA}	Eigenfrequency of the HA	[rad/s]
K_{HA}	Stiffness of the HA	[N/m]
M_{HA}	Moving mass of the HA	[kg]
L_1	Actuator stroke of chamber A	[m]
L_2	Actuator stroke of chamber B	[m]
V_L	Dead volume in oil supply pipe lines	[m ³]

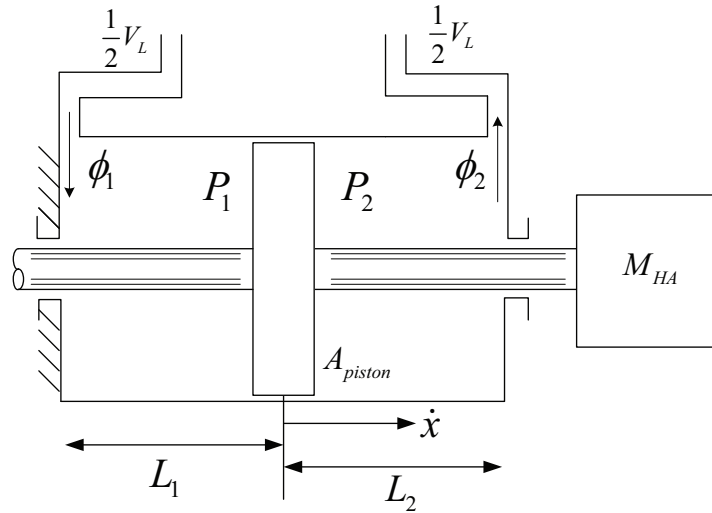


Figure 5.13 – Hydraulic Actuator, displaying the parameters of Equation 5.2.1.

The moving mass of the hydraulic actuator is set to 10 [kg]³. The other parameters for calculation of the actuator stiffness are already provided in the text. Calculation

³The mass of the HA rod is 8 [kg] and a load cell mass of 2 [kg] is included

of the hydraulic actuator eigenfrequency depends on the piston position. The system has its lowest eigenfrequency (120 [Hz]) when the piston is in its center position, see Figure 5.14.

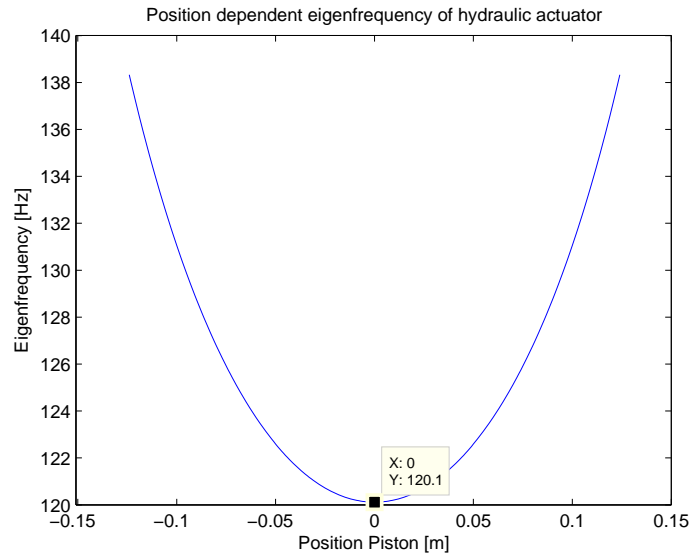


Figure 5.14 – Eigenfrequency of HA, depending on the piston position.

From simulations show that the eigenfrequency is highly dependent on the amount of dead oil volume in supply pipe lines. It is not wanted that the eigenfrequency of the hydraulic actuator interacts with the applied loading frequencies and the eigenfrequencies of the mechanical system. Therefore it is advisable to place the servo valve as close as possible on the hydraulic actuator to shorten supply distance. The lower the dead volume, the higher the eigenfrequency of the hydraulic actuator.

Literature [9, 22, 23] did not take into account the effect the mechanical stiffness of the hydraulic actuator casing. It is assumed that the mechanical stiffness of the casing can be left out of consideration, with respect to the bulk modulus of the oil and compressibility of the oil.

Figure 5.15 shows the frequency dependent behaviour of the hydraulic actuator between the input flow and output position. Linearization is performed without friction static / coulomb present in the hydraulic actuator. The linearization is performed around the initial operating point of the hydraulic actuator, where the piston is centered. Before the eigenfrequency of the hydraulic actuator a -20 [dB/decade] slope is present, due to the fact that flow is applied, which results into velocity of the hydraulic actuator rod. After the eigenfrequency of the hydraulic actuator an additional second order mass effect is present, which results into a -60 [dB/decade] slope.

5.2. Servo-Hydraulic System Model

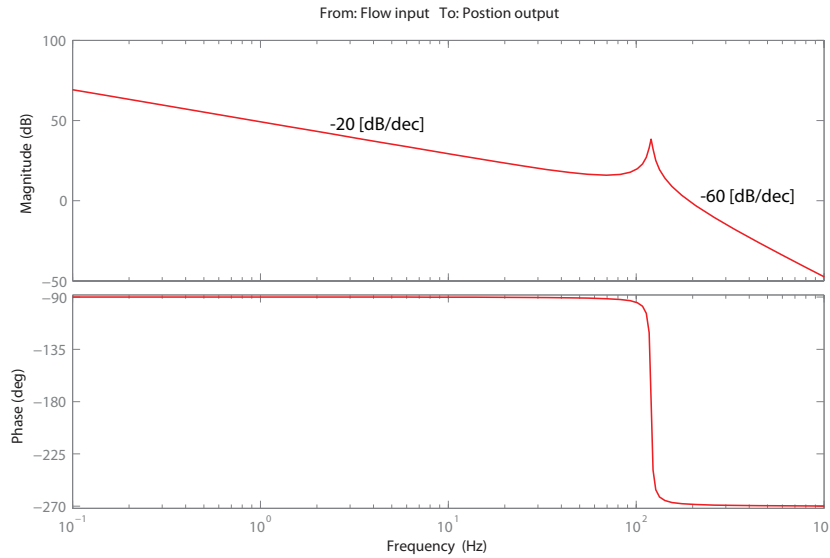


Figure 5.15 – Bode plot, presenting linearized frequency dependent behaviour of HA for a flow input and position output, including viscous friction.

5.2.2 Servo Valve Model

This section describes the modelling of the servo valve, which provides hydraulic fluid flow to the hydraulic actuator chambers. A basic servo valve model, the motion dynamics, pressure dynamics and finally the full system dynamics is presented. This section models the servo valve which is used in the demonstration test setup.

Basic Servo Valve Model

Section 4.2.2 introduced the equations of a servo valve model. Servo valves are characterized around a nominal flow operating point, having a pressure drop across the valve at nominal flow whilst the flow is dependent on the input current. The nominal flow of the servo valve is calculated using:

$$Q_{SV} = Q_N \sqrt{\frac{\Delta P_V}{\Delta P_N}}$$

Q_{SV}	Servo valve flow output		$[\text{dm}^3/\text{min}]$
Q_N	Nominal flow	10	$[\text{dm}^3/\text{min}]$
ΔP_V	Valve pressure drop	0 - 250	[bar]
ΔP_N	Nominal pressure drop	70	[bar]

Equation 5.2.2 is obtained from the manufacturer data, see Appendix B.2.4. Figure 5.16 shows the reference flow output of the manufacturer and the flow output of the MATLAB-Simulink model, which included a “four way directional valve”.

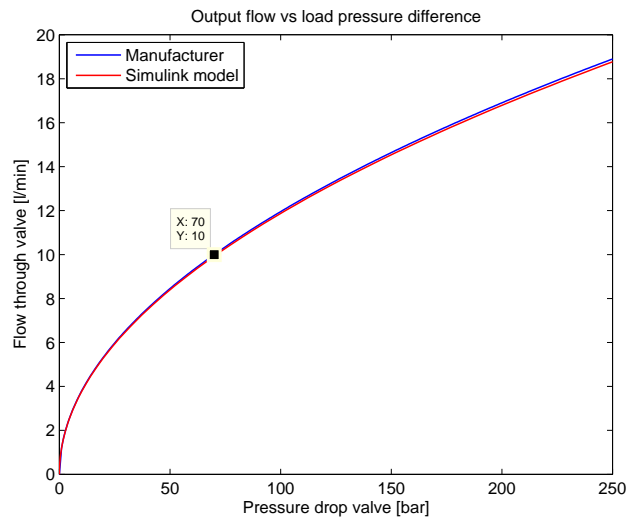


Figure 5.16 – Output flow vs pressure drop graph, presenting manufacturer specifications and MATLAB-Simulink model results.

For the flow output, motion dynamics and pressure dynamics are of importance to include in the model. Which are presented in the next section.

Motion Dynamics

Motion dynamics of a servo valve is characterized by a second order model, as became clear in Section 4.2.2. Equation 4.17 is used for the modelling of the motion dynamics of the servo valve. Valve hysteresis is neglected, in this equation. The second order model is extracted from the manufacturers bode response plot, by calculating the eigenfrequency ω_n , damping ζ and valve gain K_v factors. These parameters are obtained for worst case response of the servo valve provided by the manufacturer. The output of the second order model is multiplied with the spool port gain, representing the maximum stroke of the servo valve spool. Estimated parameters are:

Valve eigenfrequency	ω_n	75	[Hz]
Valve damping	D_v	0.8891	[-]
Valve gain	K_v	1	[-]
Valve spool position gain	S_{port}	0.0015	[m]

5.2. Servo-Hydraulic System Model

Calculation of the parameters from manufacturer data is presented in Appendix D.2.2.

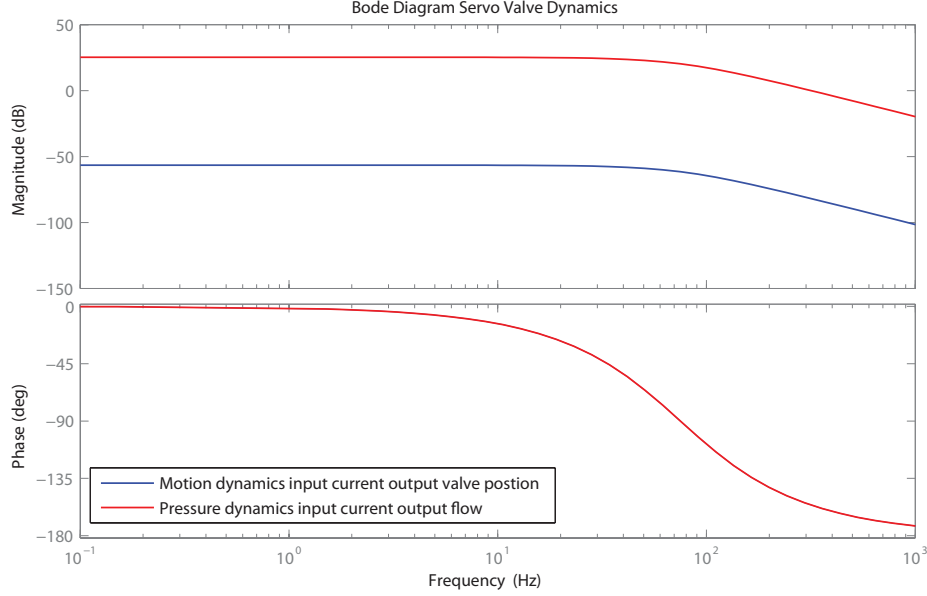


Figure 5.17 – Servo valve motion dynamics, between current input and position output or flow rate output.

The 2nd order servo valve motion dynamics is presented in a bode plot, see Figure 5.17. The second order model is an approximation of the servo valve motion dynamics, whereas the real servo valve response consists out of a higher order model. This servo valve model is updated and verified using measurements subsequently to minimize the error between the real response and the modelled response.

Pressure Dynamics

As stated in Section 4.2.2 the modelling consists of two dynamic contributions, motion dynamics and pressure dynamics. This section covers the physical model of the pressure dynamics, which is represented by Equations 4.24 and 4.25. The valve is modelled critical centered. Leakage flow and valve hysteresis are neglected in the model. The valve opening area can be calculated using Equation (5.2.2), which is obtained from Viersma [23]. The factor 0.5 is included because the rated valve pressure drop is supplied over two supply lines to chamber A and B of the HA.

$$A_{port} = \left(\frac{Q_N}{C_d} \right) \sqrt{\frac{\rho_{oil}}{(2 \cdot 0.5 \cdot \Delta P_N)}}$$

Pressure drop	ΔP_N	$70 \cdot 10^5$	[Pa]
Opening area orifice	A_{port}	$3.3175 \cdot 10^{-6}$	[m ²]
Discharge coefficient	C_D	0.611	[-]

Using the model it is possible to determine the transfer function between input valve position x_v and output valve flow Q_v . It is assumed that the supply pressure is constant, therefore the model has as constant pressure drop over the valve. According to Equation (4.21) the transfer function output flow divided by input valve position is constant, if the delta pressure is constant. Therefore a constant magnitude is obtained.

Total Servo Valve System Dynamics

Finally, pressure dynamics and motion dynamics of the servo valve are coupled to each other. The transfer function between input current and output flow is calculated and presented in Figure 5.17. Figure 5.17 shows that the trend is the similar to the position output, but that the magnitude has changed due to the combination of the motion and pressure dynamics.

5.2.3 Servo-Hydraulic Model

Previous sections covered the hydraulic actuator model and the servo valve model. In this section, both models are coupled to obtain the servo-hydraulic system model, representing the dynamics of a servo valve and hydraulic actuator.

Servo-Hydraulic System Model

The total servo-hydraulic system model, is used for modelling of structural fatigue testing setups. For time simulation responses an external mechanical mass-spring-damper system is included, representing the effective mass, stiffness and damping of the TA. This mechanical system is included because, no internal pressure will be present if no external load is applied.

Time Domain Simulation

Figure 5.18 shows the time domain response of the servo-hydraulic system coupled with the external mechanical system. The friction of Section 5.2.1 is included in this system, which is noticed in the responses of velocity, pressure and force. It is seen in Figure 5.18 that the position drifts away, this is an initiation of the actuator position. The drift will stabilize due to the external coupled force which results into a symmetric pressures in the HA chambers. Because of this position drift a controller is needed, to obtain

5.2. Servo-Hydraulic System Model

reference tracking of the reference signal. A controller will control the applied position or force of the HA.

Frequency Domain Simulation

Servo-hydraulic systems are non-linear, to obtain a Frequency Response (FR) function, linearization is used. Linear models will be used for controller tuning. Details on the linearization method used is provided in Appendix E.3. The linearization was performed without the mechanical system and applied when the HA rod and SV spool are in their center position. Coulomb friction and static friction are not taken into account, but the mass of the hydraulic actuator rod is.

Figure 5.19 shows the FR function for position and velocity output of the servo-hydraulic system. This FR function is a combination of the servo valve system response and the the hydraulic actuator system response. Above the eigenfrequency of the servo valve a -40 [dB/decade] slope is added representing the mass effect of the SV, increasing phase delay of the system. Combining this -40 [dB/decade] slope with the -60 [dB/decade] slope mass effect of the HA results into a -100 [dB/decade] slope, above the eigenfrequency of the HA.

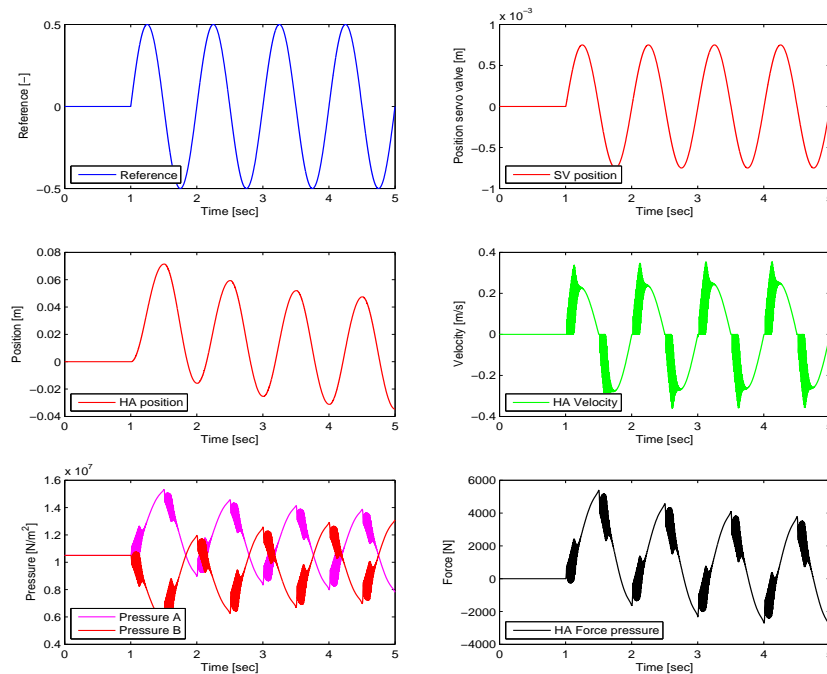


Figure 5.18 – Hydraulic system time response, showing the drift of the HA position and the friction response in the velocity and pressure signals.

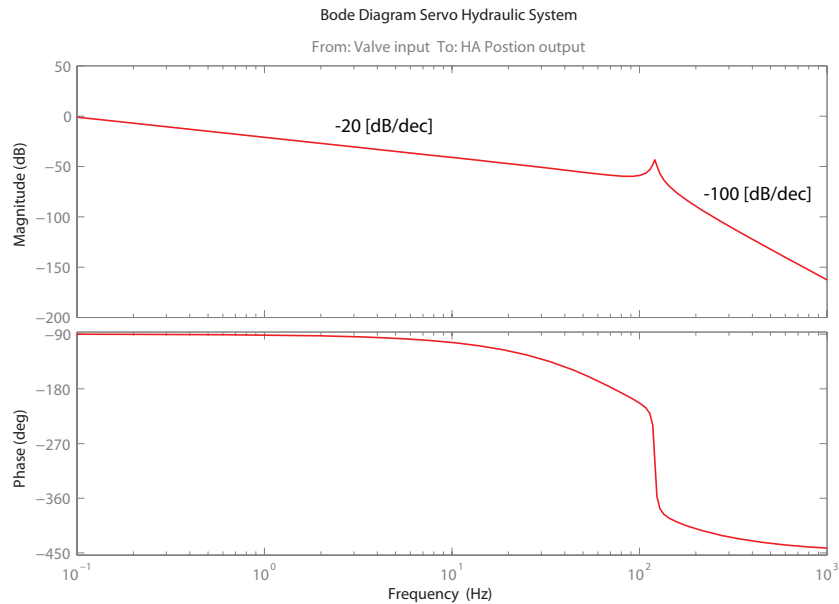


Figure 5.19 – Linearized FR of servo-hydraulic system, between valve current input to position output.

5.3 Coupling Mechanical Model and Servo-Hydraulic model

Next step in the demonstration test setup model is coupling of the mechanical model and the servo-hydraulic model. Details on coupling method used is presented in Appendix E.1 and Appendix E.2. This section presents simulation results of the coupled system model. First the time domain simulations are presented thereafter the linear frequency domain FR are presented.

The coupled system model represents the plant model as used for controller tuning. Therefore the coupled system model is of great importance.

5.3.1 Time Domain Simulations

Figure 5.20 presents the time responses of the coupled mechanical and servo-hydraulic system. This model includes; friction, actuator rod and piston mass, but excludes the interface structure.

5.3.2 Frequency Domain Simulations

This section presents the linearized frequency response models for either the HA position output or LC force output. These are used as plant models in the controller tuning.

5.3. Coupling Mechanical Model and Servo-Hydraulic model

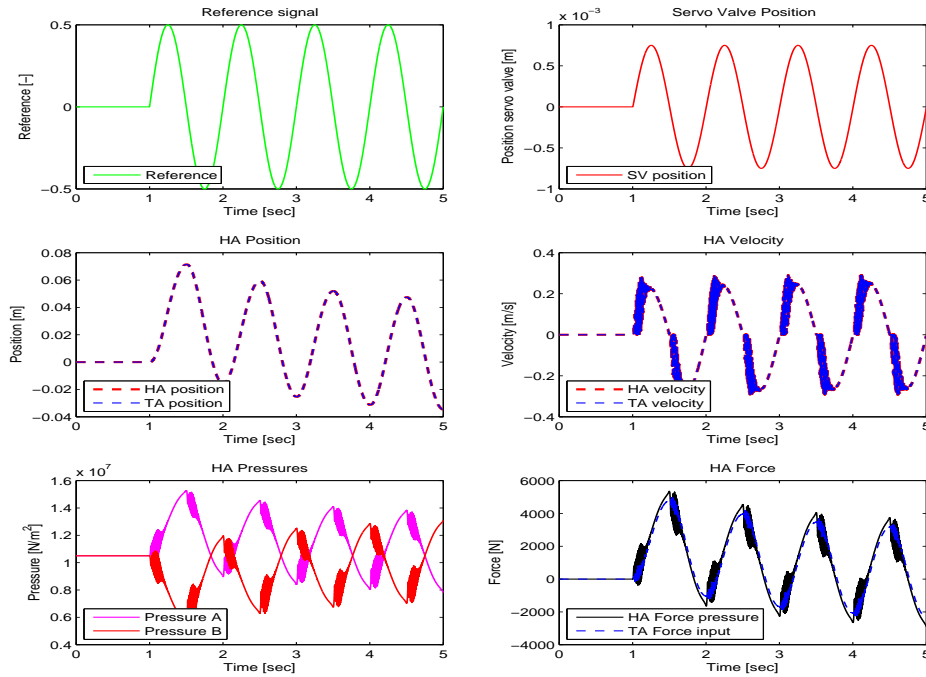


Figure 5.20 – Time response signals of the coupled mechanical and servo-hydraulic system.

First the position output results are presented thereafter the force output results are presented.

HA Postion Frequency Response

Figures 5.21 presents the linearized open-loop FR between valve input and position output or velocity output.

Coupled eigenfrequency results are displayed in Table 5.1. Due to the coupling of the Hydraulic System (HS) with the Mechanical System (MS), the eigenfrequencies

Modes	Value [Hz]
1st TA	52.4
2nd TA and HA	104
3rd TA	198
4th TA	398

Table 5.1 – Coupled Eigenfrequencies of TA and HA, obtained from the frequency response between input current and position output.

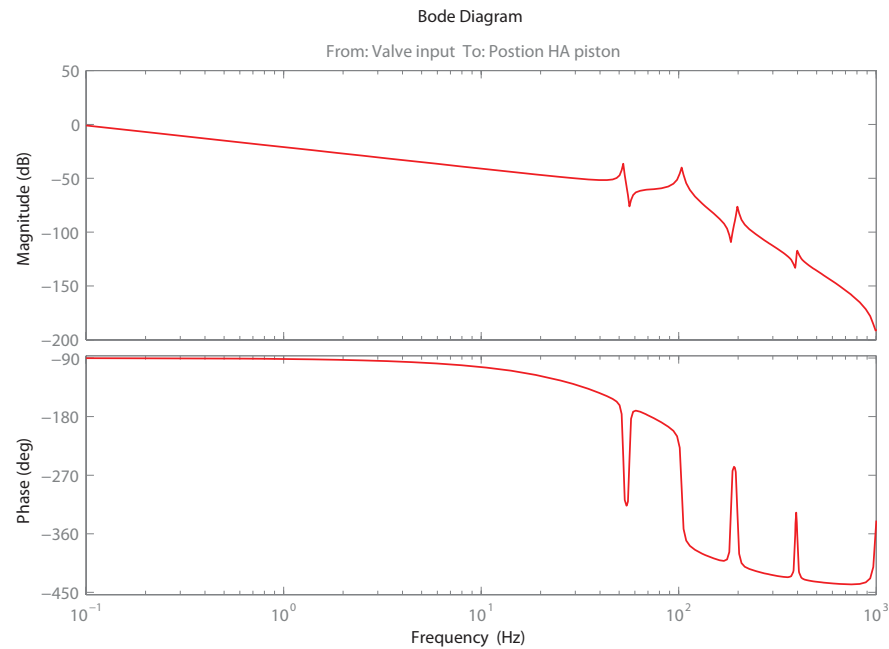


Figure 5.21 – Linearized FR between valve input and TA position output.

shift. This is due to the added stiffness provided by the hydraulic actuator oil column. Because system resonance could be performance limiting due to their influence on control tuning. A shift of the eigenfrequencies to higher frequencies can be considered as a positive effect.

Load Cell Force Frequency Response

Figure 5.22 shows the frequency response between the valve input and the force output of the system. It is noticed that the eigenfrequencies of the TA occur as anti-resonance frequencies the FR. Theoretically (if damping is neglected) there is zero force needed to excite the TA at its resonance frequencies. In this section the linearized models of the coupled mechanical system with the hydraulic system have been derived. These models are used in the next section to investigate system performance on the controller tuning.

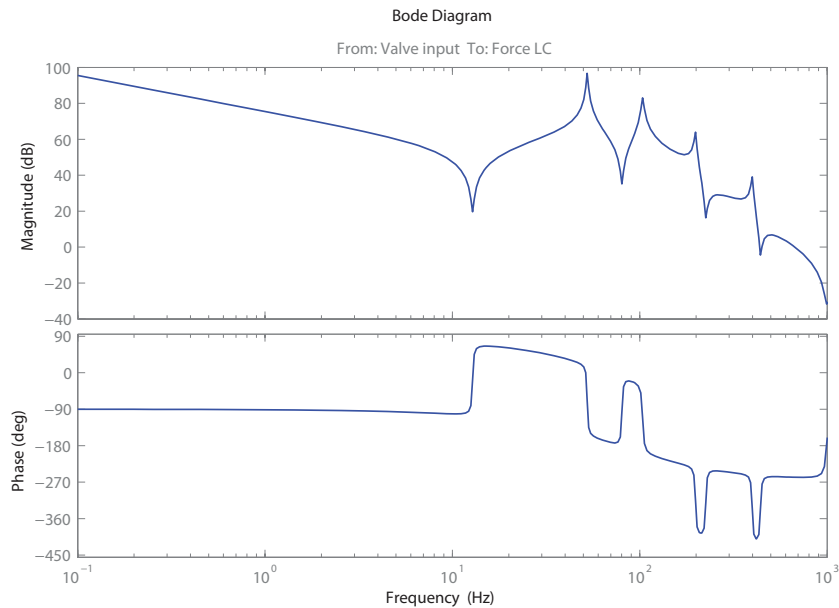


Figure 5.22 – Linearized FR between valve input and force output.

5.4 Controller Models

This section treats the control architecture as presently is used to control fatigue test setups. The tuning of control parameters is performed on the basis of experience. As a result it is not known if optimal system performance is achieved.

This section covers the integration of a controller architecture in combination with the modelled mechanical and hydraulic system models. This model can then be used to check the system performance for different controller settings. The section does not discuss different controller architectures. The simulation models can be used to develop new controllers. This is not included because it is out of scope of this thesis.

5.4.1 Objective of Control

The objective of control is to track the reference signal as exact as possible. The tracking is dependent on the system behaviour, controller settings and the reference signal applied.

Tracking of the reference signal is needed because the HA behaves like an integrator, see Section 5.2.1. The integrator action results in a zero pole, in the transfer function. It is concluded that servo-hydraulic systems are marginal stable systems, because of the zero pole. Without feedback drift in position and force responses is present. The

reference signal is subsequently not tracked.

5.4.2 Implementation Control Model

Previous section outlined the need for control in structural testing systems. This section will implement the control model of Section 4.3.2. Figure 5.23 shows the layout of the full system including a controller.

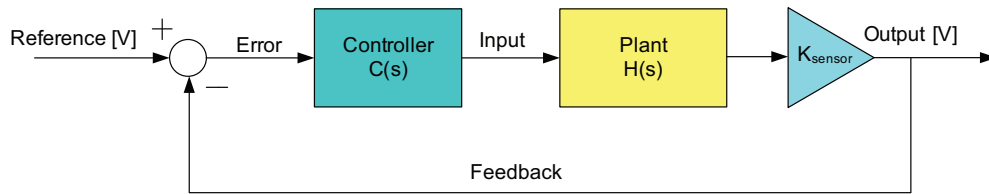


Figure 5.23 – Full system model, including feedback control loop.

There are two types of control standards in structural fatigue testing, either:

- Position control: the position of the HA is measured as output.
- Force control: the applied force on TA is measured as output.

The reference signal is generally a voltage signal which corresponds to the stroke or force which needs to be applied. The physical position or force signal from the plant is scaled to voltage by including a sensor gain K_{sensor} (see Figure 5.23).

Control Architecture

The controller architecture as implemented in the full system model is presented in Figure 5.24 and the corresponding controller transfer function (derived from the control architecture) is given by Equation 5.4.2. This controller architecture is derived from the controller architecture presented in Figure 4.8.

From the controller architecture presented in Figure 5.24 is the controller transfer function derived, which is:

$$H_{controller} = \frac{\text{Input plant}}{\text{Error}} = \frac{K_p s^2 + (293K_i + \frac{1}{2.3}K_p)s + \frac{293}{2.3}K_i}{s^2 + (293K_d + \frac{1}{2.3})s}$$

Knowing the transfer function of the controller, it is important to know its behaviour for the controller tuning. Therefore the behaviour of the three parameters K_p, K_i and K_d are analysed in the frequency domain. Figure 5.25 presents the effect of the three most important gains in the controller. Their different effects are discussed below.

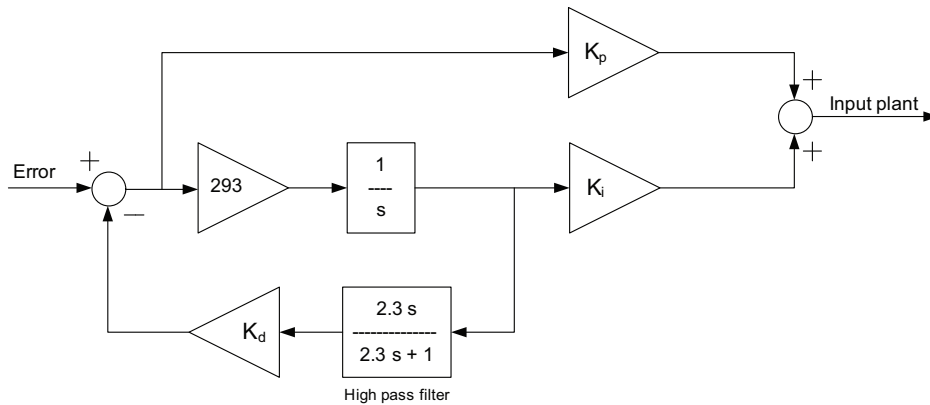


Figure 5.24 – Implemented controller architecture, including proportional gain K_p , integration gain K_i , and damping gain K_d .

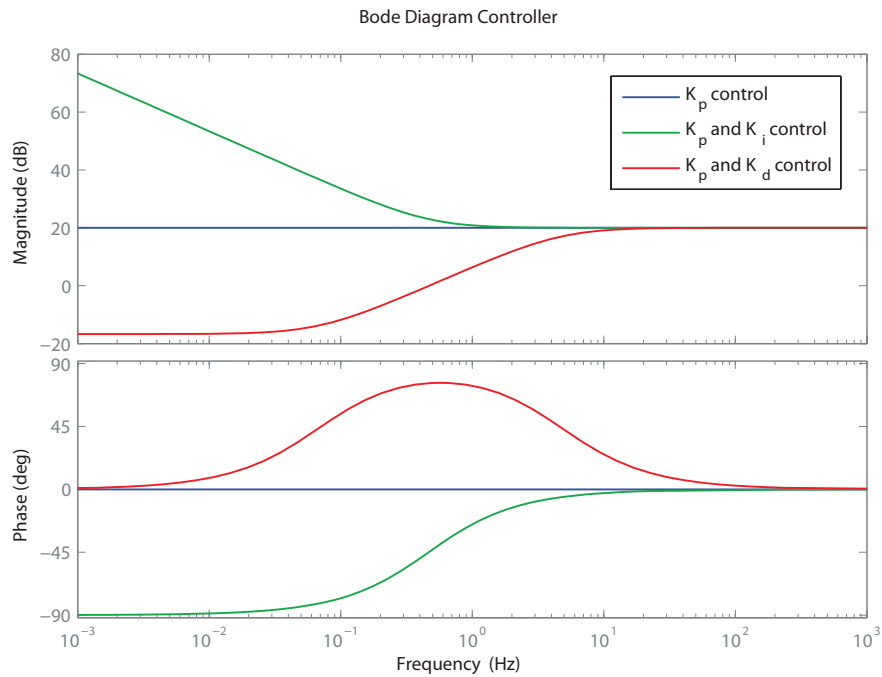


Figure 5.25 – Bode diagram controller, showing effects of proportional, integrator and differentiator gains.

Proportional gain; influences the magnitude of the input signal to the plant. The proportional gain amplifies the error signal. It improves system response. If the proportional gain is too high, overshoot and resonance occurs. If the system is only P controlled then the controller has a transfer function as in Equation 5.4.2.

$$H_{controllerP} = K_p$$

Integral gain; reduces the static error. It integrates to the error signal. Due to the integral gain the system response becomes faster. Figure 5.25 shows the integral bode response, with using a proportional gain. Figure 5.25 shows that the integral gain is active at low frequencies with a -20 [dB/decade] slope. The controller model acts as a PI compensator, see Equation 5.4.2.

$$H_{controllerPI} = \frac{K_p s^2 + (293K_i + \frac{1}{2.3}K_p) s + \frac{293}{2.3}K_i}{s^2 + (\frac{1}{2.3})s}$$

Damping gain; the damping gain reduces the amount of overshoot due to the proportional gain. The damping gain slows system response down. If only a proportional gain and damping gain are used, then the controller model acts like a lead compensator, see Equation 5.4.2 and Figure 5.25.

$$H_{controllerPD} = \frac{K_p s + \frac{1}{2.3}K_p}{s + (293K_d + \frac{1}{2.3})}$$

Sensor Gain

The sensor gain K_{sensor} in Figure 5.23 converts the output of the plant from engineering units to a voltage signal. The sensor gain included depends on either position feedback or force feedback. The sensor gain is determined by:

$$K_{sensor} = \frac{V_{max}}{Y_{max}}$$

K_{sensor}	Sensor gain	[V/m] or [V/kN]
V_{max}	Maximum input voltage	[V]
Y_{max}	Maximum output	[m] or [kN]

For position control, the displacement of the hydraulic actuator provides the feedback. The sensor gain for position feedback is calculated by:

$$K_{sensor \ position} = \frac{V_{max}}{Y_{max}} = \frac{10}{0.125} = 80 \text{ [V/m]}$$

The sensor gain for force feedback is calculated by:

$$K_{sensor \ force} = \frac{V_{max}}{Y_{max}} = \frac{10}{25 \cdot 10^3} = 4 \cdot 10^{-4} \text{ [V/N]}$$

These gains are implemented in the simulation model for position and force feedback.

5.4.3 Tuning controller parameters

The controller parameters for structural test setups can be obtained using the following three options:

- *Time domain tuning*; uses the non-linear simulation model for tuning of the controller parameters during continuous time simulation. A reference signal is applied, and on the basis of the response signals, the controller parameters are tuned. This is done using systematic tuning of K_p, K_i and K_d by hand, engineering sense. Advantage of this method is that non-linearities are included in the system. Disadvantage of this method is that that it requires a lot of computational effort.
- *Frequency domain tuning*; uses a linear simulation model for tuning the controller parameters in the frequency domain. On the basis of control theory it is possible to gain optimal and stable system performance. The advantage of this method is that a measure of the system performance in terms of closed loop bandwidth is obtained. The disadvantage is that non-linearities such as coulomb-friction are excluded. Using *Time domain tuning* it is possible to optimize controller parameters on the non-linear model.
- *Demonstration test setup tuning*; uses engineering sense to tune the controller parameters when the structural test setup is build an in operation. This is the current approach of obtaining controller parameters. Advantage of this method is that tuning controller parameters by hand obtains knowledge on the system response. Disadvantage of this method is that there is a possibility that optimal system performance is not reached.

The next sections present the controller tuning for the obtained position control and force control models, using both *Time domain controller tuning* and *Frequency domain controller tuning*.

Position control model

To obtain controller parameters of the position control configuration the controller is tuned using time domain simulation. The time domain simulation is performed at a frequency of 5 [Hz], since this is the frequency range of fatigue loading profiles. Figure 5.26 shows the time responses for a controller which is tuned in time domain. The parameters used where:

Reference Amplitude	R_A	0.31	[V]
Reference frequency	R_f	5	[Hz]
Proportional gain	K_p	3.5	[-]
Integration gain	K_i	2.1	[-]
Differentiation gain	K_d	0.6	[-]

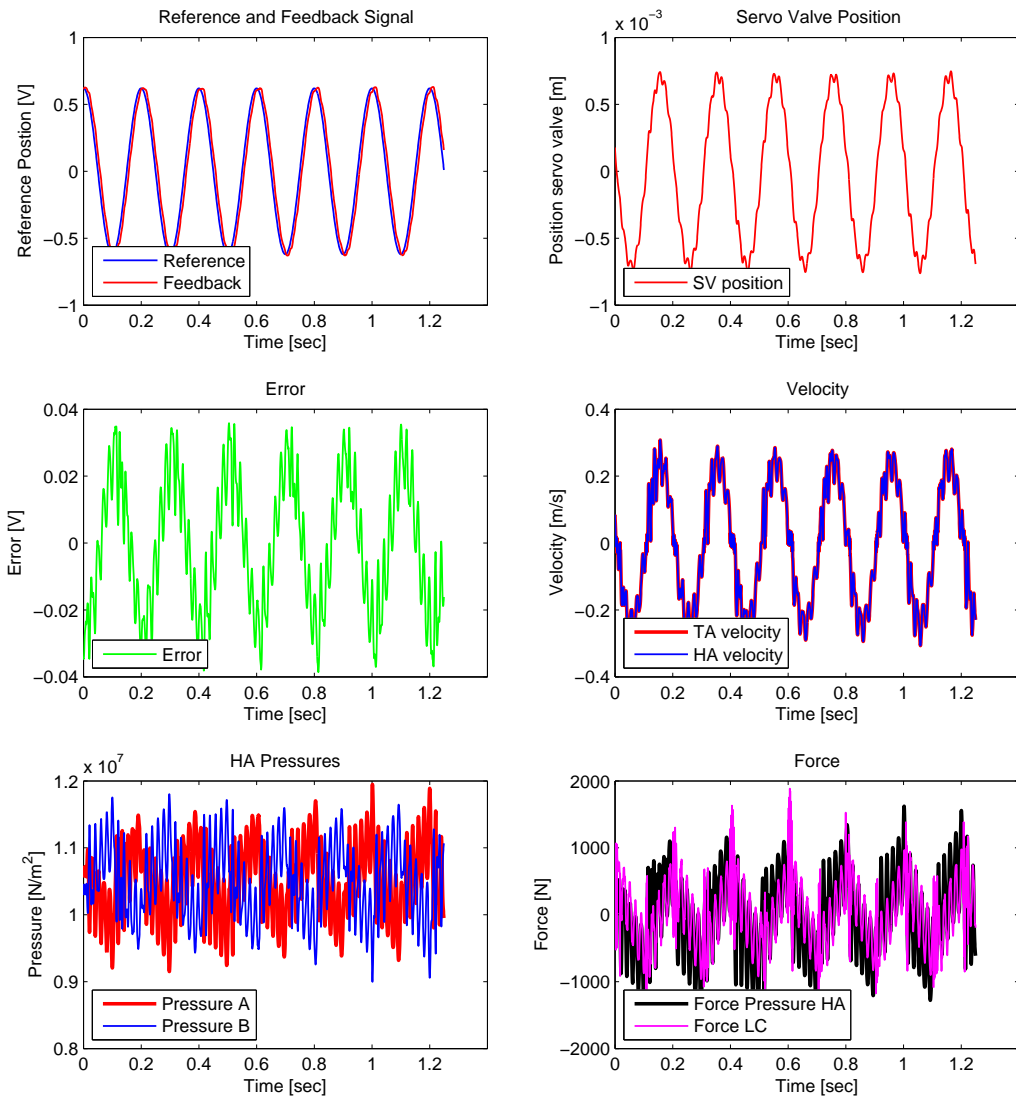


Figure 5.26 – Closed loop position control time responses.

5.4. Controller Models

The simulation is performed using static, coulomb and viscous friction. Which parameters are described in Section 5.2.1. Effects of friction are seen in the applied error, force and pressure signals. The maximum error between command and feedback in Figure 5.26 is 1.0%. From Figure 5.26 it can be concluded that the implementation of the controller obtains a stable system for 5 [Hz], which does not drift as in Figure 5.18.

The next step is to analyse system stability in the frequency domain. The stability of a controlled system over a certain frequency range, can be checked analytically by their linearized system models. Figure 5.27a shows the linearized system model of the plant and controller, for open loop and closed loop response. Figure 5.27b displays the implemented controller bode response plot.

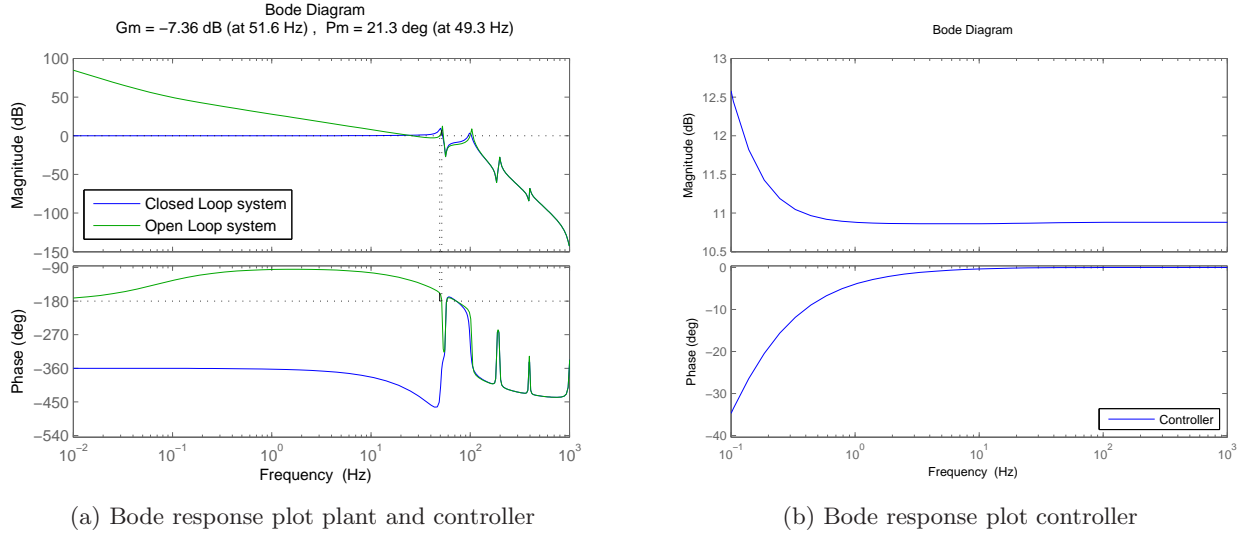


Figure 5.27 – Closed loop system unstable response at 52 [Hz] ($K_d = 0.6$), using position feedback.

From the open loop system response in Figure 5.28a it is possible to determine stability of the system, by calculating its gain and phase margin. The *gain margin*, corresponds to the value that the controller gain can be increased before system instability occurs. The *phase margin*, is the difference in phase between the open loop system and the -180 degrees when the magnitude of the open loop system $|CH(j\omega)| = 1$. A positive phase margin is needed for system stability [5].

The gain margin of the open loop damped system is -7.36 [dB] at 51.5 [Hz], and the phase margin is 21.3 [deg] at 49.3 [Hz]. As a result it is concluded that the damped system becomes unstable at frequencies above 50 [Hz]. From Figure 5.28a is concluded

that the gain margin is 1.23 [dB] at 41.7 [Hz], and the phase margin is 4.1 [deg] at 34.7 [Hz]. The system is stable. However the error between reference and feedback signal in the time domain increases to 3.5 [%] at 5 [Hz].

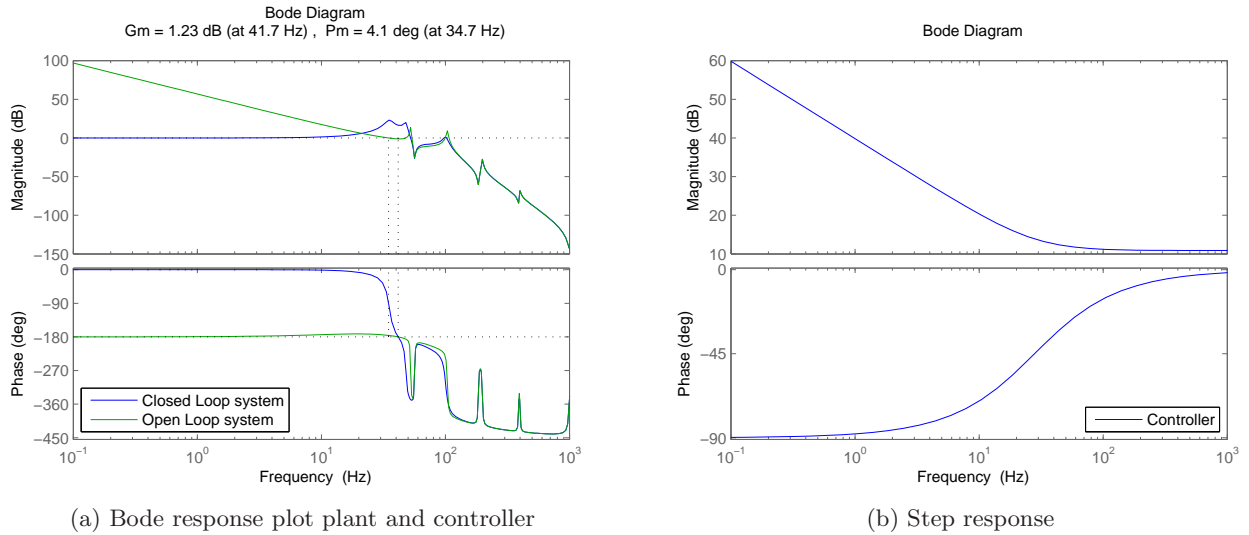


Figure 5.28 – Closed loop system stable response ($K_d = 0$), using position feedback.

Figure 5.28a presents the closed loop and open loop frequency response of the total system, including controller. The effect of the controller on the closed loop system, is that the -20 [dB/decade] slope of the open loop system is results into a 0 [dB/decade] slope. The obtained bandwidth of the closed loop system is 53 [Hz]. The bandwidth is specified as the -3 [dB] crossing of the magnitude from the closed loop system. The step time of the system is 0.576 seconds. It is possible to improve the system performance, because the system became unstable due to its eigenfrequencies. A recommendation for further research, is to apply a lag filter to damp out the eigenfrequencies of the system.

Force control model

Force control uses the applied force on TA as feedback signal. This force is measured in test setups using a load cell between HA and TA. To obtain the controller setting for force control, *frequency domain tuning* was used. This because the *time domain tuning* did not provide reasonable tracking performance at 5 [Hz]. Obtained closed loop, open loop and controller frequency response are presented in Figure 5.29.

5.4. Controller Models

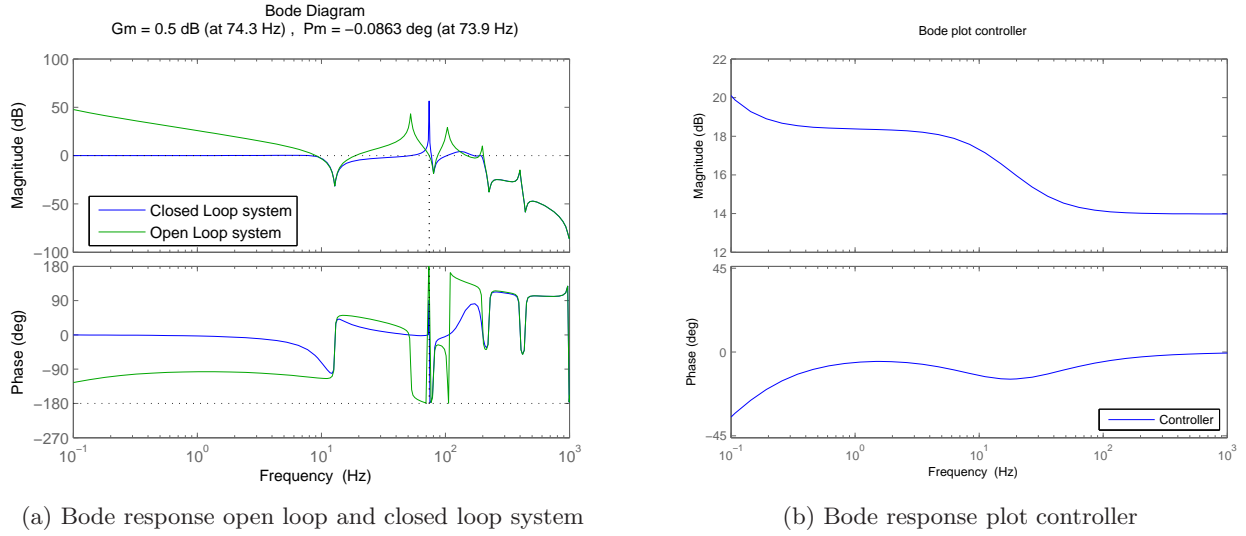


Figure 5.29 – Closed loop system frequency responses, using force feedback.

The applied parameters for the time domain and frequency domain analyses are:

Reference Amplitude	R_A	0.62	[V]
Reference frequency	R_f	5	[Hz]
Proportional gain	K_p	5	[-]
Integration gain	K_i	2.5	[-]
Differentiation gain	K_d	0.3	[-]

To obtain a measure for stability of the force controlled system, the gain and phase margin are analysed. To obtain a measure for the performance the closed loop bandwidth of the system is analyzed. The gain margin of the open loop system is 0.5 dB at 74.3 [Hz]. The phase margin is -0.08 deg at 73.9 [Hz]. It is therefore concluded that instability occurs at 74 [Hz]. The tuning of the force controller is very challenging with this controller, since a resonance peak occurred at 74 [Hz] in the closed loop response. It was not possible to reduce this peak with the current controller tuning. Therefore there is room for improvement in the system control.

The bandwidth of the closed loop system is 10 [Hz], which is much smaller than the bandwidth of the position controlled system. Limitation of this bandwidth caused by the anti-resonance occurring at 12.8 [Hz]. Bandwidth could be increased by designing a new controller, which filters out the anti-resonance of the plant at 12.8 [Hz], see Figure 5.29a. Design of a new controller is not performed in this thesis, but is an option to include in further research.

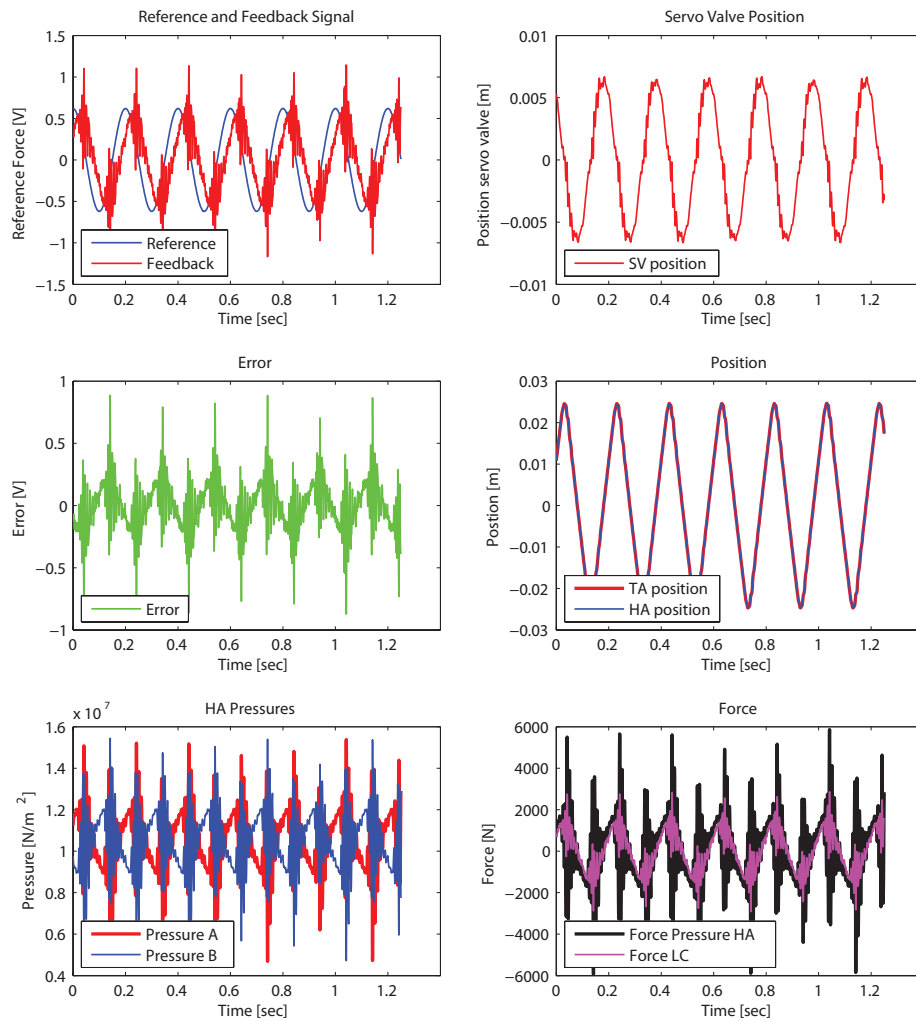


Figure 5.30 – Closed loop position control time responses.

Figure 5.30 shows the obtained time responses from the controller tuning. A large error between reference and feedback signal is present. This is due to the phase shift between these responses, and the resonances occurring. The resonance occur because of friction. The phase shift is present because of the low eigenfrequency of the mechanical system, therefore the phase delay starts sooner then in the position controlled system. If friction is not present it is possible to reduce the error significantly till 3 [%]. This was gained by time domain tuning.

This section treated the controller tuning for the worst case, with a reference signal of 5 [Hz] and 80 [%] oil flow through the servo valve. During the controller tuning it is noticed that the for lower frequencies better results were obtained, resulting in smaller errors. It is also noticed that change of friction parameters does change the controller settings a lot. Which indicates that it is hard to develop robust control for multiple friction settings. Especially Coulomb and static friction are of importance, since they introduce resonances. Mechanical play is neglected in the tuning of the controllers. A study on the robust control of test setups could be a topic for future research.

5.5 Summary

5.5.1 Summary Mechanical modelling

The section mechanical modelling presented the state space modelling methods to describe the dynamic behaviour of a mechanical system. FE modelling will be used to obtain the full structural test setup model. The dynamic state space model is obtained from a modal state space representation of the TA. An important mechanical connection in fatigue testing setups are IS. IS connect the HA with the TA and therefore transmit the loading from the HA to the TA. Mechanical play disturbs the load transmission through IS, because free movement creates an impulse force on the TA which is an uncontrolled loading. Uncontrolled loading is unwanted in fatigue testing and can damage the TA.

5.5.2 Summary Servo-Hydraulic modelling

The section servo-hydraulic modelling presented models to model the HA and SV. The dynamic behaviour of a hydraulic actuator and its eigenfrequency calculation were presented. Friction models parameters are hard to obtain and the best option is to measure them. An first estimated friction curve from the measurements was included. Servo valve models were generated by modelling the pressure dynamics and motion dynamics. The nominal flow of the model was checked if this correspond to the nominal flow of the manufacturer. Finally, frequency response functions were calculated, characterizing the frequency dependent behaviour of the servo valve. This section ended with the coupling of the hydraulic actuator model with the servo valve model, which obtained the frequency response of the servo-hydraulic system.

5.5.3 Summary Coupling Mechanical system with Servo-Hydraulic system

In this section obtained the coupled system behaviour of the mechanical system and hydraulic system. Time simulations showed the time response of this system. Finally linearized models were obtained showing the frequency dependent behaviour, these models were used in the controller modelling section.

5.5.4 Summary Controller modelling

The chapter ended with the implementation of a controller. Control is needed since servo-hydraulic systems are marginal stable. To stabilize and to track reference signals a controller is implemented. Tuning in of the controller is performed using either *Time domain tuning* or *Frequency domain tuning*. Stability was analysed on the basis of, gain margin and phase margin. It was noticed that the resonances in the high frequency part, can obtain unstable response if the controller is tuned. Time domain analyses showed the effect of friction in the models. To obtain a measure for the exact system performance these models have to be verified. The models used are a first estimation for the demonstration test setup. Therefore there is room for improvement of the performance of the models.

CHAPTER

6

MEASUREMENTS AND VERIFICATION ON DEMONSTRATION TEST SETUP

The previous chapter discussed the modelling of structural test setups. Models of the mechanical system, hydraulic system and control system of the demonstration test setup were obtained. The objective of this chapter is to verify the modelling of the demonstration test setup to prove the capability of modelling structural test setups, for analyzing its system performance.

Measurements need to be performed to verify the simulation models, that predict system behaviour and performance. Assumptions made in the modelling can be verified and updated. This will result in better model development in the future. This chapter will present the performed measurements and results for demonstration test setup modelling model verification. Verification will be performed in two manners:

- *Component verification*, each component itself is verified to characterize component behaviour.
- *Coupled verification*, components are coupled to systems to characterize full system behaviour.

In order to correlate the model and measurements, model updating will be performed and will subsequently also be a topic of discussion in this chapter. Like in the previous chapter, this chapter is divided in to four sections:

- Mechanical system measurements and verification.
- Hydraulic system measurements and verification.
- Coupled mechanical and hydraulic system measurements and verification.
- Control system measurements and verification.

The components of the different systems are presented in Figure 6.1.

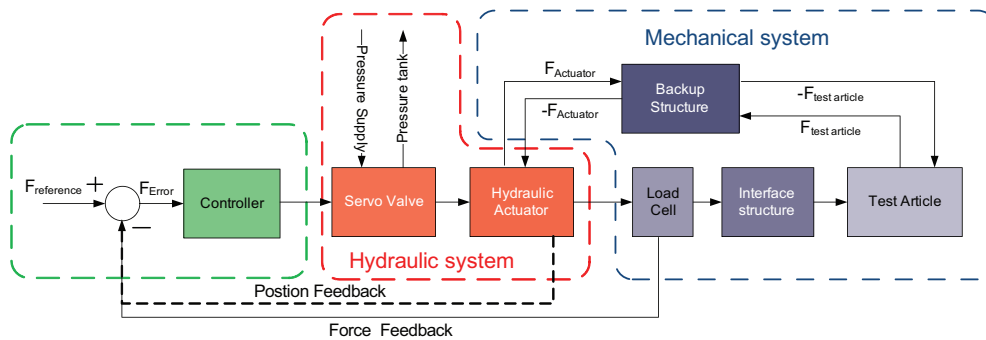


Figure 6.1 – Block description of the demonstration test set-up

6.1 Mechanical System Measurements and Verification

This section describes the measurement and verification of the mechanical system model of Section 5.1. First the measurement layout is presented. Thereafter measurement results are presented and discussed. This section concludes with the updating of the mechanical model.

6.1.1 Measurement Layout

The measurement layout for the verification of the test article modelling is presented in Figure 6.2. Verification will be performed using Experimental Modal Analysis (EMA). EMA was performed using an impact hammer and an accelerometer, see Figure 6.2. Measurements were performed in the X direction, because the HA will be coupled in this direction. The system is excited on different locations using the impact hammer and responses are measured. The Frequency Response Functions (FRFs) between the impact hammer and the accelerometer are calculated. From these FRFs eigenfrequencies and eigenmodes are extracted by using experimental modal analysis. The system is analysed till 500 Hz, to ensure that the first four eigenmodes can be identified.

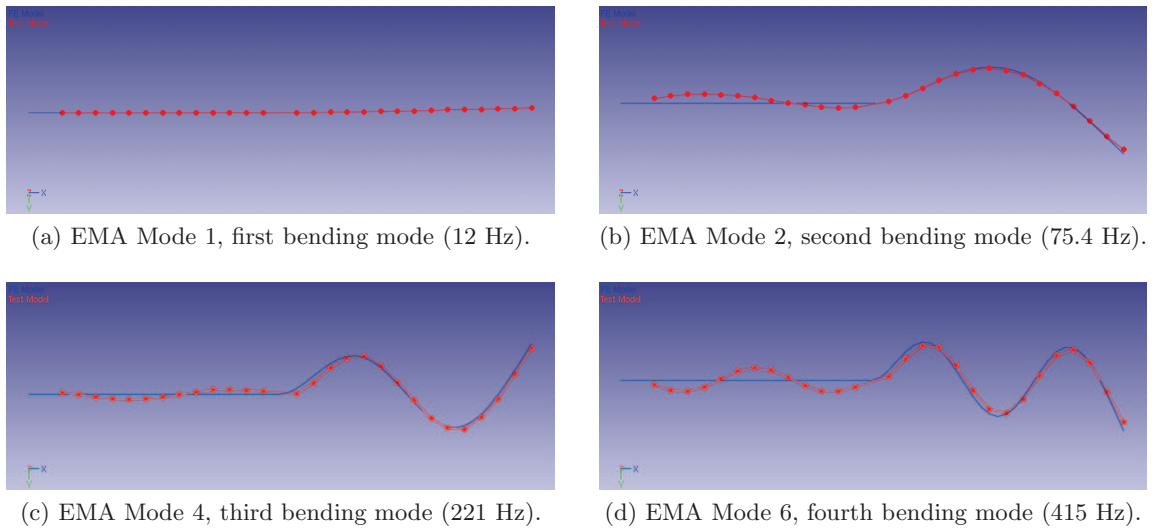


Figure 6.3 – First four modes of EMA analysis, showing the Abaqus analysis (in blue) and measured modes (in red).

FE modes Y direction		EMA modes Y direction			
Mode number	Freq [Hz]	1	2	3	4
		12	75.4	221	415
1. 1st bending	12.81	99.1	0.9	0.3	0.9
2. 2nd bending	81.55	0.1	91.9	0.2	0.1
3. 3rd bending	224.79	1.6	0	96.9	0.2
4. 4th bending	438.88	1.2	0.3	3.5	88.9

Table 6.1 – MAC table, correlating modes between FE ABAQUS analysis and EMA analysis.

Table 6.1 presents the MAC results, related to the eigenfrequency results of the EMA analysis and the FE analysis. From Table 6.1 it is concluded that the experimental modes correlate good with the modelled modes. Especially the first three modes correlate good, because , all values are above 90. The fourth mode has almost a value of 90. A better correlation will be obtained if the rear section is neglected. From the obtained eigenfrequencies is concluded that the eigenfrequencies of the model are higher then the measurement. Since the clamping is not ideal, model updating is needed. The model updating is presented in the next section.

6.1.3 Mechanical System Model Updating

The results in previous section presented the correlation of the eigenmodes between measurement and FE analysis. The eigenfrequencies measured are not the same as the modelled eigenfrequencies. Table 6.2 presents the differences between the modelled eigenfrequencies and the measured eigenfrequencies.

FE Analysis [Hz]		EMA Analysis		Error [%]	
Matlab	Abaqus	EMA [Hz]	Damp [%]	Matlab	Abaqus
12.81	12.81	12	0.23	6.75	6.74
80.31	80.17	75,4	0.126	6.51	6.33
224.9	224.23	221	0.79	1.76	1.46
440.7	438.88	422	2.18	4.43	4.00

Table 6.2 – Error calculation between eigenfrequencies of FE analysis and EMA analysis.

From Table 6.2 is concluded that the error between the modelled and the measured eigenfrequency is relatively large, especially the first eigenfrequency. The discrepancy factors caused by: the mass, cross sectional dimensions, inertia and elasticity modulus were excluded. The clamped length could therefore be a modelling error. Furthermore it is not possible to obtain an rigid clamping in reality, by using clamping blocks. Deriving the relation between the eigenfrequencies and the physical properties of the beam, it is possible to obtain an equation of the eigenfrequency with respect to the clamped length. This Equation is presented in Equation 6.1.3. Derivation of Equation 6.1.3 is provided in Appendix G.1.

$$\frac{\Delta\omega}{\omega_{ref}} = -2\frac{\Delta L}{L_{ref}}$$

$\Delta\omega$	Difference in frequency between experiment and FE model	[rad/s]
ω_{ref}	Reference frequency experiment	[rad/s]
ΔL	Difference in clamping length of beam	[m]
L_{ref}	Reference length of beam	[m]

By applying Equation 6.1.3 to the FE MATLAB model, the error between measured eigenfrequency and modelled eigenfrequency was significantly reduced by updating the new clamping length ($L_{new} = L_{ref} + \Delta L$), see Table 6.3. A new clamping length $L_{new} = 3.1013$ meter was obtained. From the EMA analysis the amount of damping

present in the structure was obtained. The average damping over the first four bending modes resulted in a damping of 0.83%. This damping value is used as an update for the FE model of the TA. The final obtained frequency response of the TA is presented in Figure 6.4.

Original FE model [Hz]	EMA [Hz]	Updated FE model [Hz]	Updated Error [%]
12.81	12	11.99	0.06
80.31	75.4	75.15	0.33
224.9	221	210.43	4.78
440.7	422	412.37	2.28

Table 6.3 – Updated Matlab FE model results, presenting the obtained error between measurement and FE model.

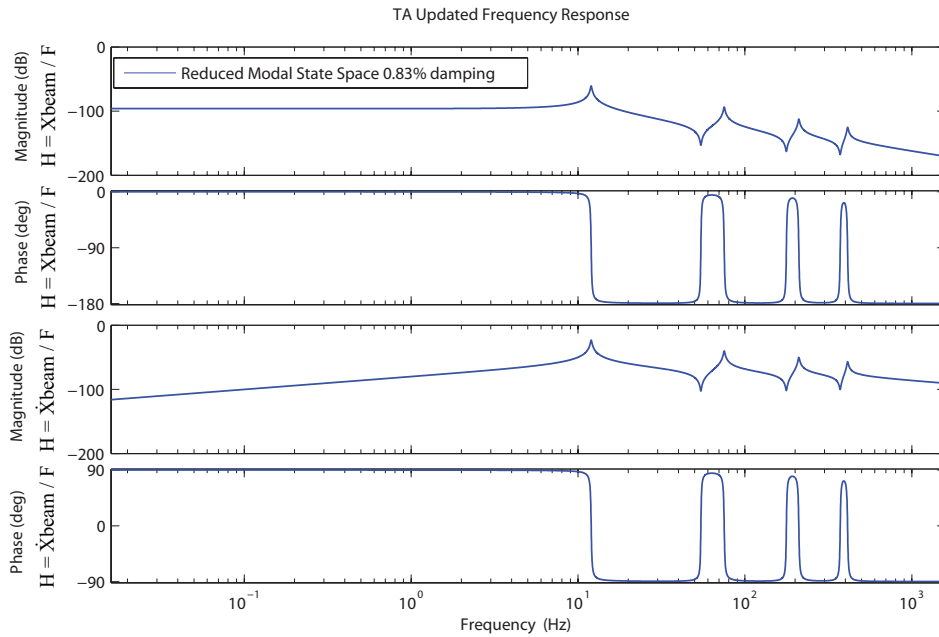


Figure 6.4 – Frequency response of the TA, after updating clamping length and structural damping.

6.1.4 Interface structures

Measuring the pin, coupling bracket and rod diameters resulted in a maximum mechanical play of 0.17 [mm]. The added mass of the IS to the TA was measured and resulted in 10.15 [kg]. This added mass will be included in the model. It was not present on the TA during identification of the eigenfrequencies and eigenmodes. Stiffness and

damping of the IS were calculated, but not measured. Before interface structures can be included in the modelling it is recommended to measure the amount of damping present.

6.2 Servo-Hydraulic measurements and verification

Section 5.2.3 presented the modelling of the servo-hydraulic system. This section presents the measurement and verification of these servo-hydraulic models and is divided in three main sections, namely:

- Measurement Layout; discusses the general layout of the measurements performed.
- Servo valve measurements and verification; presents the measured frequency responses of the servo valve.
- Hydraulic actuator measurements and verification; presents the measured frequency response of the hydraulic actuator.

6.2.1 Measurement Layout

The components that will be identified are the servo valve and the hydraulic actuator. A general overview on the the measurement layout is provided in Figure 6.5.

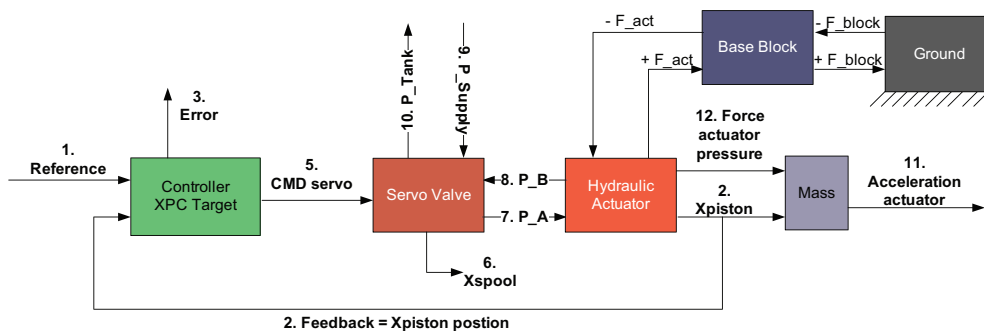


Figure 6.5 – Schematic overview on the hydraulic system measurement setup layout used for the verification of the servo-hydraulic models.

The numbers in Figure 6.5 refer to the channel numbers which are measured. The HA was measured in an uncoupled state, there was no stiffness added to the hydraulic actuator.

Servo Valve Measurements

Servo valve measurements are performed to identify its the open loop frequency response:

$$H_{SV1} = \frac{(6.) \text{ Spool Position}}{(5.) \text{ Command Servo}}$$

Verification of the frequency response, can be achieved in two different manners, namely:

- *Uncoupled state*, the servo valve is not coupled to the hydraulic actuator.
 - Step reference signal.
- *Coupled state*, the servo valve is coupled with the hydraulic actuator.
 - Sinusoidal reference signals 0.125 [Hz], 0.25 [Hz] – 32 [Hz] at 20%,40%,60% and 80% oil flows through the servo valve.
 - Frequency sweep reference signal, 0.125 [Hz] – 200 [Hz].

In the uncoupled state the servo valve is isolated from the hydraulic actuator. Flow from the servo valve to the hydraulic actuator is restricted. In this state the frequency response of the spool in its oil column is measured.

In the coupled state the servo valve is attached to the hydraulic actuator. In this state the servo valve frequency response is determined using different oil flows through the servo valve. This characterization is performed because dynamics of the servo valve is dependent on the amount of flow through the servo valve. Calculation of different reference signals is provided in Appendix F.2.2. The frequency sweep measurement is performed in the coupled state to characterize the servo hydraulic system frequency response.

Hydraulic Actuator Measurements

The objective of hydraulic actuator measurements is to measure its friction and the open loop frequency response characteristics. The Friction is measured using a ramp reference signal. This ramp reference signal determines the velocity of the hydraulic actuator piston. For speeds between 40 – 400 [mm/s], the pressures of the hydraulic actuator chambers were measured and the HA force was calculated. The hydraulic actuator force versus the velocity provides a “Stribeck” friction curve, characterizing the friction in the hydraulic actuator. Further details on the performed measurements can be found in Section 6.2.3. The open loop frequency response of the hydraulic actuator can be characterized by the following transfer functions:

$$H_{SV2} = \frac{(2.) X_{\text{piston}}}{(6.) X_{\text{spool}}}$$

$$H_{HA} = \frac{(12.) \text{ Force Actuator}}{(6.) \text{ Xspool}}$$

The numbers refer back to the numbers in Figure 6.5.

Coupled Hydraulic System Measurements

To verify the coupled hydraulic system frequency response, the coupled state system measurements were used. Transfer functions between the input and output of the hydraulic system are:

$$H_{HS1} = \frac{(2.) \text{ Xpiston}}{(5.) \text{ Command Servo}}$$

$$H_{HS2} = \frac{(12.) \text{ Force Actuator}}{(5.) \text{ Command Servo}}$$

These measured frequency responses are used to verify the linearized models of Section 5.3.

6.2.2 Servo Valve measurements and verification

The servo valve is an important component in the hydraulic system, because it needs to accurately regulate the flow to the hydraulic actuator. The hydraulic actuator depends on the provided flow, the bandwidth of the servo valve is very important. The bandwidth of the hydraulic actuator is dependent on the bandwidth of the servo valve.

Uncoupled Servo Valve Frequency Response Measurements

For the uncoupled measurements, the servo valve flow to the hydraulic actuator was closed. To measure the frequency response of the servo valve, a step reference signal was applied. Measurement settings were:

Step input	10	[mA]
Sample frequency	1000	[Hz]
Number of averages	10	[–]

Figure 6.6 presents the measured frequency response and simulation model frequency responses. The measurements in Figure 6.6 obtained a servo valve bandwidth of 130 [Hz]. This bandwidth was updated to 75 [Hz], which is presented in Figure 6.6. A bandwidth of 75 [Hz] obtains also good phase tracking in comparison to the measurement. The difference in phase between measurement and model above 100 [Hz], is due to sampling rates and Zero Order Hold (ZOH) effects.

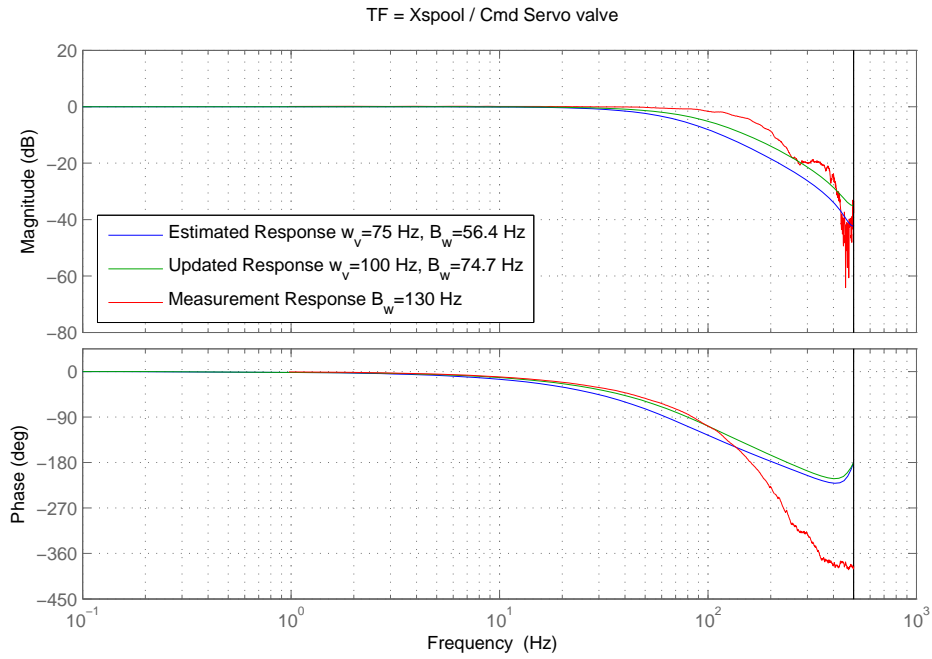


Figure 6.6 – Servo valve frequency response, measured bandwidth = 130 Hz, updated bandwidth model = 74.7 Hz, first estimated bandwidth model = 56.4 Hz.

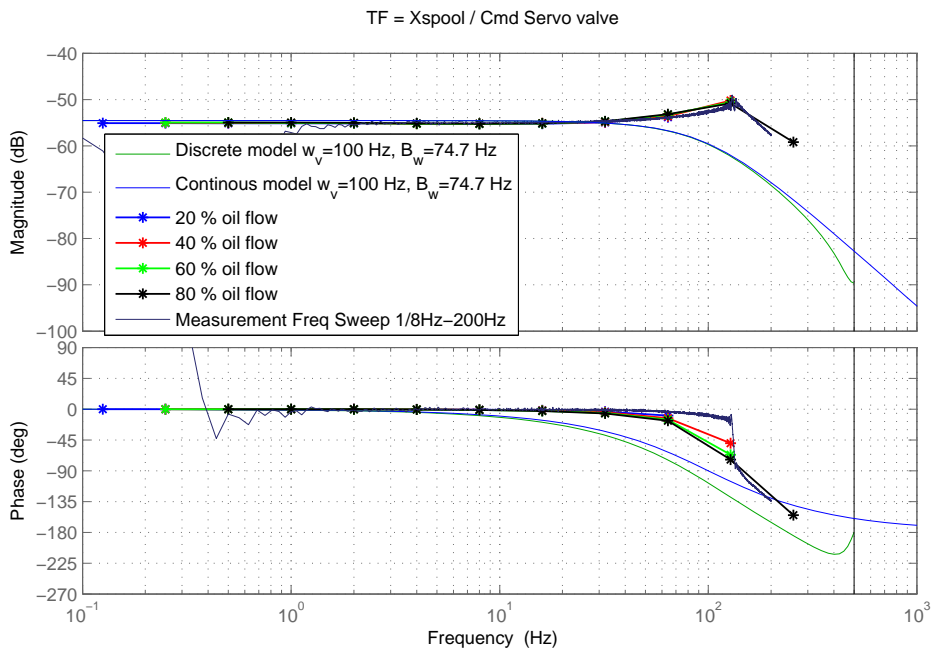


Figure 6.7 – Open Loop frequency response of the servo valve coupled to the HA for the estimated model, updated model and the measurements.

Coupled Servo Valve Frequency Response Measurements

Figure 6.7 presents the frequency response measurements of the servo valve coupled to the HA. The servo valve frequency response was measured for different flow inputs (20 – 80 %) and using a frequency sweep signal.

A difference in magnitude is present between the measurement and first estimation of the linear simulation model (blue), see Figure 6.7. This magnitude difference is due to the signal conditioning units, which scale the servo valve command signal from Volt to Ampere on a range of ± 50 [mA]. The servo valve has a range of ± 40 [mA]. This introduces a servo valve amplification gain of 1.25. An updated response was included (green), see Figure 6.7.

From the measurements it can be seen that at 130 Hz an eigenfrequency peak is present in the measurement signals. This eigenfrequency is due to the hydraulic actuator eigenfrequency.

6.2.3 Hydraulic Actuator measurements and verification

This section describes the measurement results and verification of the hydraulic actuator physical characteristics. First the friction measurements are presented. Thereafter the measured frequency responses are covered both are compared with their simulation models.

Friction measurements

The friction in the hydraulic actuator was measured by moving the actuator at different constant velocities, between 40 – 400 [mm/s]. A constant velocity was generated using a position ramp signal (red), see Figure 6.8. The velocity signal (green) in Figure 6.8 was obtained by differentiating the position signal.

The friction force in Figure 6.8 was obtained by measuring the pressures in each chamber of the hydraulic actuator. Both pressures are subtracted from each other and multiplied with the piston area, which resulted in the amount of friction. Figure 6.8 highlights the friction positive and negative. It is seen that the friction is not symmetric. This could be due to difference in the friction by the HA seals.

Figure 6.9 presents the measured friction “stribeck-curves”. Three different results were obtained, namely:

- *Single average result*; each measurement one value is chosen which characterizes the friction at a specific velocity.

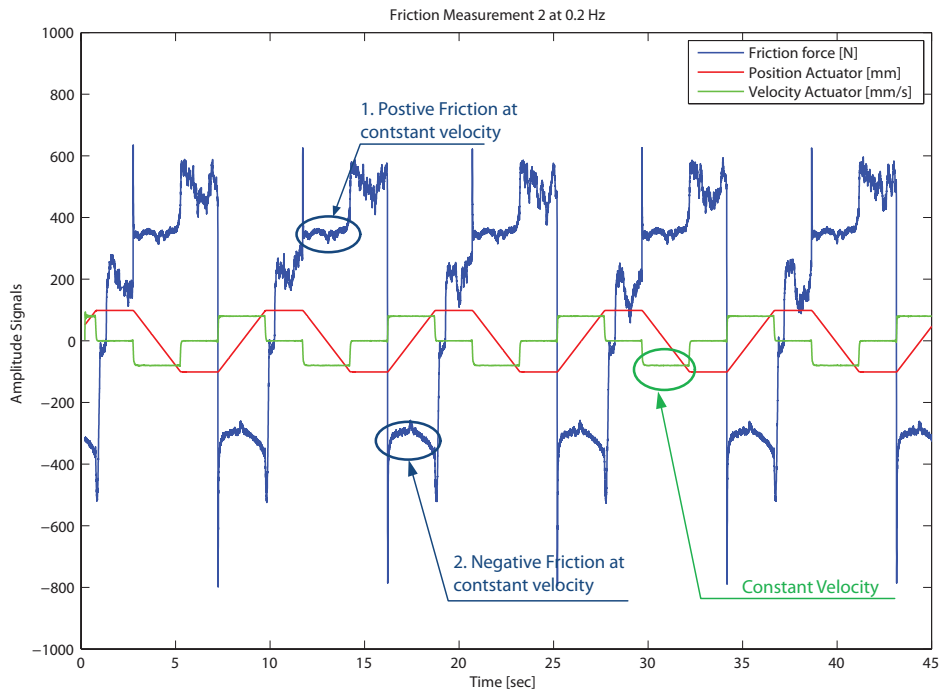


Figure 6.8 – Friction measurement results, presenting the position, velocity and friction force of the hydraulic actuator.

- *Averaged result*; where the friction positive and negative were averaged, creating a non-symmetric friction curve.
- *Symmetric averaged result*; where the friction positive and negative are averaged with each other to obtain a symmetric friction profile.

Figure 6.10 presents the implemented friction model of Section 5.2.1 versus the “*symmetric averaged friction*” model obtained from the measurements. It is concluded that the implemented friction model does not represent the measured friction curve requiring an update of the friction curve. The updating of the friction curve is performed in multiple steps:

- Coulomb friction fit,
- Static friction fit,
- Viscous friction fit.

The different friction curves are presented in Figure 6.10. From the measured friction curve, coulomb friction and viscous friction could be well estimated. The static friction did not have a good estimation because measurements with a velocity below 40 [mm/s]

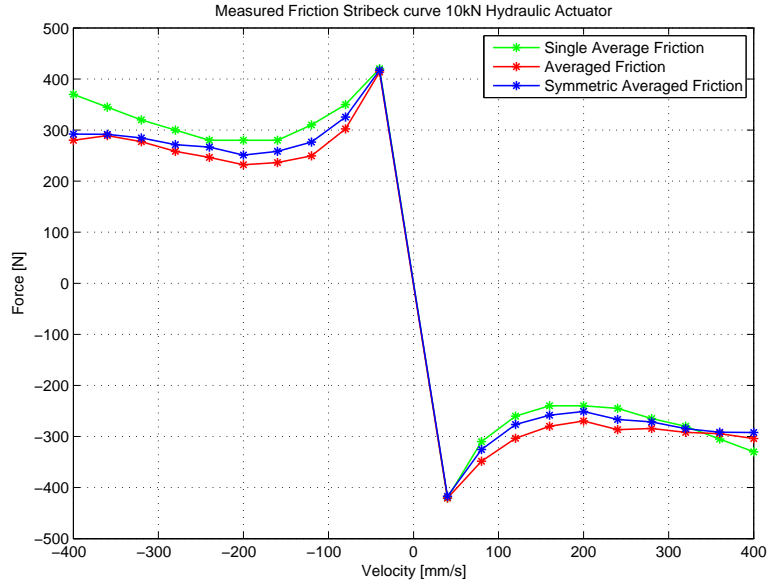


Figure 6.9 – Measured Friction curve, showing a non averaged and averaged friction curve.

need still to be performed to obtain better results. Updating of the friction model resulted in the following parameters:

Coulomb friction	F_{c0}	250	[N]
Viscous friction	F_{v0}	105	[N s/m]
Static friction	F_{s0}	650	[N]
Linear transition	\dot{x}_{min}	22.8571	[s/m]
Linear velocity threshold	\dot{x}_{th}	$1 \cdot 10^{-4}$	[m/s]

Hydraulic Actuator Frequency Response measurements

This section discusses the obtained results from the frequency response measurements of the hydraulic actuator compared with the modelling results.

To compare linear models with the measured frequency responses the linear model is updated using the new viscous friction parameter. The only uncertain parameter in the hydraulic actuator model is the dead oil volume of the HA, which is influenced by the eigenfrequency of the HA, see Equations (5.2.1) and (5.2.1) in Section 5.2.1. The eigenfrequency of the hydraulic actuator is obtained by calculating the Auto Power Spectrum (APS) of the hydraulic actuator rod acceleration, see Figure 6.11. The APS displays the amount of energy present at each frequency. Figure 6.11 shows that the hydraulic actuator eigenfrequency is present at 130 [Hz].

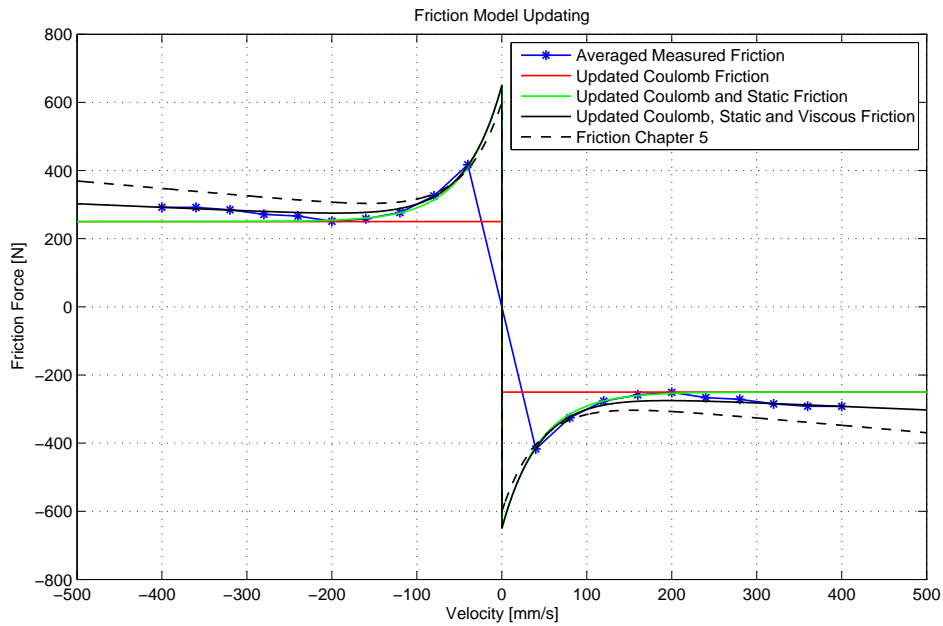


Figure 6.10 – Updated coulomb, static and viscous friction model versus the measured friction model.

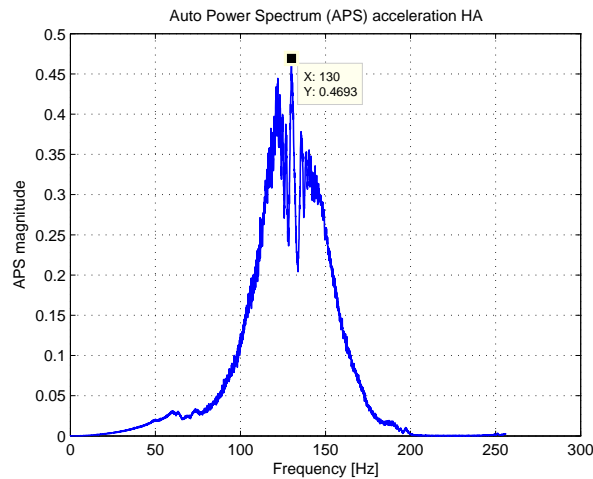


Figure 6.11 – Measured auto power spectrum of HA, showing the eigenfrequency of the HA at 130 [Hz].

Using the eigenfrequency of the HA it is possible to recalculate dead oil volume of the stiffness Equation 5.2.1. The eigenfrequency is also dependent on the mass of the hydraulic actuator. This mass was calculated. It is possible to tune both the mass and the dead volume. It was chosen to tune the dead volume, which resulted in:

6.2. Servo-Hydraulic measurements and verification

Dead volume in oil supply pipe lines	V_l	$7.42 \cdot 10^{-5}$	$[\text{m}^3]$
Mass of hydraulic actuator	M_{act}	11.086	$[\text{kg}]$

Figure 6.12 presents the measured open loop frequency response between the piston position and the valve position. The magnitude shows good correlation with the model up to 40 [Hz], where the phase shows much more delay at higher frequencies. The magnitude of the measurement at the eigenfrequency lower then the discrete linearized model. Therefore more damping is present in the real system then that the discrete linearized model predicts.

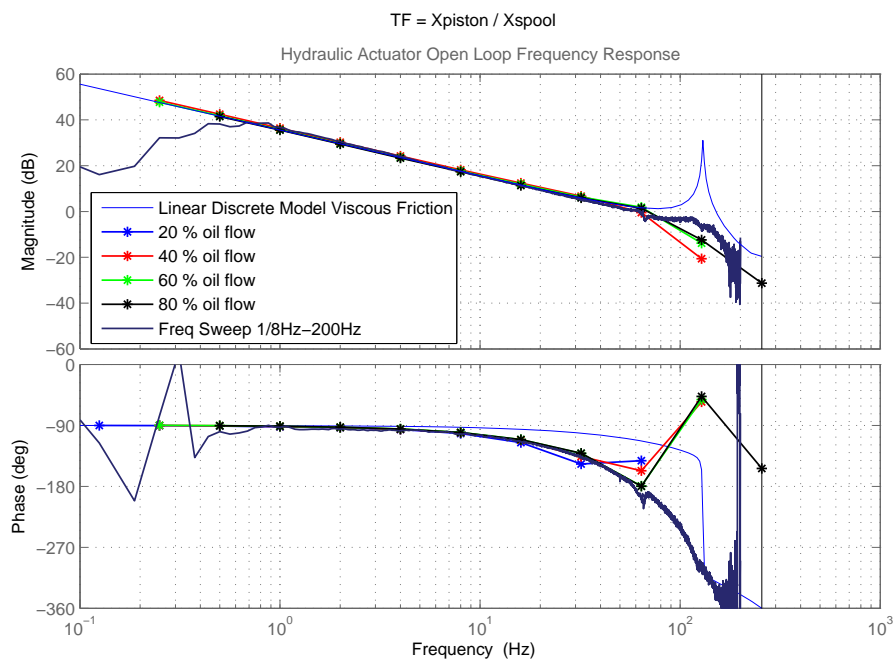


Figure 6.12 – Updated frequency response between piston position and spool position.

Figure 6.13 presents the measured results between the force of the actuator and the valve spool position. The force of the actuator is calculated by the pressure difference of the hydraulic actuator chambers. From the magnitude in Figure 6.13 can be concluded that the measurements has the same trend as the linear model, but the magnitude does not match. This is due to the fact that non-linear coulomb and static friction are not taken into account by the linear model. Which is identified by simulation of the non-linear model in time domain, and thereafter calculate the magnitude and phase of the simulation in the frequency domain. Which is done for the non-linear model with 40 [%] oil flow. The frequency response of this non-linear model is displayed in Figure 6.13.

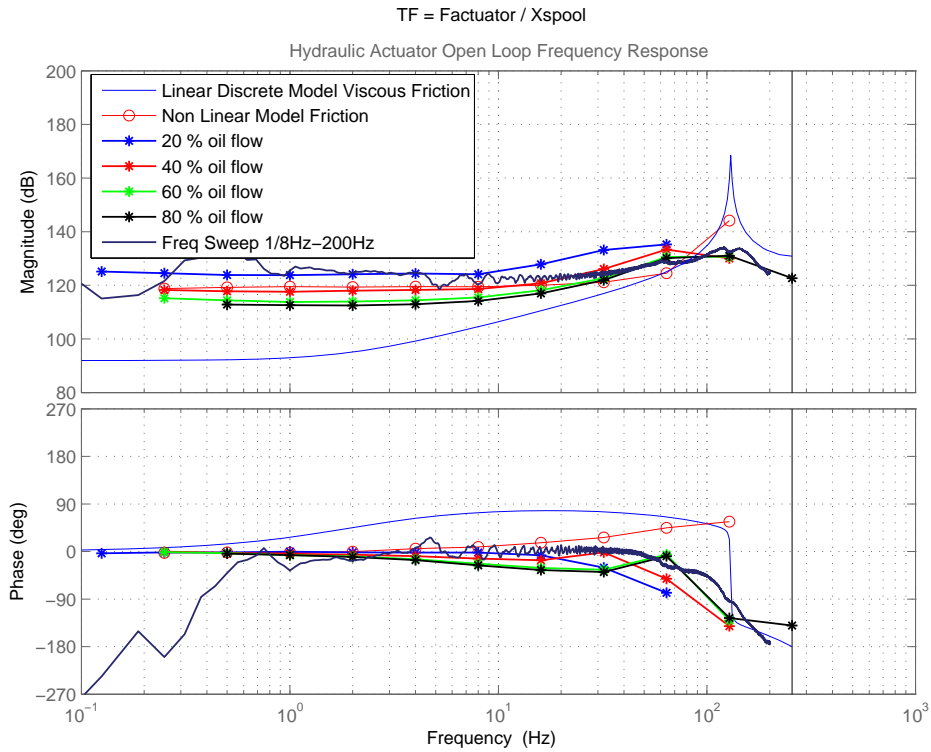


Figure 6.13 – Updated frequency response of FRF between force actuator and spool position.

Figure 6.13 shows that the measured 40 percent oil flow and modelled non-linear 40 percent oil flow model show the same trend at frequencies up to 16 Hz. The magnitude of the model has still a small error with the measurement, which is a factor of 1.0528. The difference in real friction and modelled friction has a factor of 1.0435, see Figure 6.10. This clarifies the difference between model and measurement. Simulations and measurements are performed at a piston velocity of 121 [mm/s]. The difference between model and measurement above 16 Hz is accepted in this Frequency Response (FR), since the force calculated by the pressure difference is not used for control.

In general frequency response functions which include the force of the actuator by calculating the pressure difference, are hard to characterize because the force is dependent on the friction of the actuator. Therefore it is not advisable to control the actuator on the force calculated by pressure difference, but on the force measured by a load cell.

6.2.4 Servo-Hydraulic System Measurement and Verification

Using the open loop measurements of the hydraulic actuator and servo valve it is possible to verify the coupled servo-hydraulic system response. Figure 6.14 and Figure 6.15 present the coupled hydraulic system frequency response.

From Figure 6.14 is concluded that the frequency sweep measurement obtain good verification up to 150 Hz with the linear model. From the frequency sweep is seen that a phase shift is present at 130 Hz, which is the eigenfrequency of the HA. Figure 6.14 represents the servo-hydraulic system model of the demonstration test setup.

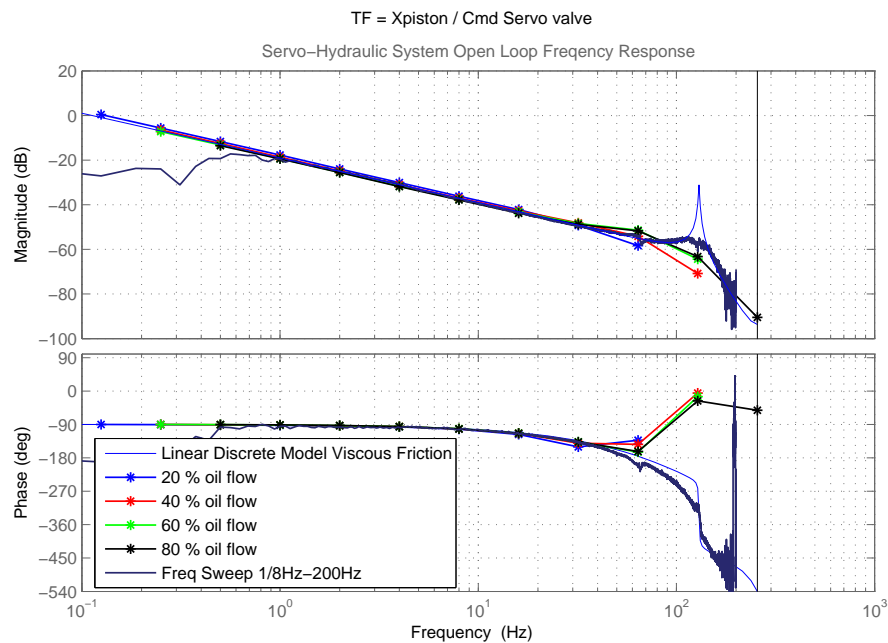


Figure 6.14 – Open Loop frequency response of the hydraulic system, between piston position output and servo valve current input.

The frequency response between the force of the hydraulic actuator and the servo valve command is presented in Figure 6.15. The linear model has discrepancy at low frequencies with respect the measurement, since Coulomb and static friction are not taken into account. This results in a large magnitude difference at low frequencies, see Figure 6.15. Actuator force frequency response model will only be used for characterization of the friction response, between model and measurement. The non-linear model which includes friction does represent the measurement up to 16 Hz, in Figure 6.15.

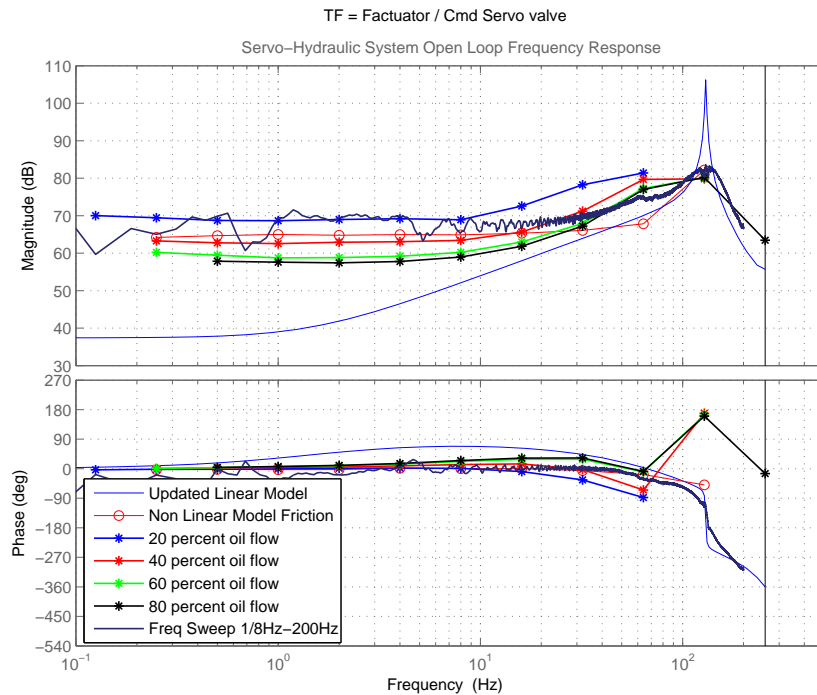


Figure 6.15 – Open loop frequency response of HA, between force actuator and servo valve command.

6.3 Coupled Mechanical System and Hydraulic System Measurement and Verification

This section will focus on the measurement and verification of the coupled system between hydraulic system and mechanical system. The open loop model characteristics presented in Section 5.3. The open loop coupled system defines the plant model used for the control loop. The objective of this section is the measurement and verification of the coupled system dynamics which represents the plant model in the total system architecture.

6.3.1 Measurement Layout

The measurements are performed with the following configurations:

- *Position feedback configuration*, where the piston position provides feedback for the controller.
- *Force feedback configuration*, where the load cell provides force feedback to the controller.

The focus of this section will be on verifying the following transfer functions:

6.3. Coupled Mechanical System and Hydraulic System Measurement and Verification

- H_{HS-MS1} = Piston position / Command Servo Valve,
- H_{HS-MS2} = Force Load Cell / Command Servo Valve.

These transfer functions describe the open loop behaviour of the plant model in the control loop. The linear transfer functions of the simulation model are used for controller modelling. The next subsections describe the measurement configurations used to measure the frequency responses.

Measurement Layout Coupled System using Position Feedback

Figure 6.16 presents the position feedback configuration and its measurement signals. The signals 1 – 13 are measured. The conversion from the controller output (signal 4) to the servo valve input (signal 5) is not displayed.

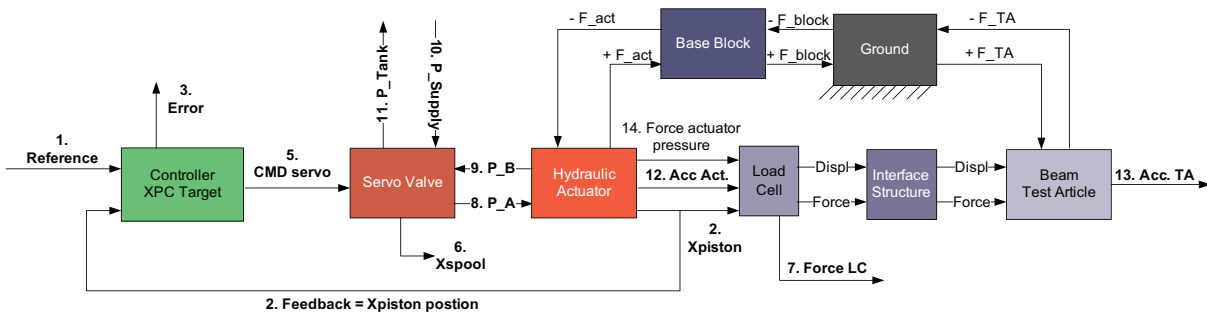


Figure 6.16 – Measurement signals of the coupled system using position feedback.

Measurements performed in the position feedback configuration are:

- Sinusoidal reference signals 0.25 [Hz], 0.5 [Hz] - maximal 128 [Hz] at 20%, 40%, 60% and 80% oil flows through the servo valve.
- Frequency sweep reference signal, 0.125 Hz – 128 Hz.

Controller tuning is performed on the demonstration test setup itself. At each sinusoidal signal the controller parameters were tuned. The frequency sweep measurement was performed using a fixed proportional gain as controller setting. Appendix F.3.2 provides the controller settings for each measurement.

Measurement Layout Coupled System using Force Feedback

Figure 6.17 presents the closed loop force feedback configuration and its measurement signals. For the force controlled sinusoidal measurements, it was not possible to measure frequencies of and above 8 [Hz], because the first anti-resonance in the force FRF is present at 8.7 [Hz]. It was not possible to obtain a stable system response, for

frequencies close to the anti-resonance. To measure the response above 8 [Hz] a frequency sweep measurement was performed up to 128 [Hz], using a fixed proportional gain. Measurement and controller settings are provided in Appendix F.3.3.

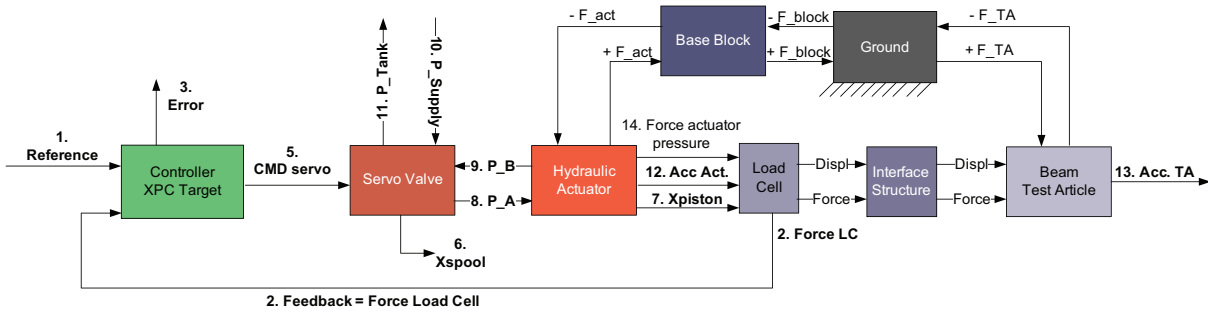


Figure 6.17 – Measurement signals of coupled system using force feedback.

6.3.2 Position Coupled System Measurement and Verification

Figure 6.18 presents the open loop frequency response between the piston position and the servo valve command signals.

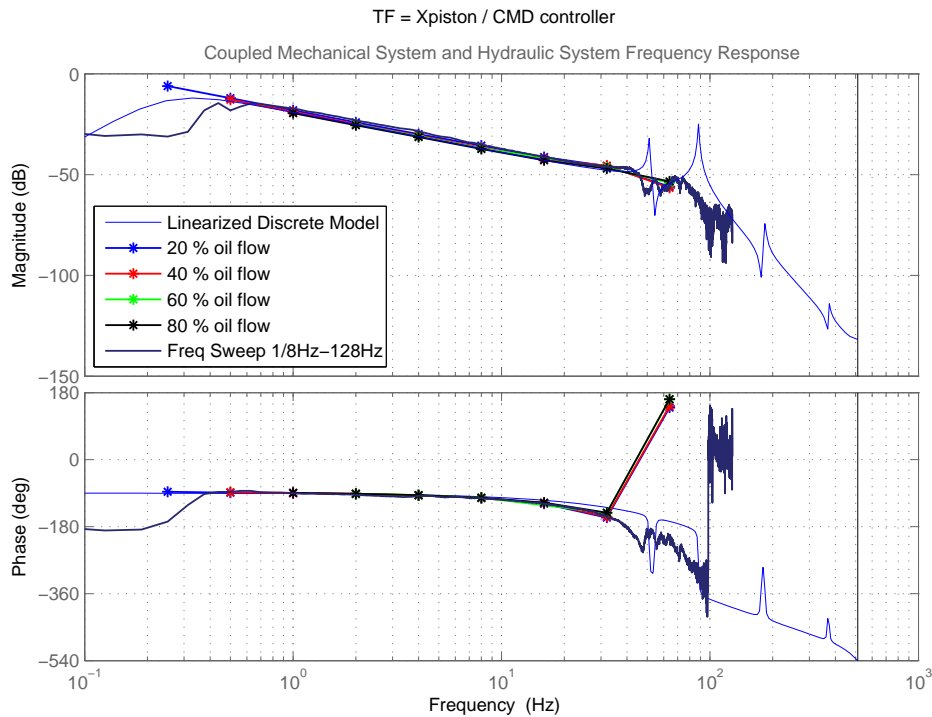


Figure 6.18 – Coupled system frequency response between piston position and command servo valve, where position feedback was used.

6.3. Coupled Mechanical System and Hydraulic System Measurement and Verification

It is concluded that the magnitude frequency response of the measurement matches the frequency response of the linear model up to 40 Hz. The phase response of the linear model matches the measurements up to 10 Hz. At frequencies above 10 Hz the phase response of the measurement shows more delay than the phase response of the linear model. This indicates that in the real system more damping is present.

Figure 6.19 presents the measured frequency response between the force of the load cell and the servo valve command signals. The measurements were performed using position feedback configuration.

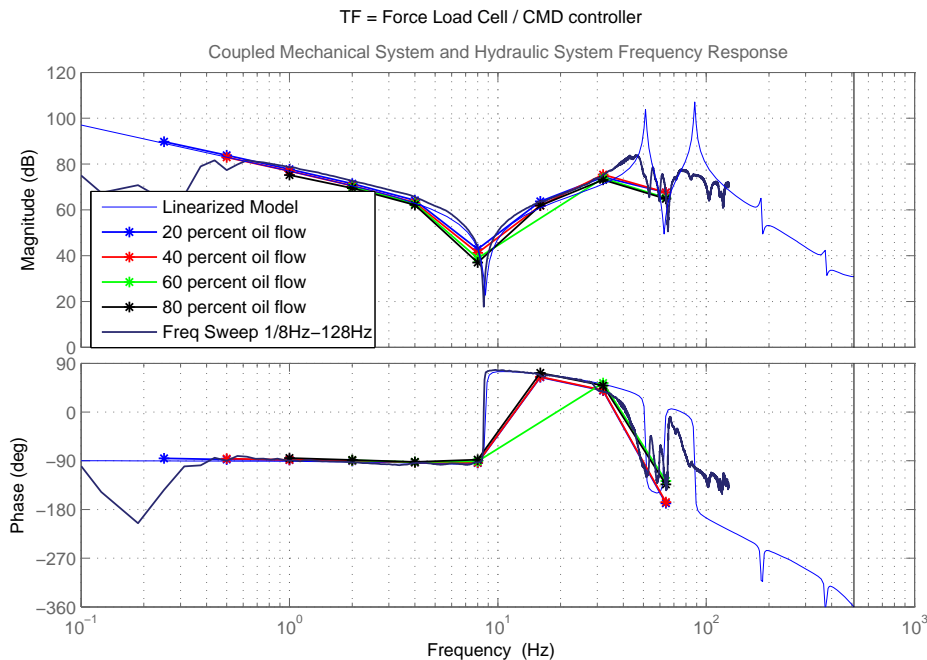


Figure 6.19 – Coupled system frequency response between load cell force and command servo valve, using position feedback configuration.

It is concluded that the measurements show good correlation with the model up to 40 [Hz], including the first eigenfrequency of the TA. It is not possible to compare the higher order dynamics between measurement and model, because the measurement showed a lot more damping than the linear model. The first anti-resonance in Figure 6.19 showed good correlation with the model. The difference between model and measurement is 1.8 [%]. The measurement of 16 [Hz] at 60 [%] oil flow was not included in Figure 6.19, because it appeared to be a wrong measurement.

6.3.3 Force Coupled System Measurement and Verification

This section presents the results obtained from the measurements performed using the force feedback loop (see Figure 6.17). Figure 6.20 presents the verification of the open loop frequency response, between the load cell force and the servo valve command signal. From Figure 6.20 is concluded that the measured sinusoidal responses represent the linear model. The frequency sweep measurement obtained good results up to 40 [Hz]. Above 40 [Hz] the measurement did not show reasonable correlation with the linear model.

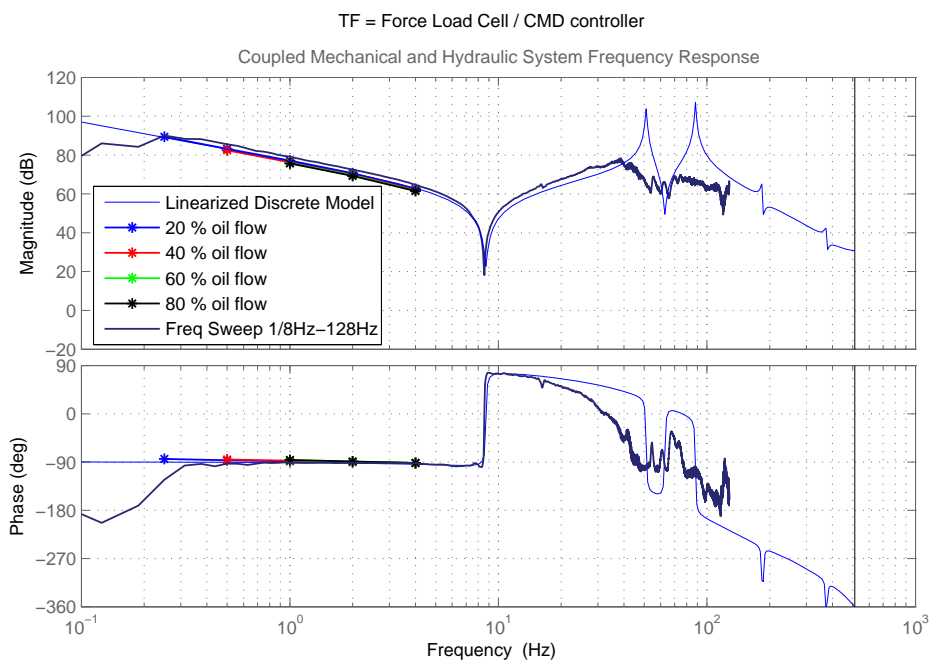


Figure 6.20 – Coupled system open loop frequency response between force load cell and Servo valve command signals, using force feedback loop.

Figure 6.21 presents the frequency response between the piston position and the servo valve command signal. The strange behaviour of the model at low frequencies till 0.5 [Hz] is due to the discretization of the linear model. It is concluded that:

- $H = \text{piston position} / \text{servo valve command}$, correlates the linear model up to 40 Hz.
- $H = \text{force actuator} / \text{servo valve command}$, correlates the linear model up to 40 Hz.

6.4. Verification of Controller Parameters

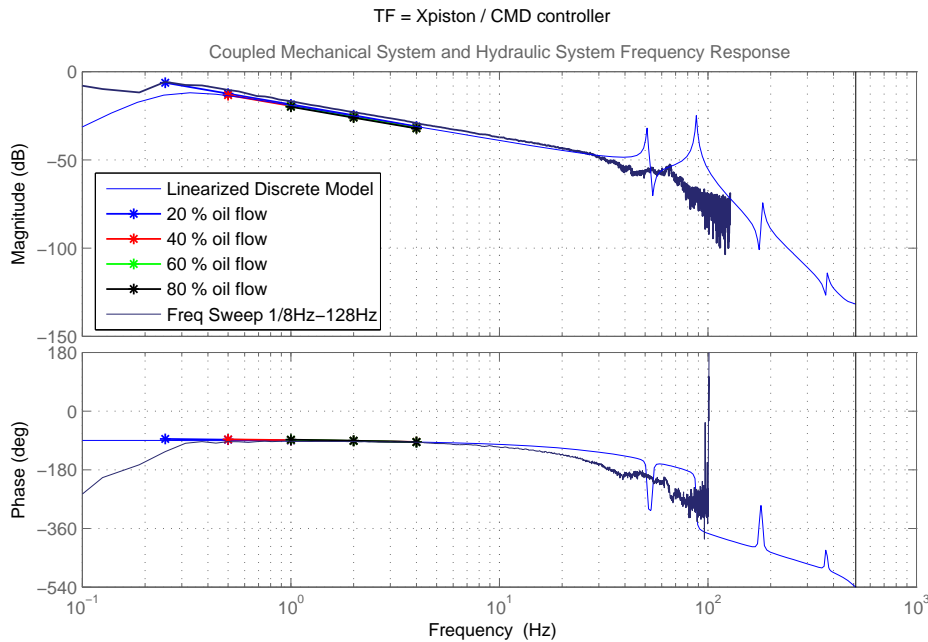


Figure 6.21 – Coupled system open loop frequency response between piston position and servo valve command signals, using force feedback loop.

The force output frequency response the difference between the measured and modelled first eigenfrequency is 1.8 %. From these results it is concluded that no further model updating will be performed, since there are no uncertain parameters any more to perform updating.

6.4 Verification of Controller Parameters

Previous section presented the open-loop system models of the coupled mechanical and hydraulic system. This section presents the closed loop measurement and verification of the full system model.

This section is divided into four subsections. First the measurement layout is presented, followed by the open loop controller model verification. The closed loop measurement is then verified using position feedback. Followed by the verification of the force feedback controlled system.

6.4.1 Measurement Strategy

The measurements were performed using the same measurement layout presented in Figure 6.22. The objective is to measure and verify the frequency responses of:

6.4. Verification of Controller Parameters

errors.

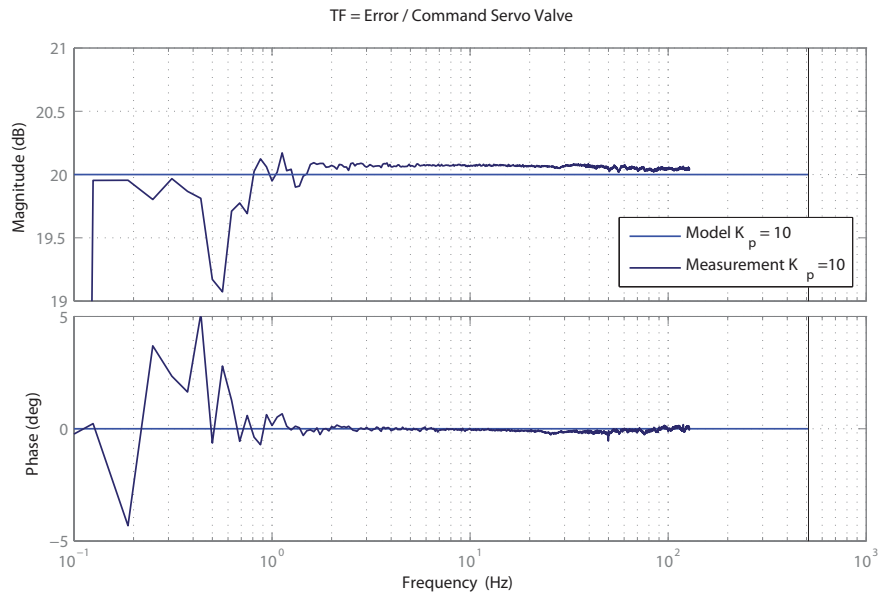


Figure 6.23 – Open loop frequency responses of the controller and simulation, using the position feedback configuration.

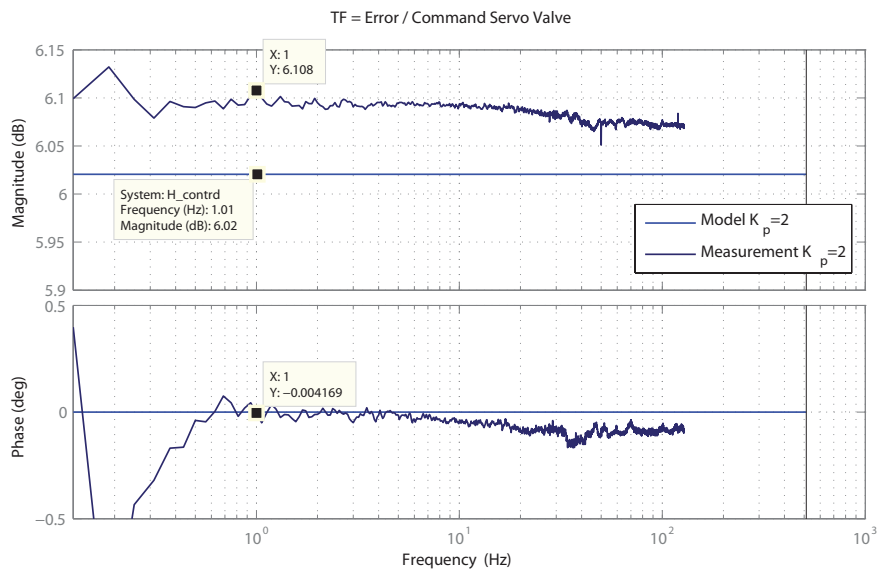


Figure 6.24 – Open loop frequency response of the controller and simulation, using force feedback configuration.

Figure 6.24 presents the open loop verification of the controller model using force feedback configuration, with a proportional gain $K_p = 2$. Below 0.5 [Hz], there is a discrepancy between model and measurement, because of measurement errors. The measurement used an higher sample rate then the position feedback measurement, which resulted into a better measurement of the low frequency content. From these measurements it is concluded that the controller is verified using proportional control.

For future measurements it is also advised to investigate the behaviour of the controller using the integral gain (K_i) and damping gain (K_d).

6.4.3 Position Feedback Measurement and Verification

Figure 6.25 presents the closed loop frequency response between reference signal and feedback signal, using position feedback. To match the frequency response of the measurement with the model a scaling gain in the signal conditioning is present. The signal conditioning is located between voltage output of the controller and current input of the servo valve is present. This scaling gain is for position feedback configuration a factor $K_{conditioning} = 1/20$.

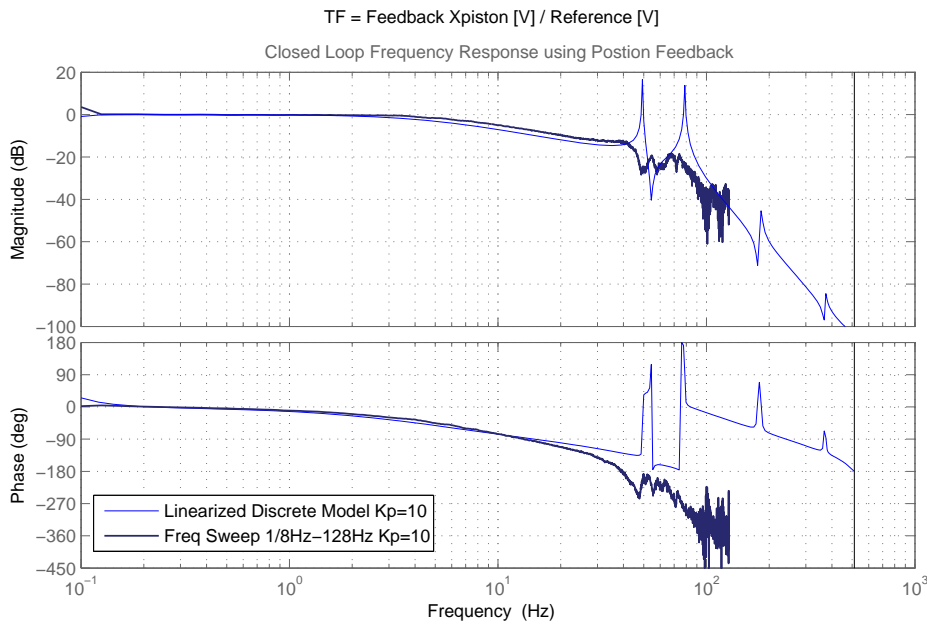


Figure 6.25 – Closed Loop Frequency Response between reference signal and position signal, using position feedback.

From Figure 6.25 is concluded that the magnitude of the linear model represents the frequency sweep measurement up to 40 [Hz]. The phase between measurement and linear

model shows a delay. This delay is due to a time of 6 to 7 [ms], in the demonstration test setup. The origin of this dead time was investigated by analyzing the measurement signals but was not found, and considered to be an electrical delay. In the open loop response this time delay was not present. The difference in phase between model and measurement is at 40 [Hz] is 90 [deg], which results in a time delay of 4 [ms]. The time delay at 20 [Hz] is 1.25 [ms] and at 30 [Hz] 2.5 [ms], therefore the phase delay can be considered as a dynamic effect. This is probably the presence of damping and or Zero Order Hold effects.

6.4.4 Force Feedback Measurement and Verification

Figure 6.26 presents the closed loop frequency response between the load cell signal and the reference signal, using force feedback. To match the frequency response of the model with the measurement, a scaling gain of the conditioning of $K_{conditioning} = 1/10$ is present.

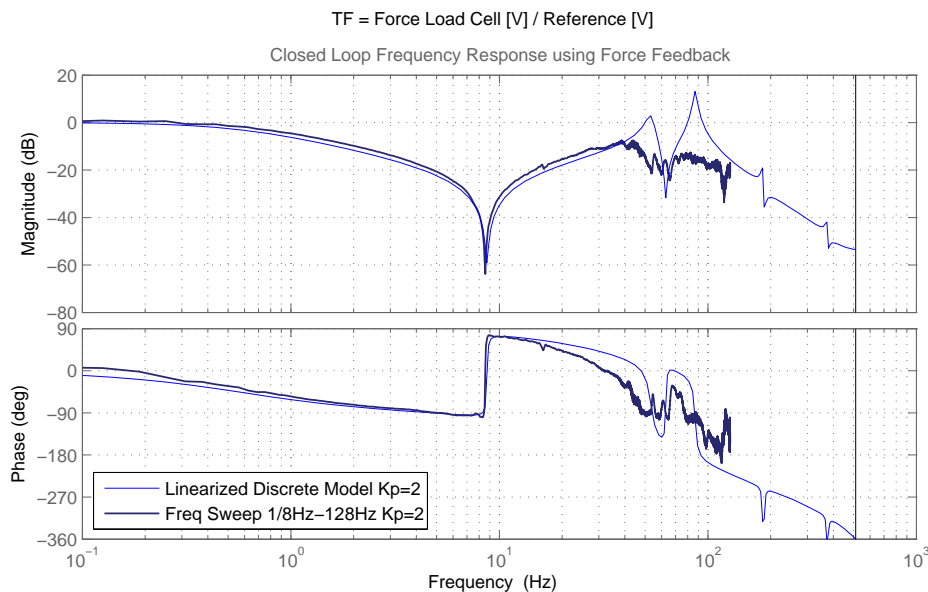


Figure 6.26 – Closed loop frequency response between reference signal and force signal, using force feedback.

From Figure 6.26 is concluded that the measurement represents the linear model up to 40 [Hz]. The phase delay present above 20 [Hz] is due to the dead time in the closed loop response. The models did not yet included the dead time, which is recommended for further research.

Using the closed loop models makes it possible to predict the system performance of a structural test setup. It is possible to determine the stability of the system and performance over a certain frequency range. This is of interest to increase the to improve robustness and test speed of the fatigue test. To obtain a complete validated model of the demonstration test setup, the difference in proportional gain of the closed loop system has to be declared. A first step is already made by finding the scaling factors.

6.5 Summary Measurement and Verification

This section presents a summary of the measurement and verification process of the different systems presented in this chapter.

6.5.1 Summary Mechanical System

The measurements performed on the mechanical system verified the first four eigenmodes and eigenfrequencies of the TA. The eigenmodes were analysed by calculating the Model Assurance Criterion (MAC) values between model and measurement. MAC values above 90 [%] were obtained on the first three TA modes. The TA eigenfrequencies obtained a large difference between model and measurement. This difference was reduced by updating the clamping length of the TA, because non-ideal clamping is present in the mechanical system.

6.5.2 Summary Hydraulic System

The servo-hydraulic system components were measured. The servo valve obtained a bandwidth of 130 Hz. Friction in the hydraulic actuator (HA) was characterized, by performing velocity measurements. The eigenfrequency of the HA was measured at 130 [Hz], by measuring the Auto Power Spectrum of the acceleration on the HA rod. The updated eigenfrequency and friction of the HA in combination with the servo valve, verified a frequency response of the piston position up to 150 [Hz].

6.5.3 Summary Coupled Mechanical and Hydraulic System

Measurements performed on the coupled mechanical and hydraulic system, showed a representative open loop frequency response of the system. This open loop frequency response is of great importance because it is used as plant model for tuning controller parameters. Both position and force frequency responses were validated with the linear model up to 40 [Hz].

6.5.4 Summary Control System

Finally the control model and closed loop response were measured and verified. The open loop verification of the controller obtained correlation with the model up to 128 [Hz]. To match the model with the measurement a conditioning unit gain had to be implemented. For position feedback this gain was $K_{conditioning} = 1/20$ and for force feedback this gain was $K_{conditioning} = 1/10$. The magnitude of the measurements showed good correlation with the measurement up to 40 [Hz] including the feedback gain. For exact correlation of the phase above 20 [Hz] it is needed to include the delay time in the closed loop response.

CHAPTER

7

CONCLUSION AND RECOMMENDATIONS

This thesis started with the need to be able to predict the actual behaviour of a structural test setup, to reduce costs and risks. To fulfill this need a virtual testing methodology for structural test setups is developed and verified. This is done by creating physical simulation models of a demonstration test setup and by verification of these models. This chapter presents the conclusions and recommendations of this thesis project, regarding the development of a virtual testing methodology for structural fatigue testing setups.

7.1 Conclusions

First, the conclusions regarding the present and proposed testing methodology are given. Followed, by the conclusions about fatigue loading profiles. Thereafter the modelling of fatigue test setup is discussed. Finally, the conclusions regarding the measurement and verification of the models are presented.

7.1.1 Testing Methodology

The current structural testing methodology was analyzed and a novel structural testing methodology was proposed. From the current structural testing methodology is

concluded; design of the hydraulic system and mechanical system are two separate processes, resulting in unknown system performance. Backup structures are designed using static calculations, therefore dynamic behaviour is unknown during the design stage. Only the static behaviour of the mechanical system is considered during the design process. The hydraulic system is determined on the basis of maximum applied loads and displacements. Servo valves are chosen on the basis of estimation of the required flow through the servo valve during the fatigue test. No dynamic physical behaviour is known since there is no dynamic hydraulic system analysis performed on forehand. Controller tuning is based on experience and therefore controller settings could not be optimal. The performance of a structural test setup is only known if the test setup is actually built. As a result it is concluded that during design the interaction between mechanical system, hydraulic system and control system is not taken into account.

To obtain a performance prediction of the structural test setup it is concluded that the design of the mechanical system and the hydraulic system need to be combined. In order to facilitate an integrated design process, simulation testing is proposed using simulation models. The simulation models couple the mechanical system, hydraulic system and control system, to investigate integrated system performance. Using these computational models, costs and risks are reduced. The objective of the new design methodology is to achieve robust designs of fatigue test setups and to achieve system performance increase of the test setup which leads to an increase of test speed.

7.1.2 Fatigue Loading Profiles

Fatigue loading profiles that are applied to the test structure are built upon loading conditions with sinusoidal interpolation between the conditions, See Section 2.2. A frequency domain analysis was performed on a specific loading profile highlighted that the step-time between the loading conditions determines the frequency content of the fatigue load profile. The frequency content of the fatigue loading profile remains below 5 [Hz] for a step-time of 0.2 seconds. Generally step-times are set between one to two seconds. 5 [Hz] will be used as the frequency range of the reference signal. As a result dynamic models will be constructed. For a general frequency content, multiple fatigue load profiles need to be analyzed.

7.1.3 Modelling of Test Setups

The modelling of test setups was performed by modelling the components of a demonstration test setup. This demonstration test setup used only one hydraulic actuator, servo valve, and control system. These were coupled with a mechanical structure. This section presents the conclusions regarding the modelling of the demonstration

test setup.

Mechanical System Modelling

It is chosen to apply state space modelling on the dynamic models of the mechanical system. The state space models are needed to couple the mechanical system with the hydraulic system. It is chosen to apply the normalized state space method, since this provided a reduction in computational time. It reduces computational time due to a reduction in states compared with the physical state space model.

Interface structures modelling showed that mechanical play could introduce significant forces on the test article. It is concluded that play has to be avoided. If this is not possible it has to be reduced to an allowable level. Damping and play affects the introduced forces on the test article. The amount of damping was not obtained from measurements and mechanical play is different for each interface structure, because these uncertainties mechanical play was not taken into account in the model of the demonstration test setup. Further research on mechanical play needs to be performed.

Hydraulic System Modelling

Modelling of the servo valve showed that it is not possible to model all the different components of the servo valve, because a lot of parameters were unknown. The servo valve dynamic characteristics is therefore approximated with a second order dynamic model, which was fitted with the frequency response of the manufacturer.

Hydraulic actuator modelling indicated that the eigenfrequency of the hydraulic actuator is highly depended on the dead oil volume of the oil supply lines between the HA and the SV. The dead oil volume is an uncertainty parameter, because detailed drawings did not provide enough information on supply line dimensions. Furthermore, the bulk modulus of the hydraulic oil was assumed to be a constant value because the manufacture did not specify this parameter. After an literature study, it was concluded that no estimation rules are present for the characterization of friction in a hydraulic actuator. Making it necessary to obtain friction values and characteristics experimentally.

Supply components for the demonstration test setup, such as the hydraulic pump and transmission lines were neglected in the modelling, because pressure dynamics has 2 [%] fluctuation in the supply pressure to the servo valve. It is assumed that there is not an affect on the system performance of the demonstration test setup.

Coupled system modelling

Open loop system simulation, showed the integrator action of the hydraulic actuator by a -20 [dB/decade] slope present in the frequency response. It is concluded that a controller is needed to compensate the integrator behaviour of the hydraulic actuator. The position frequency response shows a shift in eigenfrequencies of the test article. It is concluded that this shift originates from the coupling of the mechanical system to the oil column of the hydraulic actuator. The force frequency response shows the eigenfrequencies of the test article as antiresonances.

Control System Modelling

Modelling of the mechanical and hydraulic system resulted into the physical behaviour of the coupled system. To control the hydraulic system a control architecture is implemented. The objective of the controller is to track the reference signal as exact as possible. For reference signal tracking, *time domain tuning* or *frequency domain tuning* can be used. Frequency domain tuning has the advantage that control theory can be used to determine the system performance and stability. A disadvantage is that non-linear effects are excluded. Time domain tuning includes these non-linear effects, but demands more computational effort. It is concluded that frequency domain tuning can be used as a first estimate, and that the system can be optimized using time domain tuning.

7.1.4 Measurement and Verification

To verify the obtained simulation models of the demonstration test setup, measurement and verification is performed. Which is done by measuring the dynamic behaviour of the demonstration test setup. This section treats the conclusions regarding the verification of the simulation models and the measurements performed.

Mechanical System

To verify the FE model of the mechanical system, experimental modal analysis was performed. It is concluded from the experimental modal analysis, that the first four eigenmodes correlate the FE model. The experimental and simulation modes correlated for at least 89.9 [%]. There was a 6.75 [%] error between the first measured eigenfrequency and the modelled eigenfrequency. Updating was performed, reducing the error between model and measurement. It was concluded that the error between model and measurement of the first eigenfrequency reduced to 0.06 [%], whilst the maximum error is present at the 3rd eigenfrequency of 4.78 [%]. Furthermore, average damping of 0.83 [%] were derived from the measurements.

Hydraulic System

The measurements of the servo valve, showed that the servo valve has a bandwidth of 130 [Hz]. To approximate the measured frequency response a second-order model was tuned to a bandwidth of 75 [Hz] and having satisfactory phase response.

Friction measurements showed that the hydraulic actuator has a non-symmetric friction curve of the hydraulic actuator. It is assumed that the difference in friction is caused by different seals in the HA. It is expected that a better characterization of the friction is obtained by low velocity measurements. The pressure measurements of the HA chambers were performed using not accurately calibrated pressure sensors. The calibration was performed by reading the voltage output and the manometer pressure. Therefore, friction forces can be measured more accurately.

Measuring the Auto Power Spectrum of the hydraulic actuator rod acceleration obtained and eigenfrequency of the hydraulic actuator at 130 [Hz]. This resulted in model updating of the dead oil volume of the supply lines to the hydraulic actuator, since the model predicted an eigenfrequency of 120 [Hz]. From the measurement it is concluded that the frequency response of the hydraulic actuator piston position shows correlation with the linear model up to 40 [Hz]. The actuator force frequency response showed correlation up to 16 [Hz].

Coupled Mechanical and Hydraulic System

The verification of the coupled mechanical and hydraulic system is of importance because it represents the plant model in the control loop of structural fatigue test setups. From the measurements of the coupled system, it is concluded that the position coupling and the force coupling frequency response corresponds to the linear models up to 40 [Hz].

Control System

The control system models were verified up to 120 [Hz] for both position and force feedback. For the closed loop system response a scaling gain of the conditioning unit needed to be included to obtain satisfactory results. It is concluded that the closed loop frequency responses of force and position match the model up to 40 [Hz]. Above 20 [Hz] the phase delay increases, which is due to a dead time in the closed loop, which is measured to be around 6-7 [ms].

7.1.5 Concluding the Thesis Assignment

The aim of this thesis assignment was to investigate improvement of the structural testing methodology currently being employed. Use of models for structural testing setups design and analysis also known as virtual testing was developed in this thesis. Simulation models were developed and verified. These models can be used to predict and optimize structural test setups, for more detailed performance optimization. As a result costs and risks will be reduced by using performance optimization on allowable system tolerances. Further investigation is needed, and the recommendations are provided in the next section.

7.2 Recommendations

This section presents the recommendations for future work. The recommendations are given in three sub-sections, which are:

- Mechanical system, presenting recommendations of future modelling and measurements on the mechanical system of structural fatigue test setups.
- Hydraulic system, presenting recommendations for future models and measurements on the hydraulic system.
- Control system, presenting recommendations which could improve full system performance.

7.2.1 Mechanical System

Backup Structure and Test Article

The mechanical structure of the demonstration test setup, did consist out of a test article. The backup structure was neglected in the modelling. Structural test setups consist out of both. Therefore it is recommended to include also the backup structure in the model, and to investigate their coupled system dynamics. The eigenfrequencies of the coupled system has to be far above the bandwidth of the reference signals applied, to ensure that the dynamics of the coupled system is not excited.

Interface Structures

Currently damping of interface structures is not yet investigated. If play can not be avoided, this is an important parameter to include in the modelling for the allowable design tolerances of mechanical play.

7.2.2 Hydraulic System

Servo Valve

The choice of the servo valve is dependent on the amount of flow consumed by the hydraulic actuator. To characterize servo valve response even better it is recommended to measure flow response of the servo valve. Using flow, pressure drop and input signal the full system response of the servo valve is known.

Hydraulic Actuator

For future verification of the hydraulic actuator, it is recommended to use accurately calibrated pressure sensors. These are necessary because friction of the actuator is measured using the pressure difference between the chambers. To obtain better friction curves it is also recommended to measure the friction at low actuator speeds. Low actuator speeds characterize the static friction of the hydraulic actuator, which is an important non-linear effect in the hydraulic actuator.

The demonstration test setup used one hydraulic actuator. Structural test setups use multiple hydraulic actuators. Therefore, it is recommended to investigate the system response when multiple hydraulic actuators are used. Interaction between multiple actuators was not investigated in this thesis.

Hydraulic components

The hydraulic components that are used for hydraulic fluid supply, such as hydraulic pump, transmission lines and manifold blocks are not included in the modelling of the hydraulic system. They are assumed to behave ideal and therefore their performance is neglected. Using multiple hydraulic actuators and servo valve it is possible that there is an influence on system performance. For example the hydraulic pump capacity is too low to supply sufficient hydraulic fluid flow. It is therefore advised to investigate if these components limit the system performance of full scale test setups.

7.2.3 Control System

Linear simulation models of the demonstration test setup were obtained in this thesis. These linear simulation models can be used to tune the response of the closed loop system. Resulting in a controlled system over a certain frequency range. For future research it is recommended to investigate and verify the controller performance on fatigue testing setups. Currently there is a scaling gain present in the signal conditioning, which is determined experimentally. Further research is needed to validate this scaling gain.

With the obtained models it is also possible to investigate alternative control strategies and their effect on system performance.

This thesis proved the potential of virtual testing of structural test setups. For future research it is recommended to extend the models to a full scale test setup.

BIBLIOGRAPHY

- [1] AIRBUS. Airbus flap, <http://www.silver-aerospace.nl/track/airbus.html>, February 2010.
- [2] BOEING. Boeing 747, <http://www.boeing.com/randy/images/747a01lg.jpg>, February 2010.
- [3] COTRELL, J., MUSIAL, W., AND HUGHES, S. Necessity and requirements of a collaborative effort to develop a large wind turbine blade test facility in north america. Tech. rep., NREL/TP-500-38044, National Renewable Energy Laboratory (NREL), Golden, CO., 2006.
- [4] DE CUYPER, J. *Linear feedback control for durability test rigs in the automotive industry*. PhD thesis, Katholieke Universiteit Leuven, 2006.
- [5] FRANKLIN, G., POWELL, J., EMAMI-NAEINI, A., AND POWELL, J. *Feedback control of dynamic systems*. Addison-Wesley Reading (Ma) etc., 1994.
- [6] GAWRONSKI, W. *Advanced structural dynamics and active control of structures*. Springer Verlag, 2004.
- [7] GÉRADIN, M., AND RIXEN, D. *Mechanical vibrations: theory and application to structural dynamics*. Wiley New York, 1997.
- [8] JANUS, A. <http://blog.nasm.si.edu/2009/03/19/winged-wonders/>, March 2009.
- [9] JELALI, M., AND KROLL, A. *Hydraulic servo-systems: modelling, identification, and control*. Springer, 2003.

-
- [10] JOSEF KRYGER TADICH, J. W.-H. Full scale testing of blades: now, and for the future. *Proceedings of EWEC 2007: European Wind Energy Conference & Exhibition* (2007).
- [11] KWON, Y., AND BANG, H. *The finite element method using MATLAB*. CRC, 2000.
- [12] M. NAWIJN, B.A.T. NOORDMAN, F. G. Virtual testing of non-generic aircraft components. *Aircraft structural design conference, Liverpool, United Kingdom* (2008).
- [13] MATHWORKS. *Simscape 3 Reference guide*, 3.3 ed., March 2010.
- [14] MATHWORKS. *Simscape 3 Users guide*, March 2010.
- [15] MATHWORKS. *Simulink Control Design Users guide*, 3.1 ed., march 2010.
- [16] MOOG. Poster test system, <http://www.moog.com.cn/english/markets/automotive-test-simulation/automotive-structural-testing/7-8-poster-test-system/>, 2010.
- [17] MUSIAL, W. Wind turbine testing and certification. *Presentation National Wind Technology Center NREL* (2004).
- [18] R. HOUWINK, R. V., AND TEN HOEVE, H. Computer aided sequencing of loads and stresses for fatigue analysis and testing. *National Aerospace Laboratory NLR* (2001).
- [19] SHABANA, A. *Vibration of discrete and continuous systems*. Springer, 1997.
- [20] TEN HAVE, A. European approaches in standard spectrum development. *ASTM special technical publication*, 1006 (1989), 17–35.
- [21] VAN MUIJDEN, B. P. R. V. R. H. M. H. J. A generic flexible aircraft loads database system for fatigue analysis. *National Aerospace Laboratory NLR* (2007).
- [22] VAN SCHOTHORST G. *Modelling of long-stroke hydraulic servo-systems for flight simulator motion control and system design*. PhD thesis, 1997.
- [23] VIERSMA, T. *Analysis, Synthesis, and Design of Hydraulic Servosystems and Pipelines*. TU Delft, 1990.
- [24] WHITE, D. New method for dual-axis fatigue testing of large wind turbine blades using resonance excitation and spectral loading. Tech. rep., NREL/TP-500-35268, National Renewable Energy Lab., Golden, CO (US), 2004.

APPENDIX

A

THESIS ASSIGNMENT DEFINED BY NLR

Onderwerp Afstudeeropdracht Elasto-mechanisch servo-hydraulisch modelleren van opstellingen voor constructiebeproeving

Achtergrond Bij beproeving van constructies worden deze constructiedelen bevestigd in een testframe en (meestal) computergestuurd servo-hydraulisch belast met voorgeschreven krachten en/of verplaatsingen. Vooral niet-lineaire verschijnselen verstoren ideaal dynamisch gedrag wat resulteert in onzekerheid van responsies in hogere frequenties, zowel bij het sturen van belastingsvolgordes als het (gecontroleerd) ontlasten door beveiligingsystemen.

Doelstelling

- **Bedrijf:** Via gevalideerde modellering van testopstellingen verhogen van efficiëntie van ontwikkeling en bedrijf van constructietests.
- **Student:** Op ingenieurs niveau problemen analyseren en oplossingen implementeren.

Scope Modelleren van een bestaande testopstelling in bijvoorbeeld Matlab Simulink. Hierbij spelen zowel het testframe als het proefstuk een elasto-mechanische rol. Het hydraulisch systeem (kleppen, cylinders, accu's, hydraulische voeding enz.) vormt de

hydraulische servo-component. Samen met de software/hardware regelaar dient het geheel gemodelleerd te worden. De te modelleren opstelling is ofwel een relevante dummyopstelling, of (indien mogelijk) een bestaande testopstelling.

Uitvoeren van virtuele tests, waarbij enerzijds de actuele testopstelling, anderzijds de numerieke modellering wordt gebruikt, om zodoende een vergelijking te maken tussen model en werkelijkheid.

Via numerieke parameterstudies, waarbij constructieve stijfheid, speling, wrijving, hydraulische eigenschappen etc. worden gevarieerd, duiden van efficiëntieverbeteringen aangaande ontwerp en bedrijf van testopstelling.

Wellicht buiten het bereik van de afstudeeropdracht is het ultieme doel het nauwkeurig kunnen modelleren van een servo-hydraulische-elasto-mechanische opstelling om vanuit die modelleringscapability de grenzen beter op te zoeken in termen van “efficiënt ontwerp” / “gebalanceerde systeemsamenstelling” / “sneller testen” / “voorspelbaarder sturen binnen vooraf bekende toleranties” etc,

Paul Arendsen

APPENDIX

B

DEMONSTRATION TEST SETUP COMPONENT DETAILS

B.1 Mechanical system

B.1.1 Load Cell

Properties

Manufacturer	Interface
Model	1210BF-5K-B
Serial number	82834
Capacity	5 klbs = 5 klbs * 4.4482 kN/klbs = 22.24 kN
Loadcell sensitivity A	4.144 mV/V (@ 5 klbs)
Loadcell sensitivity B	4.141 mV/V (@ 5 klbs)
Mass	3 kg
Deflection	0.05 [mm] at 22.24 [kN]
Natural frequency	6.6 [kHz]

Signal Conditioning Setup

The calibration values of the signal condition unit are:

Full scale value	25 kN
Gain	214.7 V/V
Excitation	10 V

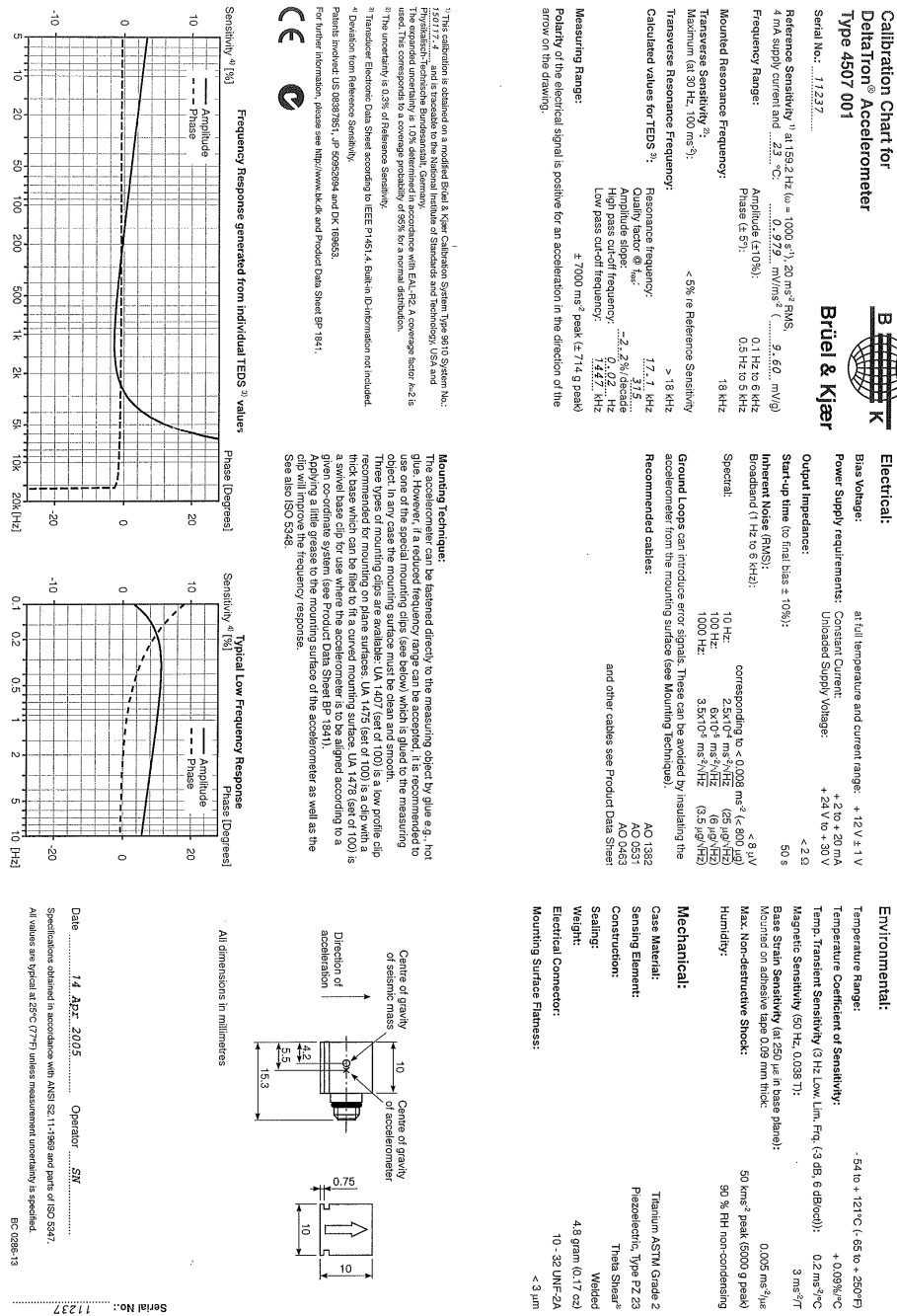
The gain is for calibration is calculated using Equation B.1.1.

$$LC_{gain} = \frac{10}{\left(V_{ex} \cdot S \cdot \frac{F_r}{F_{ps}}\right)}$$

Excitation Voltage	V_{ex}	10 V
Sensor sensitivity	S	$4.144 \cdot 10^{-3}$ V/V
Full scale value	F_r	25 kN
Capacity	F_{ps}	22.24 kN

B.1.2 Acceleration Sensors Calibration Values

B.1. Mechanical system



Frequency Response generated from individual TEDS³⁾ values

Typical Low Frequency Response

Mounting Technique:

The accelerometer can be fastened directly to the measuring object by glue e.g. hot glue. However, if a reduced frequency range can be accepted, it is recommended to use one of the special mounting tips (see below) which is glued to the measuring object. Three types of mounting clips are available: UA 1407 (set of 100) is a low profile clip recommended for mounting on plane surfaces; UA 1475 (set of 100) is a clip with a thick base which can be fitted to a curved mounting surface; UA 1478 (set of 100) is a swivel base clip for use where the accelerometer is to be aligned according to a specific angle. See also Product Data Sheet (PDS) for details. Applying a little grease to the mounting surface of the accelerometer as well as the clip will improve the frequency response. See also ISO 5348.

All dimensions in millimetres

Centre of gravity of seismic mass
Centre of gravity of accelerometer
Direction of acceleration

Date: 14 Apr 2005 Operator: SM

Specifications obtained in accordance with ANSI S2.1-1989 and parts of ISO 9347. All values are typical at 25°C (77°F) unless measurement uncertainty is specified. BC 0288-13

Serial No.: 11237

Figure B.1 – Acceleration sensor calibration data, HA channel 12 sensor

Appendix B. Demonstration Test Setup Component Details



**Calibration Chart for
DeltaTron® Accelerometer
Type 4507 001**

Serial No.: ...11236...

Reference Sensitivity¹⁾ at 169.2 Hz ($\omega = 1000 \text{ s}^{-1}$): 20 ms^{-2} RMS
4 mA supply current and 23 °C: 0.950 mV/ms^2 (\dots), 9.71 mV/g

Frequency Range:
Amplitude ($\pm 10\%$): 0.1 Hz to 6 kHz
Phase ($\pm 5^\circ$): 0.5 Hz to 5 kHz

Mounted Resonance Frequency:
Transverse Sensitivity²⁾: < 5% re Reference Sensitivity
Maximum (at 30 Hz, 100 ms^{-2}): > 18 kHz

Transverse Resonance Frequency:
Quality factor @ f_{res} : 19.3 kHz
Amplitude slope: 2.6% / decade

High pass cut-off frequency: 0.02... kHz
Low pass cut-off frequency: 0.7/1... kHz

Calculated values for TEDS³⁾:
Resonance frequency: 19.3 kHz
Quality factor @ f_{res} : 2.6% / decade
Amplitude slope: 2.6% / decade

High pass cut-off frequency: 0.02... kHz
Low pass cut-off frequency: 0.7/1... kHz

Measuring Range:
Polarity of the electrical signal is positive for an acceleration in the direction of the arrow on the drawing.

Electrical:

Bias Voltage: at full temperature and current range: +12 V \pm 1 V

Power Supply requirements: Constant Current: +2 to +20 mA
Unloaded Supply Voltage: +24 V to +30 V

Output Impedance: < 2 Ω

Start-up time (to final bias $\pm 10\%$): 50 s

Inherent Noise (RMS): < 8 μV
Broadband (1 Hz to 6 kHz): 2.5 $\times 10^{-4}$ ms^{-2} ($\pm 800 \mu\text{g}$)
10 Hz: 8 $\times 10^{-5}$ $\text{ms}^{-2}/\sqrt{\text{Hz}}$ (25 $\mu\text{g}/\sqrt{\text{Hz}}$)
100 Hz: 3.5 $\times 10^{-5}$ $\text{ms}^{-2}/\sqrt{\text{Hz}}$ (3.5 $\mu\text{g}/\sqrt{\text{Hz}}$)

Spectral:
corresponding to < 0.008 ms^{-2} ($\pm 800 \mu\text{g}$)
10 Hz: 8 $\times 10^{-5}$ $\text{ms}^{-2}/\sqrt{\text{Hz}}$ (25 $\mu\text{g}/\sqrt{\text{Hz}}$)
100 Hz: 3.5 $\times 10^{-5}$ $\text{ms}^{-2}/\sqrt{\text{Hz}}$ (3.5 $\mu\text{g}/\sqrt{\text{Hz}}$)

Ground Loops can introduce error signals. These can be avoided by insulating the accelerometer from the mounting surface (see Mounting Technique).

Recommended cables:
AO 1382
AO 0531
and other cables see Product Data Sheet

Environmental:

Temperature Range: -54 to +121°C (-65 to +250°F)
+0.05%/°C

Temp. Coefficient of Sensitivity: +0.05%/°C

Temp. Transient Sensitivity (3 Hz, Low Lim. Freq. (3 dB, 6 dB/oct)): 0.2 $\text{ms}^{-2}/\text{°C}$
3 $\text{ms}^2/\text{°C}$

Magnetic Sensitivity (50 Hz, 0.038 T): 0.005 $\text{ms}^{-2}/\mu\text{s}$
50 km^2 peak (6000 g peak)
90 % RH non-condensing

Base Strain Sensitivity (at 250 μs in base plane):
Mounted on adhesive tape 0.09 mm thick: 50 km^2 peak (6000 g peak)
90 % RH non-condensing

Max. Non-destructive Shock: 90 % RH non-condensing

Mechanical:

Case Material: Titanium ASTM Grade 2

Sensing Element: Piezoelectric, Type PZ 23

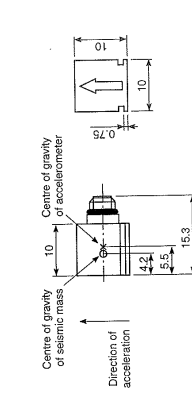
Construction: Thera Shear®
Welded

Sealing: 4.8 gram (0.17 oz)

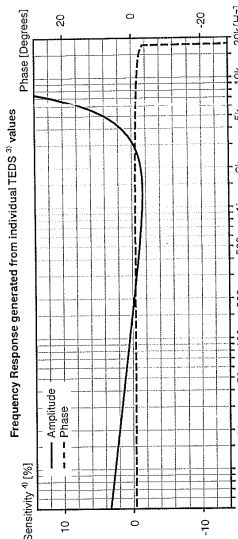
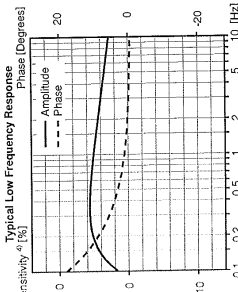
Weight: 10 - 32 INF-2A

Electrical Connector: < 3 μm

Mounting Surface Finishes:



Mounting Technique:
The accelerometer can be fastened directly to the measuring object by glue e.g., hot glue. However, if a reduced frequency range can be accepted, it is recommended to use one of the special mounting clips (see below) which is glued to the measuring object. The types of mounting clips are available: UA 1407 (set of 100) is a low profile clip recommended for mounting on plane surfaces. UA 1475 (set of 100) is a clip with a thick base which can be fitted to a curved mounting surface. UA 1478 (set of 100) is a swivel base clip for use where the accelerometer is to be aligned according to a given co-ordinate system (see Product Data Sheet). The use of the special mounting clip will improve the frequency response. See also ISO 5346.



Serial No.: 11236

Date: 14 April 2005 Operator: SW

Specifications obtained in accordance with ANSI S2.1-1989 and parts of ISO 5347.
All values are typical at 25°C (77°F) unless measurement uncertainty is specified.
BC 0286-13

Figure B.2 – Acceleration sensor calibration data, TA front channel 13 sensor

B.1. Mechanical system

**Calibration Chart for
DeltaTron® Accelerometer
Type 4507 001**

Serial No.: ...11236...

Reference Sensitivity¹⁾ at 150 Hz ($\omega = 1000 \text{ s}^{-1}$): 20 ms^{-2} RMS
4 mA supply current and 23 °C

Frequency Range:
Amplitude ($\pm 10\%$): 0.1 Hz to 6 kHz
Phase ($\pm 5^\circ$): 0.5 Hz to 5 kHz

Mounted Resonance Frequency:
Transverse Sensitivity²⁾: < 5% re Reference Sensitivity
Maximum (at 30 Hz, 100 ms^{-2}): > 18 kHz

Transverse Resonance Frequency:
Quality factor @ f_{res} : 19.3 kHz
Amplitude slope: 2.6% / decade

Calculated values for TEDS³⁾:
High pass cut-off frequency: 0.02... kHz
Low pass cut-off frequency: 0.77... kHz

Measuring Range:
Polarity of the electrical signal is positive for an acceleration in the direction of the arrow on the drawing.

Electrical:

Bias Voltage: at full temperature and current range: +12 V ± 1 V

Power Supply requirements: Constant Current: +2 to +20 mA
Unloaded Supply Voltage: +24 V to +30 V

Output Impedance: < 2 Ω

Inherent Noise (RMS): 50 s
Broadband (1 Hz to 6 kHz): < 8 μV
Spectral: corresponding to < 0.008 ms^{-2} (< 800 μg)
10 Hz: $2.5 \times 10^{-4} \text{ ms}^{-2}/\sqrt{\text{Hz}}$ (25 $\mu\text{g}/\sqrt{\text{Hz}}$)
100 Hz: $8 \times 10^{-5} \text{ ms}^{-2}/\sqrt{\text{Hz}}$ (8 $\mu\text{g}/\sqrt{\text{Hz}}$)
1000 Hz: $3.5 \times 10^{-6} \text{ ms}^{-2}/\sqrt{\text{Hz}}$ (3.5 $\mu\text{g}/\sqrt{\text{Hz}}$)

Ground Loops can introduce error signals. These can be avoided by insulating the accelerometer from the mounting surface (see Mounting Technique).

Recommended cables:
AO 1382
AO 6531
and other cables see Product Data Sheet

Environmental:

Temperature Range: -54 to + 121°C (- 65 to + 250°F)
+ 0.05%/°C

Temperature Coefficient of Sensitivity: 0.2 $\text{ms}^{-2}/\text{°C}$

Temp. Transient Sensitivity (3 Hz, Low. Lim. Fq. (3 dB, 6 dB/oct)): 3 ms^2/T

Magnetic Sensitivity (50 Hz, 0.038 T): 0.005 $\text{ms}^{-2}/\mu\text{s}$

Base Strain Sensitivity (at 250 μs in base plane): 50 km^{-2} peak (6000 g peak)

Mounts on adhesive tape 0.09 mm thick: 90 % RH non-condensing

Max. Non-destructive Shock: 90 % RH non-condensing

Humidity: 90 % RH non-condensing

Mechanical:

Case Material: Titanium ASTM Grade 2

Sensing Element: Piezoelectric, Type PZ 23

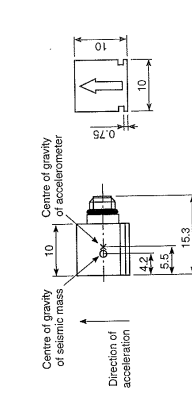
Construction: Thera Shear®
Welded

Sealing: 4.8 gram (0.17 oz)

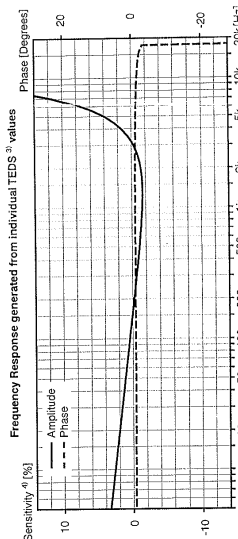
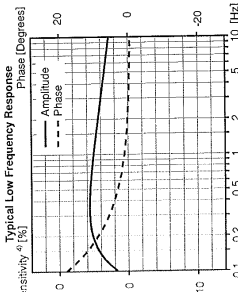
Weight: 10 - 32 INF-2A

Electrical Connector: < 3 μm

Mounting Surface Flatness: < 3 μm



Mounting Technique:
The accelerometer can be fastened directly to the measuring object by glue e.g., hot glue. However, if a reduced frequency range can be accepted, it is recommended to use one of the special mounting clips (see below) which is glued to the measuring object. The types of mounting clips are available: UA 1407 (set of 100) is a low profile clip recommended for mounting on plane surfaces. UA 1475 (set of 100) is a clip with a thick base which can be fitted to a curved mounting surface. UA 1478 (set of 100) is a swivel base clip for use where the accelerometer is to be aligned according to a given co-ordinate system (see Product Data Sheet). The use of the special mounting clip will improve the frequency response. See also ISO 5346.



Serial No.: 11236
Date: 14 Apr. 2005
Operator: SW
Specifications obtained in accordance with ANSI S2.1-1989 and parts of ISO 5347.
All values are typical at 25°C (77°F) unless measurement uncertainty is specified.
BC 028E-13

Figure B.3 – Acceleration sensor calibration data, TA rear channel 14 sensor

B.2 Hydraulic system

B.2.1 Hydraulic Actuator

Hydraulic Actuator Technical Drawing

Type number	CI0450-0786A
Serie number	0504-4117
NLR number	DOW 106

Calculation of Hydraulic Actuator Rod Mass

The mass of the hydraulic actuator rod and piston is calculated using Figure B.4.

Density	7800	$[\text{kg}/\text{m}^3]$
Mass piston and rod	8.086	$[\text{kg}]$

B.2.2 Temposonic

The hydraulic actuator is supplied with a MTS temposonic of type:

GH-M-0250M-R02-1-V2

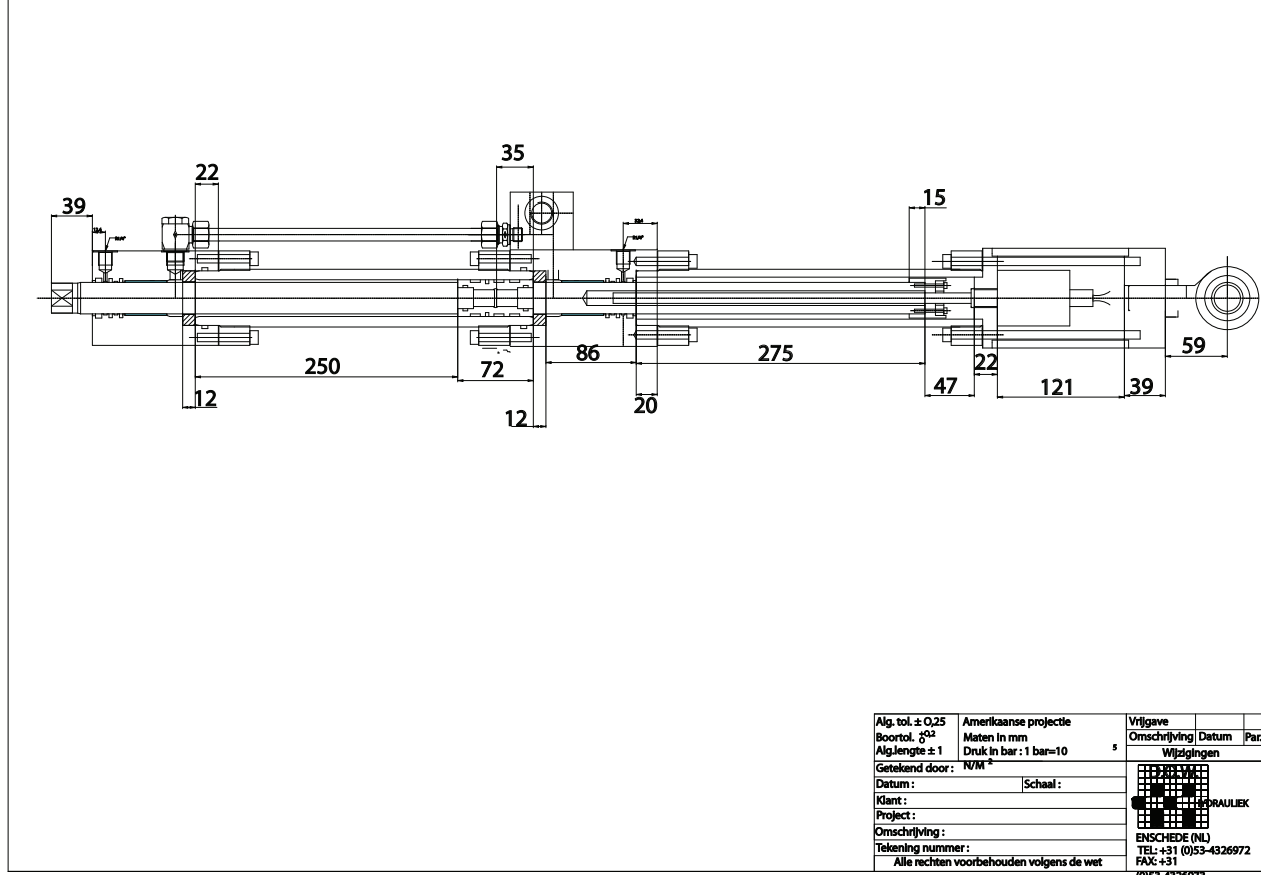


Figure B.4 – Hydraulic actuator technical drawing.

Temposonics®

Absolute, berührungslose Positionssensoren



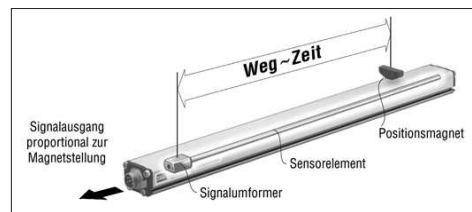
G-Serie Analog + Digital

Temposonics®-GP und GH
Messlänge 50 - 7600 mm



100 % von außen einstellbar!

- Lineare Absolutmessung ohne Referenzmarkenanfahrt
- LED Anzeige für Sensordiagnose
- Komfortable Messbereichseinstellung von außen
- Berührungslos ohne mechanischen Verschleiß
- Hochgenau: Linearität besser 0,02 %
- Wiederholbarkeit 0,001 %
- Direkter Analogausgang
- Start/Stop Impulsschnittstelle



Magnetostriktion	Formfaktor
------------------	------------

Basis der absoluten Temposonics® Linearwegsensoren ist das von MTS erfundene **magnetostriktive** Messverfahren, das den Istweg berührungslos von außen erfasst. Ein außen geführter Positionsmagnet löst im Sensorelement eine Körperschallwelle als Messimpuls aus. Dessen Laufzeit wird physikalisch hochgenau gemessen und im Sensor in marktübliche Normausgänge umgeformt. Das **verschleißfreie** magneto-mechanische Wirkprinzip ohne Referenzpunktanfahrt, garantiert langlebige und verschleißfreie Sensoren ohne Nachkalibrierung.

Temposonics® mit platzsparenden Gehäuseformen und breitem Messlängenspektrum sind anwendungsfreundlich, modular aufgebaute Sensoren für den harten Dauereinsatz in der Automatisierungstechnik.

- Das Sensorgehäuse in Profil- oder Stabform schützt das Sensorelement mit der Messstrecke, in dem das Nutzsinal entsteht.
- Der Sensorkopf trägt die Elektronik zur aktiven Signalaufbereitung. Die 2-fach gekapselten Schnittstellenmodule bieten Betriebsicherheit und optimalen EMV-Schutz.
- Der passive Positionsgeber, ein einfacher Dauermagnet fährt mechanisch völlig entkoppelt über den Sensor und markiert durch dessen Wand hindurch den Weg.



Figure B.5 – Temposonic sensor data page.

Technische Daten

Eingang	
Messgröße	Weg, Füllstand
Messlänge	
Analog	Profil/Stab: 50 - 2500 mm
Digital	Profil: 50 - 5000 mm, Stab: 50 - 7600 mm
Ausgang	
Spannung	0...10 / 10...0 / -10...+10 / +10...-10 VDC (Eingangswiderstand Steuerung: > 5 kOhm)
Strom	4(0)...20 / 20...4(0) mA (min/max. Bürde: 0/500 Ohm)
Digital (Start/Stop-Impuls)	RS 422 Differenzsignal
Messgenauigkeit	
Positionsmessung:	
- Null/Endpunkt einstellen	100 % des Messbereichs (Min. Bereich 50 mm)
- Auflösung	Analog: Praktisch unendlich Digital: 0,1 mm; 0,01; 0,005 mm je nach Folgeelektronik
- Linearität	< ± 0,02 % F.S. (Minimum ± 50 µm)
- Wiederholbarkeit	< ± 0,001 % F.S. (Minimum ± 2,5 µm)
- Hysterese	< 4 µm
- Messfrequenz	Analog: < 1 ms typisch (Messlängenabhängig) Digital: abhängig von Messlänge und Folgeelektronik
- Restwelligkeit	< 0,01 % F.S.
Einsatzbedingungen	
Magnetfahrgeschwindigkeit	beliebig
Betriebstemperatur Elektronik	-40 °C ... +80 °C (KB: -40 °C ... +85 °C)
Betriebstemperatur im aktiven Messbereich	-40 °C ... +105 °C
Taupunkt, Feuchte	90% rel. Feuchte, keine Betauung
Schutzart	Profil: IP65 / Stab: IP67, IP68 bei Kabelabgang
Schocktest	100 g (Einzelschock nach IEC-Standard 68-2-27)
Vibrationstest	15 g / 10 - 2000 Hz nach IEC-Standard 68-2-6
Normen, EMV Test	Störaussendung nach EN 50081-1 Störfestigkeit nach EN 50082-2 EN 61000-4-2/3/4/6, Level 3/4, Kriterium A, CE-geprüft
Formfaktor, Material	
Diagnoseanzeige	LEDs neben Stecker
Profilform:	
Sensorkopf	Aluminium
Messstab	Aluminium
Positionsgeber	Magnetschlitten oder abhebbarer U-Magnet
Stabform:	
Sensorkopf	Aluminium
Maßstab mit Flansch	Edelstahl 1.4301 / AISI 304
- Betriebsdruck	350 bar, 700 bar Spitze
Positionsgeber	Ring- oder U-Magnete
Einbau	
Einbaulage	Beliebig
Profil	verschiebbare Montageklammern oder M5 Nutenstein in T-Spur Bodennut
U-Magnet, abhebbar	Mitnahme und Schrauben für Magnet aus amagnetischem Material
Stab	Schraubflansch M18 x 1,5 oder 3/4" -16 UNF-3A, Mutter M18
Positionsgeber	Mitnahme und Schrauben aus amagnetischem Material (s. Bedienungsanleitung)
Elektrischer Anschluss	
Anschlussart	6 pol. Gerätestecker M16 oder 2 m Kabelabgang Achtung: Der Profilsensor muß über den Flachstecker am Sensorkopf geerdet werden.
Betriebsspannung	24 VDC (-15 / +20 %)
- Verpolungsschutz	bis -30 VDC
- Überspannungsschutz	bis 36 VDC
Stromaufnahme	100 mA typisch
Restwelligkeit	< 1 % S-S
Spannungsfestigkeit	500 VDC (0 V gegen Gehäuse)

Linearitätsprotokoll

Temposonics™-GP, Messlänge 1000 mm
Zulässige Abweichungen: ± 0,2 mm
Gemessene Abweichung: ± 0,12 mm
unkorrigiert

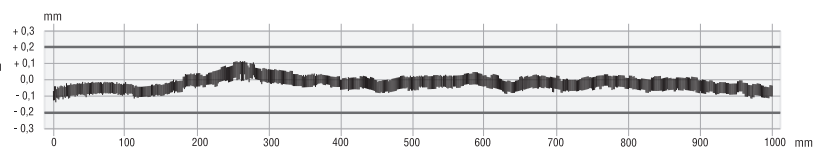


Figure B.6 – Temposonic sensor data page.

B.2.3 Pressure Sensors

Pressure-A	Pressure-B
Microgage P-102	Microgage P-102
Transducer full bridge	Transducer full bridge
Excitation 5.0 Volt	Excitation 5.0 Volt
Sensitivity Range ± 80 mV / V	Sensitivity Range ± 80 mV / V
Pressure Range 3000 psi	Pressure Range 3000 psi
Serial number 30903	Serial number 30907
Calibration gain 51.966 V/V	Calibration gain 50.09 V/V

Pressure-supply	Pressure-tank
Microgage P-102	Microgage P-102
Transducer full bridge	Transducer full bridge
Excitation 5.0 Volt	Excitation 5.0 Volt
Sensitivity Range ± 80 mV / V	Sensitivity Range ± 80 mV / V
Pressure Range 3000 psi	Pressure Range 3000 psi
Serial number 30916	Serial number 30393
Calibration gain 52.005 V/V	Calibration gain 48.274 V/V

Table B.1 – Pressure sensors technical data

The pressure sensor calibration gains were determined by comparing the measured pressure on the signal conditioning unit with the measured pressure on the manometer. This experimental determining of the pressure sensor gains was used since the pressure sensors were not calibrated.

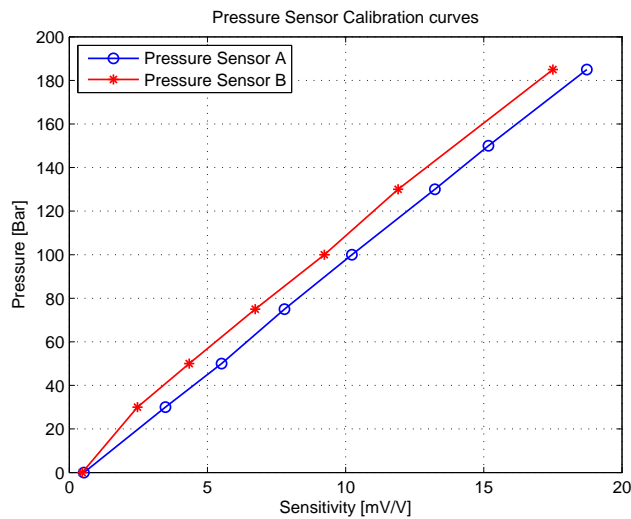


Figure B.7 – Pressure sensor calibration curves of pressure sensors A and B.

B.2.4 Servo Valve



Model 552E Servovalve



- Nominal flows rates 1 to 75 l/min @ 70 bar
- Sapphire Technology™
- Spool position control, integrated electronics
- High & Very-High-Response characteristics
- Higher resolution lower hysteresis
- External pilot supply

Star Hydraulics Ltd.
8A Beta Close
Tewkesbury Industrial Centre
Tewkesbury
Gloucestershire GL20 8SR
England U.K.

Tel.: 01684 296176
Fax.: 01684 850714

Email: sales@star-hydraulics.co.uk
Web: <http://www.star-hydraulics.co.uk>

Appendix B. Demonstration Test Setup Component Details

Nominal flow ratings	4, 10, 20, 40, 60, 75 l/min at 70 bar Δp For other flow ratings contact factory
Hysteresis	< 0.5% without dither
Threshold	< 0.1% without dither
Null bias	< 1%
Null shift	
with 40°C temp change	< 2%
with 70 bar supply pressure change	< 2%
with return pressure 0 to 35 bar	< 2%
Pressure gain	< 1% rated input signal for 60% of supply pressure
Seal materials available	FPM, NBR, EPDM
Operating temperature range	-20 °C to 85 °C
Proof pressure	
at pressure port	150% max supply pressure
at return port	100% max supply pressure
Burst pressure	
return port open	250% max supply pressure
External leakage	zero
Degree of protection	IP 65 (BS EN 60529 : 1992)
Weight	1.5 kg
Mounting position	Any, fixed or movable
Supply filtration	
minimum	$\beta_{10} \geq 75$ (10 micron abs)
recommended	$\beta_5 = 200$ (5 micron abs)
Fluid cleanliness level	
minimum	ISO 4406 - 16/13 NAS 1638 - class 7
recommended	ISO 4406 - 13/10 NAS 1638 - class 4
Supply pressure	
min. to effect spool movement	3.5 bar
minimum recommended	15 bar
maximum continuous	210 bar (FPM & EPDM) 315 bar (NBR)
Viscosity	VG 10 to 100 ISO 3448
Fluid type	Petroleum based mineral oils For operation with other media contact factory

General Information

Hydraulic Data

Figure B.9 – Servo valve manufacturers manual.

B.2. Hydraulic system

Calculating output flow

The output flow for a given pressure drop can be calculated using the following:

$$q = q_N \sqrt{\frac{\Delta p_N}{\Delta p_V}}$$

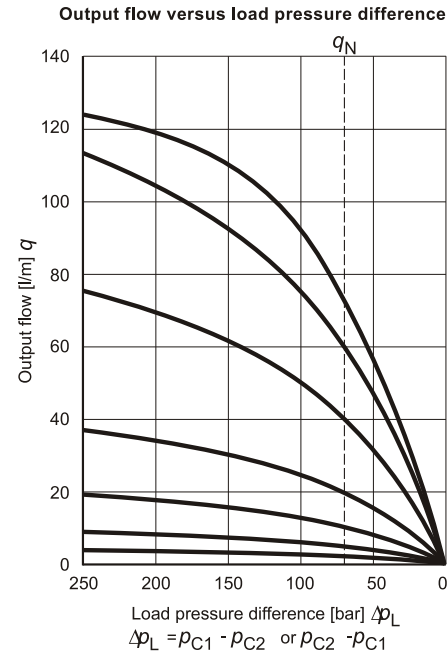
Where:

q = Output flow [l/min]

q_N = Rated flow [l/min]

Δp_N = Valve pressure drop [bar]

Δp_V = Rated valve pressure drop [bar]

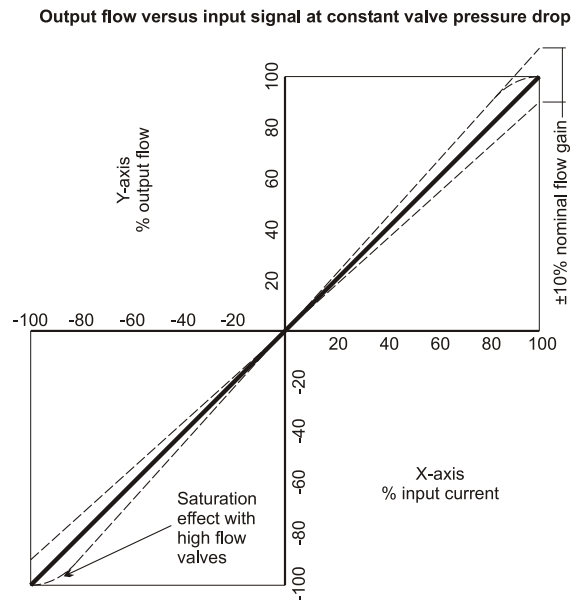


Flow Characteristics

Internal leakage

This comprises of both pilot stage flow (tare leakage) and the second stage null leakage, typical values for this size of valve would be:

Rated flow	Internal leakage at 140 bar
4 l/min	< 1.0 l/min
10 l/min	< 1.2 l/min
20 l/min	< 1.6 l/min
40 l/min	< 1.6 l/min
60 l/min	< 1.6 l/min
75 l/min	< 1.6 l/min



The flow tolerance for standard servovalves is $\pm 10\%$ of the nominal rated flow at $\pm 100\%$ input signal.

The rated flow is quoted at 70 bar Δp and 100% rated input signal.

Figure B.10 – Servo valve manufacturers manual.

Connections

	Pin	Voltage Command	Current Command
Supply voltage +15/0/-15 VDC ±3% Ripple < 50 mVp-p	A	+15 VDC	$I_{max} = 200 \text{ mA}$
	B	-15 VDC	$I_{max} = 200 \text{ mA}$
	C	⊥	
Command signal 	D	0...±10 VDC	$R_e \geq 50 \text{ k}\Omega$
	E		0...±10 mA
Spool position output 	F	0...±10 VDC	load resistance 10 kΩ
	G	Protective grounding	

	Pin	Voltage Command	Current Command
Supply voltage +24 VDC ±3% Ripple < 50 mVp-p	A	+24 VDC	$I_{max} = 200 \text{ mA}$
	B	⊥	
	C	Not used	
Command signal 	D	0...±10 VDC	$R_e \geq 50 \text{ k}\Omega$
	E		0...±10 mA
Spool position output 	F	0...±10 VDC	load resistance 10 kΩ
	G	Protective grounding	

Spool stroke is proportional to command signal. +10 VDC to pin D causes 100% rated flow in the direction of P→C2, C1→R.

One input D or E must be connected to ⊥ if a single ended driver is used.

Connection cable to be 6-core, 0.75 mm², screened. External diameter 6.5~9.5 mm. Connect screening to ⊥ on supply side only.

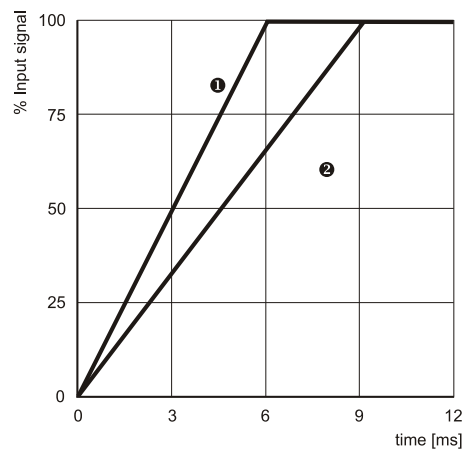
Standard connector is MS3106E-14-SA-7S (MIL-C-5015). Please contact factory for more options.



Figure B.11 – Servo valve manufacturers manual.

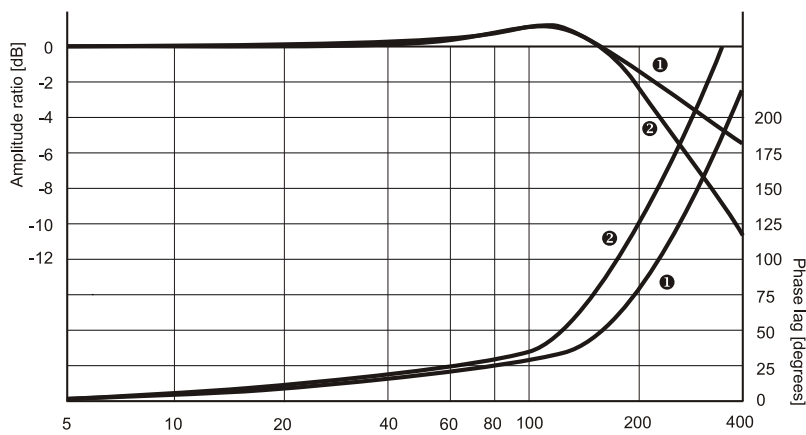
B.2. Hydraulic system

Transient Response (HR)

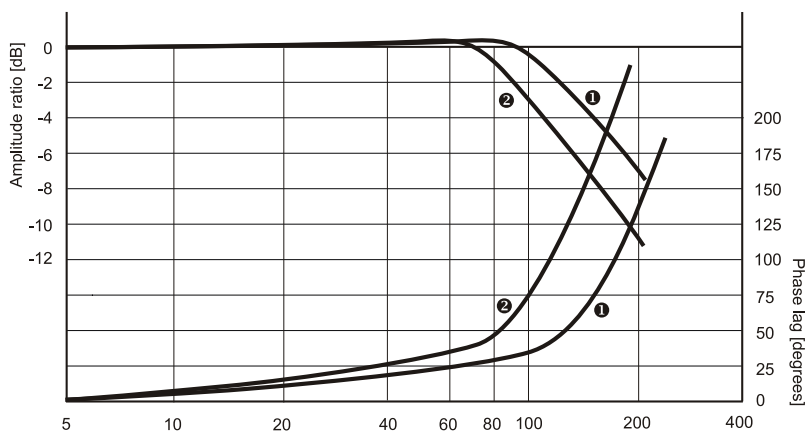


[1] Rated flow = 20 l/min
 [2] Rated flow = 75 l/min
 Supply pressure = 210 bar

Frequency Response (HR)



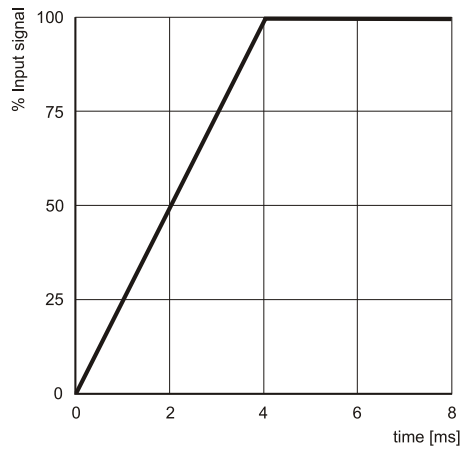
Input signal = 5%
 [1] Rated flow = 20 l/min
 [2] Rated flow = 75 l/min
 Supply pressure = 210 bar



Input signal = 40%
 [1] Rated flow = 20 l/min
 [2] Rated flow = 75 l/min
 Supply pressure = 210 bar

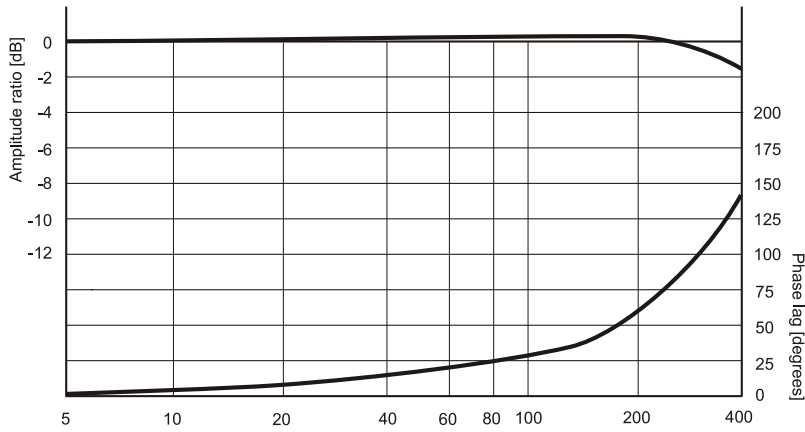
Figure B.12 – Servo valve manufacturers manual.

Transient Response (VHR)

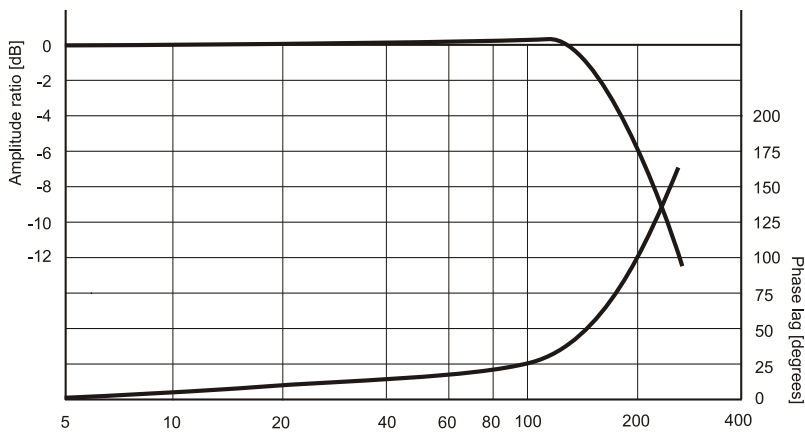


Rated flow = 4 to 40 l/min
Supply pressure = 210 bar

Frequency Response (VHR)



Input signal = 5%
Rated flow = 4 to 40 l/min
Supply pressure = 210 bar



Input signal = 40%
Rated flow = 4 to 40 l/min
Supply pressure = 210 bar

Figure B.13 – Servo valve manufacturers manual.

B.2. Hydraulic system

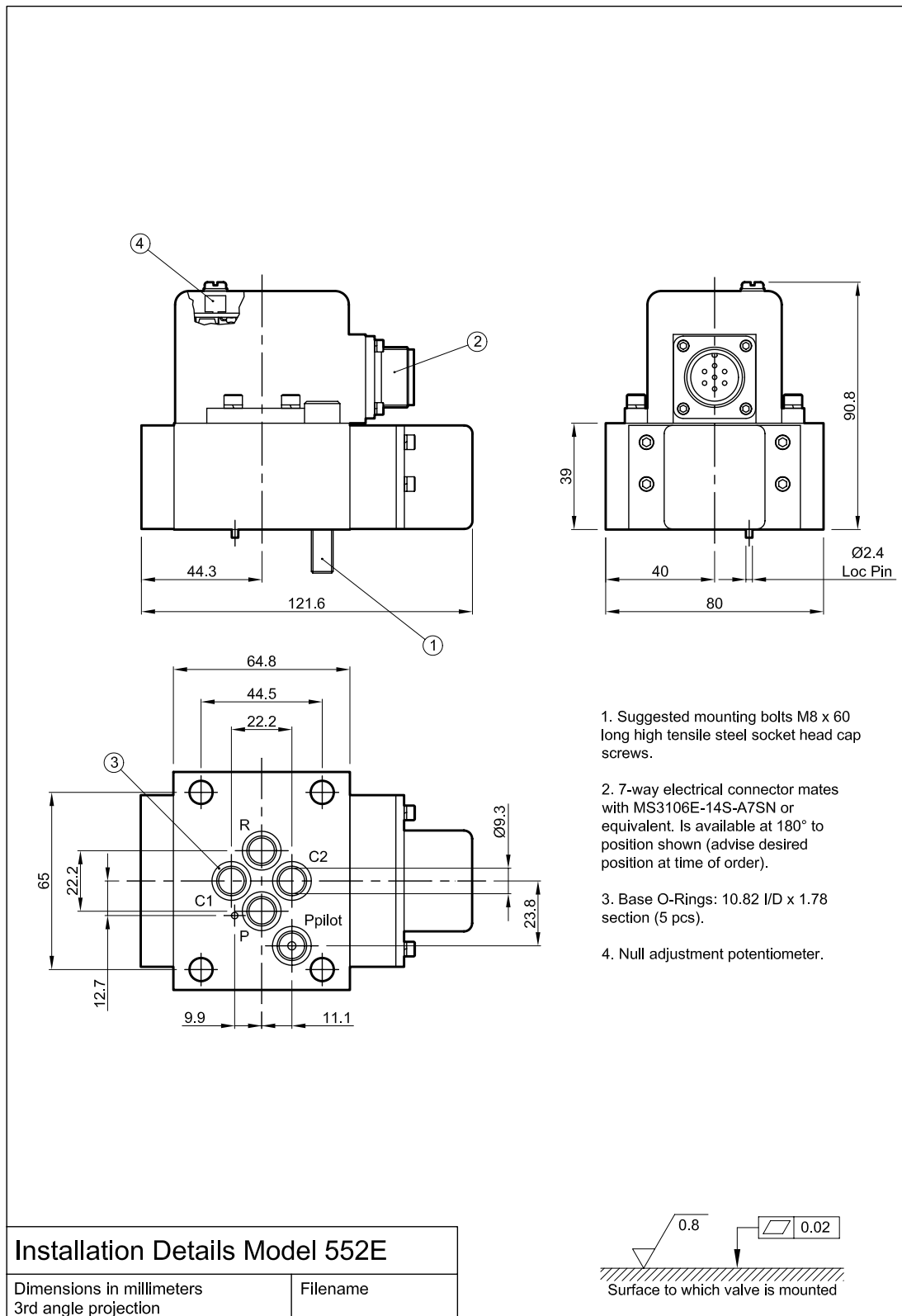


Figure B.14 – Servo valve manufacturers manual.

B.3 Measurement System

B.3.1 Signal Conditioning Units

Signal Conditioning A

Signal conditioning B has the following setup:

- AC1 Conditioning = Servo Valve driver
- DC2 Conditioning = Position sensor hydraulic actuator
- DC3 Conditioning = Load Cell

Signal Conditioning B

Signal conditioning B has the following setup:

- DC1 Conditioning = Pressure Tank sensor
- DC2 Conditioning = Pressure Supply sensor

Signal Conditioning C

Signal conditioning C has the following setup:

- DC1 Conditioning = Pressure B sensor
- DC2 Conditioning = Pressure A sensor

APPENDIX

C

DERIVATIONS MODELLING THEORY

This Appendix presents the derivations of the equations used in the modelling theory for the mechanical system, hydraulic system and control system.

C.1 Mechanical Modelling

This section presents first the derivation of FE model, thereafter the assembly and boundary conditions are presented. Finally this section concludes with the derivation of the state space methods.

C.1.1 Finite Element Modelling

Static Equations

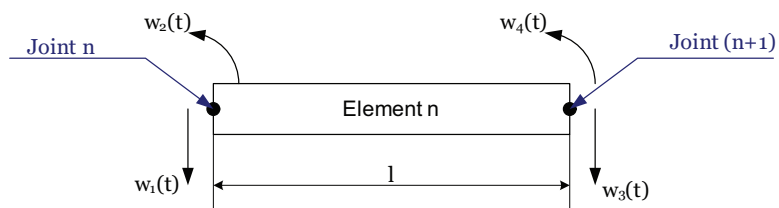


Figure C.1 – Element n , representing the degrees of freedom.

The displacements of the beam element can be calculated using a cubic equation in x (as in the case of static deflection of a beam):

$$w(x, t) = a(t) + b(t)x + c(t)x^2 + d(t)x^3$$

The unknown displacements $a(t)$, $b(t)$, $c(t)$ and $d(t)$ must satisfy the following conditions:

$$\begin{aligned} w(0, t) &= w_1(t), & \frac{\partial w}{\partial x}(0, t) &= w_2(t) \\ w(l, t) &= w_3(t), & \frac{\partial w}{\partial x}(l, t) &= w_4(t) \end{aligned}$$

If equation C.1.1 is substituted in equation C.1.1 the result is:

$$\begin{aligned} a(t) &= w_1(t) \\ b(t) &= w_2(t) \\ c(t) &= \frac{1}{l^2}[-3w_1(t) - 2w_2(t)l + 3w_3(t) - w_4(t)l] \\ d(t) &= \frac{1}{l^3}[2w_1(t) + w_2(t)l - 2w_3(t) + w_4(t)l] \end{aligned}$$

If the constants of equation C.1.1 are substituted in equation C.1.1, then this equation can be re written to the form of:

$$\begin{aligned} w(x, t) &= \left(1 - 3\frac{x^2}{l^2} + 2\frac{x^3}{l^3}\right) w_1(t) + \left(\frac{x}{l} - 2\frac{x^2}{l^2} + \frac{x^3}{l^3}\right) l w_2(t) \\ &\quad + \left(3\frac{x^2}{l^2} - 2\frac{x^3}{l^3}\right) w_3(t) + \left(-\frac{x^2}{l^2} + \frac{x^3}{l^3}\right) l w_4(t) \end{aligned}$$

This equation can be rewritten as:

$$w(x, t) = \sum_{i=1}^4 N_i(x) w_i(t)$$

here are $N_i(x)$ the shape functions.

$$\begin{aligned} N_1(x) &= 1 - 3\frac{x^2}{l^2} + 2\frac{x^3}{l^3} \\ N_2(x) &= x - 2l\frac{x^2}{l^2} + l\frac{x^3}{l^3} \\ N_3(x) &= 3\frac{x^2}{l^2} - 2\frac{x^3}{l^3} \\ N_4(x) &= -\frac{x^2}{l} + \frac{x^3}{l^2} \end{aligned}$$

These result in the following matrices:

$$\mathbf{N} = \begin{pmatrix} N_1 & N_2 & N_3 & N_4 \end{pmatrix}$$

$$\mathbf{w} = \begin{pmatrix} w_1 & w_2 & w_3 & w_4 \end{pmatrix}$$

Dynamic Equations

The kinetic energy, bending strain energy and virtual work of the element can be expressed as:

$$T(t) = \frac{1}{2} \int_0^l \rho A \left(\frac{\partial w(x,t)}{\partial t} \right)^2 dx \equiv \frac{1}{2} \dot{\mathbf{w}} \mathbf{M} \dot{\mathbf{w}}^T$$

$$V(t) = \frac{1}{2} \int_0^l EI \left(\frac{\partial^2 w(x,t)}{\partial x^2} \right)^2 dx \equiv \frac{1}{2} \mathbf{w} \mathbf{K} \mathbf{w}^T$$

$$\delta W(t) = \int_0^l f(x,t) \delta w(x,t) dx \equiv \delta \mathbf{w} \mathbf{F}$$

Where $\dot{\mathbf{w}} = \frac{\partial \mathbf{w}}{\partial t}$. From these formula's the K and M and F matrices can be calculated.

$$\mathbf{M} = \rho A \int_0^l \mathbf{N}^T \mathbf{N} dx$$

$$\mathbf{K} = EI \int_0^l \ddot{\mathbf{N}}^T \ddot{\mathbf{N}} dx$$

$$\mathbf{F} = \int_0^l \mathbf{N}^T \mathbf{F}^e dx$$

Where $\ddot{N} = \frac{\partial^2 N}{x^2}$. The result is the following mass and stiffness matrices.

$$\mathbf{M} = \frac{\rho Al}{420} \begin{bmatrix} 156 & 22l & 54 & -13l \\ 22l & 4l^2 & 13l & -3l^2 \\ 54 & 13l & 156 & -22l \\ -13l & -3l^2 & -22l & 4l^2 \end{bmatrix}, \quad \mathbf{K} = \frac{EI}{l^3} \begin{bmatrix} 12 & 6l & -12 & 6l \\ 6l & 4l^2 & -6l & 2l^2 \\ -12 & -6l & 12 & -6l \\ 6l & -2l^2 & -6l & 4l^2 \end{bmatrix}$$

Element stiffness matrix	\mathbf{K}	[N/m]
Element mass matrix	\mathbf{M}	[kg]
Element length	l	[m]
Density	ρ	[kg/m ³]
Elasticity modulus	E	[N/m ²]
Inertia	I	[m ⁴]

C.1.2 Assembling Mass and Stiffness matrices

Local matrices can be combined to obtain global system matrices. Figure C.2 shows three local elements. Each of these elements has its own element matrix E , an element matrix can be a mass matrix or stiffness matrix. The local coordinates of the elements

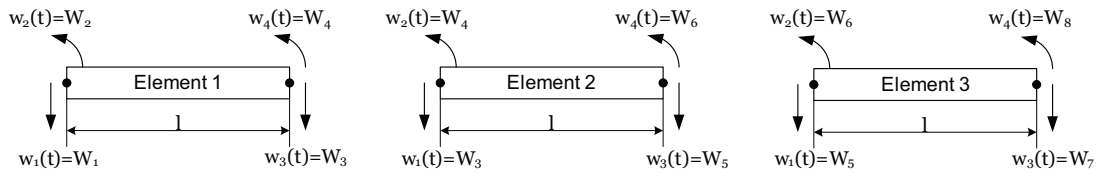


Figure C.2 – Multiple Elements Global coordinates

are translated to global coordinates, resulting in a global matrix. Elements presented in Figure C.2 are characterized in three element matrices \mathbf{E}_1 , \mathbf{E}_2 and \mathbf{E}_3 .

$$\mathbf{E}_1 = \begin{bmatrix} a_{11} & a_{12} & a_{13} & a_{14} \\ a_{21} & a_{22} & a_{23} & a_{24} \\ a_{31} & a_{32} & a_{33} & a_{34} \\ a_{41} & a_{42} & a_{43} & a_{44} \end{bmatrix}, \quad \mathbf{E}_2 = \begin{bmatrix} b_{11} & b_{12} & b_{13} & b_{14} \\ b_{21} & b_{22} & b_{23} & b_{24} \\ b_{31} & b_{32} & b_{33} & b_{34} \\ b_{41} & b_{42} & b_{43} & b_{44} \end{bmatrix}, \quad \mathbf{E}_3 = \begin{bmatrix} c_{11} & c_{12} & c_{13} & c_{14} \\ c_{21} & c_{22} & c_{23} & c_{24} \\ c_{31} & c_{32} & c_{33} & c_{34} \\ c_{41} & c_{42} & c_{43} & c_{44} \end{bmatrix}$$

The global matrix is defined as:

$$\mathbf{E}_g = \mathbf{E}_1 + \mathbf{E}_2 + \mathbf{E}_3$$

Assembling the element matrices leads to a global is done as represented in Equation C.1.2.

$$\mathbf{E}_g = \begin{bmatrix} a_{11} & a_{12} & a_{13} & a_{14} & 0 & 0 & 0 & 0 \\ a_{21} & a_{22} & a_{23} & a_{24} & 0 & 0 & 0 & 0 \\ a_{31} & a_{32} & a_{33} + b_{11} & a_{34} + b_{12} & b_{13} & b_{14} & 0 & 0 \\ a_{41} & a_{42} & a_{43} + b_{21} & a_{44} + b_{22} & b_{23} & b_{24} & 0 & 0 \\ 0 & 0 & b_{31} & b_{32} & b_{33} + c_{11} & b_{34} + c_{12} & c_{13} & c_{14} \\ 0 & 0 & b_{41} & b_{42} & b_{43} + c_{21} & b_{44} + c_{22} & c_{23} & c_{24} \\ 0 & 0 & 0 & 0 & c_{31} & c_{32} & c_{33} & c_{34} \\ 0 & 0 & 0 & 0 & c_{41} & c_{42} & c_{43} & c_{44} \end{bmatrix}$$

After defining the global matrix it is possible to apply boundary conditions on the rotations and translations of the beam. If for example the beam is clamped on the left side then the global displacement $W_1 = 0$ and the global rotation $W_2 = 0$, see Figure C.2. The result is that the first two columns and the first two rows disappear in the global matrix, resulting in the following global element matrix.

$$E_{g-fixed-free} = \begin{bmatrix} a_{33} + b_{11} & a_{34} + b_{12} & b_{13} & b_{14} & 0 & 0 \\ a_{43} + b_{21} & a_{44} + b_{22} & b_{23} & b_{24} & 0 & 0 \\ b_{31} & b_{32} & b_{33} + c_{11} & b_{34} + c_{12} & c_{13} & c_{14} \\ b_{41} & b_{42} & b_{43} + c_{21} & b_{44} + c_{22} & c_{23} & c_{24} \\ 0 & 0 & c_{31} & c_{32} & c_{33} & c_{34} \\ 0 & 0 & c_{41} & c_{42} & c_{43} & c_{44} \end{bmatrix}$$

The global matrix obtained represents a clamped beam as is displayed in Figure C.3.

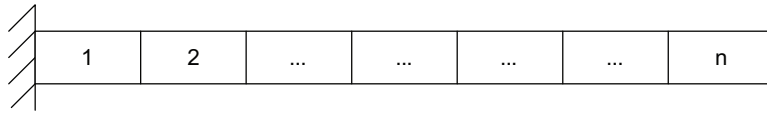


Figure C.3 – Finite Element clamped beam, consisting of n elements.

C.1.3 State Space representations

This section presents the derivations of the physical and normalized state spaces.

State Space Equations

The general dynamic equations are described by Equation (C.1.3).

$$\mathbf{M}_{MS}\ddot{\mathbf{w}} + \mathbf{C}_{MS}\dot{\mathbf{w}} + \mathbf{K}_{MS}\mathbf{w} = \mathbf{F}_{extern}$$

Mechanical system mass matrix	\mathbf{M}_{MS}	[kg]
Mechanical system stiffness matrix	\mathbf{K}_{MS}	[N/m]
Mechanical system damping matrix	\mathbf{C}_{MS}	[Ns/m]
Mechanical system external applied force matrix	\mathbf{F}_{extern}	[N]
Mechanical system displacement matrix	\mathbf{w}	[m]

Mass, Stiffness and Damping matrices of equation 4.2 can be written into state-space [19]. To obtain a first order system a state vector \mathbf{z} is introduced, see Equation 4.3.

$$\mathbf{z} = \begin{bmatrix} \mathbf{w} \\ \dot{\mathbf{w}} \end{bmatrix}$$

The time derivative of this state vector is:

$$\dot{\mathbf{z}} = \begin{bmatrix} \dot{\mathbf{w}} \\ \ddot{\mathbf{w}} \end{bmatrix}$$

If equation C.1.3 is pre-multiplied by the inverse mass matrix the result is:

$$\ddot{\mathbf{w}} + \mathbf{M}_{MS}^{-1}\mathbf{C}_{MS}\dot{\mathbf{w}} + \mathbf{M}_{MS}^{-1}\mathbf{K}_{MS}\mathbf{w} = \mathbf{M}_{MS}^{-1}\mathbf{F}_{extern}$$

$$\ddot{\mathbf{w}} = -\mathbf{M}_{MS}^{-1}\mathbf{C}_{MS}\dot{\mathbf{w}} - \mathbf{M}_{MS}^{-1}\mathbf{K}_{MS}\mathbf{w} + \mathbf{M}_{MS}^{-1}\mathbf{F}_{extern}$$

The general representation of a state space form is defined as in equation 4.4.

$$\dot{\mathbf{z}} = \mathbf{Az} + \mathbf{Bu}$$

$$\mathbf{y} = \mathbf{Cz} + \mathbf{Du}$$

Equation C.1.3 can be written in to state space form [6, 11]:

$$\begin{bmatrix} \dot{\mathbf{w}} \\ \ddot{\mathbf{w}} \end{bmatrix} = \begin{bmatrix} \mathbf{0} & \mathbf{I} \\ -\mathbf{M}_{MS}^{-1}\mathbf{K}_{MS} & -\mathbf{M}_{MS}^{-1}\mathbf{C}_{MS} \end{bmatrix} \begin{bmatrix} \mathbf{w} \\ \dot{\mathbf{w}} \end{bmatrix} + \begin{bmatrix} \mathbf{0} \\ -\mathbf{M}_{MS}^{-1}\mathbf{F} \end{bmatrix} \begin{bmatrix} \mathbf{u} \end{bmatrix}$$

$$\mathbf{y} = \begin{bmatrix} \mathbf{I} & \mathbf{0} \\ \mathbf{0} & \mathbf{I} \end{bmatrix} \begin{bmatrix} \mathbf{w} \\ \dot{\mathbf{w}} \end{bmatrix} + \begin{bmatrix} \mathbf{0} \\ \mathbf{0} \end{bmatrix} \begin{bmatrix} \mathbf{u} \end{bmatrix}$$

Normalized State Space Equations

The derivation of normalized state space equations starts from Equation (C.1.3). To obtain the eigenmodes and eigenfrequencies, the system is expressed through modal expansion:

$$\mathbf{w}(\mathbf{t}) = \sum_{s=1}^n \eta_s(t) \mathbf{v}_s$$

If Equation (C.1.3) is substituted in Equation (C.1.3) and is pre multiplied by each eigenmode $\mathbf{v}_{(r)}$, the result is the normalized equations:

$$\mathbf{v}_{(r)}^T \left(\mathbf{M}_{MS} \sum_{s=1}^n \mathbf{v}_{(s)} \ddot{\eta}_s(t) + \mathbf{C}_{MS} \sum_{s=1}^n \mathbf{v}_{(s)} \dot{\eta}_s(t) + \mathbf{K}_{MS} \sum_{s=1}^n \mathbf{v}_{(s)} \eta_s(t) \right) = \mathbf{v}_{(r)}^T \mathbf{F}_{extern}$$

The normalized form can be written as:

$$\ddot{\eta}_r + \sum_{s=1}^n \frac{\beta_{rs}}{\mu_r} \dot{\eta}_r + \frac{\gamma_r}{\mu_r} \eta_r = \phi_r(t)$$

Where:

$$\mu_r = \mathbf{v}_{(r)}^T \mathbf{M}_{MS} \mathbf{v}_{(r)}$$

$$\beta_{rs} = \mathbf{v}_{(r)}^T \mathbf{C}_{MS} \mathbf{v}_{(s)}$$

$$\gamma_r = \mathbf{v}_{(r)}^T \mathbf{K}_{MS} \mathbf{v}_{(r)}$$

$$\phi_r(t) = \frac{\mathbf{v}_{(r)}^T \mathbf{F}_{extern}}{\mu_r}$$

Which can be expressed in terms of eigenfrequencies and damping:

$$\ddot{\eta}_r + 2\zeta\omega_n\dot{\eta}_r + \omega_n^2\eta_r = \phi_r(t)$$

Where:

$$\omega_n^2 = \frac{\mathbf{v}_{(r)}^T \mathbf{K}_{MS} \mathbf{v}_{(r)}}{\mathbf{v}_{(r)}^T \mathbf{M}_{MS} \mathbf{v}_{(r)}} = \frac{\gamma_r}{\mu_r}$$

$$\zeta = \frac{\mathbf{v}_{(r)}^T \mathbf{C}_{MS} \mathbf{v}_{(s)}}{2\sqrt{\mathbf{v}_{(r)}^T \mathbf{K}_{MS} \mathbf{v}_{(r)} \mathbf{v}_{(r)}^T \mathbf{M}_{MS} \mathbf{v}_{(r)}}} = \frac{\beta_{rs}}{2\sqrt{\gamma_r \mu_r}}$$

Finally the normalized state space equations are obtained:

$$\begin{bmatrix} \dot{\eta} \\ \dot{\eta} \end{bmatrix} = \begin{bmatrix} \mathbf{0} & \mathbf{I} \\ -\Lambda & -2\zeta\Lambda^{1/2} \end{bmatrix} \begin{bmatrix} \eta \\ \dot{\eta} \end{bmatrix} + \begin{bmatrix} \mathbf{0} \\ -\Phi_r \end{bmatrix} \begin{bmatrix} \mathbf{u} \end{bmatrix}$$

$$\mathbf{y} = \mathbf{C} \begin{bmatrix} \mathbf{V} & \mathbf{0} \\ \mathbf{0} & \mathbf{V} \end{bmatrix} \begin{bmatrix} \eta \\ \dot{\eta} \end{bmatrix} + \begin{bmatrix} \mathbf{0} \\ \mathbf{0} \end{bmatrix} \begin{bmatrix} \mathbf{u} \end{bmatrix}$$

C.2 Servo-Hydraulic Modelling

This section presents the important formulas for modelling the hydraulic actuator and servo valve.

C.2.1 Fundamental Modelling Hydraulic actuators

The dynamics of the hydraulic actuator is expressed in Figure C.4. And the general layout is presented in Figure C.5. First the equations for the pressure dynamics are

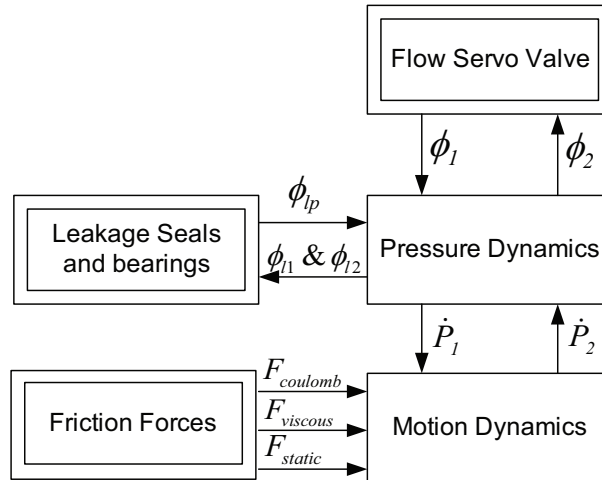


Figure C.4 – Block scheme representing the dynamics of the HA and their inputs [22].

derived. Thereafter the equations for the motion dynamics are derived.

Pressure Dynamics

Using continuity of hydraulic fluid flow the pressure dynamics each chamber can be expressed as:

$$\Phi_1 - \Phi_{lp} - \Phi_{l1} = \dot{V}_1 + \frac{V_1}{E(P_1)} \dot{P}_1$$

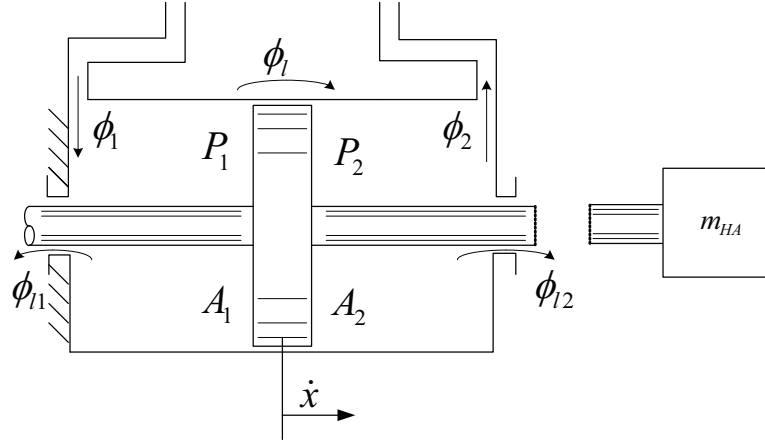


Figure C.5 – Schematic of hydraulic actuator, with the different parameters used for modelling [22].

$$\Phi_2 + \Phi_{lp} - \Phi_{l1} = \dot{V}_2 + \frac{V_2}{E(P_2)} \dot{P}_2$$

$$\dot{P}_1 = \frac{E(P_1)}{(V_0 + x_p A_p)} (\Phi_1 - \dot{x}_p A_p - \Phi_{lp} - \Phi_{l1})$$

$$\dot{P}_2 = \frac{E(P_2)}{(V_0 + x_p A_p)} (-\Phi_2 + \alpha \dot{x}_p A_p + \Phi_{lp} - \Phi_{l2})$$

Φ_i	Servo valve flows 1 and 2	$[l/min]$
Φ_{lp}	Leakage flow piston	$[l/min]$
Φ_{li}	Leakage flow seals 1 and 2	$[l/min]$
V_0	Dead oil volume of oil pipelines between SV and HA	$[m^3]$
x_p	Piston displacement	$[m]$
A_p	Piston area	$[m^2]$
α	Correction factor for difference in piston area	$[-]$
E	Bulk modulus oil	$[GPa]$
\dot{P}_i	Pressure sensitivity with respect to time	$[Pa/sec]$
V_i	Oil volume of the chamber	$[m^3]$
\dot{V}_i	Volume chamber sensitivity with respect to time	$[m^3/s]$

Equations of motion

$$\sum m_{HA} \ddot{x}_p = (P_1 - P_2) A_p + \sum F$$

Where:

$$\begin{aligned} \sum F &= F_{external} - F_{coulomb} - F_{viscous} - F_{static} - F_{end-stop} \\ \sum m_{HA} &= m_{piston} + m_{rod} + m_{fluid,1} + m_{fluid,2} \end{aligned}$$

The fluid masses can be calculated using:

$$\begin{aligned} M_{fluid,1} &= \rho_{fl} [V_{pl,1} + (x_{p0} + x_p) A_p] \\ M_{fluid,2} &= \rho_{fl} [V_{pl,2} + (x_{p0} - x_p) \alpha A_p] \end{aligned}$$

$M_{fluid,i}$	Fluid mass of chamber i	[kg]
$V_{pl,i}$	Volume supply pipe line i	[m ³]
Φ_{li}	Leakage flow seals 1 and 2	[l/min]
x_{p0}	Piston start position	[m]
x_p	Piston displacement	[m]
A_p	Piston area	[m ²]

C.2.2 Fundamental Modeling Servo Valve

The complete servo valve dynamics is presented in Figure C.6. This section will treat the modelling of the pressure dynamics, spool dynamics and non-linear spool port flows of the servo valve described in Figure C.6, based on [9, 22]. The modelling of the other components in Figure C.6 is provided by [22].

Pressure Dynamics

In order to describe the pressure dynamics, it is needed to know the flows through the nozzles and through the inlet and outlet. With these results it is possible to obtain the equations for the pressure dynamics.

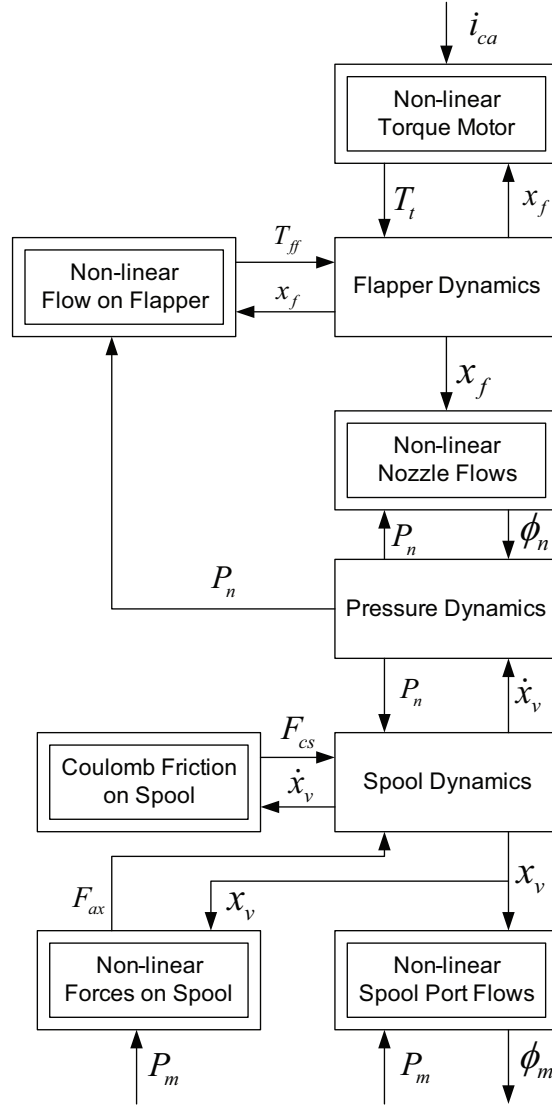


Figure C.6 – Blok scheme representation of a servo valve dynamics and there in and outputs [22].

Nozzle flows The nozzle flows Φ_{n1} , Φ_{n2} and Φ_{n3} are characterized by:

$$\Phi_{n1} = C_d \pi D_n (x_{f0} + x_f) \sqrt{2 \frac{P_{n1} - P_{n3}}{\rho_{fl}}}$$

$$\Phi_{n2} = C_d \pi D_n (x_{f0} + x_f) \sqrt{2 \frac{P_{n2} - P_{n3}}{\rho_{fl}}}$$

$$\Phi_{n3} = C_d A_{n3} \sqrt{2 \frac{P_{n1} - P_{n3}}{\rho_{fl}}}$$

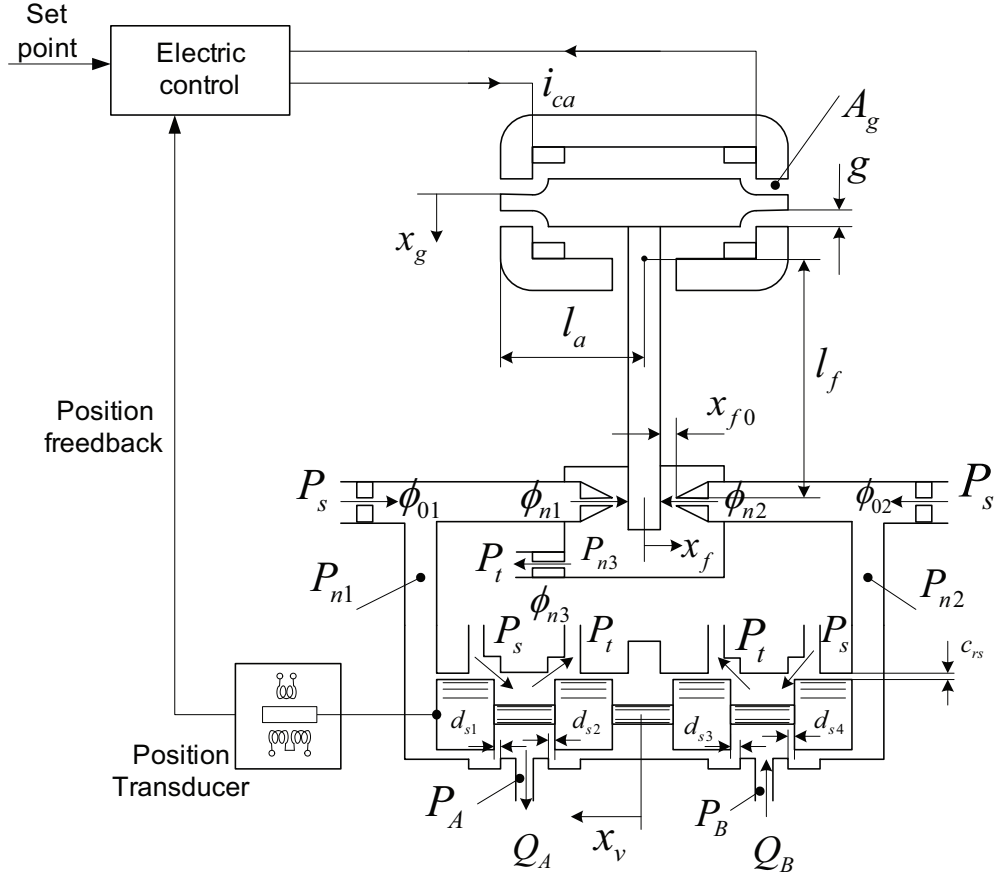


Figure C.7 – Servo valve physical layout, including all the different parameters [22].

C_d	Discharge coefficient for turbulent flows	[-]
ρ_{fl}	Density hydraulic fluid	[kg/m ³]
x_{f0}	Flapper-nozzle distance in neutral position	[m]
x_f	Flapper displacement	[m]
D_n	Nozzle diameter	[m]
P_{ni}	Nozzle pressure i	[Pa]
A_{ni}	Nozzle area i	[m ²]

Inlet flows The inlet flows Φ_{01} and Φ_{02} are characterized by:

$$\Phi_{01} = C_d A_0 \sqrt{2 \frac{P_s - P_{n1}}{\rho_{fl}}}$$

$$\Phi_{02} = C_d A_0 \sqrt{2 \frac{P_s - P_{n2}}{\rho_{fl}}}$$

Φ_i	Inlet flow	$[\text{m}^3/\text{s}]$
A_0	Orifice area of inlet restrictions	$[\text{m}^2]$
P_s	Supply pressure	$[\text{Pa}]$
P_{ni}	Nozzle pressure i	$[\text{Pa}]$

Pressure dynamics The pressure dynamics is obtained from the mass balanced defined by the nozzle and inlet flows.

$$\begin{aligned}\dot{P}_{n1} &= \frac{E}{V_{n1}} (\Phi_{01} - \Phi_{n1} + A_v \dot{x}_v) \\ \dot{P}_{n2} &= \frac{E}{V_{n2}} (\Phi_{02} - \Phi_{n2} - A_v \dot{x}_v) \\ \dot{P}_{n3} &= \frac{E}{V_{n3}} (\Phi_{n1} + \Phi_{n2} - \Phi_{n3})\end{aligned}$$

P_{ni}	Nozzle pressure i	$[\text{Pa}]$
E	Bulk modulus oil	$[\text{Pa}]$
V_{ni}	Valve chamber volumes	$[\text{m}^3]$
A_v	Valve spool area	$[\text{m}^2]$
x_v	Valve position	$[\text{m}]$

Spool Dynamics

For a two-stage flapper nozzle valve the equations of motion for the dynamics of the spool position are described by:

$$m_v \ddot{x}_v = A_v (P_{n2} - P_{n1}) - w_v \dot{x}_v - F_{cv} - F_{ax}$$

m_v	Mass of the valve	$[\text{kg}]$
w_v	Viscous friction of the valve	$[\text{Ns/m}]$
F_{cv}	Coulomb friction of the valve	$[\text{N}]$
F_{ax}	Axial flow forces	$[\text{N}]$

The coulomb friction and axial flow forces were not investigated. Detailed equations on calculating these forces are provided in literature [22].

Spool port flows

The Spool port flows are related to the valve dynamics, and are an important non-linear effect in the servo valve dynamics. The valve dynamics places the valve at a

certain position x_v , providing an opening of the orifices. Flow through an orifice can be calculated using equation by [9]:

$$Q = A \cdot v = AC_d \sqrt{\frac{2\Delta P}{\rho}} \text{sign}(\Delta P)$$

Q	Orifice flow	$[\text{m}^3/\text{s}]$
A	Orifice opening area	$[\text{m}^2]$
v	Velocity of the oil	$[\text{m}/\text{s}]$
C_d	Discharge coefficient	$[-]$
ΔP	Pressure drop between inlet and outlet	$[\text{Pa}]$
ρ	Density of oil	$[\text{kg}/\text{m}^3]$

Where the orifice opening area is calculated by:

$$A(h) = \begin{cases} h \cdot A_{max}/h_{max} + A_{leak} & \text{for } h > 0 \\ A_{leak} & \text{for } h < 0 \end{cases}$$

$$h = x_{v0} + x_v \cdot or$$

A	Orifice opening area	$[\text{m}^2]$
A_{leak}	Orifice leakage area	$[\text{m}^2]$
x_{v0}	Initial valve position	$[\text{m}]$
x_v	Valve position	$[\text{m}]$
or	Orifice orientation indicator, -1 or +1	$[-]$
h	Orifice opening	$[\text{m}]$

Knowing the equations for the flow through an orifice, it is possible to obtain the servo valve flows through and from the hydraulic actuator us, which are:

$$Q_A = Q_{P_S-P_A} - Q_{P_A-P_T}$$

$$Q_B = Q_{P_B-P_T} - Q_{P_S-P_B}$$

Q_A	Valve flow to HA chamber A	$[\text{m}^3/\text{s}]$
Q_B	Valve flow from HA chamber B	$[\text{m}^3/\text{s}]$
$Q_{P_S-P_A}$	Orifice flow from supply to HA chamber A	$[\text{m}^3/\text{s}]$
$Q_{P_A-P_T}$	Orifice flow from HA chamber A to tank	$[\text{m}^3/\text{s}]$
$Q_{P_S-P_B}$	Orifice flow from supply to HA chamber B	$[\text{m}^3/\text{s}]$
$Q_{P_B-P_T}$	Orifice flow from HA chamber B to tank	$[\text{m}^3/\text{s}]$

If Equation C.2.2 is substituted into Equations 4.24 and 4.25 the result is:

$$Q_A = A_{v1}C_d\sqrt{\frac{2(P_S - P_A)}{\rho}}\text{sign}(P_S - P_A) - A_{v2}C_d\sqrt{\frac{2(P_A - P_T)}{\rho}}\text{sign}(P_A - P_T)$$

$$Q_B = A_{v3}C_d\sqrt{\frac{2(P_B - P_T)}{\rho}}\text{sign}(P_B - P_T) - A_{v4}C_d\sqrt{\frac{2(P_S - P_B)}{\rho}}\text{sign}(P_S - P_B)$$

P_s	Supply pressure	[Pa]
P_t	Return pressure of tank	[Pa]
P_A	Pressure chamber A of HA	[Pa]
P_B	Pressure chamber B of HA	[Pa]
A_{vi}	Valve opening area of port i	[m ²]

APPENDIX

D

DEMONSTRATION TEST SETUP MODEL PARAMETERS

D.1 Mechanical System Model

D.1.1 Test Article

It was chosen to use a mechanical steel beam as test article. The mechanical beam has a symmetric cross sectional area, which dimensions are:

Height	H_{tot}	100	[mm]
Width	W_{tot}	100	[mm]
Thickness	T_{tot}	5	[mm]
Total length	L_{tot}	6	[m]
Clamping length	L_{clamp}	3	[m]

It was chosen to use a symmetric cross sectional area since dynamic properties in both directions will be the same. This is an advantage since then it is possible to determine clamping effects of the support structure.

Physical properties of the test article are:

Mass	M_{tot}	85	[kg]
Density	ρ_{beam}	7456, 14	[kg/m ³]
Cross sectional Area	A	0.0019	[m ²]
Inertia	I	$2.8658 \cdot 10^{-6}$	[m ⁴]
Elasticity Modulus	E_{steel}	$210 \cdot 10^9$	[Pa]
Elastic yield strength	$\sigma_{p0.2}$	240	[N/mm ²]

Stresses and Displacements Test Article

This section calculates the bending stiffness of the TA and the maximum applied force, which results in the maximum displacement.

The bending stiffness is calculated using Equation D.1.1.

$$K_{bending} = \frac{dF}{d\delta} = \frac{3EI}{L^3}$$

Bending stiffness	$K_{bending}$	$6.6869 \cdot 10^4$	[N/m]
-------------------	---------------	---------------------	-------

The normal stress can be determined using Equation D.1.1.

$$\sigma = \frac{Me}{I}$$

where:

$$e = \frac{H_{tot}}{2}$$

Maximal applied force results from:

$$F_{max} = \frac{I\sigma_{p0.2}}{eL_{clamp}}$$

Finally the maximum deflection is calculated using Equation D.1.1.

$$\delta = \frac{FL^3}{3EI}$$

Maximum Applied Force	F_{max}	4585.3	[N]
Maximum Applied Deflection	δ_{max}	68.57	[mm]

D.1.2 Interface Structures

Physical Parameters

2x Coupling bracket		6.0172	[kg]
Bolts and nuts		0.6877	[kg]
Coupling Rod		0.986	[kg]
2x Spines		2.0729	[kg]
Coupling Pin		0.3869	[kg]

Diameter pin	D_{pin}	25	[mm]
Length pin	L_{pin}	100	[mm]
Diameter rod	D_{pin}	30	[mm]
Length rod	L_{pin}	500	[mm]

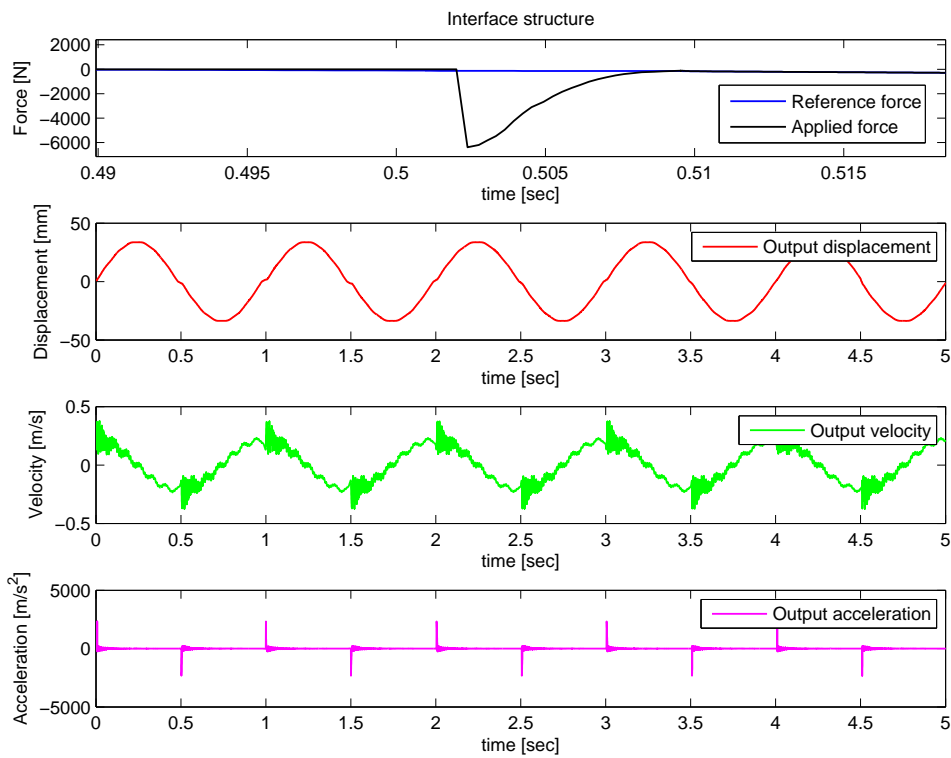


Figure D.1 – Interface structure, effect of mechanical play on sinusoidal reference signal of 0.5 Hz.

Stiffness Calculation

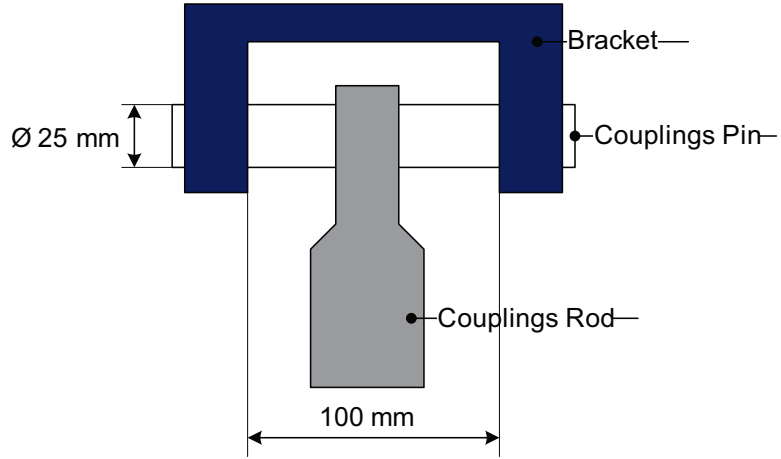


Figure D.2 – Interface structure coupling bracket and pin.

$$I_{pin} = \frac{\pi}{64} d^4$$

Inertia pin	I_{pin}	$1.9175 \cdot 10^{-8}$	$[m^4]$
-------------	-----------	------------------------	---------

Using Equation D.1.1 the bending stiffness of the 1/2 couplings pin is calculated.

Bending stiffness 1/2 couplings pin	K_{pin}	$9.66 \cdot 10^7$	$[N/m]$
Bending stiffness full couplings pin	K_{pin}	$1.93 \cdot 10^8$	$[N/m]$

The stiffness of the couplings rod is determined using Equation D.1.2.

$$\sigma = \epsilon E$$

Which can be written as:

$$\frac{F}{A} = \frac{\Delta L}{L_{rod}} E$$

The stiffness of the couplings rod is then:

$$K_{rod} = \frac{F}{\Delta L} = \frac{AE}{L_{rod}}$$

Couplings rod stiffness	K_{rod}	$2.9688 \cdot 10^8$	$[N/m]$
-------------------------	-----------	---------------------	---------

Damping Calculation

The critical damping is calculated by:

$$D_c = 2m_{IS}\sqrt{\frac{K_{pin}}{m_{IS}}}$$

The damping is calculated with:

$$D_{pin} = \zeta D_c$$

Resulting in:	Damping	ζ	0.1	[-]
	Couplings pin damping	D_{pin}	$9.380 \cdot 10^4$	[Ns/m]

Summarizing the parameters used for modelling the interface structure are:

Positive play gab	g_p	$0.085 \cdot 10^{-3}$	[m]
Negative play gab	g_n	$-0.085 \cdot 10^{-3}$	[m]
1/2 Stiffness IS positive	K_{IS}	$100 \cdot 10^6$	[N/m]
1/2 Damping IS positive	D_{IS}	$10 \cdot 10^4$	[Ns/m]
Mass IS	M_{IS}	2	[kg]

D.1.3 Backup Structure Stiffness

To determine the stiffness ratio between the stiffness of the TA and the support structure, the stiffness of the baseblock is calculated. Physical dimensions of this block are:

Length base block	L_{bb}	1000	[mm]
Height HA	$H_{couplingHA}$	300	[mm]
Thickness wall	T_{bb}	50	[mm]

The obtain a safe measure for the block stiffness the thickness of the is divided by a factor of 2 since the wall is not completely solid. Also the length is divided by a factor 2 in the calculation since it is assumed that the loading is not completely distributed over the full length. The inertia is calculated using Equation D.1.3. And the stiffness is determined using Equation D.1.1.

$$I_{bb} = \frac{1}{12}T_{bb}H_{couplingHA}^3$$

Inertia	I_{bb}	$5.6250 \cdot 10^{-5}$	$[\text{m}^4]$
Base block Stiffness	K_{bb}	$7.1 \cdot 10^7$	$[\text{N/m}]$

The stiffness ratio between support structure and TA is then:

$$K_{ratio} = \frac{K_{bb}}{K_{TA}} = \frac{7.1 \cdot 10^7}{6.7 \cdot 10^4} = 1.1 \cdot 10^3$$

To determine the stiffness ratio between the stiffness of the TA and the clamping structure, the bending stiffness of the clamping bolts is calculated. The clamping is provided by the clamp force and the bending force of the bolts. In worst case only the bending stiffness is present. Physical dimensions of these bolts are:

Length 1/2 bolt	L_{bolt}	50	$[\text{mm}]$
Diameter bolt	D_{bolt}	15	$[\text{mm}]$

Further more the standard properties as used for the steel beam are used. The bending stiffness can be estimated using Equation D.1.1 and the bolt inertia is calculated with:

$$I_{bolt} = \frac{\pi}{64} D_{bolt}^4$$

Calculation obtained the following results:

Inertia	I_{bolt}	$3.98 \cdot 10^{-8}$	$[\text{m}^4]$
Stiffnes 1/2 bolt	$K_{1/2bolt}$	$1.25 \cdot 10^7$	$[\text{N/m}]$
Stiffnes 1 bolt	K_{1bolt}	$2.50 \cdot 10^7$	$[\text{N/m}]$
Stiffnes 2 bolts	K_{2bolt}	$5.00 \cdot 10^7$	$[\text{N/m}]$

4 Bolts will clamp the TA. In the worst case 2 bolts will receive the loading. The stiffness ratio is then:

$$K_{ratio} = \frac{K_{bb}}{K_{TA}} = \frac{5.0 \cdot 10^7}{6.7 \cdot 10^4} = 747.7$$

Therefore it is assumed that the support structure rigidly clamps the TA.

D.2 Hydraulic System Model

D.2.1 Hydraulic Fluid

It was chosen to use ESSO UNIVIS 46 as hydraulic fluid. Hydraulic fluid parameters used in the model are:

D.2. Hydraulic System Model

Viscosity	C_{oil}	21.36	[cSt]
Density	ρ_{oil}	855.6	[kg/m ³]
Bulk Modulus	E_{oil}	$1.295 \cdot 10^9$	[Pa]
Amount of trapped air	α_{oil}	0	[%]
System temperature	T_{oil}	60	[C]

$$1 \text{ cSt} = 10^{-6} \text{ m}^2/\text{s}$$

It is assumed that no air is present in the system. Resulting in a constant bulk modulus over the pressure range.

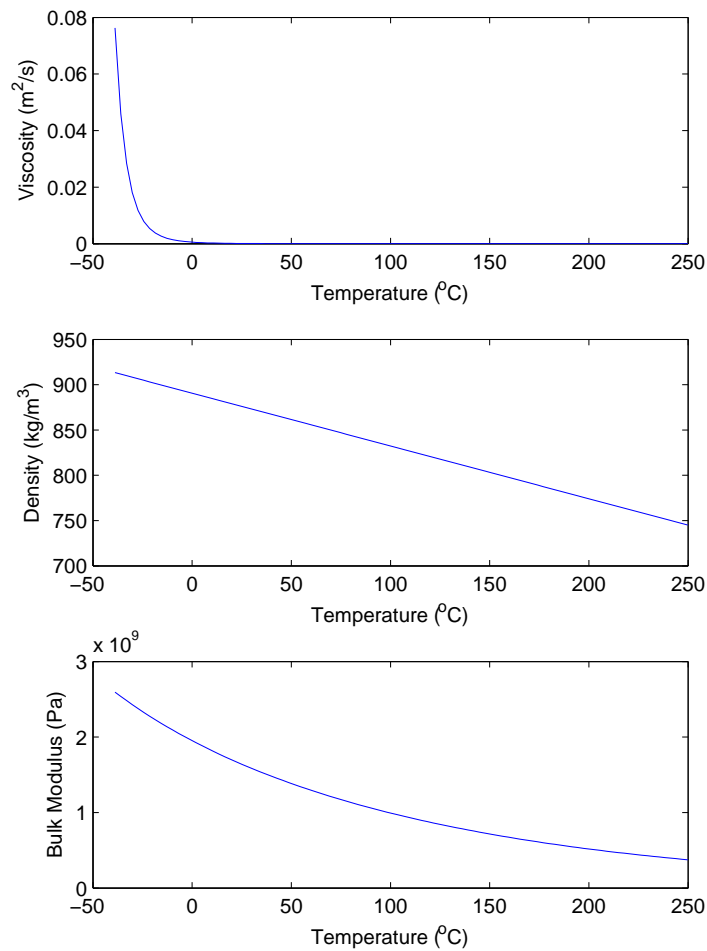


Figure D.3 – Hydraulic fluid properties of ESSO UNIVIS 46 hydraulic fluid.

D.2.2 Servo Valve Model

Servo Valve Response

To estimate the servo valve response, the eigenfrequency, damping and static gain are estimated from the servo valve response.

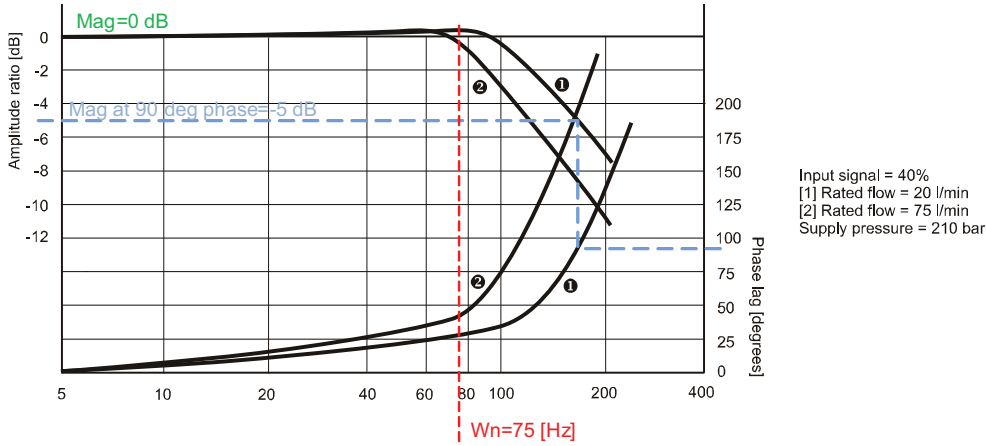


Figure D.4 – Servo valve estimation parameters

The response of the servo valve is calculated by:

$$G_{sv} = \frac{K_v \omega_v^2}{s^2 + 2D_v \omega_v s + \omega_v^2}$$

where:

$$D_v = \frac{1}{2 \cdot 10^{M90/20}}$$

$$K_v = 10^{M0/20}$$

The servo valve eigenfrequency is estimated, to be located at the place where the magnitude is maximal. The servo valve gain K_v is estimated when to be the magnitude $M0$ at 5 [Hz]. The magnitude $M90$, is the magnitude when the phase is 90 degrees. From this magnitude the servo valve damping D_v is calculated. Calculating these parameters from the frequency response of the manufacturer results in:

Valve eigenfrequency	ω_n	75	[Hz]
Valve damping	ζ_v	0.8891	[-]
Valve gain	K_v	1	[-]
Valve spool gain	S_{port}	0.0015	[m]

The valve spool gain is needed, since the output of the second order model is normalized. To scale the output to the physical valve displacement this gain is included.

Servo Valve parameters

The opening area of the servo valve is calculated using:

$$A_{port} = \left(\frac{Q_N}{C_d} \right) \sqrt{\frac{\rho_{oil}}{(2 \cdot 0.5 \cdot \Delta P_N)}}$$

The opening area is estimated at nominal flow and constant pressure drop over de valve. This is done because the nominal flow determines the operation point of the servo valve. This resulted in the following parameters:

Nominal flow	Q_N	10	[l/min]
Pressure drop	P_N	$70 \cdot 10^5$	[Pa]
Density hydraulic fluid	ρ_{oil}	855.7	[kg/m ³]
Discharge coefficient	C_D	0.611	[-]

To simulate the servo valve response, the following parameters are included in the model:

Supply pressure	P_s	$210 \cdot 10^5$	[Pa]
Orifice Opening area	A_{port}	$3.3175 \cdot 10^{-6}$	[m ²]
Underlap of port i in neutral position	d_{si}	$1 \cdot 10^{-6}$	[mm]
Discharge coefficient	C_D	0.611	[-]

D.2.3 Basic Hydraulic Actuator Model

The parameters of the hydraulic actuator, are calculated form the technical drawing presented in Appendix B.2.1. It is assumed that the dead volume of each chamber is equal to the chamber volume.

Dead oil volume of each chamber	V_0	$1.37 \cdot 10^{-4}$	[m ³]
Piston area	A_p	$5.497 \cdot 10^{-4}$	[m ²]
Correction factor	α	1	[-]
Maximum distance full extraction	x_E	0.125	[m]
Maximum distance full retraction	x_R	-0.125	[m]
Moving mass actuator	M_{act}	10	[kg]

Friction Model

Friction model parameters are estimated from the measurements.

Coulomb friction	F_c	260	[N]
Viscous friction	F_v	218.75	[N/(m/s)]
Static friction	F_s	600	[N]
Linear transition	$1/\dot{x}_{min}$	25	[s/m]
Linear velocity threshold	\dot{x}_{th}	$1 \cdot 10^{-4}$	[m/s]

D.2.4 Hydraulic Actuator Rod Stiffness

The rod stiffness is calculated by:

$$K_{rod} = \frac{AE}{l}$$

The area is the area of the rod diameter. And the length is the rod length obtained from the technical drawing in Appendix B.2.1.

Including the parameters results in:

$$K_{rod} = \frac{\frac{\pi}{4}(30 \cdot 10^{-3})^2 210 \cdot 10^9}{0.676} = 390 \cdot 10^6 \text{ [N/m]}$$

The mass of the rod is calculated to be 8.085 [Kg]. Using this mass the eigenfrequency of the rod is calculated:

$$\omega_{rod} = \sqrt{\frac{K_{rod}}{M_{rod}}} = \sqrt{\frac{390 \cdot 10^6}{8.085}} = 1106 \text{ [Hz]}$$

Calculating the critical damping results in:

$$c_{critical} = 2M_{rod}\omega_{rod} = 2 \cdot 8.085 \cdot 1106 = 1.1237 \cdot 10^5 \text{ [Ns/m]}$$

Assuming 2 % damping results in:

$$C_{rod} = \zeta c_{critical} = 0.02 \cdot 1.1237 \cdot 10^5 = 2.2473 \cdot 10^3 \text{ [Ns/m]}$$

APPENDIX

E

SIMULINK MODELLING

E.1 Energy Based Modelling

MATLAB-Simulink [14] uses an energy based method for the inclusion of servo-hydraulic systems. Input energy and output energy of the system need to be equal, assuming continuity. The in and outputs of each port have two variable, which product is the energy. These variables are defined as a *through variable* and *across variable*. The energy is defined as:

$$Energy = Across \times Through$$

The through and across variables are measured as:

- Through variable, which are measured in series with an element.
- Across variable, which are measured in parallel to an element.

Through and across variables characterizing the energy flow for mechanical systems and servo-hydraulic systems are displayed in Table E.1.

The amount of energy passed through a system is calculated using Equation E.1.

Input energy and output energy of the system need to be equal. From Equation E.1 and Figure E.1 can therefore be concluded, that Equation E.1 is present for an ideal hydraulic system.

Port type	Across variable	Through variable
Mechanical system	Translational velocity	Force
Servo Hydraulic system	Pressure	Flow rate

Table E.1 – Energy flow variables used in energy based modelling of MATLAB-Simulink.

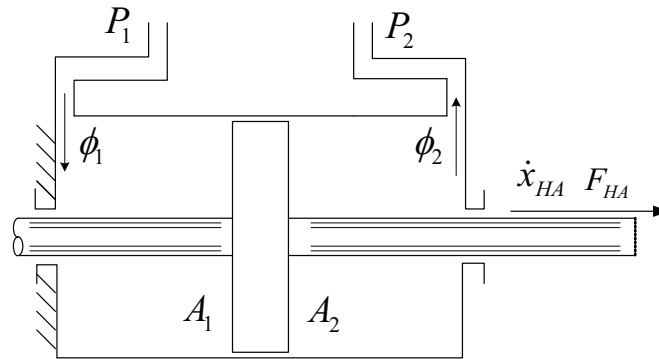


Figure E.1 – Hydraulic Actuator variables which characterize the energy flows.

$$P_1\phi_1 - P_2\phi_2 = \dot{x}_{HA}F_{HA}$$

Therefore MATLAB-simulink assumes continuity in energy flow through power systems. More details are provided in the MATLAB-Simulink user guide [14].

E.2 Force Input Calculation

To couple an hydraulic actuator which has a velocity and force output with the mechanical system, the input force is needed. To do so MATLAB-Simulink provides an ideal force sensor.

Figure E.2 presents the force input block, which is used to calculate the force input for the state space model. This calculation is done by using an ideal force sensor [13]. The sensor has three connections, two input and one output which are:

- R, input port representing the velocity and force of the hydraulic actuator.
- C, input port represents the velocity reference of the mechanical system.
- F, is the physical output force to the mechanical system.

Because of the energy approach (as discussed in previous section), port R is supplied with force (through variable) and velocity (across variable) provided by the hydraulic

E.2. Force Input Calculation

actuator. The force represents our physical output, and the velocity represents the mechanical translation. To be able to sense the force also a mechanical translational reference signal C must be present. In reality force is measured between hydraulic actuator and test article, by using a load cell. The force is measured in the same manner. To do this the velocity output of the state space model provides feedback to the mechanical translational reference port C . Resulting in a measured force between the hydraulic actuator and test article.

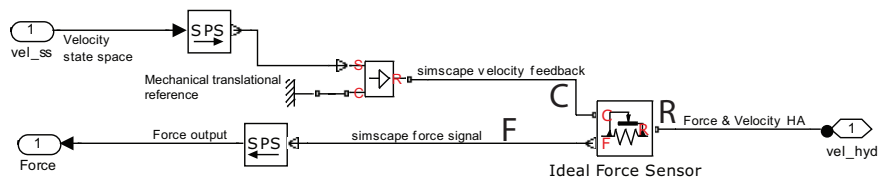


Figure E.2 – Force input block, representing the method for calculating the force provided by the HA.

The velocity output signal of the state space model is not yet a Simulink-Simscape signal. To obtain a Simulink-Simscape signal a conversion block SPS needs to be used (see Figure E.2). An ideal velocity source and a translational reference are used to obtain a physical reference in Simulink-Simscape of the velocity signal.

E.3 Linearization of Simulation Models

This section will presents the linearization method as used in MATLAB-Simulink for obtaining linear system models [15]. Linear models of the system are used for controller parameter estimation. First the linearization method is discussed. Thereafter the linearization settings are presented.

E.3.1 Linearization Background

A non-linear system can be expressed into a state space representation by:

$$\begin{aligned}\dot{x}(t) &= f(x(t), u(t), t) \\ y(t) &= g(x(t), u(t), t)\end{aligned}$$

Where $x(t)$ represents the system states, $u(t)$ the inputs and $y(t)$ the outputs. The variables vary continuous with time. A linear approximation of the non-linear system is obtained around an operating point at $t = t_0$, $x_0 = x(t_0)$ and $u_0 = u(t_0)$. To obtain a linearized model first new set of variables centered about the operating point are introduced, which describe system states, inputs and outputs:

$$\begin{aligned}\delta x(t) &= x(t) - x_0 \\ \delta y(t) &= y(t) - y_0 \\ \delta u(t) &= u(t) - u_0\end{aligned}$$

This results in linearized state space equations in terms of $\delta x(t)$, $\delta y(t)$ and $\delta u(t)$, which are:

$$\begin{aligned}\delta \dot{x}(t) &= A\delta x(t) + B\delta u(t) \\ \delta y(t) &= C\delta x(t) + D\delta u(t)\end{aligned}$$

Where A,B,C and D are the Jacobians of the system evaluated at the operating point:

$$\begin{aligned}A &= \frac{\partial f}{\partial x_{t_0, x_0, u_0}} & B &= \frac{\partial f}{\partial u_{t_0, x_0, u_0}} \\ C &= \frac{\partial g}{\partial x_{t_0, x_0, u_0}} & D &= \frac{\partial g}{\partial u_{t_0, x_0, u_0}}\end{aligned}$$

The Jacobians are the sensitivities at each operation point. To obtain from this linear model the linear transfer function, the system has to be transfered using Laplace transformation. To obtain the linear transfer function the system the Laplace transform of

the output is divided by the Laplace transform of the input.

$$P_{lin}(s) = \frac{\delta Y(s)}{\delta U(s)}$$

The linear transfer functions obtained are used for verification of the measurements.

E.3.2 Linearization Settings

For linearization options where set to obtain linearized models, which are:

Linearization algorithm:	Analytical block by block.
Operating point:	$t = 0$.

For linearization of the simulink models an analytical block by block linearization is used. This means that each simulation block (for example a Hydraulic Actuator simulation block) is linearized individually. These linearized sub-models are combined to obtain a full linear model.

The operation point for linearization is obtained at $t = 0$. This means that the initial values of the system are used as operation point. For example the HA is positioned at $t = 0$ at 0.125 [m] of its actuator stroke.

APPENDIX

F

MEASUREMENT SETTINGS

F.1 Mechanical System

Measurement settings used to measure the eigenfrequencies and eigenmodes where:

Sample frequency	F_{sample}	1280	[Hz]
Block size	B_{size}	1800	[-]
Number of averages	$N_{averages}$	10	[-]
Number of points	$N_{measure}$	28	[-]
Distance between points	D_{point}	0.2	[m]
Hammer signal	Force window		[-]
Accelerometer signals	Hanning window		[-]
Directions measured	Y and Z		[-]

F.2 Hydraulic System

F.2.1 Servo Valve

This section presents the derivation of the operation points required to generate a constant amount of flow through the servo valve, at different frequencies. These operation points are used to perform measurements for verification.

The maximum output flow is:

$$\phi_{servo} = 10[\text{l}/\text{min}] = \frac{10 \cdot 10^{-3}}{60}[\text{m}^3/\text{sec}] = 1.67 \cdot 10^{-4}[\text{m}^3/\text{sec}]$$

The maximum flow needed by the HA, is related to the piston area and the maximum piston speed, which is defined as:

$$\phi_{actuator} = \dot{x}_{piston-max} A_{piston}$$

Where the piston speed is depended on the frequency and the amplitude of the stroke.

$$x = x_{piston} \sin(\omega t)$$

Differentiating with respect to time leads to:

$$\dot{x} = x_{piston} \omega \cos(\omega t)$$

The maximum piston speed is then:

$$\dot{x}_{piston-max} = x_{piston} \omega = x_{piston} 2\pi f$$

which results in the maximum hydraulic actuator flow:

$$\phi_{actuator} = x_{piston} 2\pi f A_{piston}$$

The amount of flow consumed by the actuator is equal to the amount of flow through the servo valve. Assuming continuity of flow and assuming an exact 1:1 ratio over all frequencies between input and output of the servo valve, results in:

$$\phi_{servo} = \phi_{actuator}$$

$$\phi_{servo} = x_{piston} 2\pi f A_{piston}$$

Which can be written as:

$$x_{piston} = \frac{\phi_{servo}}{2\pi f A_{piston}}$$

Defining different oil flows ϕ_{servo} , 20%, 40%, 60% and 80% of the maximum servo valve flow results into Figure F.1.

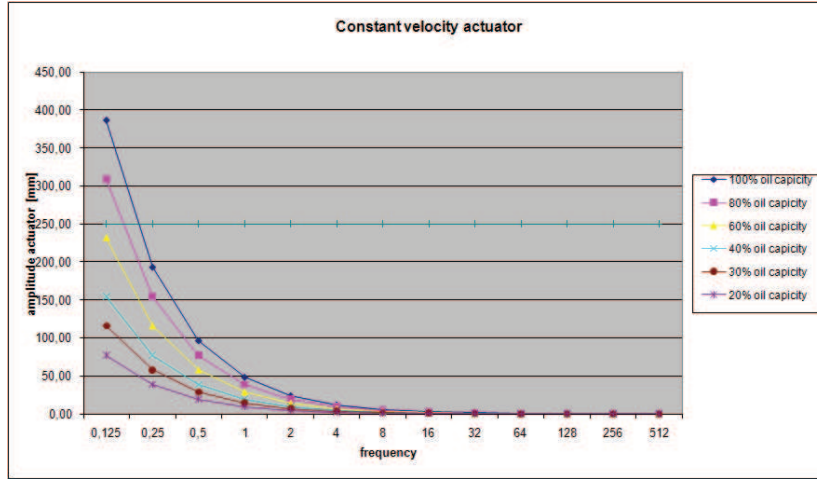


Figure F.1 – Piston displacement at different oil flows at different frequencies.

To define the input voltages to obtain the output displacements at each frequency, it is assumed that the piston position is linear related to the input voltage. Friction in the HA is neglected. It is assumed that:

$$5 \text{ Volt} = 125 \text{ mm}$$

This obtained the measurement settings to measure the hydraulic system using different percentages of flow through the servo valve. These settings are presented in the next section.

F.2.2 Measurement Settings Oil Flows

The next tables present the calculated reference signals to measure the frequency response at different frequencies with 20%, 40%, 60% or 80% oil flow through the servo valve. The maximum amplitude of the piston is limited to 125 [mm]. And the maximum input force is limited to 2500 [N].

20% oil capacity					
Freq [Hz]	Amplitude piston [mm]	Total amplitude piston [mm]	Velocity piston [mm/s]	Input force [N]	Reference Amplitude [V]
0,125	77,20	154,39	60,63	4511,46	3,09
0,25	38,60	77,20	60,63	2255,73	1,54
0,5	19,30	38,60	60,63	1127,86	0,77
1	9,65	19,30	60,63	563,93	0,39
2	4,82	9,65	60,63	281,97	0,19
4	2,41	4,82	60,63	140,98	0,10
8	1,21	2,41	60,63	70,49	0,05
16	0,60	1,21	60,63	35,25	0,02
32	0,30	0,60	60,63	17,62	0,01
64	0,15	0,30	60,63	8,81	0,01
128	0,08	0,15	60,63	4,41	0,00

Table F.1 – Measurement settings for 20% oil flow through the servo valve.

40% oil capacity					
Freq [Hz]	Amplitude piston [mm]	Total amplitude piston [mm]	Velocity piston [mm/s]	Input force [N]	Reference Amplitude [V]
0,125	154,39	308,79	121,26	9022,91	6,18
0,25	77,20	154,39	121,26	4511,46	3,09
0,5	38,60	77,20	121,26	2255,73	1,54
1	19,30	38,60	121,26	1127,86	0,77
2	9,65	19,30	121,26	563,93	0,39
4	4,82	9,65	121,26	281,97	0,19
8	2,41	4,82	121,26	140,98	0,10
16	1,21	2,41	121,26	70,49	0,05
32	0,60	1,21	121,26	35,25	0,02
64	0,30	0,60	121,26	17,62	0,01
128	0,15	0,30	121,26	8,81	0,01
256	0,08	0,15	121,26	4,41	0,00

Table F.2 – Measurement settings for 40% oil flow through the servo valve.

F.3 Control System Settings

This section presents the controller settings as used during measurements.

F.3.1 Servo-Hydraulic Settings

The controller settings for verification of the hydraulic actuator coupled with the servo valve are:

F.3. Control System Settings

60% oil capacity					
Freq [Hz]	Amplitude piston [mm]	Total amplitude piston [mm]	Velocity piston [mm/s]	Input force [N]	Reference Amplitude [V]
0,125	231,59	463,18	181,89	13534,37	9,26
0,25	115,80	231,59	181,89	6767,18	4,63
0,5	57,90	115,80	181,89	3383,59	2,32
1	28,95	57,90	181,89	1691,80	1,16
2	14,47	28,95	181,89	845,90	0,58
4	7,24	14,47	181,89	422,95	0,29
8	3,62	7,24	181,89	211,47	0,14
16	1,81	3,62	181,89	105,74	0,07
32	0,90	1,81	181,89	52,87	0,04
64	0,45	0,90	181,89	26,43	0,02
128	0,23	0,45	181,89	13,22	0,01
256	0,11	0,23	181,89	6,61	0,00

Table F.3 – Measurement settings for 60% oil flow through the servo valve.

80% oil capacity					
Freq [Hz]	Amplitude piston [mm]	Total amplitude piston [mm]	Velocity piston [mm/s]	Input force [N]	Reference Amplitude [V]
0,125	308,79	617,58	242,52	18045,82	12,35
0,25	154,39	308,79	242,52	9022,91	6,18
0,5	77,20	154,39	242,52	4511,46	3,09
1	38,60	77,20	242,52	2255,73	1,54
2	19,30	38,60	242,52	1127,86	0,77
4	9,65	19,30	242,52	563,93	0,39
8	4,82	9,65	242,52	281,97	0,19
16	2,41	4,82	242,52	140,98	0,10
32	1,21	2,41	242,52	70,49	0,05
64	0,60	1,21	242,52	35,25	0,02
128	0,30	0,60	242,52	17,62	0,01
256	0,15	0,30	242,52	8,81	0,01
512	0,08	0,15	242,52	4,41	0,00

Table F.4 – Measurement settings for 80% oil flow through the servo valve.

Sweep measurement	Bandwidth [Hz]	Fsample [Hz]	Block Size	Amplitude [mV]	K_p	Averages
0.125 Hz - 200 Hz	256	512	4096	200 P.P.	5	10

Table F.5 – Measurement settings, used for a frequency sweep measurement of the servo valve and hydraulic actuator.

	20 percent oil flow	40 percent oil flow	60 percent oil flow	80 percent oil flow
Frequency [Hz]	K_p	K_p	K_p	K_p
0,125	2,5			
0,25	5	3	4	
0,5	7,5	5	5	7
1	7,5	10	15	10
2	12	15	20	15
4	15	25	30	27
8	25	30	35	35
16	25	30	35	40
32	25	30	35	40
64	25	30	35	40

Table F.6 – Measurement settings, used for measuring coupled servo valve and hydraulic actuator response.

F.3.2 Coupled System Position Feedback Settings

The controller settings for the coupled hydraulic system with the mechanical system, using position feedback are:

Sweep measurement	Bandwidth [Hz]	Fsample [Hz]	Block Size	Amplitude [mV]	K_p	Averages
0.125 Hz - 128 Hz	512	1024	8192	50 P.P.	10	10

Table F.7 – Controller settings, used for a frequency sweep measurement for position closed loop response.

F.3. Control System Settings

Freq. [Hz]	20% oil capacity			40% oil capacity			60% oil capacity			80% oil capacity		
	Kd	Kp	Ki	Kd	Kp	Ki	Kd	Kp	Ki	Kd	Kp	Ki
0,25	0	5	0,001									
0,5	0,005	8	0,04	0	5	0,005						
1	0	8	0	0	10	0,002	0,01	15	0,08	0,01	20	0,05
2	0,02	10	0,25	0	10	0,05	0,005	20	0,01	0,01	25	0,05
4	0	10	0,25	0	15	0,02	0,01	20	0,05	0,01	22	0,05
8	0	10	0,8	0	25	0	0,01	29	0,025	0,01	28	0,05
16	0	30	0	0	30	0	0,02	25	0,04	0,01	30	0,04
32	0	20	0	0	20	0	0,005	25	0,005	0,015	27	0,05
64	0	30	0	0	35	0	0	45	0,01	0,01	45	0,01

Table F.8 – Controller settings, for position feedback.

F.3.3 Coupled System Force Feedback Settings

The controller settings for the coupled hydraulic system with the mechanical system, using force feedback are:

Sweep measurement	Bandwidth [Hz]	Fsample [Hz]	Block Size	Amplitude [mV]	K_p	Averages
0.125 Hz - 128 Hz	1024	2048	16384	200 P.P.	2	10

Table F.9 – Controller settings, used for a frequency sweep measurement for force closed loop response.

Freq. [Hz]	20% oil capacity			40% oil capacity			60% oil capacity			80% oil capacity		
	Kd	Kp	Ki	Kd	Kp	Ki	Kd	Kp	Ki	Kd	Kp	Ki
0,25	0	1	0,0011									
0,5	0	1,5	0,01	0	1	0,008						
1	0	1,5	0,038	0	1,5	0,042	0	1,8	0,042	0	1	0,039
2	0	2	0,16	0	1,5	0,17	0	1,5	0,18	0	1,5	0,185
4	0	1,5	0,8	0	2	0,85	0	1,8	0,9	0	2	0,85

Table F.10 – Controller settings, for force feedback.

F.3.4 Measurement System

To measure the sinusoidal signals of the different reference flows, the following measurement settings were used:

Where:

Reference [Hz]	BW [Hz]	Fs [Hz]	Bs [Hz]	ΔF [Hz]	Δt [s]	cycli/avg	nr. avg
0,125	1	2	128	0,007813	128	16	5
0,25	2	4	128	0,015625	64	16	5
0,5	4	8	128	0,03125	32	16	10
1	8	16	128	0,0625	16	16	10
2	16	32	128	0,125	8	16	20
4	32	64	128	0,25	4	16	32
8	64	128	256	0,25	4	32	32
16	128	256	512	0,25	4	64	16
32	256	512	1024	0,25	4	128	8
64	512	1024	2048	0,25	4	256	4
128	1024	2048	4096	0,25	4	512	2
256	2048	4096	8192	0,25	4	1024	1
512	4096	8192	16384	0,25	4	2048	1

Table F.11 – Measurement settings for measuring different sinusoidal signals.

- BW = bandwidth measured.
- Fs = sample frequency = $BW \cdot 2$.
- Bs = Block size, which is the number of data points measured.
- ΔF = resolution measured = BW / BS .
- Δt = resolution in time = $1 / \Delta F$.
- cycli/avg = the amount of sinusoids present in one measured block.
- nr. avg = the total amount of measurement blocks measured.

APPENDIX

G

MODEL UPDATING

G.1 Test Article Model Updating

This section presents the derivation of the relation between the clamping length of the TA and its eigenfrequency. To obtain this relation the kinetic and potential energies of the TA are derived. First the displacement field is presented.

G.1.1 Displacement Field

The displacement field and its time derivatives of a clamped beam can be written as:

$$\begin{aligned}u &= (1 - x/l)^2 \cos(\omega t) \\ \dot{u} &= -(1 - x/l)^2 \omega \sin(\omega t) \\ \ddot{u} &= -(1 - x/l)^2 \omega^2 \cos(\omega t)\end{aligned}$$

Displacement	u	[m]
Clamping length	l	[m]
Variable length	x	[m]
Eigenfrequency	ω	[rad/s]
time	t	[sec]

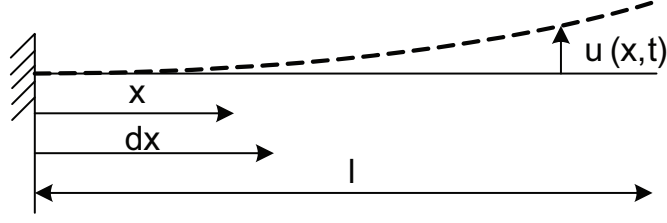


Figure G.1 – Beam displacement field, presenting the variables used to calculate the displacement of the TA.

G.1.2 Kinetic Energy Beam

The kinetic energy of the TA is calculated by:

$$E_k = \frac{1}{2} \int_0^l \dot{u}^2 dm = \frac{1}{2} \int_0^l \dot{u}^2 \rho A dx$$

Kinetic energy	E_k	[Joule]
Variable mass	dm	[kg]
Cross sectional area TA	A	[m ²]
density	ρ	[kg/m ³]

The velocity squared of the TA at displacement x is calculated using:

$$\dot{u}^2 = (1 - x/l)^4 \omega^2 \sin^2(\omega t)$$

Substituting above into Equation G.1.2 obtains:

$$E_k = \frac{1}{2} \int_0^l (1 - x/l)^4 \omega^2 \sin^2(\omega t) \rho A dx$$

$$\int_0^l (1 - x/l)^4 dx = \int_0^l \frac{x^4}{l^4} - 4 \frac{x^3}{l^3} + 6 \frac{x^2}{l^2} - 4 \frac{x}{l} + 1 dx$$

$$\int_0^l (1 - x/l)^4 dx = \left[\frac{x^5}{5l^4} - \frac{x^4}{l^3} + 2 \frac{x^3}{l^2} - 2 \frac{x^2}{l} + x \right]_0^l = \frac{1}{5} l$$

$$E_k = \frac{1}{10} l \omega^2 \rho A \sin^2(\omega t)$$

G.1.3 Potential Energy

The potential energy of the TA is calculated by:

$$U_e = \frac{1}{2} \int_0^l M d\theta$$

Potential energy	U_e	[Joule]
Bending moment	M	[Nm]

The bending moment is calculated using:

$$M(x, t) = EI \frac{\partial^2 u}{\partial x^2}(x, t)$$

Elasticity modulus	E	$[\text{N/m}^2]$
Inertia	I	$[\text{m}^4]$

The slope of the deformed beam is given by:

$$\theta = \frac{\partial u}{\partial x}$$

Angle beam	θ	[rad]
------------	----------	-------

Substituting Equations G.1.3 and G.1.3 into Equation G.1.3 results in:

$$U_e = \frac{1}{2} \int_0^l EI \frac{\partial^2 u}{\partial x^2} \frac{\partial^2 u}{\partial x^2} dx = \frac{1}{2} \int_0^l EI \left(\frac{\partial^2 u}{\partial x^2} \right)^2 dx$$

Where:

$$\frac{\partial^2 u}{\partial x^2} = \frac{2}{l^2} \cos(\omega t)$$

Rewriting results in:

$$U_e = \frac{1}{2} \int_0^l EI \left(\frac{2}{l^2} \cos(\omega t) \right)^2 dx = 2 \int_0^l \frac{EI}{l^4} \cos^2(\omega t) dx$$

Integration over the length of the beam obtains:

$$U_e = 2 \frac{EI}{l^4} \cos^2(\omega t) [x]_0^l = 2 \frac{EI}{l^4} \cos^2(\omega t) l$$

Rewriting results in the the potential energy of the beam:

$$U_e = 2\frac{EI}{l^3}\cos^2(\omega t)$$

G.1.4 Equilibrium

To obtain the relation between the eigenfrequency and the length of the beam, the kinetic and potential energy maximum values are stet equal to each other.

$$E_k = U_e$$

Equation G.1.4 results in:

$$\frac{1}{10}l\omega^2\rho A\sin^2(\omega t) = 2\frac{EI}{l^3}\cos^2(\omega t)$$

The maximum values of the kinetic and potential energy are:

$$\frac{1}{10}l\omega^2\rho A = 2\frac{EI}{l^3}$$

Resulting in the relation between eigenfrequency and the length of the TA.

$$\omega = \sqrt{20\frac{EI}{\rho Al^4}}$$

G.1.5 Eigenfrequency Length Correlation

Equation G.1.4 can be written as:

$$\omega = Cl^{-2}$$

Where:

$$C = \sqrt{20}\frac{EI}{\rho A}$$

Differentiating results into:

$$\frac{d\omega}{dl} = -\frac{2C}{l^3}$$

$$d\omega = -\frac{2C}{l^3}dl$$

Multiplying both sides with the inverse of Equation G.1.5 results into:

$$\frac{d\omega}{\omega} = -\frac{2C}{l^3}\frac{l^2}{C}dl$$

Finally the relation between the difference in eigenfrequency and the difference in

G.1. Test Article Model Updating

clamping length is written as:

$$\frac{d\omega}{\omega} = -2\frac{dl}{l}$$

Equation G.1.5 is used for the updating of the clamping length of the TA.

The interface structure mass is added to the test article tip, which obtained the following frequency response.

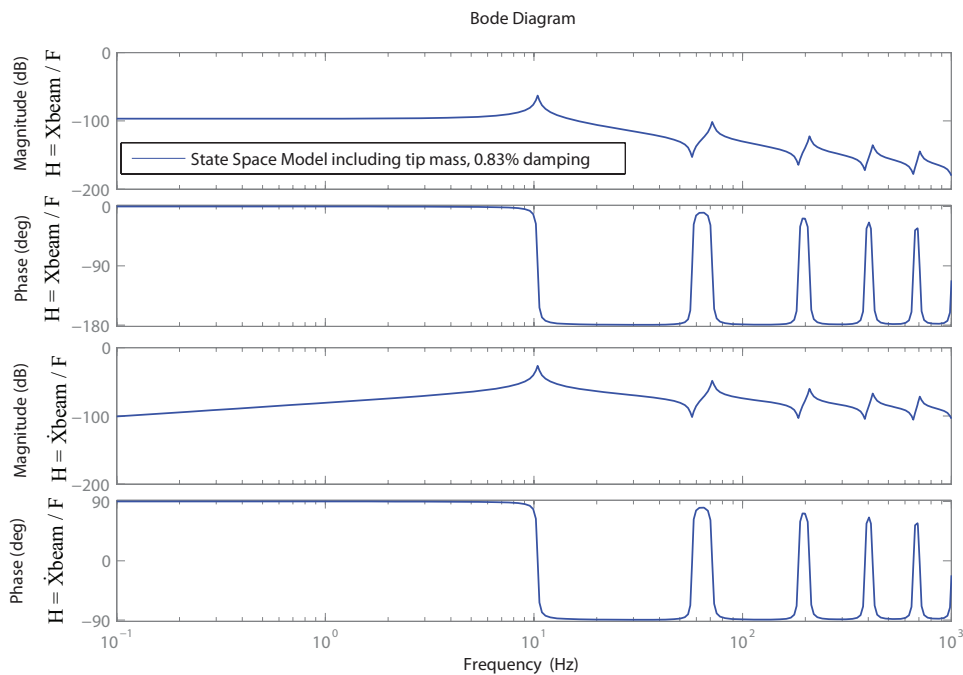


Figure G.2 – Update state space model, including tip mass of interface structure.

The updated mechanical parameters are:

Clamping length TA	L_{clamp}	3.1013	[m]
Damping TA	ζ_{TA}	0.83	[%]
Mass tip TA	M_{tip}	10.15	[kg]
Coupling Rod		0.986	[kg]
2x Spines		2.0729	[kg]
Coupling Pin		0.3869	[kg]
Brackets		6.017	[kg]
Bolts and nuts		0.6877	[kg]

G.2 Hydraulic System Model Updating

G.2.1 Hydraulic Actuator Model Updating

The updated mass and friction parameters of the hydraulic actuator are:

Moving mass actuator	M_{act}	11.09	[kg]
Load Cell	3		[kg]
Rod and piston	8.0859		[kg]

The updated friction parameters with respect to the symmetric averaged measurement are:

Coulomb friction	F_{c0}	250	[N]
Viscous friction	F_{v0}	105	[N/(m/s)]
Static friction	F_{s0}	650	[N]
Linear transition	\dot{x}_{min}	22.8571	[s/m]
Linear velocity threshold	\dot{x}_{th}	$1 \cdot 10^{-4}$	[m/s]

APPENDIX

H

MEASUREMENT RESULTS

H.1 Mechanical System

H.1.1 Test Article

To measure the modes of the test article, the frequency responses are measured. Each measurement obtains the eigenfrequencies and the modal amplitude at the point measured, see Figure H.1. To obtain information on the correctness of the measurement the coherence is calculated between the input force and output acceleration, see Figure H.2.

Figure H.3 presents the obtained correlated modes of the rear beam. The MAC values between model and measurement are presented in Table H.1.

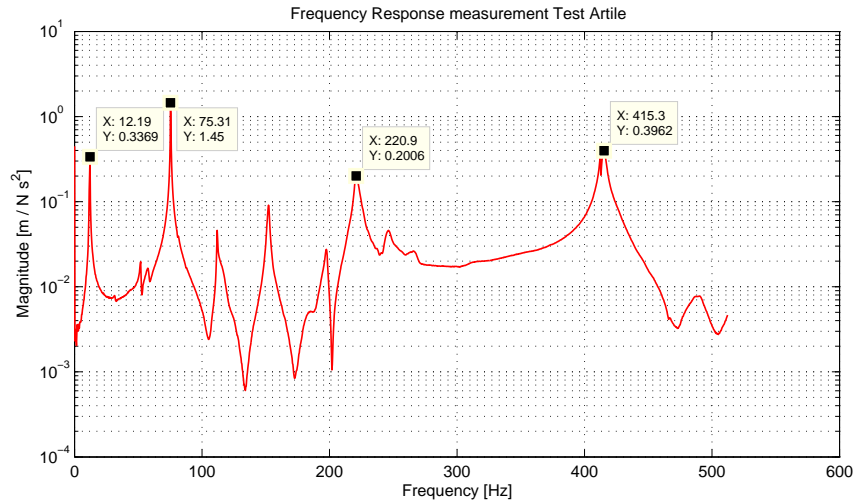


Figure H.1 – Frequency response measurement between acceleration output (tip beam) and force input (point 0.6 m from tip beam).

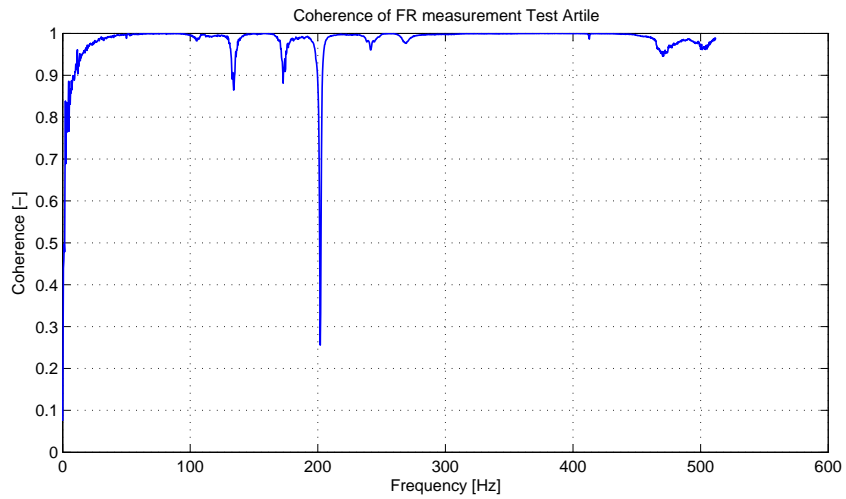
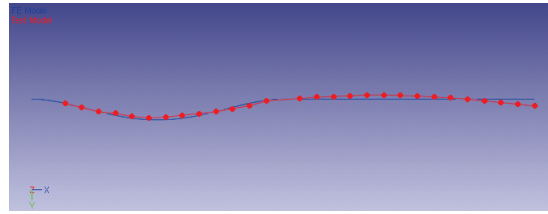
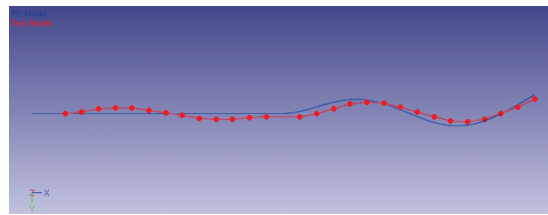


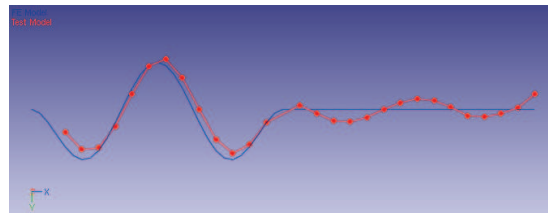
Figure H.2 – Coherence test article measurement, between force input and acceleration output.



(a) EMA Mode 3, first bending rear beam mode (52 Hz).



(b) EMA Mode 5, second bending rear beam mode (221 Hz).



(c) EMA Mode 7, third bending rear beam mode (422 Hz).

Figure H.3 – First three modes of rear beam obtained by EMA analysis, showing the ABAQUS analysis (in blue) and measured modes (in red).

FE modes Y direction		EMA modes Y direction						
Mode number	Freq [Hz]	1	2	3	4	5	6	7
		12	75.4	52.1	221	245	415	422
1. 1st bending front	12.81	99.1	0.9	1.2	0.3	4.4	0.9	0.2
2. 1st rear	80.17	0.4	6.6	95.4	0.8	0	1.4	0.2
3. 2nd bending front	81.55	0.1	91.9	2.3	0.2	0.4	0.1	1.5
4. 2nd rear	224.22	1.6	0	1.1	96.9	68.1	0.2	0.1
5. 3rd bending front	224.79	1.6	0	1.1	96.9	68.1	0.2	0.1
6. 4th bending front	438.88	1.2	0.3	1.5	3.5	10.5	88.9	5.4
7. 3rd rear	440.67	0	0.5	0	0.5	2.8	8	88.9

Table H.1 – MAC correlation table of all modes correlated between FE ABAQUS analysis and EMA analysis.

H.1.2 Interface Structure

Hole and pin diameters of the interface structure coupling between base block and the hydraulic actuator are:

Bracket hole diameter	B_{h1}	25.04	[mm]
Pin diameter	P_{d1}	24.95	[mm]
Fork hole diameter	F_{h1}	25.01	[mm]

Hole and pin diameters of the interface structure coupling between hydraulic actuator and test article are:

Bracket hole diameter	B_{h2}	24.95	[mm]
Pin diameter	P_{d2}	24.9	[mm]
Fork hole diameter	F_{h2}	24.98	[mm]

Maximal mechanical play of the test setup is calculated by the difference between the pin diameters and the maximum bracket or fork diameter, resulting in:

$$g_{tot} = (B_{h1} - P_{d1}) + (F_{h2} - P_{d2})$$

$$g_{tot} = (25.04 - 24.95) + (24.98 - 24.9) = 0.17[\text{mm}]$$

H.2 Hydraulic System

This section presents detailed measurement results, on the hydraulic system.

H.2.1 Servo Valve

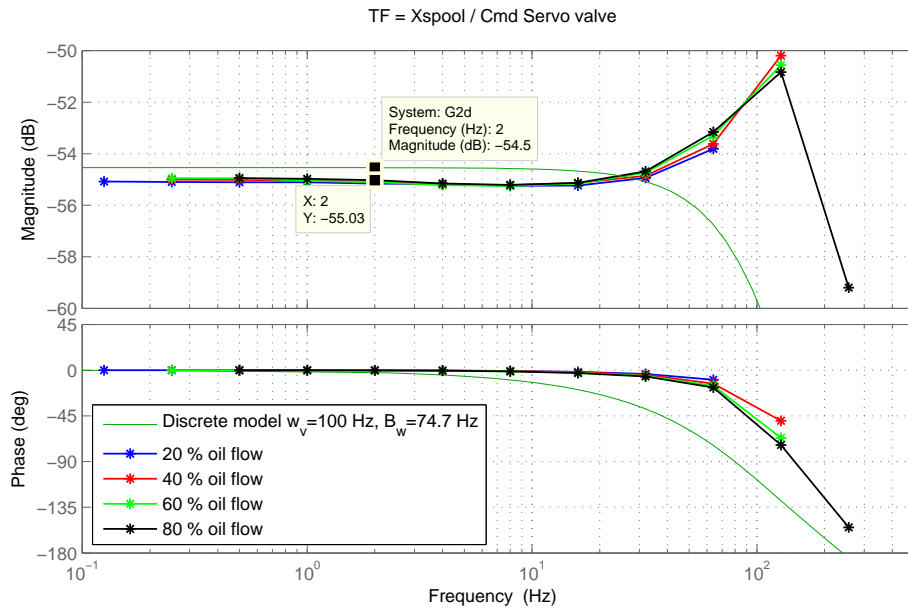


Figure H.4 – Detailed measurement results of SV response, between valve position and current input, coupled with the HA.

H.2.2 Hydraulic Actuator

Figure H.5 and Figure H.6 present a detailed plot on the hydraulic actuator frequency response.

H.2.3 Supply and Return Pressures

Figures H.7 and H.8 present the supply and return pressure time signals of the HA in uncoupled state. Which means that the HA is not coupled to any structure. The HA is sinusoidal at 8 [Hz] and consuming 80 [%] of the nominal flow. From these results it is possible to calculate the amount of supply pressure fluctuation. This is done by calculating the error between average pressure and maximum amplitude of the pressure.

$$P_{average} = \frac{1.96 \cdot 10^7 - 1.88 \cdot 10^7}{2} = 1.92 \cdot 10^7 \text{ [N/m}^2\text{]} \text{ [N/m}^2\text{]} \text{ [N/m}^2\text{]} \text{ [N/m}^2\text{]}$$

$$Error_{pressure} = \frac{1.96 \cdot 10^7 - 1.92 \cdot 10^7}{1.92 \cdot 10^7} = 2 \text{ [\%]}$$

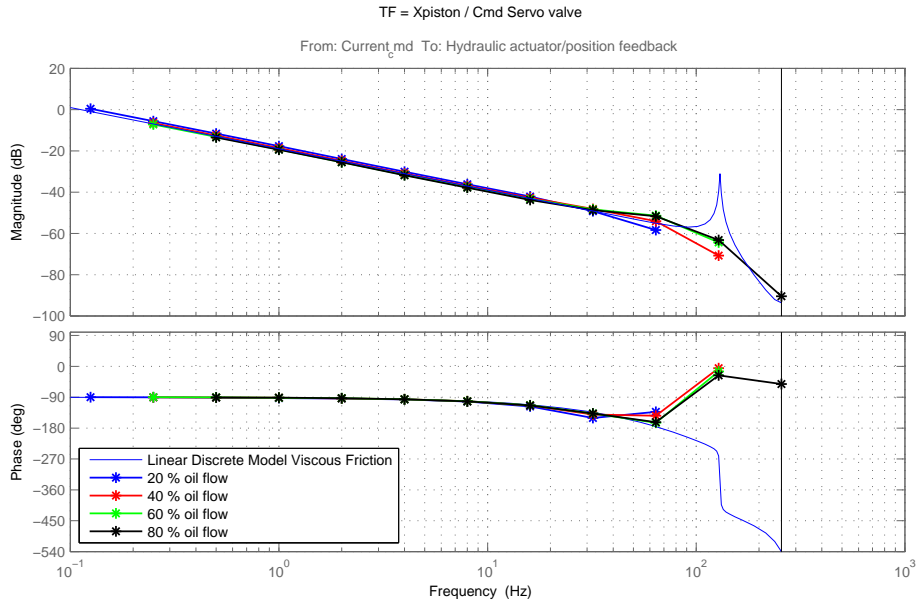


Figure H.5 – Hydraulic actuator frequency response between piston position and servo valve command, using sinusoidal signals.

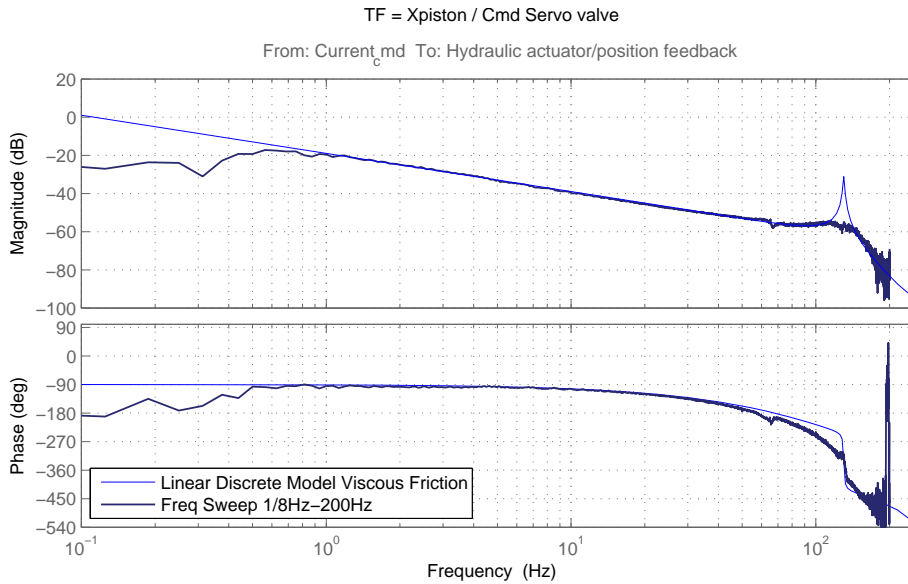


Figure H.6 – Hydraulic actuator frequency response between piston position and servo valve command using a frequency sweep.

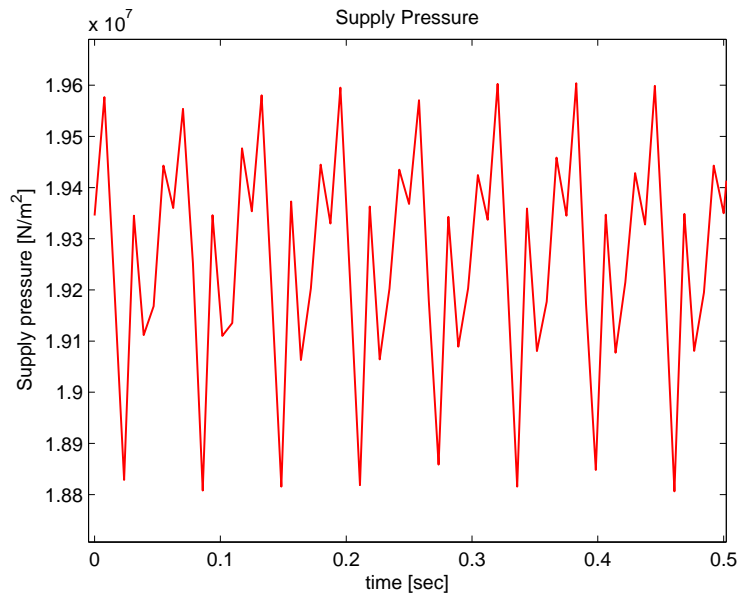


Figure H.7 – Supply Pressure fluctuation at HA rod 8 [Hz] and 80 [%] of the nominal flow.

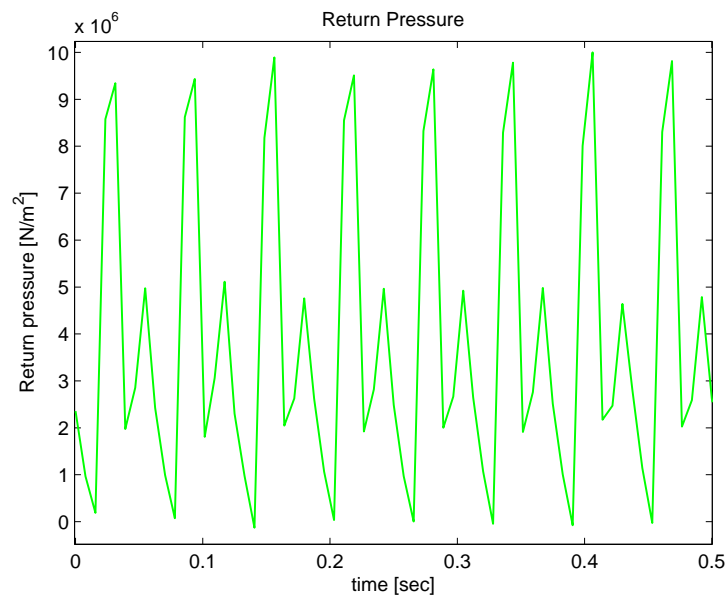


Figure H.8 – Return Pressure fluctuation, HA rod at 8 [Hz] and SV providing 80 [%] of the nominal flow.

H.3 Coupled Mechanical and Hydraulic System

H.3.1 Measurements Semi-Open Loop Configuration

To verify the frequency responses obtained by position and force feedback measurements, also a semi-open loop measurement is performed. In these measurements a feedback gain is implemented to simulate frequency response of the open loop system. To perform real open loop simulations the feedback gain has to be set to 0.

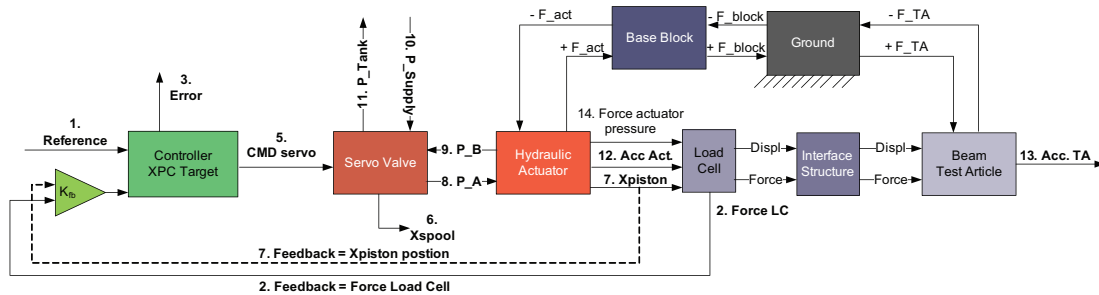


Figure H.9 – Semi-open loop measurement configuration, implementing feedback gain for force and position feedback loops.

Measurements performed for semi-open loop force and position frequency responses are:

- Frequency sweep 0.125 Hz - 256 Hz, with a feedback gain of 0.1.
- White noise 0.08 Hz - 256 Hz, with a feedback gain of 0.01.

These measurements resulted in the results presented in Figure H.10 and Figure H.11:

H.3. Coupled Mechanical and Hydraulic System

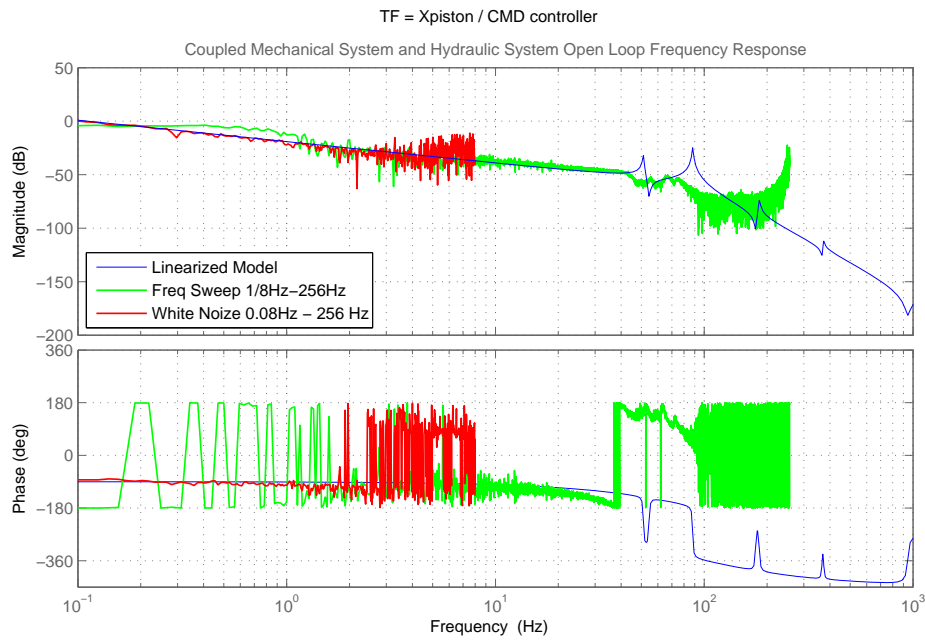


Figure H.10 – Coupled system open loop frequency response, between piston position and command servo valve, using small position feedback.

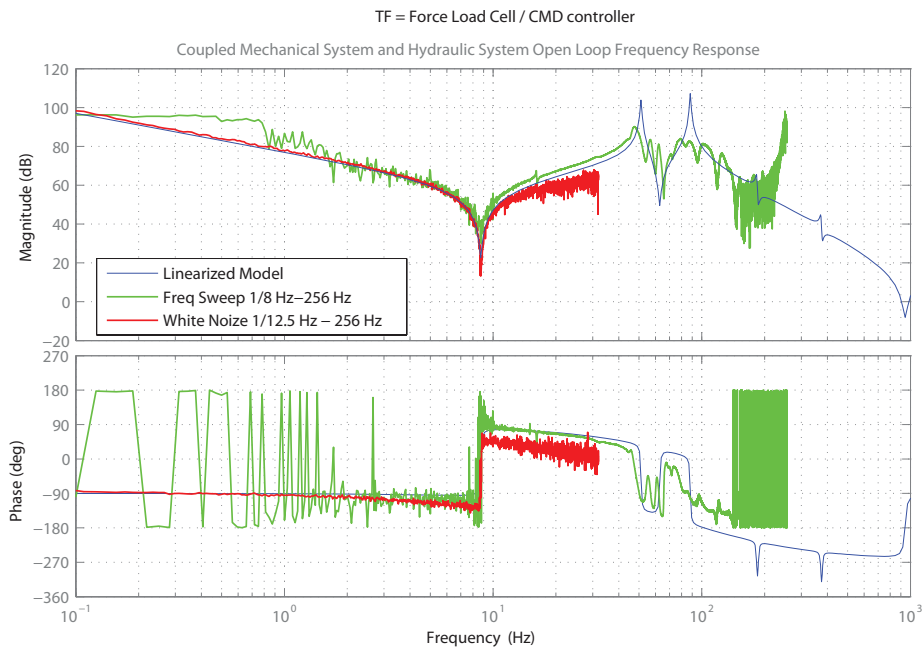


Figure H.11 – Coupled system open loop frequency response, between force load cell and command servo valve, using small force feedback.

H.4 Control System

H.4.1 Open Loop FR Controller and Plant

The open loop Frequency Response of the controller and the plant are presented in Figure H.12 and Figure H.13.

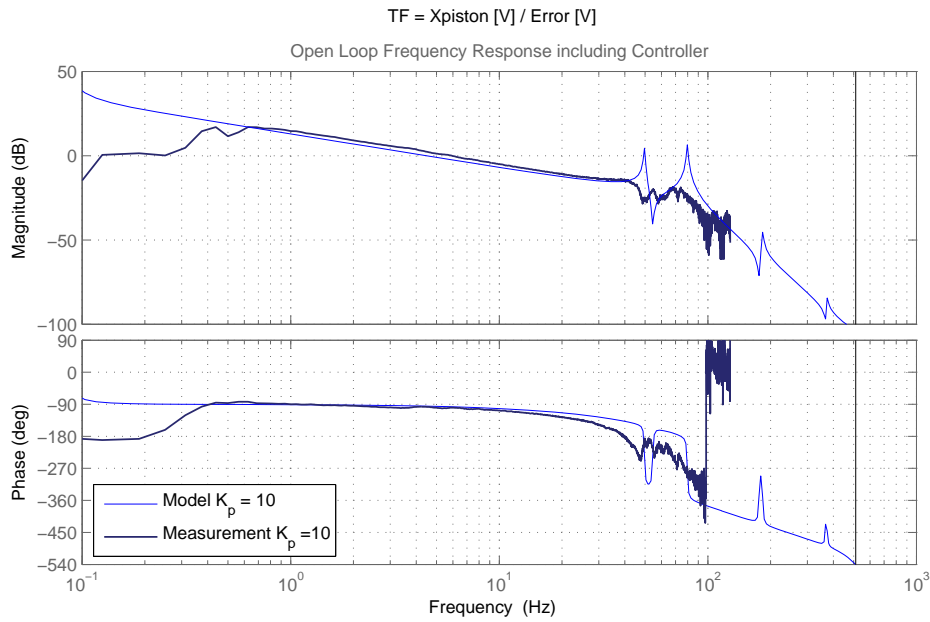


Figure H.12 – Open loop frequency response of the controller and plant, using position feedback configuration.

H.5 Signal Conditioning

The open loop frequency responses of the signal conditioning units are presented in Figure H.14. Each signal conditioning unit is measured between its input and output.

H.5. Signal Conditioning

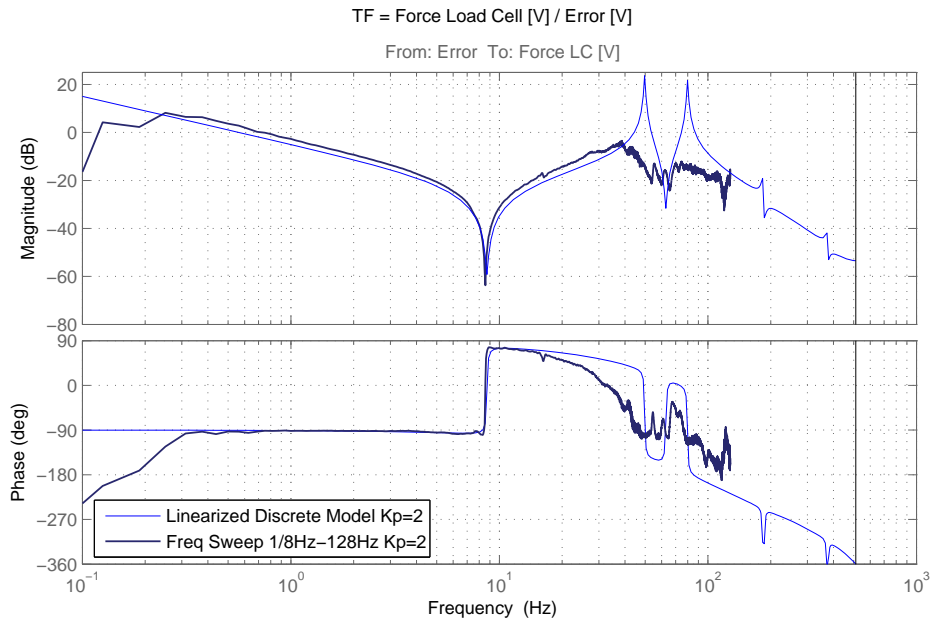


Figure H.13 – Open loop frequency response of the controller and plant, using load cell force feedback configuration.

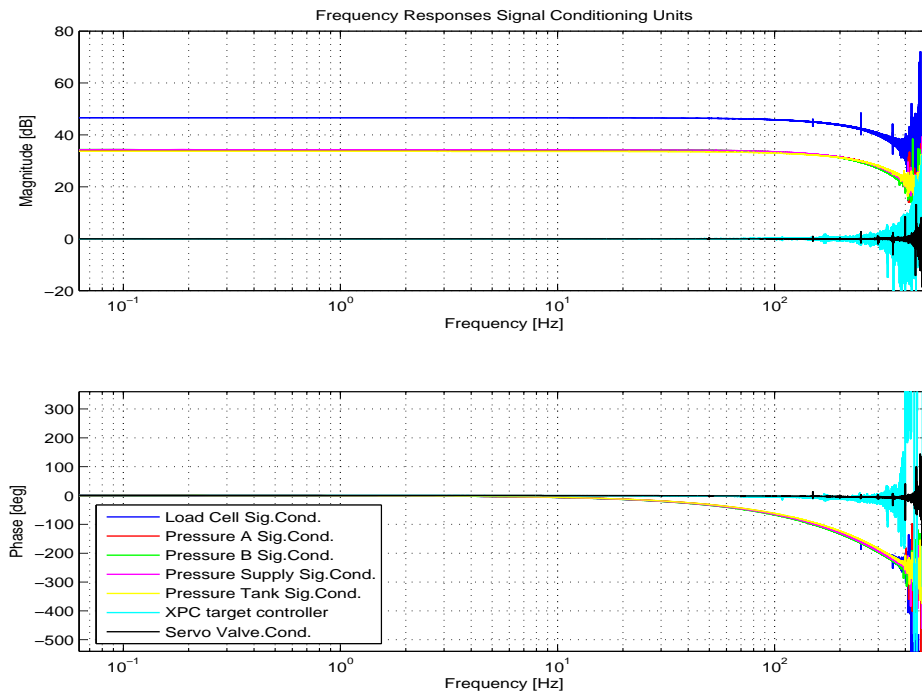


Figure H.14 – Signal Conditioning Units frequency responses open loop.